Leibniz-Institut für Arbeitsforschung an der TU-Dortmund

Dissertation

Alterations of the glyoxylate metabolism in hepatic steatosis – a risk factor for hyperoxaluria

zur Erlangung des akademischen Grades des Doktors der Naturwissenschaften (Dr. rer. nat.) an der Fakultät für Chemie und Chemische Biologie der Technischen Universität Dortmund

vorgelegt von

Adelina Jashari (M.Sc.)

Dortmund 2020

Gutachter: 1. Prof. Dr. med. Jan Hengstler

2. Prof. Dr. Carsten Watzl

Datum der Einreichung: 15.07.2020

Datum der Disputation: 16.09.2020

Abstract

Non-alcoholic fatty liver disease (NAFLD) comprises a wide spectrum of liver diseases ranging from simple hepatic steatosis to more severe liver diseases, like non-alcoholic steatohepatitis (NASH), cirrhosis or hepatocellular cancer (HCC), and is the leading cause of liver diseases worldwide. Features of the metabolic syndrome, such as insulin resistance, hypertension, obesity, hyperlipidaemia, and extrahepatic diseases, like cardiovascular diseases and kidney stone disease, strongly associate with NAFLD. A previously identified steatosis-associated downregulation of the alanine-glyoxylate aminotransferase (*AGXT)* was suggested to be one molecular link explaining the connection of NAFLD with the development of calcium oxalate kidney stones. AGXT is responsible for the hepatic glyoxylate detoxification and its deficiency results in primary hyperoxaluria type 1 (PH1), which is a hereditary disorder with characteristic symptoms such as recurrent urolithiasis, nephrocalcinosis and the formation of calcium oxalate kidney stones. Furthermore, the *AGXT* downregulation in steatotic conditions was proposed to be influenced by DNA methylation since the *AGXT* promoter is hypermethylated in steatosis.

In the course of this thesis, further alterations of the glyoxylate metabolism were revealed in the *ob/ob* and Western diet (WD) mouse models of NAFLD contributing to a better understanding of the steatosis-associated modifications. These alterations indicating an increased hepatic oxalate production in steatotic conditions were confirmed by elevated oxalate excretion of steatotic hepatocytes from WD-fed and *ob/ob* mice upon hydroxyproline exposure. Furthermore, the increased oxalate production in the fatty liver was validated *in vivo* by elevated oxalate levels in the plasma from the hepatic vein of WD-fed mice, representing the blood outflow from the liver. Additionally, oxalate levels in the plasma and urine of *ob/ob* mice were increased to a higher extent due to the consumption of dietary hydroxyproline compared to *ob/+* mice, showing an enhanced susceptibility towards hydroxyproline also *in vivo*. The selective sensitivity of steatotic hepatocytes to hydroxyproline contrasted with that of primary hepatocytes from *Agxt* knock-out (*Agxt*$^{-/-}$*)* mice, which excreted more oxalate when exposed to all oxalate precursors than hepatocytes from wild type control mice. This suggested, that only mitochondrial glyoxylate detoxification is compromised in hepatic steatosis. Rescuing the *Agxt* expression in the hepatocytes of *ob/ob* mice by adeno-associated virus (AAV)-mediated gene transfer was able to reduce oxalate production from hydroxyproline. Moreover, inhibition of hydroxyproline catabolism normalised the oxalate excretion from *ob/ob* hepatocytes to the levels of *ob/+* hepatocytes after consumption of hydroxyproline. These results provided clear evidence that the downregulation of *Agxt*, at least partially, responsible for the steatosis-accompanied increased hepatic oxalate production in NAFLD mouse models, supporting the hypothesis of the steatosis-associated downregulation of *Agxt* being a molecular link explaining the strong association between NALFD and kidney stone disease.

The translational relevance of these findings was studied in a cohort of overweight and obese children and adolescents with biopsy proven NAFLD and corresponding 24 h urine samples.

The steatosis percentage positively correlated with the amount of urinary excreted oxalate, showing the relevance of steatosis induced hyperoxaluria in human NAFLD.

In order to further understand the deregulation of *Agxt* expression in steatosis and the dependency to DNA methylation, its transcriptional upregulation in response to glucagon was studied in *ob/ob* and 6 weeks WD-fed mice. Since there is a cAMP response element (CRE) binding site within the hypermethylated region of the *Agxt* promoter it was hypothesised that the glucagon-cAMP-PKA-Creb signalling, that regulates *Agxt* transcription, may be blunted in steatosis. When treated with glucagon, an increase of the *Agxt* mRNA expression was missing in *ob/ob* mice but not in 6 weeks WD-fed mice, most probably due to the higher hypermethylation of the *Agxt* promoter in *ob/ob* mice. This supported the importance of the *Agxt* promoter hypermethylation regarding the regulation of the *Agxt* gene expression. These results were confirmed *in vitro* in glucagon stimulated primary hepatocytes from the two different NAFLD mouse models and in an *in vitro* steatosis model. Furthermore, the phosphorylation of Creb was lost earlier in hepatocytes from *ob/ob*, 6 weeks WD-fed mice and in an *in vitro* steatosis model compared to their corresponding controls. The impaired responsiveness of *AGXT* mRNA expression and the earlier CREB dephosphorylation could also be shown in primary human hepatocytes (PHHs) with an increased triglyceride content. All in all, these findings support the thesis that steatosis associated *AGXT* promoter hypermethylation might repress the *AGXT* gene expression leading to an impaired response towards glucagon. Altogether, considering that Agxt has an additional role in gluconeogenesis, the earlier CREB dephosphorylation together with the impaired transcriptional response of *AGXT* towards glucagon might be possible feedback mechanisms in order to reduce hepatic glucose production and NAFLD associated hyperglycaemia. As a side effect, this may lead to steatosis-linked increased hepatic oxalate production.

Zusammenfassung

Die nicht-alkoholische Fettlebererkrankung (NAFLD) entsteht durch die übermäßige Akkumulation an Triglyceriden innerhalb von Hepatozyten. Das klinische Erscheinungsbild von NAFLD umfasst die simple Fettleber, die nicht-alkoholische Steatohepatitis (NASH), Leberzirrhose und das Leberzellkarzinom. NAFLD ist stark assoziiert mit verschiedenen Merkmalen des metabolischen Syndroms sowie mit kardiovaskulären- und Nierenerkrankungen wie der Ausbildung von Kalziumoxalatsteinen. In einer vorangegangenen Studie wurde die Fettleber-assoziierte Herunterregulierung von *AGXT* als mögliche molekulare Verbindung suggeriert, welche die starke Assoziierung von NAFLD zur Ausbildung von Kalziumoxalatsteinen erklären könnte. Die Hauptfunktion von AGXT ist die Umwandlung des toxischen Glyoxylats zu Glycin innerhalb der Leber. Individuen mit einem nicht funktionalen oder fehlenden AGXT leiden unter der sogenannten primären Hyperoxalurie Typ 1 (PH1), welche eine autosomal-rezessiv vererbbare Krankheit darstellt. Charakteristische Symptome von PH1 sind eine wiederkehrende Urolithiasis, Nephrokalzinose sowie die Ausbildung von Kalziumoxalatsteinen innerhalb der Niere. Des Weiteren wurde die These aufgestellt, dass die Herunterregulierung von *AGXT* in steatotischen Bedingungen aufgrund der Hypermethylierung im *AGXT* Promotor entstehen könnte.

Im Rahmen dieser Arbeit wurden weitere Steatose-bedingte Expressionsveränderungen von im hepatischen Glyoxylatmetabolismus beteiligten Enzymen in *ob/ob* und Western Diät (WD) gefütterten Mäusen festgestellt. Diese Veränderungen deuteten auf eine erhöhte Oxalatproduktion in der Fettleber hin. Dies konnte durch eine gesteigerte Ausscheidung an Oxalat aus primären Hepatozyten von *ob/ob* und WD-gefütterten Mäusen, die mit der Oxalatvorläufersubstanz Hydroxyprolin behandelt wurden, bestätigt werden. Außerdem wurde die erhöhte hepatische Oxalatproduktion der steatotischen Leber durch höhere Oxalatekonzentrationen im Blut, welches aus der Leber hinaus fließt, von WD Mäusen untermauert. Zusätzlich wurde festgestellt, dass über die Nahrung aufgenommenes Hydroxyprolin die Oxalatkonzentrationen in *ob/ob* Mäusen im Plasma und Urin stärker anhebt als in *ob/+* Kontrollmäusen. Dies bestätigte die zuvor beobachtete verstärkte Empfindlichkeit von *ob/ob* Hepatozyten gegenüber Hydroxyprolin auch *in vivo*. Die selektive Sensitivität von steatotischer Hepatozyten gegenüber Hydroxyproline stand im Gegensatz zu primären Hepatozyten aus *Agxt* knock-out (*Agxt*$^{-/-}$) Mäusen, welche im Vergleich zu Wildtyp-Kontrollhepatozyten mehr Oxalat aus allen Oxalatvorläufersubstanzen produzierten. Dieses Ergebnis deutete darauf hin, dass in der steatotischen Leber nur die mitochondriale Glyoxylatdetoxifizierung kompromittiert ist. Darüber hinaus führte die Wiederherstellung der *Agxt* Expression durch einen adeno-assoziierten Virus (AAV) vermittelten Gentransfer in *ob/ob* Hepatozyten zu einer Reduktion der Oxalatproduktion aus Hydroxyprolin. Außerdem normalisierte die Inhibition des Hydroxyprolinkatabolismus die Oxalatausscheidung von *ob/ob* Hepatozyten auf das Niveau von *ob/+* Kontrollhepatozyten nach der Behandlung mit Hydroxyprolin. Aufgrund dieser Ergebnisse konnte gezeigt werden, dass die Herunterregulierung von Agxt, zumindest zu einem gewissen Teil, für die Steatose-bedingten

Erhöhung der hepatischen Oxalatproduktion verantwortlich ist. Weiterhin wird die Hypothese, dass die Herunterregulierung von Agxt in der Fettleber ein molekularer Mechanismus ist, der die Verbindung von NAFLD zur Entstehung von Kalziumoxalatsteinen erklären könnte, durch diese Ergebnisse unterstützt.

Die translationale Relevanz dieser Befunde wurden in einer Kohorte von übergewichtigen und adipösen Kindern und Jugendlichen mit einer durch eine Leberbiopsie nachgewiesenen Fettlebererkrankung untersucht, wobei auch die Oxalatmenge in 24 h Urinproben analysiert wurde. Der Steatosegrad korrelierte positiv mit der Menge an ausgeschiedenem Oxalat im Urin. Dies verdeutlichte die Relevanz von Steatose-induzierter Hyperoxalurie in NALFD im Menschen.

Um die Deregulierung der *Agxt* Expression in der Steatose und dessen Abhängigkeit zur DNA Methylierung zu verstehen, wurde dessen transkriptionelle Hochregulierung in Antwort auf Glukagon in *ob/ob* und WD Mäuse untersucht. Da sich innerhalb der hypermethylierten *Agxt* Promotorregion eine CRE Bindungsstelle befindet, wurde die Hypothese aufgestellt, dass der Glukagon-cAMP-PKA-Creb Signalweg, welche die *Agxt* Transkription reguliert, in der Steatose abgeschwächt ist. Eine Erhöhung der *Agxt* mRNA Expression in Antwort auf Glukagon fehlte in *ob/ob*, jedoch nicht in WD Mäusen. Dies geschah vermutlich aufgrund einer stärkeren Promotorhypermethylierung in *ob/ob* Mäusen, was den Einfluss der Hypermethylierung im *Agxt* Promotor hinsichtlich der Genexpressionsregulierung untermauerte. Diese Ergebnisse konnten *in vitro* in Glukagon stimulierten primären Hepatozyten aus den zwei verschiedenen NAFLD Mausmodellen als auch in einem *in vitro* Steatose-Modell reproduziert werden. Außerdem wurde eine frühere Creb-Dephosphorylierung in primären Hepatozyten von *ob/ob* Mäusen, von WD Mäusen und im *in vitro* Steatose-Modell beobachtet. Die gestörte Antwort der *AGXT* mRNA Expression sowie die schnellere CREB-Dephosphorylierung nach Glukagonstimulation konnte ebenfalls in primären humanen Hepatozyten eines steatotischen im Vergleich zu einem nicht-steatotischen Donor gezeigt werden. Zusammenfassend unterstützen diese Ergebnisse die These, dass die Steatose-assoziierter *AGXT* Promotorhypermethylierung zu einer Repression der *AGXT* Genexpression führt. In Anbetracht der Rolle von Agxt in der Glukoneogenese, könnten die beobachteten Effekte in steatotischen Bedingungen Rückkopplungsmechanismen darstellen, die die mit NAFLD-assoziierte erhöhte Glukoseproduktion und somit erhöhte Glukosekonzentrationen im Blut reduzieren. Als Nebeneffekt würde dies zu einer Steatose-bedingten gesteigerten hepatische Oxalatproduktion führen.

Abbreviations

%	Percent
Adj	Adjusted
AGXT	Alanine-glyoxylate aminotransferase
APS	Ammonium persulphate
BCA	Bicinchoninic acid
BisTris	Bis-(2-hydroxy-ethyl)-amino-tris(hydroxymethyl)-methane
BMI	Body mass index
BSA	Bovine serum albumin
°C	Degrees Celsius
$CaCl_2$	Calcium chloride
cAMP	Cyclic adenosine monophosphate
cDNA	Complementary DNA
CpG	5'—cytosine—phosphate—guanine—3'
CRE	cAMP response element
CREB/pCREB	cAMP response element binding protein/ phosphorylated cAMP response element binding protein
CRTC2	CREB regulated coactivator 2
Ct	Cycle threshold
d	days
DAPI	4',6-diamidino-2-phenylindole
DEPC	Diethyl pyrocarbonate
DMEM	Dulbecco's modified Eagles' medium
DNA/RNA	Deoxyribonucleic acid/Ribonucleic acid
DNMT	DNA methyltransferase
DPPIV	Dipeptidyl peptidase 4

DTT	Dithiothreitol
EDTA	Ethylenediaminetetraacetic acid
EGTA	Ethylene glycol-bis (β-aminoethyl ether)-N, N, N’, N'-tetra acetic acid
Eif2a	Eukaryotic translation initiation factor 2A
e.g.	For example
Et al.	And others
ESKD	End stage kidney disease
FM	Full media
g/mg/µg	gram/milligram/microgram
G6P	Glucose-6-phosphatase
GAPDH	Glyceraldehyde 3-phosphate dehydrogenase
GCGR	Glucagon receptor
Gluc	Glucagon
GRHPR	Glyoxylate reductase/hydroxypyruvate reductase
h	hours
HAO1	4-hydroxy-2-oxoglutarate aldolase 1
HRP	Horseradish peroxidase
Hepes	4-(2-hydroxyethyl)-1-piperazineethanesulfonic acid
HOGA1	Horseradish peroxidase
H&E	Haematoxylin and Eosin Y
Hyp	Hydroxyproline
i.E.	that is
IfADo	Leibniz-Institut für Arbeitsforschung an der TU Dortmund
IFNγ	Interferon gamma
IHC	Immunohistochemistry
Il-6/Il-10	Interleukin-6/-10

IR	Insulin resistance
JNK	c-Jun N-terminal kinase
KH_2PO_4	Potassium dihydrogen phosphate
l/ml/µl	Litre/millilitre/microlitre
LC-MS/MS	Liquid chromatography-mass spectrometry/mass spectrometry
LDHA	Lactate dehydrogenase A
LPS	Lipopolysaccharide
M/mM/µM/nM	Molar/millimolar/micromolar/nanomolar
$MgSO_4$	Magnesium sulphate
MTS	Mitochondria target sequence
n	Number of biological replicates
Na_2HPO_4	Sodium hydrogen phosphate
NaCl	Sodium chloride
NAFL	Non-alcoholic fatty liver
NAFLD	Non-alcoholic fatty liver disease
NASH	Non-alcoholic steatohepatitis
NCD/WD/HFD	Normal chow diet/ western diet/ high fat diet
NF-κB	Nuclear factor kappa-light-chain-enhancer of activated B cells
NF-Y	Nuclear transcription factor Y
nm	Nanometre
NP-40	Nonidet P-40 substitute
OA; OA/BSA	Oleic acid; Oleic acid complexed to BSA (6:1)
o/n	Over night
PAGE	Polyacrylamide gel electrophoresis
PBS	Phosphate-buffered saline
PCK1	Phosphoenolpyruvate carboxykinase 1

PFA	Paraformaldehyde
PH (1, 2, 3)	Primary hyperoxaluria (type 1, 2 or 3)
PHH	Primary human hepatocytes
PKA	Protein kinase A
PKCα	Protein kinase Cα
PMH	Primary mouse hepatocytes
PRODH2	Proline dehydrogenase 2
PTS1	Peroxisomal targeting sequence type 1
PVDF	Polyvinylidene fluoride
qRT-PCR	Quantitative real-time polymerase chain reaction
RFU	Relative fluorescence units
Rpm	Rounds per minute
ROS	Reactive oxygen species
RRBS	Reduced representation bisulphite sequencing
RT	Room temperature
SDS	Sodium dodecyl sulphate
siRNA	Small interfering RNA
SREBP-1c	Sterol regulatory element-binding protein-1c
STZ	Streptozotocin
T2D	Type 2 diabetes
TBS-T	Tris-buffered saline
TEMED	Tetramethylethylenediamine
TG	Triglyceride
TLR	Toll-like receptor
TNF	Tumour necrosis factor
Tris	Tris(hydroxymethyl)aminomethane

UBC	Ubiquitin C
UPR	Unfolded protein response
Vs	Versus
v/v; w/v	Volume per volume, weight per volume
xg	Standard gravity

1 Introduction

1.1 Non-alcoholic fatty liver disease

Non-alcoholic fatty liver disease (NAFLD) describes the accumulation of fat within the liver due to causes which are independent of alcohol abuse. Therefore, NAFLD can only be diagnosed when secondary causes leading to hepatic lipid infiltration, such as heavy alcohol abuse, steatogenic medication, virus infections or genetic disorders (Chalasani et al. 2012) can be excluded. Heavy alcohol consumption with respect to NAFLD is defined as 30 g absolute ethanol per day for men and 20 g for women (Ratziu et al. 2010).

The term “NAFLD” encompasses a wide spectrum of fatty liver diseases ranging from simple fatty liver (NAFL) to the progressive form of steatosis, the non-alcoholic steatohepatitis (NASH) (Benedict and Zhang 2017). In some cases, NASH can further progress to terminal liver diseases like liver cirrhosis or hepatocellular cancer (HCC) (Anstee et al. 2019a). NAFL is characterised by the presence of more than 5% hepatic steatosis without any inflammation or further hepatocellular injury (European Association for the Study of the Liver (EASL) 2016), whereas, NASH includes the spectrum of more severe liver diseases, which are defined by the occurrence of inflammation, hepatocellular ballooning and fibrosis additionally to steatosis (Brunt et al. 2011). NAFLD is the most important cause of liver disease and elevated liver enzymes worldwide (Younossi et al. 2019) and is becoming the leading cause of liver transplantations (Benedict and Zhang 2017; Younossi et al. 2019). The epidemiology and demographic characteristics of NALFD vary parallel to the prevalence of obesity (Younossi et al. 2018). Numerous risk factors for the development of NAFLD have been identified with most having some form of metabolic disorder or insulin resistance at the core of its pathophysiology. Nevertheless, the exact pathogenic mechanism of NAFLD remains unclear (Benedict and Zhang 2017; Younossi et al. 2018). Furthermore, NAFLD patients exhibit an increased risk of liver-related and cardiovascular mortality (Rinella and Sanyal 2016).

1.1.1 Prevalence of NAFLD

Due to extreme variations in study parameters, demographic variations and the missing of standardized diagnosis methods, a clear and reliable occurrence rate is currently not available. Liver biopsy remains the gold standard for NAFLD diagnosis; while this invasive procedure is not practicable for the screening of a high number of patients. With this background, current estimations have posited suggesting the prevalence of NAFLD to be 20 – 30% in Western countries and 27% in Asia. Out of the NAFLD patients, only 1.5% to 6.45% of NAFLD patients display a progression to NASH (Younossi et al. 2019). Non-invasive radiological methods to diagnose NAFLD include magnetic resonance imaging (MRI) and ultrasonography. In a Spanish study, ultrasound diagnosis revealed a NAFLD prevalence of 33% in men and 20% in women in individuals with no suspected liver diseases. In Italy 20% NAFLD prevalence was measure in patients without suspected liver diseases and in India ultrasound determination revealed a NAFLD prevalence of 17% in the general population. Nevertheless, non-invasive diagnosis

methods are less accurate than histology-based evaluations of liver biopsies, which remain the gold-standard for NAFLD diagnosis (Vernon et al. 2011). Furthermore, the NAFLD prevalence seems to depend on the ethnicity, since Hispanics are reported to be the most susceptible group, followed by white and African Americans (Browning et al. 2004). An allele (rs738409 [G], encoding I148M) in the patatin-like phospholipase-3/adiponutrin (*PNPLA3*) gene is associated with increased hepatic fat accumulation and inflammation. Furthermore, this allele was most common in Hispanics which could be a possible explanation for the increased NAFLD prevalence in Hispanic patients (Romeo et al. 2008).

1.1.2 Connection between NAFLD and metabolic syndrome

The metabolic syndrome is defined by the presence of a cluster of metabolic irregularities that are either causes or consequences of insulin resistance coexisting in obese inactive patients. Different sets of criteria were suggested over the years. The newest postulation defines metabolic syndrome as a disorder that fulfils any three of the following five criteria: increased fasting plasma glucose or T2D (T2D), hypertriglyceridemia, low HDL cholesterol, increased waist circumference, or hypertension (Huang 2009; Shin et al. 2013). Furthermore, metabolic syndrome is more common in obese than in non-obese patients. However, some obese individuals do not develop the syndrome while non-obese individuals may do so. The reason for this phenomenon remains unclear (Wildman 2008; Schulze 2019).

Patients with a metabolic syndrome often display an increased hepatic triglyceride accumulation and hepatic insulin resistance. This increased hepatic fat content is only associated with insulin resistance but not with other known causes of steatosis (e.g., alcohol, viruses, and drugs). Thus, a connection between NAFLD and metabolic syndrome was suggested (Smits et al. 2013; Yki-Järvinen 2014a; Williams 2015). Furthermore, NAFLD is more prevalent in patients with existing metabolic disorders compared to those in general population (Vernon et al. 2011; Grander et al. 2016). Beside insulin resistance, also other criteria of the metabolic syndrome like hypertriglyceridemia, elevated waist circumference or T2D are associated with NAFLD. Thus, NAFLD is often considered as the hepatic manifestation of the metabolic syndrome (Kim and Younossi 2008; Gastaldelli 2010; Medina-Santillán et al. 2013). But this conclusion is controversially discussed. As a result of a variety of different definitions of metabolic syndrome and NAFLD, the two disorders are not necessarily concurrent (Yki-Järvinen 2014b; Lonardo et al. 2015; Wainwright and Byrne 2016). Smit and colleagues found no evidence that NAFLD is an independent component of the metabolic syndrome. They consider NAFLD rather as a separate condition, which is strongly associated with the metabolic syndrome (Smits et al. 2013).

1.2 The progression of NAFLD

Steatosis alone is considered a benign and non-progressive form of NAFLD. However, patients with simple steatosis might still develop NASH and/or fibrosis (Wong et al. 2010). Moreover, NAFLD and NASH can progress to cirrhosis and hepatocellular cancer (HCC) with or without fibrosis and are reported to be the most common underlying risk factor for HCC in the USA

(Sanyal et al. 2010; Baffy et al. 2012; Wong et al. 2014; Anstee et al. 2019b). Singh and colleagues studied the progression of NAFL and NASH patients towards fibrosis. They reported a fibrosis development progression time of 14.3 years for NAFL and 7.1 years for NASH patients (Singh et al. 2015).

However, the pathogenic components of NAFLD development and progression exhibit a high complexity and multiple factors with various theories presented in literature (Buzzetti et al. 2016). Already the first step in the development of NAFLD, the hepatic fat accumulation, displays various possible underlying processes, since the lipid accumulation might be a consequence of several mechanism, such as the oversupply of fatty acids and their assembly into triglycerides (Postic and Girard 2008). Additionally, the fatty acids might have different sources, like lipolysis of adipose tissue, the diet, and hepatic *de novo* synthesis of fatty acids, which are further esterified to glycerol (Donnelly et al. 2005). Furthermore, hepatic lipid accumulation can be driven by an increased lipid/triglyceride production, an impaired fatty acid degradation and/or by a reduced excretion of hepatic very low-density lipoproteins (VLDL) containing triglycerides (Postic and Girard 2008). Regarding NAFLD progression, a two-hit model has been proposed with the first hit being hepatic lipid accumulation, a sedentary lifestyle, a high fat diet, and insulin resistance. The first hits are described to increase the susceptibility of the liver to “second hits” which activate an inflammatory event with associated fibrogenesis. Examples of second hits are lipid peroxidation, reactive oxygen species, free fatty acids, and the release of cytokines (Day and James 1998; Day 2002). By now, the two-hit model is believed to be too oversimplified to comprehensively capture the complexity of NAFLD where multiple factors are collaborating with one another in a genetically predisposed individual (Buzzetti et al. 2016; Fang et al. 2018; Pierantonelli and Svegliati-Baroni 2019). In some researcher’s opinions, this model still cannot explain the rare progression rate of simple steatosis, in contrast to NASH, to more severe liver diseases. Consequently, multiple parallel hits models have been proposed trying to explain the intricacy of NAFLD progression (Buzzetti et al. 2016; Fang et al. 2018; Pierantonelli and Svegliati-Baroni 2019). Some scientists also introduced the idea of simple fatty liver and NASH being two different diseases (Tilg and Moschen 2010; Buzzetti et al. 2016).

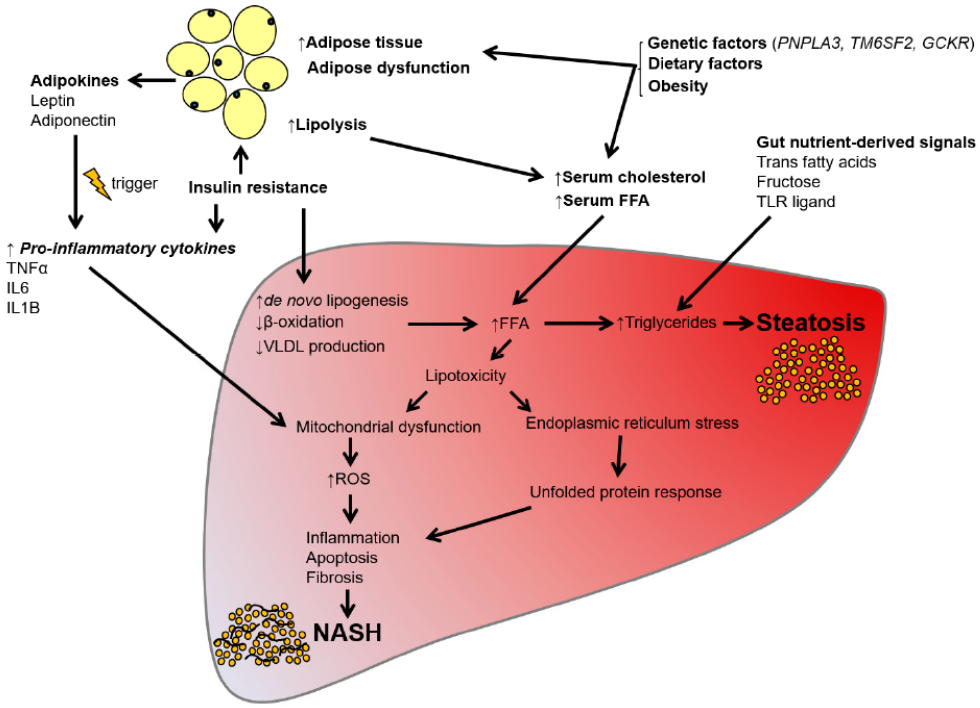

Figure 1.1: Schematic illustration of multiple parallel hits hypothesis of NAFLD development (Chen et al. 2018).

1.2.1 Role of insulin and glucagon in NAFLD

In the muscle and liver, insulin promotes glucose uptake for glucose oxidation or glycogen storage. Furthermore, insulin also regulates the lipid metabolism, as it enhances fatty acid re-esterification into triglyceride in adipocytes and the liver. The main function of insulin in the liver is the suppression of glycogenolysis and gluconeogenesis (Petersen and Shulman 2018).

Insulin resistance is the key pathogenic feature of the metabolic syndrome and a crucial risk factor for NAFLD development and progression (Marchesini et al. 1999; Ota et al. 2007; Gluvic et al. 2016). Hepatic insulin resistance develops by interrupting insulin-induced suppression of hepatic glucose production but increasing stimulation of lipogenesis reversely (Samuel and Shulman 2016). For individuals with insulin resistance, the islets of Langerhans are stimulated to increase the insulin secretion in order to overcome the deficiency in plasma glucose absorption and to reduce the hepatic glucose production leading to high glucose production rates in hepatocytes in the presence of high insulin levels in the plasma. On one hand, insulin fails to suppress hepatic glucose production in a liver with insulin resistance, but on the other hand it continues to stimulate lipogenesis, resulting in hyperglycaemia, hyperlipidaemia, hepatic steatosis, and T2D (Samuel and Shulman 2016; Petersen and Shulman 2018; Khan et al. 2019). Hence, increased insulin concentrations lead to an increasing TG synthesis in the presence of insulin resistance (Vatner et al. 2015). NAFLD patients display an increased *de novo* lipogenesis (DNL), which is not suppressed on fasting and elevated FFA plasma concentrations, compared to controls (Lambert et al. 2014). Furthermore, β-oxidation of FFAs is inhibited in states of insulin resistance, contributing to hepatic fat lipid accumulation (Postic

and Girard 2008). Moreover, genetic variations involved in insulin signalling have been associated with NAFLD pathogenesis and progression. (Dongiovanni et al. 2010).

Glucagon is a hormone of 29 amino acids produced by the pancreatic alpha cells and is known as the counter-regulatory hormone to insulin (Scott and Bloom 2018). The balance of glucagon and insulin signalling is mainly responsible for maintaining physiological euglycemia (Hædersdal et al. 2018). The secretion of glucagon is inhibited by hyperglycaemia, insulin, glucagon-like peptide 1 (GLP-1) and somatostatin (Yamato et al. 1990; Cejvan et al. 2003; Kawamori et al. 2009). The most important function of glucagon is increasing the blood glucose, through stimulation of glycogenolysis and gluconeogenesis (Scott and Bloom 2018). Hepatic lipid metabolism is also influenced by glucagon, which induces lipolysis and ketone production (Wang et al. 2016). Moreover, glucagon affects protein metabolism by increasing ureagenesis and causing amino acid uptake into hepatocytes (Fitzpatrick et al. 1977; Fehlmann et al. 1979; Boden et al. 1996). All in all, glucagon influences multiple mechanism in order to maintain energy nourishment of all organs.

Glucagon acts via a specific $G_{\alpha s}$-protein coupled sevens transmembrane receptor on the plasma membrane (GCGR), which is expressed throughout the body, and it is particularly abundant in the liver, kidney, heart and adipose tissue (Geary 2013). Binding of glucagon to its receptor leads to conformational changes that activate $G_{\alpha s}$-coupled proteins which in turn activate the adenylate cyclase (AC). Next, the AC produces cyclic adenosine monophosphate (cAMP) out of adenosine monophosphate (AMP). Elevated cAMP levels stimulate the activation of protein kinase A (PKA) which translocate to the nucleus and activates the cAMP response element-binding (CREB) protein via phosphorylation. The activated transcription factor pCREB induces transcription of the gluconeogenic enzymes like glucose 6-phosphatase and phosphoenolpyruvate carboxykinase (PEPCK) (Burgess et al. 2007; Lin and Accili 2011). Meanwhile, the activated PKA results in a number of intracellular events besides the phosphorylation of CREB, for instance the inhibition of phospho-fructokinase 2 (PFK-2) protein The subsequent increased activity of fructose 2,6-bisphosphatase (FBPase2) leads the elevated activity of fructose-1,6-bisphosphatase (FBPase-1) which results in stimulated gluconeogenesis and reduced glycolysis (Pilkis et al. 1982; Kurland and Pilkis 1995). Also, phosphorylase kinase is activated by PKA which through a number of events leads to an overall lower glycogen concentration and results in hepatic glucose release (Brushia 1999; Jiang and Zhang 2003; Miller and Birnbaum 2016; Müller et al. 2017).

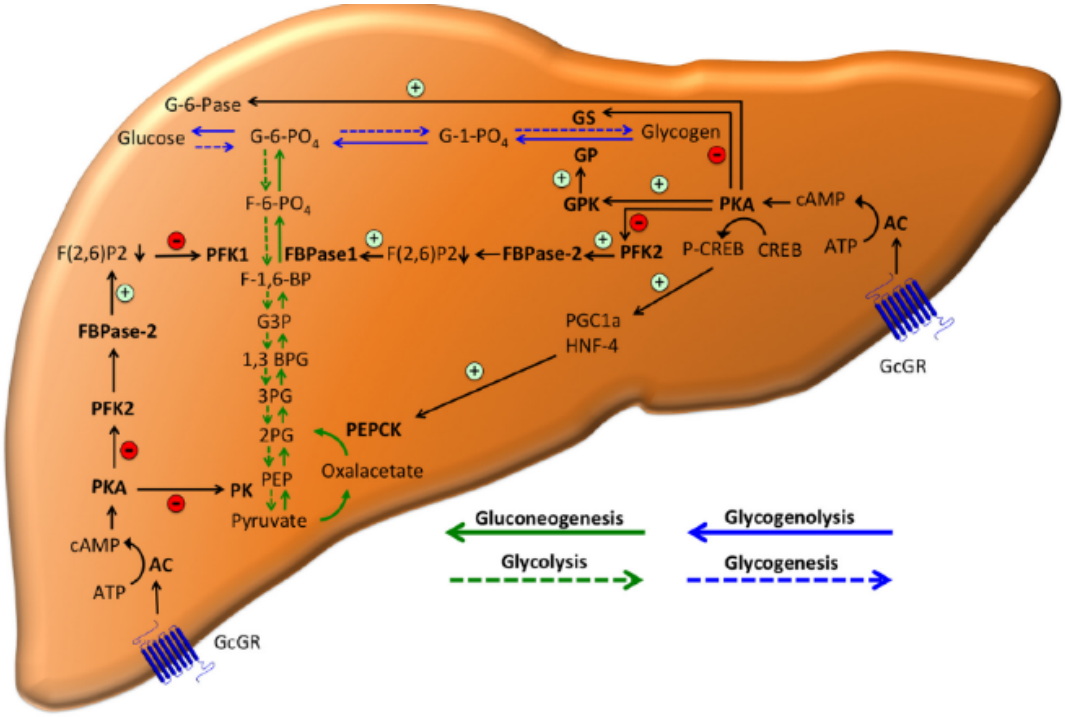

Figure 1.2: Schematic illustration of hepatic glucagon signalling (Müller et al. 2017).

Glucagon levels have been found to be elevated in all forms of diabetes, including alloxan-induced diabetes in dogs, to patients with type 1 and type 2 diabetes, even after removal of the pancreas (Müller et al. 1971; Unger et al. 1972; Buchanan and Mccarroll 1972; Mashiter et al. 1975; Alberti et al. 1975; Palmer et al. 1976). Therefore, the bihormonal abnormality hypothesis of diabetes was proposed, suggesting that glucagon elevation was as important as insulin deficiency. It has been postulated that hyperglucagonemia stimulates hepatic glucose production and potentiates the hyperglycaemic state of diabetes patients (Unger and Orci 1975). Moreover, many obese and/or pre-diabetic patients also displayed high levels of glucagon in the plasma, and an increased hepatic glucose production (Gastaldelli et al. 2000; Stern et al. 2019). Recent studies further showed in rodent models of type 1 and T2D that elevated plasma glucose levels and ketosis could be reduced by *Gcgr* knockout (*Gcgr*$^{-/-}$) (Gelling et al. 2003; Conarello et al. 2006; Lee et al. 2011). Furthermore, in the *Gcgr*$^{-/-}$ version of T2D mouse model, type 2 diabetic phenotype appears after the rescue of the Gcgr cDNA via adenoviral (Lee et al. 2012). In summary it can be said, that there is a central role of glucagon in the pathogenesis of diabetes.

Glucagon and GCGR agonists have been proposed as potential treatment agents for obesity and subsequently treat T2D through weight loss, since glucagon has been reported to reduced appetite, increase energy expenditure, and hence cause weight loss (Schulman et al. 1957; Dicker et al. 1998; Tan et al. 2013; Cegla et al. 2014; Salem et al. 2016). In order to use glucagon as a treatment for obesity without disrupting any hyperglycaemic effects, it had to be administered with another hormone such as glucagon like peptide-1 (GLP-1), which is an incretin hormone and releases insulin and thereby inhibits the gluconeogenic function of glucagon. Glucagon/GLP-1 co-agonism have been shown to lead to promising results in

improving different features of the metabolic syndrome (Day et al. 2009; Axelsen et al. 2012; Clemmensen et al. 2014; Cegla et al. 2014; Jin and Weng 2016; Seghieri et al. 2018). Glucagon antagonism had been another approach in many recent studies in various animals and in humans (Liang et al. 2004; Lau et al. 2007; Yan et al. 2009; Gu et al. 2009; Mu et al. 2012; Kim et al. 2012b; Franklin et al. 2014; van Dongen et al. 2015; Kelly et al. 2015; Okamoto et al. 2015; Kazda et al. 2016; Vajda et al. 2017; Kostic et al. 2018). However, inhibition of the GCGR led to many side effects (Guan et al. 2015; Pearson et al. 2016; Bergman et al. 2017). Despite promising experimental results, neither of these approaches, either glucagon agonism or antagonism, is at present used in clinical practice.

1.2.2 Gut microbiota-dependent endotoxin release

Dysfunctions in the gut-liver-axis (GLA), like intestinal dysbiosis, bacterial overgrowth, and alteration of mucosa permeability, had been linked to NAFLD in the recent years. It has been reported that NASH patients exhibit a higher prevalence of small intestinal bacterial overgrowth and elevated serum levels of TNFα. Moreover, an increasing leakage of the gut has been observed in NASH patients (Seo et al. 2013; Shen et al. 2014). Thus, combining bacterial overgrowth with an elevated permeability of the gut might increase the exposure of the liver to gut-derived endotoxins, consisting of lipopolysaccharides (LPS). Data showing increased serum concentrations of endotoxins in NAFLD compared to controls, support this hypothesis (Harte et al. 2010; Fukunishi et al. 2014). Increased plasma levels of endotoxins could also be measured in mouse models of NAFLD, including mice on high fat diet and genetically obese leptin deficient mice. When LPS is linked to the co-receptor CD14, it can bind to the Toll like receptor 4 (TLR4) leading to the activation of various pro-inflammatory pathways which have demonstrated effects on insulin resistance, obesity, hepatic fat accumulation and NASH development and progression (Kim et al. 2012a; Yang et al. 2014; Nyati et al. 2017).

1.2.3 Pro- and anti-inflammatory signalling in NAFLD

Lipotoxicity and insulin resistance in combination with other factors, like gut-derived endotoxins activate the release of pro-inflammatory cytokines systemically and locally in the liver. There are two main mechanisms which are involved in NAFLD inflammation and progression: c-Jun-N-terminal-kinase (c-JNK) – AP-1 and the IκBα-kinase-complexes-nuclear factor jB kinase-b (IKK-NF-κB) (Hotamisligil 2006; Wullaert et al. 2007; Czaja 2010). The importance of cytokines in the progression of NAFL to NASH is supported by studies in animal models which show that the exposure to elevated pro-inflammatory cytokines lead to histological changes which mimic NASH features (Tomita 2006). Moreover, NASH patients have been shown to display increased serum and hepatic levels of TNF-α which correlate with the severity of liver damage (Crespo 2001). Since inflammation and NF-κB activation are able to drive carcinogenesis, the chronic inflammatory state of NAFLD might contribute to the HCC progression (Pikarsky et al. 2004).

Adipose tissue releases anti-inflammatory adipokines, like adiponectin and leptin (Stojsavljević et al. 2014) and contributes to the maintenance of low inflammatory states. Leptin prevents hepatic lipid accumulation by supressing SREBP-1 expression and increases in obese individuals due to a leptin resistance and becomes fibrogenic (Kakuma et al. 2000; Ikejima 2001; Tsochatzis et al. 2008). The anti-inflammatory effects of adiponectin are achieved by the inhibition of NF-κB activation, the secretion of anti-inflammatory cytokines and inhibition of pro-inflammatory cytokines like TNF-α synthesis and IL-6 (Tilg and Hotamisligil 2006; Tilg and Moschen 2006). Mice lacking adiponectin exhibit severe liver fibrosis showing the anti-fibrotic effect of adiponectin (Xu et al. 2003; Kamada et al. 2003; Adachi and Brenner 2008). In patients with obesity the serum levels of adiponectin were found to be distinctly decreased, while they increase again upon weight loss, accompanied with decreasing levels of IL-6 (Arita et al. 1999; Bruun et al. 2003). All in all, decreased levels of adiponectin and increased leptin concentrations are associated with hepatic steatosis and NAFLD progression (Tsochatzis et al. 2006).

1.2.4 Mitochondrial malfunctioning in NAFLD

The influence of mitochondria on the pathogenesis of NAFLD are reported to be caused by structural and functional alterations in the mitochondria (Pessayre and Fromenty 2005). Mitochondrial dysfunction correlates with insulin resistance, obesity and TNF-α levels (Paradies 2014). Moreover, reactive oxygen species (ROS) and oxidized low-density lipoproteins (LDL) might lead to the activation of Kupffer cells and hepatic stellate cells causing inflammation and fibrosis (Cusi 2009). Additionally, the accumulation of free cholesterol within hepatic mitochondria might lead to the depletion of mitochondrial glutathione, and thus to an increased susceptibility of hepatocytes towards TNF signalling in steatohepatitis (Marí et al. 2006). All in all, mitochondrial malfunctioning is associated to NAFLD, however it remains unclear whether this is a consequence or a cause for NAFLD progression.

1.2.5 The influence of ER stress on NAFLD progression

Endoplasmic reticulum (ER) dysfunctions, such as an increased protein synthesis or lack of ATP, might results in the increase of unfolded proteins within the ER, and hence to the activation of the unfolded protein response' (UPR) (Wang and Kaufman 2014). ER stress and the UPR has been linked to NAFLD since several studies reported an activation of the UPR during NAFLD. Factors that induce UPR in NAFLD include hyperglycaemia, mitochondrial injury, hypercholesterolemia, depletion of phosphatidylcholine and oxidative stress (Seki et al. 2005). Moreover, UPR leads to the activation of JNK, which stimulates inflammation and apoptosis and has been reported to be associated with NASH (Hotamisligil 2006; Czaja 2010). Silencing of JNK was shown to decrease steatosis and steatohepatitis (Schattenberg et al. 2006). Additionally, UPR is also able to activate the SREBP-1c pathway leading to the preservation of hepatic lipid accumulation and further stimulation of ER stress and UPR (Kapoor and Sanyal 2009). One of the main regulators of UPR is the x-box binding protein-1 (XBP-1). Its nuclear translocation is stimulated by insulin thought the PI3K insulin signalling pathway (Park et al. 2010). The interaction of PI3K and XBP-1 can affect and is influenced by

the cellular response to ER stress (Winnay et al. 2010). Therefore, XBP-1 has been suggested to be connect steatosis, insulin resistance and inflammation (Tilg and Moschen 2010).

1.2.6 Genetic and epigenetic factors

A certain genetic background has been shown to predispose an individual for the development of a fatty liver (Vernon et al. 2011). Genetic factors, especially in the form of single nucleotide polymorphisms, have been shown to also impact the development of NAFLD by influencing hepatic FFA flux, oxidative stress, and the response to endotoxins and cytokine production and active (Browning et al. 2004; Anstee et al. 2011; Loomba and Sanyal 2013).

Epigenetic modifications are stable modifications at transcriptional level, such as DNA methylation, histone modifications and changes in the activity of microRNAs (miRNAs). Those modifications do not alter the basic DNA sequences and contribute to the cell homeostasis (Tollefsbol 2011; Zeybel et al. 2013). In literature is has been hypothesized that the disruption of this balance might lead to an increased susceptibility for NAFLD (Podrini et al. 2013; Lee et al. 2014, 2017; de Mello et al. 2017). In a mouse models with diet-induced NASH, an association between epigenetic alterations and the development of NASH has been observed (Pogribny et al. 2009). Especially DNA methylation, which is mostly influenced by dietary deficiency of methyl donors, is considered to be an important determinant in the progression of simple steatosis to NASH (Jaenisch and Bird 2003). DNA methylation occurs at the C5 position of cytosine residues next to guanine (CpG sites) and is catalysed by DNA methyltransferases (DNMTs) (Tollefsbol 2011). When the regulatory region of a gene is hypermethylated, its expression is silenced or impaired (Cedar 1988). Liver biopsy samples from NAFLD patients, collected before and after weight loss due to bariatric surgery, show that NAFLD-related DNA methylations are partially reversible (Ahrens et al. 2013). Further, an imbalance between histone acetylation and deacetylation is reported to be an underlying cause for the progression of NAFLD to hepatocellular cancer (Tian et al. 2013). Additionally, atypical miRNA profiles are found in NAFLD and specific miRNAs have been shown to be involved in the progression from steatosis to more severe forms of NAFLD (Cheung et al. 2008; Li 2012; Panera 2014; Moylan et al. 2014).

1.3 Extrahepatic consequences of NAFLD

1.3.1 Association of cardiovascular diseases with NAFLD

NAFLD is associated with obesity, insulin resistance and further features of the metabolic syndrome (Kim and Younossi 2008; Wainwright and Byrne 2016), which are also risk factors for the development of cardiovascular disease (Misra et al. 2009; Targher et al. 2010). Moreover, an increased prevalence of coronary, cerebrovascular and peripheral vascular disease has been reported in T2D patients with NAFLD compared to diabetic patients without NAFLD, suggesting NAFLD to be an independent risk factor of cardiovascular disease (Targher et al. 2007, 2010) A recent study reported that NAFLD independently elevated the risk for coronary artery disease (Arslan et al. 2007). Furthermore, children with NAFLD displayed a significant increase in carotid artery thickness compared to lean patients (Pacifico et al. 2008).

A further study suggested premature atherosclerosis in patients with NAFLD (Volzke et al. 2005). Additionally, cardiovascular disease is one of the most important causes of morbidity and mortality in patients with NAFLD (Matteoni et al. 1999; Adams et al. 2005; Ekstedt et al. 2006).

1.3.2 Formation of kidney stones is connected to NAFLD

A distinct association between the NAFLD severity and an increased risk of chronic kidney disease has been reported (Musso et al. 2014). The development of kidney stones has also been linked to individual traits of the metabolic syndrome as well as to the metabolic syndrome itself. For example, visceral obesity is strongly associated to an increased risk of kidney stone formation (Akarken and Zorlu 2015). The combination of hypertension and an elevated body mass index (BMI) is related to an enhanced probability of calcium oxalate stones and increased urinary oxalate and uric acid levels (Taylor 2005; Negri et al. 2008; Polat et al. 2015; Shavit et al. 2015). On the other hand, a study from Torricelli and colleagues reported that the connection of dyslipidaemia to the risk kidney stone formation is not depending on obesity or other features of the metabolic syndromes (Torricelli et al. 2014). Moreover, it has been shown that overweight and obese men are more likely to develop calcium oxalate stones compared to overweight and obese women (Siener et al. 2004). Patients with metabolic syndrome mostly develop calcium oxalate stones, which are in the most abundant form of kidney stones in general (Kadlec et al. 2012). Furthermore, the frequency of kidney stones in NAFLD patients was 19% higher compared to individuals without NAFLD, suggesting NAFLD to be a risk factor for renal stone formation (Einollahi et al. 2013; Nam et al. 2016). Also, the severity of T2D has been reported to be an important risk factor for the development of kidney stone disease.

All in all, the metabolic syndrome leads to an increased risk for the development of kidney stones, and the more traits of the syndrome are present in a patient, the greater the probability (Ramaswamy and Shah 2014). However, there is no molecular link reported that could explain the increased prevalence of kidney stone disease with regard to metabolic syndrome and NAFLD.

1.4 Calcium oxalate deposits in kidneys

Calcium oxalate stones are the most frequent kidney stones followed by calcium phosphate deposits (Coe 2005). In the USA the prevalence of kidney stones is approximately 10.1%. The highest prevalence was observed in males older than 60 years, at 17.8% followed by males 40-59 years old at 12.6%. The trend changes in the 20-39-year-old age group, where females displayed a higher prevalence compared to males (7.5% vs. 4.5%). Female patients over 60 years showed a prevalence of 9.8%. Comparison of data from 2007 and 2013 show that young females (20-39 years) showed a significant increase in the prevalence of kidney stones (3.9% to 7.5%). The data for males and older females has remained stable (Chen et al. 2019).

Various mechanisms might be of importance in the process of calcium kidney stones development. Nevertheless, high urinary concentrations of calcium and/or oxalate are crucial factors underlying the kidney stone formation (Evan 2010). The amount of oxalate excreted in one day ranges from 30 to 44 mg/day, while men excrete slightly higher amounts. Hyperoxaluria is present, when the urinary oxalate levels equal or are above 45 mg/day (500 µmol/day) (Curhan et al. 2001). When normalized to the body surface area, normal oxalate excretion should be below 450 µmol/1.73 m^2 per day while hyperoxaluria is diagnosed with values over 500 µmol/1.73 m^2 per day (Salido et al. 2012). The supersaturation of salts, which is present when the salt concentration of a solution transcends a certain threshold so that the salt precipitates, is the first and basic step in the development of kidney stones. This condition can occur due to low urine volume or excessive excretion of oxalate, calcium or both (Evan 2010). The concentrations of calcium and oxalate vary within the nephron, which is the functional subunit of the kidney, because of the water reabsorption. Within the nephron, the concentrations of calcium and oxalate reach their peak in the descending limb of the loop of Henle where calcium oxalate crystal start to develop. Further, this can be observed in the collection duct of the kidney because of the final water adjustment in the urine (Robertson 2004). A schematic illustration of a nephron is depicted below (Figure 1.5). To sum up, metabolites which are released by the liver are able to affect the physiology of the kidney.

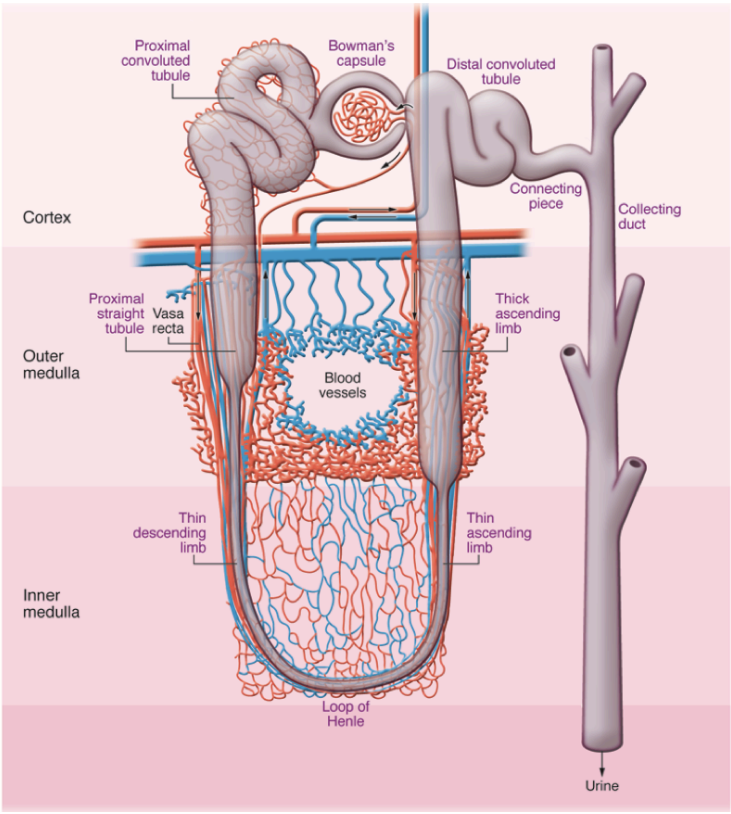

Figure 1.3: Schematic illustration of the anatomy of a nephron (Bonventre et al. 2011). This scheme depicts the anatomy of a nephron with region identified in the figure. Outer medulla vasculature is shown with capillaries in red and venous system in blue.

1.5 Hepatic formation of oxalate

Oxalate is a metabolic end product in mammals and is excreted *via* kidneys into the urine. The diet is an important exogenous source of oxalate; especially spinach, rhubarb, tea, strawberries, beets, nuts, wheat bran, chocolate, sorrel, sesame, carambola and coffee exhibit high oxalate concentrations (Duncan et al. 2002; Siener et al. 2006). Endogenous oxalate is produced by erythrocytes and the liver, while the majority of endogenous oxalate production takes place in the liver (Holmes and Assimos 1998; Holmes et al. 2001, 2016; Baker et al. 2004; Behnam et al. 2006). Ascorbic acid, metabolism of amino acids and the immediate precursors of oxalate within the liver, such as glycolate and glyoxylate, are the main endogenous oxalate sources (Gambardella 1977; Chai et al. 2004; Massey et al. 2005; Knight et al. 2006; Fargue et al. 2016). Hydroxyproline derives from collagen-containing foods, such as gelatine and meat-rich as wells as from the endogenous tissue-collagen turnover which is the primary endogenous source of hydroxyproline, because it is not reused for collagen synthesis, but newly produced by posttranslational modification of proline during its biosynthesis (Adams and Frank 1980; Phang et al. 2001; Salido et al. 2012). The daily release of hydroxyproline upon collagen turnover is estimated to be 240 – 420 mg, which in turn leads to the generation of 140 – 240 mg glyoxylate per day (Knight et al. 2006). The main source for glycolate are vegetables and fruits (Harris and Richardson 1980). Further, glyoxylate is generated mainly by intermediary metabolism within the liver, with glycine, hydroxyproline and glycolate being the best-known sources in human (Salido et al. 2012). The endogenous glyoxylate formation is located within peroxisomes and mitochondria of hepatocytes and the oxidation of glyoxylate is primary catalysed by lactate dehydrogenase (LDH), which is localised in the cytosol of hepatocytes (Salido et al. 2012). In peroxisomes, the D-amino acid oxidase catalyses the generation of glyoxylate from glycine and the hydroxyacid oxidase 1 (HAO1) converts glycolate into glyoxylate (Salido et al. 2012). However, the peroxisomes can also import glyoxylate from the cytosol and mitochondria since its membrane is permeable to small mono- and divalent anions due to the channel-forming protein PXMP2 (Rokka et al. 2009). In mitochondria, glyoxylate is an intermediate metabolite of the hydroxyproline catabolism (Adams and Frank 1980).

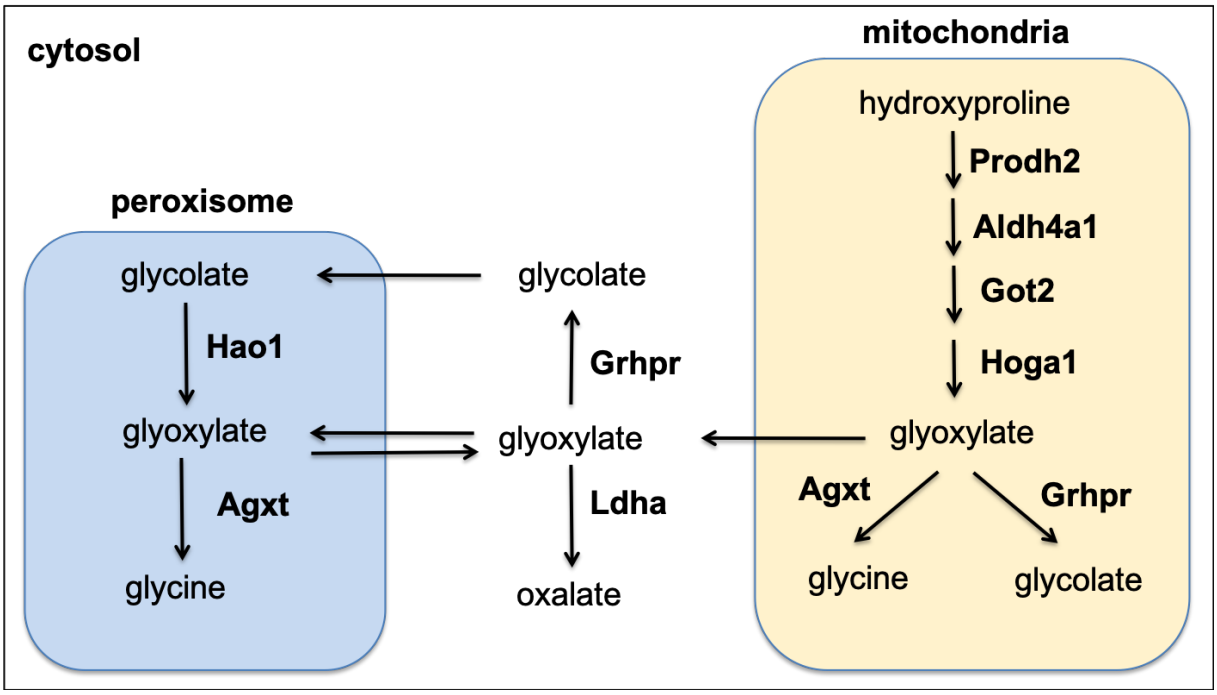

Figure 1.4: Simplified depiction of the glyoxylate metabolism in mouse hepatocytes. The figure does not cover the entire glyoxylate metabolism. Prodh2 = proline dehydrogenase 2; Aldh4a1 = aldehyde dehydrogenase 4 family member a1; Got2 = glutamic-oxaloacetic transaminase).

Because of its toxicity, glyoxylate needs to be converted to a non-toxic compound. The detoxification of peroxisomal and mitochondrial glyoxylate is catalysed by the alanine-glyoxylate-aminotransferase (Agxt) in mice, since murine Agxt is located in both peroxisomes and mitochondria (Cellini et al. 2007). In contrast, human AGXT is localised only within peroxisomes (Noguchi and Takada 1978). Besides AGXT, the cytosolic and mitochondrial glyoxylate reductase/hydroxypyruvate reductase (GRHPR) is able to detoxify glyoxylate to glycolate in order to limit a glyoxylate and/or oxalate accumulation (Salido et al. 2012). Glyoxylate detoxification and avoidance of excessive oxalate production is important since the dysfunction of this process can lead to diseases like primary hyperoxalurias.

1.6 Dysfunctions in hepatic glyoxylate metabolism lead to primary hyperoxalurias

Primary hyperoxalurias (PHs) are hereditary disorders based on a malfunctioning glyoxylate metabolism resulting in an elevated hepatic oxalate production. The high amounts of oxalate are transferred to the kidneys and lead to frequent urolithiasis and nephrocalcinosis, and hence leading to kidney injuries, which can lead to more severe diseases like end stage renal disorder (ESKD) (Hoppe et al. 2009). The prevalence of PH is 1 to 3 persons per million with an incidence rate of 1 per 100,000 live birth each year in Europe, but the estimated number of cases might be higher because of under diagnosis (Cochat et al. 1995; Kopp and Leumann 1995; van Woerden 2003). With approximately 80% of all primary hyperoxaluria cases out of the three different types of PH, PH1 is the most prevalent, representing; 20% are diagnosed with either PH type 2 (PH2) or PH type 3 (PH3) (Salido et al. 2012). Mutations int the *AGXT* gene are responsible for PH1 due to an inefficient and/or defective detoxification of glyoxylate

by the AGXT enzyme which is described further in the Chapter 1.7. PH2 is caused by various mutations in the *GRHPR* gene, encoding the enzyme GRHPR (Cramer et al. 1999). The missing or inefficient GRHPR enzyme results in an accumulation of glyoxylate and hydroxypyruvate in the cytosol, which in turn leads increased hepatic oxalate levels (Hoppe et al. 2009). Recurrent nephrolithiasis and less frequently nephrocalcinosis are the consequences. In contrast to PH1, PH2 rarely progresses to ESRD (Milliner et al. 2001; Hoppe et al. 2009; Salido et al. 2012). PH3 develops due to mutations in the *HOGA1* gene, which encodes the mitochondrial enzyme 4-hydroxy-2-oxoglutarate (HOGA1). The cleavage of 4-hydroxy-2oxoglutarate into glyoxylate and pyruvate is catalysed by HOGA1 and represents the last step of the hydroxyproline breakdown in the mitochondria (Adams and Frank 1980; Belostotsky et al. 2010). The absence of HOGA1 leads to the conversion of 4-hydroxy-2-oxoglutarate into glyoxylate *via* cytosolic aldolases (Monico et al. 2011). Up to date, there is no evidence of ESRD resulting from PH3, however PH3 seems to be more frequent than PH2 (Salido et al. 2012).

In addition to primary hyperoxaluria, secondary hyperoxaluria, which does not arise from genetic mutations, has been reported. The high oxalate concentrations in secondary hyperoxaluria might be consequence of increased intake of oxalate enriched diet or an abuse of oxalate precursors such as vitamin C or ethylene glycol. Moreover, intestinal malabsorption due to chronic diseases like inflammatory bowel disease or cystic fibrosis might lead to secondary hyperoxaluria as well as elevated gut bacteria production and further unknown reasons (Hoppe 2003; Lorenzo et al. 2014). As mentioned before, there is no molecular mechanism known so for, which could explain the strong associated between the formation of calcium oxalate kidney stones and NAFLD (Chapter 1.3.2). Furthermore, there is little information about hyperoxaluria and NAFLD which will be analysed in this work. Therefore, in this thesis it will be investigated whether NAFLD causes hyperoxaluria.

1.7 Alanine-glyoxylate-/ Serine-pyruvate aminotransferase

The alanine-glyoxylate-/-serine-pyruvate aminotransferase 1 (AGXT1 or SPT1; EC2.6.1.44 or EC 2.6.1.51) is encoded by the *AGXT1* gene and catalyses the conversion of glyoxylate and alanine to glycine and pyruvate and of serine and pyruvate and to hydroxypyruvate and alanine.

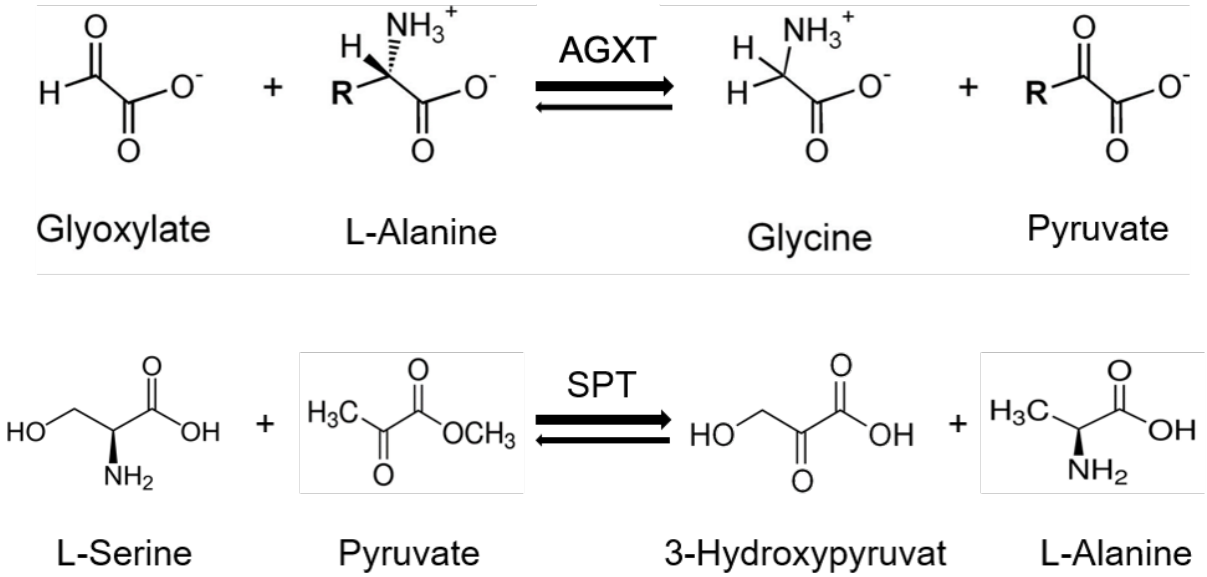

Figure 1.5: Enzymatic reactions catalysed by AGXT/SPT. Glyoxylate and pyruvate receive an amino group from alanine or serine, respectively. (Modified, (Donini et al. 2009)

Agxt, which was first found in rat liver by Noguchi and colleagues in 1978 l (Noguchi et al. 1978). The subcellular localisation of AGXT1 is dependent on the species, the species' diet and the major site of glyoxylate production (Takada and Noguchi 1982; Birdsey et al. 2004). The dietary precursor of glyoxylate in herbivores is glycolate, which is converted to glyoxylate in the peroxisome. Hence, AGXT1 is located in the peroxisomes in herbivores. In carnivores, AGXT1 is localised in mitochondria, since the major glyoxylate precursor in carnivores is hydroxyproline, which is metabolized in mitochondria. Further, in omnivores AGXT1 can be found in both, peroxisomes and mitochondria. In most humans, AGXT1 is primarily in the peroxisomes if not mistargeted to the mitochondria by mutations. This variable subcellular localization pattern is caused by species-specific N-terminal mitochondrial and C-terminal peroxisomal targeting sequences (Oda et al. 1990; Danpure 1997; Birdsey et al. 2004).

1.7.1 Subcellular targeting of AGXT

The coding sequence of the human *AGXT* gene contains eleven exons which are distributed over 10 kB on chromosome 2q36-37 (Purdue et al. 1991b). The gene encoding the AGXT enzyme, which is a homodimeric enzyme consisting of two units with 392 amino acid residues, occurs as two polymorphic variants termed the "major" and "minor" alleles. Each monomer binds its cofactor pyridoxyl-5'-phosphate (PLP) with a Schiff base (Zhang et al. 2003). In the human organism, the C-terminal of PLP contains a KKL type 1 peroxisomal targeting sequence type 1 (PTS1) for the import of AGXT into the peroxisomes *via* the PTS1 receptor Pex5p (Motley et al. 1995b). Although human AGXT is predominantly located in peroxisomes, 15-20% of the *AGXT* alleles encode a cryptic N-terminal mitochondrial targeting sequence (MTS) (Purdue et al. 1990, 1991a). This polypeptide is encoded by the "minor allele" and differs from the more common "major" allele by the presence of a $Pro_{11}Leu$ amino acid replacement which creates a motif for binding to the mitochondrial import receptor TOM20 (Purdue et al. 1990; Abe et al. 2000; Obita et al. 2003; Danpure 2006a). However, a $Pro_{11}Leu$-generated MTS is

functionally ineffective, and hence results in the import of only 5% of AGXT encoded by the minor allele into the mitochondria (Purdue et al. 1990). In patients with PH1, the interactions of disease-specific mutations in the *AGXT* gene with the characteristics of the $Pro_{11}Leu$ replacement increase the efficiency of the $Pro_{11}Leu$ generated MTS, resulting in the majority (up to 90%) of the enzyme being targeted to the mitochondria. (Danpure et al. 1989; Purdue et al. 1990, 1991a; Motley et al. 1995a; Leiper et al. 1996; Fargue et al. 2013).

The mouse Agxt gene contains eleven exons, spans 11 kB and is located to in the central portion of mouse chromosome 1. The full-length mouse Agxt cDNA is 1545 bp long and encodes a 392 amino acid protein with a molecular weight of 43.6 kDA. In mice, Agxt is localised in mitochondria and peroxisomes due to two alternative transcription initiation sites of the mouse *Agxt* gene resulting in two different *Agxt* transcripts with and without a MTS (Li et al. 1999). A high level of conservation has been found between the mouse and human *AGXT* both at cDNA and amino acid level (75% and 76% identity, respectively). However, there a sequence divergence between the two genes at their promoter regions (Purdue et al. 1991a; Li et al. 1999).

1.7.2 Regulation of AGXT

Despite the well-characterised *AGXT* gene, little is known about the regulation of *AGXT* expression. The presence of numerous transcription factor binding sites within the human AGXT promoter have been reported. For example, binding sites for the ubiquitous transcription factor SP1, the hepatic nuclear factor H-APF-1 and nuclear transcription factor y (NF-Y), NF-κB, as well as binding sites for two TGGCA-binding protein and two lipopolysaccharide-binding protein (LBP-1). Furthermore, the human *AGXT* gene also contains five interferon gamma response elements (γ-IRE) (Yang et al. 1990; Sato 2002).

It has been reported that the cAMP responsive element (CRE) and the negative glucocorticoid responsive element (GRE(-)) are located within the rat *Agxt* gene (Oda et al. 1993). Moreover, the mouse *Agxt* has also been shown to contain a CRE sequence (Li et al. 1999). Glucagon treatment has been reported to enhance *Agxt* mRNA transcription and enzyme activity in mice and in rat (Oda et al. 1993; Li et al. 1999). Importantly, due to the two alternative transcription initiation sites in mouse *Agxt*, glucagon treatment only increases the mitochondrial *Agxt* transcript. Furthermore, glutamine and insulin seem to regulate *Agxt* expression in mice and in rat, respectively (Miyajima et al. 1989; Ferrara et al. 2008).. Further research is needed in order to understand the regulatory machinery of the *AGXT* gene.

1.7.3 The role of AGXT in gluconeogenesis

As mentioned in the previous chapter, AGXT is not only able to detoxify glyoxylate in the hepatic peroxisomes, but also catalyses the conversion of serine to hydroxypyruvate. Serine is known to be physiological relevant as a substrate for hepatic gluconeogenesis, in addition to its function as a donor of one-carbon unit (Remesy et al. 1983). It is postulated that

hydroxypyruvate could be metabolized to glucose in several steps, as depicted below (Fig. 1.5).

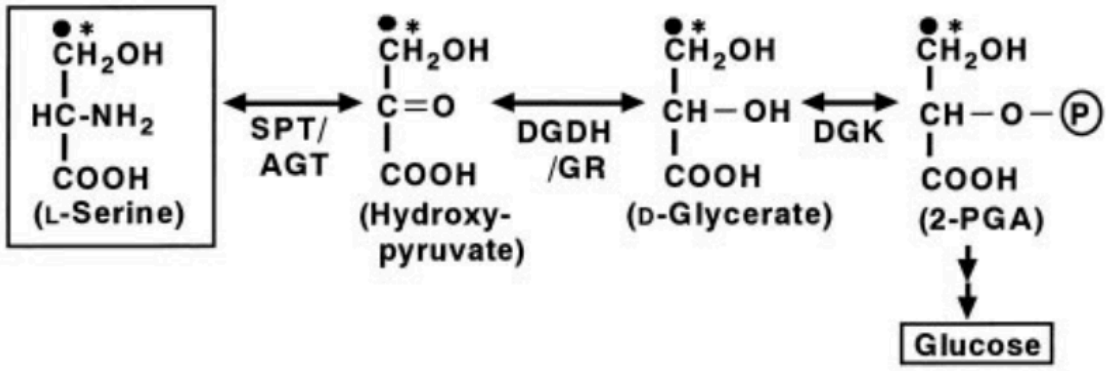

Figure 1.6: The involvement of Agxt in the production of glucose (Xue et al. 1999). 2-PGA = 2-phosphoglycerate; DGDH/GR = D-glycerate dehydrogenase/glyoxylate reductase; DGK = D-glycerate kinase In support of a potential role of Agxt in gluconeogenesis, Roswell and colleagues first reported in 1969, that the activity of Agxt in rat liver is enhanced upon glucagon treatment (Rowsell et al. 1969). The stimulation of Agxt activity by glucagon was shown to be mediated by cyclic adenosine monophosphate (cAMP), since the treatment of rats with glucagon and cAMP equally increased the activity of Agxt (Tsubaki and Hiraiwa 1971). The increased Agxt activity upon glucagon treatment was reported to occur mainly in the mitochondrial matrix of parenchymal cells. Further, it was suggested that the increased enzyme activity was accompanied by a parallel accumulation of the enzyme due to the rise of the enzyme synthesis rate (Fukushima et al. 1978). Studies in primary rat hepatocytes reported an increased mRNA expression of mitochondrial *Agxt* upon glucagon stimulation in a dose- and time dependent manner (Miyajima et al. 1989). Furthermore, it was shown that an activation of transcription underlies the increased mRNA expression. Surprisingly, it has been reported that also insulin elevates the activity of Agxt in rat liver and that the simultaneous treatment with both insulin and glucagon has an additive effect (Miyajima et al. 1989). Since the glucagon-induced increase of mitochondrial *Agxt* mRNA could be suppressed by inhibiting protein kinase A (PKA), and the effect of glucagon could be mimicked by 8-bromo-cAMP, it has been suggested that the pathway is dependent on cAMP-PKA system (Uchida et al. 1994). The identification of a cAMP responsive element (CRE) sequence in the 5'-upstream region of the rat *Agxt* gene by Oda and colleagues in 1993 suggested that the glucagon-induced *Agxt* mRNA expression is accomplished by the hepatic glucagon-cAMP-PKA-pCREB signalling pathway (Oda et al. 1993).

Importantly, the transcript for mitochondrial Agxt of the mouse liver has been shown to increase upon glucagon treatment due to the CRE sequence in the mouse *Agxt* gene (Li et al. 1999a). In our previous study, we found that the *AGXT* promoter is hypermethylated in steatotic *ob/ob* hepatocytes compared to their lean counterparts. Interestingly, one methylated cytosine is located within the CRE sequence, a half site 5'TGACG-3' (Gianmoena

et al.). Whether this affects the induction of Agxt in response to glucagon will be investigated in this thesis.

1.8 NAFLD mouse models

Since the pathogenesis of NAFLD and NASH is complex and not completely understood, animal models exhibiting different histological and pathophysiological stages of NAFLD are required to clarify the NAFLD pathogenesis. Due to the strong association of human NAFLD with traits of metabolic syndrome, such as obesity, insulin resistance and T2D, animal models need to mirror these features. Currently, the available models illustrate solely single hallmarks of NAFLD, but not the complete histopathology and physiological characteristics of human NAFLD progression from steatosis to HCC (Lau et al. 2017). The following table presents an overview of relevant NAFLD mouse models, including their ability to recapitulate features of human NAFLD. In the current work, both genetic and diet induced models were used, and therefore a more detailed description is provided below for these specific models.

Table 1-1: Overview of mouse models of NAFLD (Anstee and Goldin 2006; Schattenberg and Galle 2010; Lau et al. 2017)

Model	Obesity	IR	Steatosis	NASH	Fibrosis
Genetic					
ob/ob	✓	✓	✓	no	no
db/db	✓	✓	✓	no	no
KK-Ay	✓	✓	✓	no	no
Diet induced					
High fat diet	✓	✓	✓	✓	?
MCD diet	no	no	✓	✓	✓
High fat and high cholesterol diet	✓	?	✓	✓	✓
Combination					
db/db + MCD diet	✓	✓	✓	✓	✓
ob/ob + LPS	✓	✓	✓	✓	no

1.8.1 Leptin deficient *ob/ob* mouse model

The *ob/ob* mice carry a spontaneous mutation in the leptin gene, which leads to leptin deficiency (Ingalls et al. 1950; Zhang et al. 1994; Friedman et al. 1995). Since leptin controls the appetite, leptin-deficient mice become consequently obese, hyperphagic, hyperinsulinemic and hyperglycaemic (Mayer et al. 1953; Garthwaite et al. 1980). Administration of leptin normalizes their food intake, and hence decreases body weight and body fat (Halaas et al. 1995; Pelleymounter et al. 1995; Larcher et al. 2001). Ob/ob mice

develop steatosis, but there is no progression to NASH under normal conditions since it has been shown that *ob/ob* mice are resistant to fibrosis. However, LPS treatment provokes NASH development in *ob/ob* mice (Yang et al. 1997; Faggioni et al. 1999; Leclercq et al. 2002), suggesting their susceptibility to a "second hit". The *ob/ob* mouse model reflects the human metabolic syndrome and simple steatosis. Although it cannot be utilized to investigate the complete NAFLD spectrum, this model is useful for analysing the effects of lipid accumulation on functionality of hepatocytes as well as the progression from steatosis to steatohepatitis, which can be triggered artificially.

1.8.2 High fat diet induced NAFLD

Mice models with high fat diet (HFD)-induced NAFLD are close to the human disease, because the development of NAFLD is based on the increased dietary intake of fat and carbohydrates that drive hepatic fatty acid uptake or *de novo* synthesis (Anstee and Goldin 2006). The compositions of the different diets vary. The most important feature is that most of the calories come from fat (45 – 75%), which is sufficient to induce obesity, insulin resistance and hepatic steatosis (Schattenberg and Galle 2010). The outcome of the HFD depends on the mouse strain, sex and age. Male C57Bl6 mice on a HFD exhibit hepatocyte ballooning, decreased adiponectin levels and hyperglycaemia after 16 weeks on the diet (Eccleston et al. 2011). Furthermore, feeding male C57Bl6 mice fifty weeks with a HFD leads to steatohepatitis, slight fibrosis and hyperinsulinemia (Ito et al. 2007, p. 20). Hence, the high fat diet induced NAFLD model is a more accurate representation of human NAFLD, while one disadvantage is the long time required to obtain the desired phenotype.

1.9 Downregulation of *AGXT* in human liver disease and mouse models of NAFLD

In previous studies, our group was interested in investigating the impact of hepatic lipid accumulation on global gene expression in mouse and human. Therefore, publicly available hepatic genome-wide expression datasets of human liver tissue from patients with NASH, cirrhosis, and HCC (GSE49541, GSE25097, TCGA, E-MEXP-3291) were analysed and compared to transcriptomics and epigenetic analysis of hepatocytes from leptin deficient *ob/ob* mouse model generated within the DEEP (Deutsches Epigenom Programm) consortium with the contribution of our group.

In order to identify epigenetic alterations in NAFLD that are associated with gene expression changes liver tissue and isolated hepatocytes from control (*ob/+*) and obese (*ob/ob*) mice were analysed with respect to mRNA expression (by RNA-seq) and DNA methylation (by reduced representation bisulfite sequencing, RRBS). The profiles of chromatin accessibility (by DNase I-seq) were also examined in the isolated hepatocytes By assigning differently methylated regions (DMRs) and differentially open regions (DORs) to the closest gene, DNA methylation and chromatin accessibility were combined with gene expression changes. Altogether, 649 differentially expressed genes (DEGs) were associated with DMRs and DORs. By comparing this overlap of 649 DEGs with DMRs and DORs from the *ob/ob* mouse model

with 62 DEGs genes identified in human datasets of liver diseases, 12 genes were found to be deregulated in both, human and mouse NAFLD (Fig 1.7, Gianmoena et al., not published).

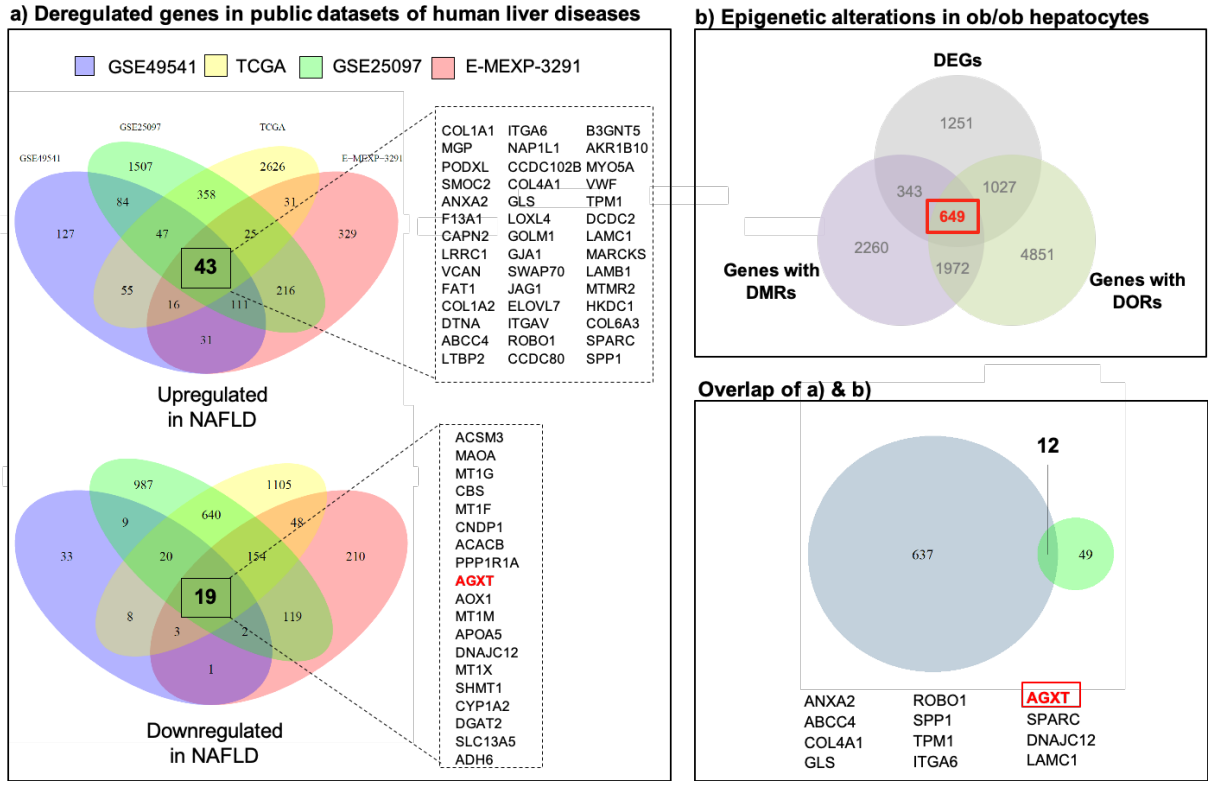

Figure 1.7: Pipeline for the identification of AGXT downregulation in mouse and human NAFLD (Modified after Gianmoena et al., not published). Among these 12 DEGs, the downregulation of the *AGXT* gene in the NAFLD condition of both species caught our interest due to its physiological relevance in PH1. Subsequent research focused on exploring the downregulation of AGXT upon NAFLD for being one possible molecular mechanism explaining the increased risk of kidney stone formation in NAFLD patients (Fig. 1.8; Gianmoena et al., not published).

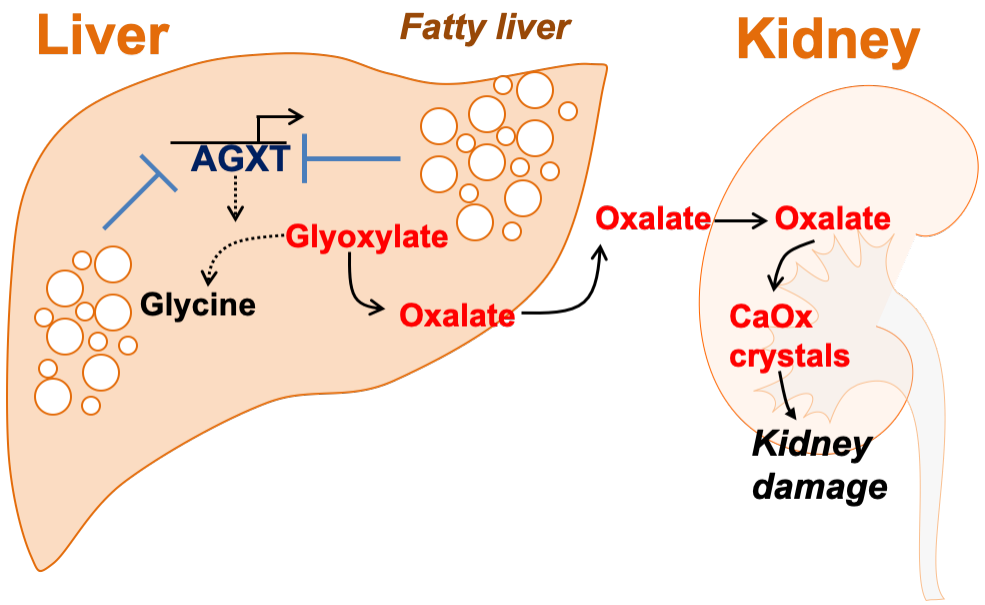

Figure 1.8: Schematic illustration of our hypothesis. The hypothesis, first postulated by Gianmoena in 2017, claims that the hepatic fat accumulation impairs the *Agxt* expression leading to an insufficient conversion of glyoxylate to glycine, which results in the formation of excessive hepatic oxalate. The increased hepatic oxalate production might lead to kidney damage due to oxalate supersaturation and the subsequent formation of calcium oxalate kidney stones. (modified after Gianmoena 2017).

1.9.1 Agxt is downregulated in hepatic steatosis and *ob/ob* mice are hyperoxaluric

The downregulation of AGXT in steatosis was validated in primary human hepatocytes, in a Western diet-induced mouse model of NAFLD, in the *ob/ob* mouse model, and in the in vitro steatosis model of primary mouse hepatocytes, as well as in a hepatic cell line (Gianmoena 2017). Further analysis showed that the downregulation of Agxt in *ob/ob* resulted in elevated urinary oxalate excretion and a reduced hepatic glycine concentration. These results indicated physiological consequence of the repressed Agxt expression due to the lack of glyoxylate detoxification in this mouse model. Furthermore, cultivated *ob/ob* hepatocytes displayed an increased susceptibility towards the glyoxylate precursor hydroxyproline, since they produced more oxalate when treated with hydroxyproline compared to ob/+ hepatocytes (Gianmoena 2017).

1.9.2 The *AGXT* promoter is hypermethylated in mice and human steatosis

DNA methylation analysis revealed a significant hypermethylation of the *AGXT* promoter in steatotic primary human hepatocytes and in primary *ob/ob* hepatocytes, indicating a possible methylation-dependent regulation of *AGXT* expression *in vivo*. The hypermethylation of the AGXT promoter upon fat accumulation could not be observed in the *in vitro* steatosis model, suggesting alternative mechanisms of transcriptional downregulation of *AGXT* (Gianmoena 2017).

1.10 Aim of the work

Previous work at IfADo identified the steatosis-associated downregulation of *AGXT* in mouse and human NAFLD which was correlated with an *AGXT* promoter hypermethylation. It was postulated that this effect might be one possible mechanism explaining the connection between NAFLD and the formation of kidney stones. The remaining questions that should be answered are whether the steatosis-associated downregulation of *AGXT* and deregulated glyoxylate metabolism lead to pathophysiological consequences, such as hyperoxaluria, both in mouse and human NAFLD, and whether the promoter hypermethylation contributes to the downregulation of AGXT expression.

For this purpose, oxalate excretion was studied in i) primary mouse hepatocytes from different mouse models of NAFLD which were exposed to different oxalate precursors, ii) *in vivo* in two different NAFLD mouse models by measuring oxalate in plasma and in the 24 h urine, also under the influence of dietary hydroxyproline and iii) in 24 h urine collected from a cohort of children with biopsy-proven NAFLD.

One major goal of this work was to mechanistically provide evidence for a causal role of Agxt in the increased oxalate generation in NAFLD. By studying *Agxt* knockout mice (*Agxt*$^{-/-}$) it should be proofed that Agxt deficiency results in increased hepatic oxalate production and elevated urinary oxalate excretion. By adeno-associated virus (AAV)-mediated gene transfer it was aimed to show that the steatosis-induced increased hepatic oxalate production can be normalised by rescuing Agxt expression in the hepatocytes of *ob/ob* mice. These interventions should confirm the hypothesis that Agxt downregulation represents one molecular link explaining the increased risk of calcium oxalate kidney stones in NAFLD.

A further goal of this work was to investigate the transcriptional upregulation of *Agxt* in response to glucagon in two different NAFLD mouse models, in an *in vitro* steatosis system as well as in primary human hepatocytes. This is of importance because glucagon-induced upregulation of *Agxt* has been shown to reduce oxalate excretion. Therefore, upregulation of *Agxt* stimulated by glucagon might be one potential treatment to reduced hepatic oxalate production in NAFLD.

2 Materials and methods

2.1 Material

2.1.1 Technical equipment

Table 2-1: Equipment

Equipment	Company
Autocalve Systec VX-150	Systec
Autoclave 5075 ELV	Tuttenauer
Autosampler SIL-20AC xr	Shimadzu
Balance	EW, Kern
Bunsen Burner	IBS Fireboy Plus, Integra Biosciences
Blot imager Vilber Fusion Fx7	Vilber Lourmat
Centrifuge with cooling function	Biofuge Fresco, Heraeus
Centrifuge with cooling function 5424R	Eppendorf
Centrifuge MiniSpin plus	Eppendorf
CO_2 incubator C150 R Hinge	Binder
Electrophoresis unit Mini-PROTEAN®	BioRad
Electrophoresis unit SE260	Höfer
EVOQ™ Elite Triple Quadrupole	Bruker
Fume hood	Waldner
LC system LC-20AD XR	Shimadzu
LC Column: PL Hi-Plex-H (100 × 4 mm)	Agilent
Magnetic stirrer IKAMAG RCT	Ikamag
Microscope BX41	Olympus
Microscope eclipse TS 100	Nikon
Microscope Primo Vert	Zeiss, Software ZEN from Zeiss
Microwave oven	Bosch
MiSeq	Illumina
Modular tissue embedding center	Thermo Fisher Scientific
NanoDrop ND-1000	Thermo Fisher Scientific
pH meter	Schott
Pipettes (10 µL, 2 µL, 100 µL, 200 µL, 1 ml, 5 ml)	Eppendorf

Pipet boy	Integra
Plate reader infinite M200 Pro	Tecan
Power pack HC	BioRad
Power pack P25T	Biometra
Precision balance EW150-3M	Kern
Precision balance ME235P	Sartorius
qPCR system ABI 7500	Applied Biosystems
QTRAP 5500 LC-MS/MS system	Sciex
Rocking platform	VWR
Shaker KS 260 basic	IKA
Slide drying oven TDO Sahara	Medite
Sliding Microtome HM 450	Microm
Sonicator sonoplus mono	Bandelin
Spin tissue Processor STP 120	Thermo Fisher Scientific
Sterile hood	Hereaus
Thermo cycler T gradient	Biometra
Thermomixer	Eppendorf
Thermo shaker PHMT Grant-bio	Keison
Thermo shaker	peqlab
Transfer chamber fast blot B44	Biometra
Transfer chamber Trans-Blot SD	BioRad
Vacuum pump	Vacuubrand
Vortex-Genie2	Bender & Hobein
Water purification	Maxima Ultra-Pure Water, ELGA
Water purification system	Milli- Q® Integral 15 System, Merck
Waterbath	GFL 1083, Gesellschaft für Labortechnik
Waterbath	Precision GP28 Thermo Scientific

2.1.2 Consumables

Table 2-2: Consumables

Consumables	**Company**
Cell scraper (25 mm)	Sarstedt
Cover slips	VWR

Embedding cassettes	Carl Roth
Glass inserts, 200µL	VWR
Glass vials (1.5 ml -4 ml)	VWR
Metabolic cage for single mouse	Tecniplast
MicroAmp® Optical Adhesive Film	Thermo Fisher Scientific
MicroAmp® Optical 96-Well Reaction Plate	Thermo Fisher Scientific
Microscope slide SuperFrost Plus	Thermo Fisher Scientific
Minisart® syringe filters (0.45 µM)	Sartorius
Needle 26G	BD bioscience
NuPAGE®4 – 12% Bis-Tris	Thermo Fisher Scientific
Pestle and Microtube	VWR
Pipettes	Eppendorf
Pipette tips (filtered/not filtered)	Sarstedt
PVDF Membrane	Perkin Elmer
PCR SinglCAP 8er-Softstrips 0.2 mL	Biozym Scientific
RNase-free Microfuge Tubes 1.5 ml	Thermo Fisher Scientific
Reaction tubes (0.5 - 50 ml)	Sarstedt
Serological pipets (5 ml, 10 ml, 25 ml)	Sarstedt
Syringe 1 ml	BD bioscience
Tissue culture plates (6-, 12-, 24, 96-well format)	Sarstedt
96-Well plates black	GreinerBio
96-Well plates transparent	Sarstedt
Whatman-Paper 3mm	VWR
Thick Blot Filter Paper, Precut	Biorad

2.1.3 Chemicals and dyes

Table 2-3: Chemicals and dyes

Chemicals/dyes	Company
Acetic acid	Carl Roth
Amino acids solution	PAN Biotech
Ammonium persulfate	Sigma-Aldrich
Bovine serum albumin (BSA)	Carl Roth

Bovine serum albumin (BSA), fatty acid free	Sigma-Aldrich
Bromphenol blue	Carl Roth
Calcium chloride	Carl Roth
Chloroform	Carl Roth
Citric acid monohydrate	Carl Roth
Collagenase from Clostridium hystolyticum	Sigma-Aldrich
p-Coumaric acid	Sigma-Aldrich
Creatinine hydrochloride	Sigma-Aldrich
Dimethyl sulfoxide (DMSO)	Sigma-Aldrich
Dithiothreitol (DTT)	Sigma-Aldrich
Triethylene glycol diamine tetra acetic acid (EGTA)	Carl Roth
Entellan®	Merck
Eosin Y disodium salt	Sigma-Aldrich
Ethanol, absolute	Carl Roth
Ethylenediaminetetraacetic acid (EDTA)	Carl Roth
Fetal Calf serum (FCS) Sera Plus	Pan-Biotech
FluorPreserve reagent	Calbiochem
Glucagon	Sigma-Aldrich, Cayman Chemicals
Glucose	Carl Roth
L-Glutamine	Sigma-Aldrich
Glycerol	Carl Roth
Glycine	Carl Roth
Glycolic acid (1,2 -13C2, 99%)	Cambridge Isotope Laboratories, Inc.
HEPES	Carl Roth
Hydrochloric acid 32%	Carl Roth
Hydrogen peroxide 30%	Merck
L-Hydroxyproline	ApplChem
Luminol	Sigma-Aldrich
Magnesium chloride	Carl Roth
Magnesium sulphate	Sigma-Aldrich
Methanol, HPLC grade	Carl Roth
Nonidet P-40 substitute (NP-40)	Roche

Oleic acid	Sigma-Aldrich
Oxalic acid (1,2-^{13}C2, 99%)	Cambridge Isotope Laboratories, Inc.
Paraffin Histowax Surgipath paraplast	Leica
Paraformaldehyde 4% (PFA)	Carl Roth
Picric acid	Sigma-Aldrich
Potassium chloride	Carl Roth
Potassium dihydrogen phosphate	Carl Roth
2-Propanol	Carl Roth
Rotihistol®	Carl Roth
SDS pellets	Carl Roth
Sodium chloride	Carl Roth
Sodium deoxycholate	Carl Roth
Sodium glycolate	Thermo Fisher Scientific
Sodium glyoxylate monohydrate	Sigma-Aldrich
Sodium hydrogen phosphate	Carl Roth
Sodium hydroxide pellets	Carl Roth
Tetrahydrofuroic acid (THFA)	Sigma-Aldrich
Tetramethylethylenediamine (TEMED)	Carl Roth
Tris	Carl Roth
Tris-HCl	Carl Roth
TritonX-100	Sigma-Aldrich
Tween20	Sigma-Aldrich
Tween80	Sigma-Aldrich
Xylol	VWR

2.1.4 Commercial buffers and reagents

Table 2-4: Commercial buffers and reagents

Buffer/reagent	Company
Acrylamide (30% (v/v))	Carl Roth
Amino acid solution	PAN-Biotech
Anode-/Cathode-buffer concentrate A & K	Carl Roth
Diethylpyrocarbonate treated (DEPC) water	Thermo Fisher Scientific
Duotrol® urine liquid level1 & 2	Biomed Labordiagnostik GmbH

Ketamine 100 mg/ml	Ratiopharm
Mayer's haemalaun solution	Merck
NuPAGE® MES SDS Running Buffer (20X)	Thermo Fisher Scientific
Phosphatase-Inhibitor-Cocktail II&III	Sigma-Aldrich
Precision Plus Protein Dual Colour standards	BioRad
Protease-Inhibitor-Cocktail	Sigma-Aldrich
QIAzol Lysis-Reagent	Qiagen
Rompun 2%	Bayer Health Care
Taqman Universal PCR Master Mix	Thermo Fisher Scientific

2.1.5 Prepared buffers and reagents

Table 2-5: Prepared buffers and reagents for gel electrophoresis and Western blotting

Buffer	Compounds	Concentration
Anode buffer	Buffer concentrate A	10%
	Methanol	20%
	in ultrapure water	
APS solution	Ammonium persulfate	10% (w/v)
	in ultrapure water	
Blocking solution	BSA in TBS-T	5% (w/v)
Cathode buffer	Buffer concentrate K	10%
	Methanol	20%
	in ultrapure water	
Chemiluminescent solution	Luminol	2.5 mM
	p-Coumaric acid	0.2 mM
	in 0.1 M Tris	
Loading buffer (5x)	Bromophenol blue	0.05% (w/v)
	DTT	0.25 M
	Glycerol	50% (v/v)
	SDS	5% (w/v)
	Tris-HCl	0.225 M
PBS (10x)	KCl	27 mM
	KH_2PO_4	18 mM
	Na_2HPO_4	100 mM

	NaCl	1.37 M
	in ultrapure water,	
RIPA buffer	Tris-HCl	50mM (pH 7.5)
	NaCl	150 mM
	NP-40	1%
	Sodium deoxycholate	0.5%
	SDS	0.5%
Running buffer (10x)	Glycine	1.92 M
	SDS	1% (w/v)
	Tris	0.25 M g
	in ultrapure water, pH 8.3	
SDS solution	SDS	10% (w/v)
	in ultrapure water	
Separation buffer	Tris	3 M
	in ultrapure water,	
	pH adjusted to 8.8	
Stacking buffer	Tris	0.47 M
	in ultrapure water,	
	pH adjusted to 6.8	
Stripping buffer	Glycine	0.2 M
	SDS	0.1% (w/v)
	Tween 20	1% (v/v)
	in ultrapure water,	
	pH adjusted to 2.2	
TBS (10x)	NaCl	1.5 M
	Tris	0.5 M
	in ultrapure water, pH adjusted to 7.4	
TBS-T	10x TBS	10% (v/v)
	Tween20	0.1% (v/v)

Table 2-6: Prepared buffers for IHC

Buffer	**Compounds**	**Concentration**

Citrate buffer	Citrate 1xH_2O	0.01 M
	in ultrapure water, pH adjusted to 6	
Haematoxylin	Mayer's haemalaun	20% (v/v)
	in ultrapure water	

Table 2-7: Prepared buffers for perfusion

Buffer	Compounds	Amount
Collagenase buffer	Amino acid solution	30 ml
	$CaCl_2$ solution (19 g/l $CaCl_2$* 2 H_2O)	10 ml
	Collagenase Type 1	100 mg
	Glucose solution (9 g/l)	155 ml
	Glutamine (7 g/ml)	2.5 ml
	HEPES (60 g/l) (pH 8.5)	25 ml
	KH buffer	25 ml
EGTA buffer	Amino acid solution	60 ml
	EGTA solution (47.5 g/l)	1.6 ml
	Glucose solution (9 g/l)	248 ml
	Glutamine (7 g/l)	4 ml
	HEPES (60 g/l) (pH 8.5)	30 ml
	KH buffer	30 ml
KH buffer	KCl	1.75 g
	KH_2PO_4	1.6 g
	NaCl	60 g
	Filled to 1 l with ultrapure water	
	Adjust pH to 7.4	
Suspension buffer	Albumin Fraction V	400 mg
	Amino acid solution	30 ml
	$CaCl_2$ solution (19 g/l $CaCl_2$* 2 H_2O)	1.6ml
	Glucose solution (9 g/l)	124 ml
	Glutamine (7 g/ml)	2 ml
		20 ml

	HEPES (60 g/l) (pH 7.6)	20 ml
	KH buffer	0.8 ml
	$MgSO_4$ solution (24.6 g/l $MgSO_4$ * 7 H2O)	

Table 2-8: Commercial assays and kits

Kits	Company
BCA Protein assay	Thermo Fisher Scientific
CellTiter-Blue® assay	Promega
DAB Peroxidase substrate kit	Vector Laboratories
High-Capacity cDNA Reverse Transcription Kit	Thermo Fisher Scientific
Triglyceride quantification assay	Abcam
VECTASTAIN Elite ABC Kit (rabbit)	Vector Laboratories

2.1.6 Cell culture reagents

Table 2-9: Medium and additives

Cells/cell lines	Medium	Company
Primary mouse and human hepatocytes	William's E medium	PAN-Biotech
	+ Dexamethasone (100 nM)	Sigma Aldrich
	+ Gentamycin (10 µg/ml)	PAN Biotech
	+ Insulin (ITS) 100x (2 ng/ml)	Sigma Aldrich
	+ Penicillin/Streptomycin (100 U/ml)	PAN-Biotech
	+ Stable L-Glutamine (2 mM)	PAN-Biotech
	(+ Sera Plus 10% for attaching)	PAN-Biotech

Table 2-10: Additional cell culture supplies

Reagents	Company
Acetic acid glacial	Carl Roth
Casyton	Roche
Collagen rat tail lyophilised	Roche
Dexamethasone	Sigma-Aldrich
DMEM10x, 1 g/l glucose	PAN-Biotech
DMSO	Sigma-Aldrich
OptiMEM	Life technologies
10xPBS	See Table 2.5

Trypan blue	Sigma-Aldrich
Trypsin 0.05% EDTA	PAN-Biotech

2.1.7 Laboratory mice

Table 2-11: Mice

Mouse	Gender	Age at arrival	Company/Source
Agxt$^{-/-}$	male & female	5-8 weeks	Prof. Eduardo Salido, Universidad de la laguna, Tenerife
Lep^{ob}/*Lep*^{ob} & *Lep* $^{ob/+}$	male	8 weeks	Janvier labs
Lep^{ob}/*Lep*^{ob}	female	8 weeks	Janvier labs
C57BL6/J	male & female	8 weeks	Janvier labs
C57BL6/N	male	8 weeks	Janvier labs

Table 2-12: Mouse feed

Reagents	Company
Pellet standard diet R/M-H 10-mm	Ssniff
Pellet standard diet R/M-H 10-mm + 1% Hydroxyproline	Ssniff
Powder standard diet R/M-H	Ssniff
Powder standard diet R/M-H + 1% Hydroxyproline	Sniff
Western diet (containing 45% kcal fat, 20% kcal fructose and 2% cholesterol)	Research Diets Inc., Catalogue-number D09100301

2.1.8 Antibodies

2.1.8.1 Primary antibodies

Table 2-13: Primary antibodies for Western blotting and immunohistochemistry

Antibody	Host	Cat#/Company
anti Agxt	Rabbit	HPA035370, Sigma-Aldrich
anti Creb	Rabbit	4820S, Cell Signalling
anti Creb (phosphor S133)	Rabbit	Ab32096, Abcam
anti Hao1	Rabbit	AV42480, Sigma-Aldrich
anti Ldha	Mouse	66287-1-Ig, Proteintech
anti Gapdh	Rabbit	#2118, Cell Signaling

anti β-Actin	Mouse	#A5316, Sigma-Aldrich

2.1.8.2 Secondary antibodies

Table 2-14: Secondary antibodies for Western blotting

Antibody	Host	Cat#/Company
anti-mouse HPR linked	Horse	#7076, Cell Signaling
anti-rabbit HPR linked	Goat	#7074, Cell Signaling

2.1.9 Taqman gene expression assays

Table 2-15: Taqman gene expression assays (Thermo Fisher Scientific)

Target gene	Mouse	Human
Agxt	Mm00507980_m1	Hs00163584_m1
Eif2a	Mm01289723	
Gapdh	4352932E	4352934E
Grhpr	Mm00519119_m1	Hs00201903_m1
Hoga1	Mm00470609_m1	
Hao1	Mm00439249_m1	Hs00213909_m1
Ldha	Mm01612132_g1	
Prodh2	Mm00457662_m1	
UBC		Hs00824723_m1

2.1.10 Adeno-associated viral vectors

Name	Description	Vector ID / Company
pAAV[Exp]-CMV>{mAgxt[NM_016702.3]}:IRES:EGFP	mouse mitochondrial AGXT under the control of CMV promoter	VB191228-2726vjg / Vector builder
pAAV[Exp]-CMV>EGFP	EGFP under the control of CMV promoter	VB150925-10026 / Vector builder

2.2 Methods

2.2.1 Housing conditions of mice

Mice were bought at an age of eight weeks from Janvier Labs and allowed to acclimatise for one week. They had access to water and food *ad libitum* and were kept under a 12 h light –

12 h dark cycle. The performed experiments were approved by the animal welfare authority. Mice were handled according to the Principles of Laboratory Care and recommendations of the Society of Laboratory Animal Science (Gesellschaft für Versuchstierkunde, GV-SOLAS, Germany).

2.2.2 Isolation of primary hepatocytes

2.2.2.1 Hepatocyte isolation

2.2.2.1.1 Mouse hepatocytes

The procedure for isolating primary mouse hepatocytes from a mouse was based on a two-step perfusion (Seglen 1976), by which the whole liver is converted into a suspension of viable hepatocytes. The perfusion was carried out under physiological conditions of the mouse and yielded hepatocytes with a viability above 90%. First, the mouse was narcotised with an intraperitoneal injection of Rompun® (25-40 mg/kg) and ketamine (50-80 mg/kg) and the anaesthesia was controlled by testing the pain sensitivity *via* the pedal reflex. In the next step, the mouse was fixed in a dorsal position on a grid table and the abdominal cavity was opened longitudinally. A blunted needle was inserted into the incised vena cava. This needle was connected to a flexible tube that passed through a pump and ended up in a bottle containing the needed buffer. The liver was first perfused with pre-warmed EGTA buffer at a flow rate of 9 ml/min for 10 to 15 min for removing blood and Ca^{2+} dependent adhesion factors. An instant loss of the livers red-brown colour was the indicator whether the needle was placed correctly. Next, the EGTA buffer was replaced by collagenase buffer (37 °C) to digest the extracellular matrix and to decrease cell to cell contacts with the same flow rate and the perfusion duration. This perfusion step was stopped when the liver became soft and lustrous. The liver was excised carefully and taken out with forceps at the thoracic blood vessels and placed in a petri dish filled with suspension buffer which was transferred into a laminar flow cabinet. Under sterile conditions, the liver capsule was opened, and the liver cells were released into the suspension buffer supported by shaking the capsule gently within the buffer. This cell suspension was filtered through a 100 µm cell strainer and transferred to a 50 ml tube and centrifuged for 5 min at 4 °C and at 50xg to roughly remove non-parenchymal cells (NPC) from hepatocytes. The supernatant, which contained NPCs, was discarded and the hepatocyte pellet was re-suspended in 10 ml suspension buffer by gently inverting the tube several times. The hepatocytes were placed on ice and an aliquot was diluted with the suspension buffer and with trypan blue solution (1:2). The stained cell suspension was pipetted into each chamber of the Neubauer counting chamber and the amount of viable and dead blue stained cells were determined.

2.2.2.1.2 Human hepatocytes

Cryopreserved primary human hepatocytes (PHHs) were purchased from Lonza and BioIVT and stored in the nitrogen tank until usage. Additionally, PHHs isolated by the group of Dr. Georg Damm from the University of Leipzig were used. The cells were isolated from liver tissue samples from patients with a primary or secondary liver tumours. The patients agreed that their cells can be used for research purposes according to the ethical guidelines of the University of Leipzig. Isolation of PHHs was performed via a two-step isolation procedure as

described above or with minor modifications (Lee et al. 2013). The isolated hepatocytes were transported on ice overnight from the clinics to our institute. The cells were re-suspended in William's E medium and counted with the Neubauer counting chamber using trypan blue to calculate the viability. The cells were cultivated in a collagen sandwich on top system as described in Chapter 2.2.2.2.

2.2.2.2 Cultivation of primary mouse and human hepatocytes

Primary hepatocytes were cultured under sterile conditions at 37 °C and 5% CO_2 within aqueous saturated vapour. The cells were plated on a collagen coated well with a thicker layer of collagen on top. For the two different collagen layers, 10 mg rat tail collagen was dissolved in either 40 ml or 9 ml 0.2% acetic acid which generated a 250 µg/ml and 1.1 mg/ml collagen solution, respectively. The dissolving process took place at 4 °C overnight. On the next day, cell culture plates were rinsed with 250 µg/ml collagen solution and left to dry for several hours or overnight inside the laminar flow. In order to increase the pH value of the monolayer, the coated plates were washed two times with William's E Medium without additives. In the next step, the wells were filled with William's E medium containing all additives and 10% sera plus and the appropriate number of freshly isolated hepatocytes was added (Table 2.19). To ensure an even distribution of the cells, the plate was gently shaken. The cells were incubated for 3 h at 37 °C for attaching to the collagen monolayer. Afterwards, the hepatocytes were washed with pre-warmed William's E medium to remove dead and non-attached cells. The second collagen layer was prepared on ice by mixing one part of 10x DMEM and nine parts of 1.1 mg/ml collagen solution for a concentration of 1 mg/ml collagen. The pH value of the DMEM-collagen solution was neutralised by carefully adding 1 M of NaOH until the solution's colour changed from yellow to pink. Next, the adequate volume of the second layer collagen solution was added to the wells and the plate was again put into the incubator for 45 min so that the collagen could polymerize. In the last step, William's E medium with additives (full media) was added. When the cells were challenged with glucagon, insulin was not added to the medium.

Table 2-16: Overview of different plate systems

Plate	Cell number	1 mg/ml collagen	William's E medium &additives
6-well plate	850000 cells/well	350 µl	2 ml
12-well plate	400000 cells/well	200 µl	1 ml
24-well plate	200000 cells/well	100 µl	0.5 ml

2.2.2.3 Cultivation of human hepatocytes from Lonza and Bio IVT

The PHHs were taken out of the nitrogen tank and defrosted carefully. Next, the hepatocytes were re-suspended in William'E cultivation medium containing 10% Sera Plus. After counting the PHHs with the Neubauer counting chamber and determining their viability with trypan blue, the cells were plated according to Table 2-16. The cells were cultivated in a collagen sandwich on top system. The plating procedure is the same as described in Chapter 2.2.2.2.

2.2.3 Collection of organs, tissue and blood from mice

Livers and kidneys were collected from mice to conduct RNA, protein and triglyceride analysis and histological staining in order to detect differences between the control and NAFLD mice. The animals were anaesthetized with an intraperitoneal injection of Rompun® (25-40 mg/kg) and ketamine (50-80 mg/kg), while the obese mice required a higher dose compared to the lean mice. Once the mice were fully narcotized, they were fixed in a dorsal position on a surgical table and the abdominal cavity was opened longitudinally. The liver was excised and weighed. The left lobe was cut into two halves. The left half was frozen in a cryo cassette and the right half was put into a histological cassette and fixed with 4 % PFA. The rest of the liver was cut into many small pieces and put into 1.5 ml reaction tubes, which were snap frozen in liquid nitrogen. In some collections the liver was crushed with pliers, which was kept in liquid nitrogen. After being crushed the liver was put into a mortar and grinded to powder. The liver powder was transferred to a 5 ml tube and stored at -80 °C. After the kidneys were excised, the left kidney was cut longitudinally, and the left half was cryo preserved and the right half was fixed with 4% PFA in histological cassettes. The right kidney was completely crushed and pulverised as described for the liver.

2.2.4 24 h urine collection

Metabolic cages were used to collect 24 h urine from single mice for two or three consecutive days in order to analyse the daily urinary oxalate excretion of mice. The mice, which were placed into the metabolic cage, had free access to water and feed powder. The excreted urine was collected in a small tube filled with 35 µL 6 M HCl to acidify the urine directly which was necessary to avoid the conversion of ascorbic acid to oxalic acid and to prevent bacterial growth. The daily uptake of water and food was recorded, and the mice were weighed before and after the time in the metabolic cages. A weight loss of more than 10% was consistently observed. The collected urine samples were transferred to a tube and centrifuged for 10 min at 179xg and room temperature to remove feed powder. The supernatant was aliquoted and stored at -80 °C for further analysis. The daily urine samples of each mouse were analysed separately before an average of the excreted compounds in the urine per mouse was calculated.

2.2.5 Gene expression analysis

2.2.5.1 RNA isolation

RNA from cells and mouse or human tissue was isolated by using QIAzol reagent (QIAgen) for phenol-chloroform extraction. QIAzol consists of guanidinium thiocyanate and phenol, which lyses cell membranes and inhibits RNases (Chomzynski 1987). Snap frozen tissue pieces or powder were added to 1 ml QIAzol. If necessary, the tissue samples were homogenised by a pestle. Next, samples were sonicated (50% power, 30 s, 5 s pulse, 2 s break) while kept on ice. Cells, cultivated on 6 well, 12 well or 24 well plates, were placed on ice, the medium was aspirated, and the cells were lysed with 1 ml, 500 µL or 250 µL QIAzol, respectively. After scraping, the cell lysates were transferred to 2 ml-reaction tubes and sonicated on ice as

mentioned before. Moreover, 1-5 million freshly isolated mouse or human hepatocytes were re-suspended in 1 ml QIAzol and sonicated in the same way. Next, 200 µL chloroform were added to each sample and the reaction tubes were shaken for approximately 20 s. The samples were incubated for several minutes at room temperature to improve the phase separation. Subsequently, the samples were centrifuged at 4 °C, 12000xg for 15 min. The aqueous phase containing the RNA was carefully transferred to a new reaction tube containing 500 µL 2-porpanol for precipitating the RNA. The samples were incubated at room temperature for 10 min followed by a 15 min centrifugation step at 12000xg at 4 °C. The supernatant was discarded, and the RNA pellet was washed with 850 µL 100% ethanol and subsequently centrifuged for 5 min at 4 °C and 10000xg. This washing step was repeated with 850 µL 75% ethanol. The supernatant was completely removed by pipetting and the RNA pellet was air-dried for several minutes. The RNA was dissolved in 15-100 µL DEPC-treated water and its concentration was determined photometrically with the Nanodrop2000 (Thermo Fisher Scientific). The RNA samples were stored at -80 °C.

2.2.5.2 cDNA synthesis

Before a real-time polymerase chain reaction (RT-PCR) for gene expression analysis was conducted, the RNA was converted to cDNA. For the reversed transcription of RNA into single stranded cDNA the high capacity cDNA reverse transcription kit (Applied Biosystems) was used. 500 ng – 2 µg RNA were mixed with appropriate volumes of 10x RT-Buffer, 10x random primers, 25x DNTP mix and reverse transcriptase. The total volume of the reaction mix was adjusted to 20 µL with DEPC water. The chosen conditions for the thermos cycler (Tgradient, Biometra) are listed in Table 2-17. All cDNA samples were diluted with DEPC water to a final concentration of 10 ng/µL and stored at -20 °C.

Table 2-17: Thermo cycler programme for reversed transcription of RNA into cDNA

Step	Temperature	Time
Incubation	25 °C	10 min
Reverse transcription	37 °C	120 min
Inactivation	85 °C	5 min
	4 °C	∞

2.2.5.3 Quantitative real-time polymerase chain reaction (qPCR)

Quantitative real-time PCR is a sensitive technique to detect and quantify changes in gene expression of a target gene (Higuchi et al. 1993). In this thesis, TaqMan probes, that hybridised to the DNA template strand between the primers and carry a fluorescent reporter on the 5'-end and a quencher on the 3'- end, were used. Hence, a fluorescence resonance energy transfer (FRET) between the quencher and the reporter suppresses the fluorescent signal. The applied DNA polymerase has a 5' – 3' exonuclease activity that leads to a separation of the TaqMan probes from the template strand which are cleaved into single nucleotides (Holland et al. 1991). Thus, the fluorescent reporter and quencher are spatially separated and a fluorescent signal, which is proportional to the amplified DNA concentration, can be

measured. The fluorescence is illustrated as a function of time and so-called Ct values, which describe the necessary number of cycles until the measured fluorescent signal crosses a threshold and enters the exponential phase.

All gene expression measurements were conducted with a 7500 Real-Time PCR System (Applied Biosystems). 25 ng cDNA were mixed with 2x universal master-mix and 20x specific TaqMan probe. The absolute volume per reaction was adjusted to 20 µL with DEPC water. All samples were measured in technical duplicates and for each probe water was used as a negative control. The standard conditions for the amplification are listed in Table 2-18.

Table 2-18: Parameters for standard amplification

Step	Temperature	Time	Cycles/Repetitions
	50 °C	2 min	1
Activation of DNA polymerase	95 °C	10 min	1
DNA denaturation	95 °C	15 s	40
Annealing and Elongation		60 °C	1 min

The levels of gene expression were calculated using the $2^{-\Delta\Delta Ct}$ method (Livak and Schmittgen 2001)which is a relative quantification approach that compares the expression levels of the gene of interest (GOI) and of a housekeeping gene (HKG) of the analysed samples in relation to control conditions (=calibrator). The expression of housekeeping genes does not alter under stressed or modified experimental conditions, therefore they serve as endogenous control genes. For this work, the expression of the housekeeping genes *Gapdh*, *Eif2a* or *UBC* were used to normalize the expression of the GOI ($\Delta Ct = Ct_{GOI} - Ct_{HKG}$). At first, this ΔCt value needs to be calculated for a test sample (ΔCt1) and separately for a control sample. In the next step, the ΔCt values of the control samples were subtracted from the ΔCt values of the test samples ($\Delta\Delta Ct = \Delta Ct1 - \Delta Ct2$) to find differences resulting from test conditions. For simplification, the calculation $2^{-\Delta\Delta Ct}$ was applied. Thus, the $2^{-\Delta\Delta Ct}$ value of control samples were set to 1; if the $2^{-\Delta\Delta Ct}$ value of the test sample is greater than 1, it indicates an upregulation of the GOI compared to the control and vice versa for $2^{-\Delta\Delta Ct}$ values below 1.

2.2.6 Protein analysis

2.2.6.1 Protein extraction

Proteins were extracted from liver tissue, kidney tissue and primary hepatocytes. Tissues and cells were lysed in RIPA lysis buffer containing 1:100 protease inhibitor and phosphatase cocktail II and III. Different procedures were applied, depending on the source material:

a) **Snap frozen tissue**: 1 ml RIPA buffer was added to a piece of tissue or tissue powder on ice. If necessary, the tissue was homogenised with a pestle, followed by a sonication for 20 s (50% power, 0.5 s pulse, 2 s break). After 20 min incubation on ice, the

homogenates were centrifuged for 10 min at 4 °C and 13000xg. The supernatants were transferred to new tubes.

b) **Primary cell culture**: 6, 12 or 24 well plates were placed on ice and medium was aspirated. If the analysation of the phosphorylation status of interesting proteins was not the aim of the experiment, the plated cells were carefully rinsed with 1xPBS before adding 300 µL, 150 µL or 75 µL RIPA buffer to each well, respectively. Cells were scraped and collected in a 1.5 ml tube. After the samples were sonicated as mentioned in a), the cell lysates were incubated for 20 min on ice. Next, the samples were centrifuged for 10 min at 13000xg and 4 °C. The supernatants were collected in new tubes.

Protein lysates were stored at -20 °C or -80 °C.

2.2.6.2 Protein quantification

The bicinchoninic acid (BCA) protein assay (Thermo Fisher Scientific) was used for the quantification of protein concentrations in the analysed samples. This method is a combination of the Biuret reaction, which outlines the conversion of Cu^{2+} to Cu^{+} by peptide bonds under alkaline conditions, and the colorimetric detection of Cu^{+} with BCA. Two BCA molecules and one Cu^{+} ion form a purple chelate complex with an absorbance at 562 nm which is proportional to the protein concentration (Smith et al. 1985).

Based on the expected protein concentration, the samples were diluted with ultrapure water. Next, 5 µL of the diluted samples were mixed with 195 µL BCA working reagent, which is composed of 49 parts of solution A and 1 part of solution B, in one well of a 96 well plate. A calibration curve of bovine serum albumin (BSA), ranging from 0 µg/ml to 2000 µg/ml, was prepared in the same way without the predilution. Each sample and BSA standard were measured in duplicates. The 96 well plate was incubated for 30 min at 37 °C previous to the absorbance measurement at 562 nm. Incubation and measurements were both done in a plate reader (Infinite M200 Pro, Tecan). On the basis of the standard curve, the protein concentrations of the samples were calculated.

2.2.6.3 Western blot

2.2.6.3.1 SDS-Polyacrylamide gel electrophoresis (SDS-PAGE)

The SDS-PAGE is a frequently utilized method to separate protein mixtures in a size dependent manner. This is achieved by applying an electric field to the gel which leads to a separation of the proteins according to their electrophoretic mobility which in turn is dependent on the weight and charge of the protein. The anionic detergent sodium dodecyl sulphate (SDS) linearizes proteins and covers their charge negatively (Shapiro et al. 1967). Hereby, the mobility of the protein is only depending on the weight.

Freshly prepared gels were cast in the Mini-PROTEAN tetra electrophoresis system (BioRad) like described in the manufacturer's instructions. A mixture for two 1.5 mm thick 10% separation gels consisted of 6.4 ml ultrapure water, 5.28 ml acrylamide solution (30% v/v), 4

ml separation buffer, 160 µL 10% (w/v) SDS solution, 6.4 µL TEMED and 160 µL 10% (w/v) APS solution. The solution was transferred between two glass plates within a vertical frame. Each gel was covered with a thin layer of 2-propanol on top to avoid oxidation and evaporation. After polymerization, the 2-propanol was removed and the mixture for the stacking gels was cast on top. This stacking gel mixture for two gels contained 4.8 ml ultrapure water, 1 ml acrylamide solution (30% v/v), 0.8 ml stacking buffer, 65 µL 10% (w/v) SDS solution, 5 µL TEMED and 100 µL 10% (w/v) APS solution. Immediately after transferring the stacking gel mixture into the cast, combs were added on top in order to form loading wells. The finished gels were stored in a humid bag at 4 ° C for a maximum of one week.

For the gel electrophoresis equal amounts of protein from each sample were mixed with 5 x loading buffer and denaturised at 95 °C for 5 min. The dithiothreitol (DTT) in the loading buffer reduced disulphide bonds of the proteins to accomplish a better protein separation during the electrophoresis. Meanwhile the gels were fixed into their chambers and filled with 1 x running buffer. The denaturised protein samples and 4 µL of Precision Plus Protein Dual Colour standard (BioRad) were added into the wells of the gels. An initial current of 20 mA/gel was applied and increased up to 40 mA/gel when the samples reached the stacking gel. The electrophoresis was terminated when the samples reached the end of the gel.

2.2.6.3.2 Protein transfer on PVDF membrane

After the gel electrophoresis, the proteins were transferred from the gel to a PVDF membrane in order to immobilise them and to make them detectable *via* antibodies. For the protein transfer the semidry blot system from Biometra or BioRad was used. Each transfer chamber consisted of two horizontal plates, which represented the anode (lower plate) and the cathode (upper plate). Blotting papers, were soaked with the anode and cathode buffer, three in the anode buffer and one in the cathode buffer per gel, respectively. The membrane was activated in methanol and stored in anode buffer for several minutes. Next, the gel was removed from its cast and left in cathode buffer to equilibrate. The three blotting papers soaked with anode buffer were laid on the anode plate of the transfer chamber and the activated membrane was put on top of them and overlaid with the gel. Air bubbles between the membrane and the gel were carefully removed with a roller. The construct was covered with one blotting paper, pre-equilibrated in cathode buffer. Thereafter, the transfer chamber was closed with the cathode plate and the transfer was performed at 234 mA/blot for 30-40 min. After the transfer, the membrane was shortly washed in 1xTBS-T and incubated in 5% BSA in 1xTBS-T for one hour, in order to block unspecific binding between the membrane and the antibody.

2.2.6.3.3 Protein detection

Following the blocking step, the membranes were incubated with a specific primary antibody, in antibody dependent dilution in 5% BSA or 5% milk powder in 1xTBS-T, overnight at 4°C and constantly shaken. On the next day, the membranes were washed three times with 1xTBS-T for 5 min each prior to incubation with the secondary horseradish peroxidase (HRP) linked antibody for one hour at room temperature (RT). The secondary antibodies were

appropriately diluted in 5% BSA 1xTBST or 5% milk powder in 1xTBS-T. Specific information about the used antibodies are listen in Table 2-19. Subsequently, the membranes were again washed three times for 5 min each with 1xTBS-T. Protein detection was performed by chemiluminescence using 5 ml ECL solution and 3 µL hydrogen peroxide. The conjugated HRP of the secondary antibody catalysed the oxidation of luminol which was accompanied by light emission at 428 nm. Light emission was captured by the Blot-Imager Vilber Fusion Fx7 (Vilber Lourmat). Thereafter, the membranes were incubated in stripping buffer for 30 min at RT, for the purpose of removing the probed antibodies off the membrane. After blocking the membranes again with 5% BSA 1xTBST or 5% milk powder for 1 h at RT, further proteins, e.g. a loading control like β-actin, can be detected. The protein signals were quantified densitometrically with the software ImageJ.

Table 2-19: Parameters for antibody incubation (Western blotting)

Primary antibody	Secondary antibody	Dilution	Incubation
anti α-tubulin	anti-mouse	1:1000/1:5000 in 5% BSA	O/N 4 °C/ 1 h RT
anti β-actin	anti-mouse	1:5000/1:10000 in 5% BSA	30 min RT/20 min RT
anti Agxt	anti-rabbit	1:1000/1:5000 in 5% BSA	O/N 4 °C/ 1 h RT
anti Creb	anti-rabbit	1:1000/1:5000 in 5% BSA	O/N 4 °C/ 1 h RT
anti Creb (phospho S133)	anti-rabbit	1:1000/1:5000 in 5% BSA	O/N 4 °C/ 1 h RT
anti Gapdh	anti-rabbit	1:5000/1:5000 in 5% BSA	O/N 4 °C/ 1 h RT
anti Hao1	anti-rabbit	1:1000/1:5000 in 5% BSA	O/N 4 °C/ 1 h RT
anti Ldha	anti-mouse	1:3000/1:5000 in 5% milk	O/N 4 °C/ 1 h RT

2.2.7 Preparation of oleic acid-BSA complex solution

The formation of lipid droplets in primary hepatocytes was induced by incubation with oleic acid (OA) bound to BSA. Under physiological conditions, free fatty acids are usually bound to serum albumin when transported within plasma (Gordon and Cherkes 1956). The approach for the preparation of the complex was similar to the protocol from Cousin and colleagues (Cousin et al. 2001) with modifications in temperature and concentrations.

At first, a 60 mM OA solution in 0.01 M NaOH was prepared by adding the appropriate volume of OA to 0.01 M NaOH and stirring the mixture for 30 min at 70 °C in the dark. Afterwards, the solution was cooled and mixed with usually three droplets of 1 M NaOH to completely dissolve the OA. Meanwhile, fatty acid free BSA was dissolved in ultrapure water in order to obtain a

2.5 mM BSA solution. In the next step, one part of 60 mM OA solution was mixed with four parts of 2.5 mM BSA solution (molecular ratio OA to BSA was 6:1). The OA/BSA-solution was stirred for 1 h at room temperature to form OA/BSA complexes. Also, four parts of 2.5 mM BSA solution were diluted with one part of 0.01 M NaOH to serve as a control solution. The OA/BSA-solution and the BSA control solution were sterile filtered (0.45 µm filter) and stored at -20 °C. The solutions were used within 3-4 weeks.

2.2.8 Induction of lipid droplet formation in primary mouse and human hepatocytes (*in vitro* steatosis model)

For the *in vitro* formation of lipid droplets, hepatocytes were incubated with OA/BSA complex solution. Based on prior studies, which were carried out to find an appropriate OA/BSA concentrations (Gianmoena 2017), a concentration of 1 mM OA/ 0.1667 mM BSA was chosen for the treatment of primary hepatocytes. The stock solutions of OA/BSA and the BSA control were diluted in William's E cultivation medium and the cells were usually treated for 72 h, including a media change after 48 h.

2.2.9 Extraction and enzymatic quantification of triglycerides (TG)

Triglyceride (TG) levels in different tissues and cells were quantified enzymatically with a triglyceride quantification kit (Abcam). Fatty acids are cleaved from the glycerol backbone by a lipase, glycerol is oxidized and then reacts with a probe to generate a fluorescent signal (535_{Ex} /587_{Em} nm).

a) **Snap frozen tissue**: Tissue pieces or powder were transferred to a 1.5 ml reaction tube and 1 ml of 5% NP-40 solution was added. If necessary, the samples were first homogenized with a pestle and then sonicated on ice (50% power, 30 s, 5 s pulse, 2 s break) to completely release the TG.
b) **Primary hepatocytes**: Freshly isolated hepatocytes (2.5 – 5 million) were centrifuged for 1 min at 2000 rpm and 4 °C, the supernatants were removed, and the cells were washed with 1xPBS. After a second centrifugation, the supernatants were aspirated, and the pellets were re-suspended in 1 ml 5% NP-40 solution. The samples were sonicated like in a) in order to release all TG.
c) **Plated primary hepatocytes**: The 6 well plate was put on ice and the medium was aspirated. Next, 300 µL of 5% NP-40 solution was added on each well, the cells were scraped and transferred to a 1.5 ml tube. The cells were sonicated like in a) to collect all TG.

The extracts were heated up to 90 °C for 3 min and then allowed to cool down to room temperature while repeatedly vortexed. The heating step was repeated, followed by a centrifugation for 2 min at top speed to remove any insoluble material. The supernatant was collected, and an aliquot was diluted appropriately.

2.2.9.1 Enzymatic quantification of triglycerides

The assay was performed in a black 96 well plate with a flat, clear bottom since fluorescence signals were measured from the bottom. The diluted sample (1-5 µL) was added to a well and the volume was adjusted to 50 µL with assay buffer. The samples were measured in duplicates. Next, 2 µL of lipase was added to each well and each sample had a background control where no lipase was added. After an incubation of 20 min at room temperature, 50 µL reaction mix (see Table 2.20) were added to each well followed by an incubation of 1hour at room temperature in the dark. Thereafter, the fluorescence signals were measured with 535 nm excitation and 587 nm emission in the plate reader (Infinite M200 Pro, Tecan). In parallel, the protein concentrations of the diluted extracts were quantified with the BCA assay in order to normalize the relative fluorescence unit (RFU). For data analysis, the blanks (buffer with/without lipase) were subtracted from each reading. Next, the samples were background-corrected to consider only the glycerol arising from tri-, di- and monoglycerides but not the free glycerol. The concentration of proteins within the extract was calculated and the RFU values were divided by the corresponding protein amount to normalize the signal.

Table 2-20: TG reaction mix for one sample

Compound	1 sample
Assay buffer	47.6 µL
Probe	0.4 µL
Enzyme mix	2 µL

2.2.10 Stimulation of oxalate formation *in vivo* and *in vitro*

The role of reduced Agxt expression was examined by the application of oxalate precursor compounds *in vivo* as well as *in vitro*. The levels of excreted oxalate in urine and cell culture supernatant were analysed *via* LC-MS/MS.

2.2.10.1 Hydroxyproline enriched diet of *ob/ob* and *ob/+* mice

Ten *ob/ob* and ten *ob/+* mice were divided into two groups of 5 mice from which the first group received a normal chow diet which was enriched with 1% hydroxyproline (1% Hyp) and the other group was fed with plain normal chow diet. Each mouse had its own cage and free access to water and food. The body weight, water and food intake were measured daily. On day seven, mice were transferred to a single mouse metabolic cage (Tecniplast) and 24 h urine was collected for three consecutive days. On day ten of the diet, the mice were again transferred to their normal single cages and scarified the next day for tissue and plasma collection. The liver and the kidneys were collected for histological staining, immunoblotting and RNA expression analysis. Further, plasma samples from the heart, portal and hepatic vein were collected to measure the systemic oxalate levels, the oxalate inflow into the liver and outflow from the liver, respectively.

2.2.10.2 Oxalate precursor treatment of primary hepatocytes from male *ob/+* and *ob/ob* and female wt and *ob/ob* mice

Isolated primary hepatocytes were cultured in 6 well plates in a collagen sandwich on top system as described before (Chapter 2.2.2.2). On the next day, the cells were treated with 1 ml of 3.16 mM, 10 mM, 31.6 mM hydroxyproline, 3.16 mM, 10 mM, 31.6 mM glycolate and with 1 ml of 0.316 mM, 1 mM and 3.16 mM glyoxylate for 48 h at 37°C and 5% CO_2. All concentrations of the different substances were diluted in full media. After 48 h of incubation, the supernatants and protein extracts were collected and stored at -80 °C.

2.2.10.3 Hydroxyproline and THFA treatment of primary hepatocytes from *ob/+* and *ob/ob* mice

Primary mouse hepatocytes of *ob/ob* and *ob/+* mice were isolated and cultivated in 6-well plates for 24 h as described in chapter 2.2.2.2. After 24 h, the hepatocytes were incubated with 0.5 ml William's E medium with additives (full media) containing 10 mM tetrahydrofuroic acid (THFA) for 1 h at 37°C and 5% CO_2. THFA is a known inhibitor of proline dehydrogenase 2 (Prodh2) which catalyses the first step of the hydroxyproline breakdown (Adams and Frank 1980; Zhang et al. 2004). Thereafter, 0.5 ml of either 6.32 mM, 20 mM or 63.2 ml of hydroxyproline diluted in full media was mixed with 10 mM THFA and added on top of the present 0.5 ml 10 mM THFA. This leads to a 1:2 dilution of the hydroxyproline concentrations while the THFA concentration remains the same. Thus, the cells wells were incubated with 3.16 mM, 10 mM and 31.6 mM hydroxyproline accompanied by 10 mM THFA for 48 h at 37°C and 5% CO_2. Afterwards, the supernatants were collected on ice and frozen at -80 °C. The cells were washed with 1xPBS and protein extracts were collected as described in chapter 2.2.6.1.

2.2.10.4 Oxalate precursor treatment of primary hepatocytes from western diet mice

Isolated primary hepatocytes from normal chow and western diet mice were cultured in 6 well plates in a collagen sandwich on top system as described before (Chapter 2.2.2.2). On the next day, the cells were treated with 1 ml of 3.16 mM, 10 mM and 31.6 mM hydroxyproline and glycolate and with 1 ml of 0.316 mM, 1 mM and 3.16 mM glyoxylate for 48 h at 37°C and 5% CO_2. All concentrations of the different substances were diluted in full media. After 48 h of incubation, the supernatants and protein extracts were collected and stored at -80 °C.

2.2.10.5 Oxalate precursor treatment of primary hepatocytes from *Agxt*$^{-/-}$ mice

Primary hepatocytes from *Agxt*$^{-/-}$ and aged matched wild type mice were cultivated as outlined in Chapter 2.2.2.2. After 24 h, the hepatocytes were treated with different concentrations of hydroxyproline, glycolate and glyoxylate. The treatment was carried out exactly as described in Chapter 2.2.10.2. Finally, supernatants and protein extracts were collected and stored at -80 °C.

2.2.10.6 Oxalate precursor treatment of primary human hepatocytes

Primary human hepatocytes were thawed and cultivated in 6 well plates for 24 h as described in Chapter 2.2.2.3. The treatment of primary hepatocytes from different donors with oxalate

precursors was performed in the same way as described in the previous chapter (2.2.10.2). Thereafter, the supernatants and protein extracts were collected and stored at -80 °C.

2.2.10.7 Oxalate precursor treatment of primary human hepatocytes with *in vitro* steatosis

Primary human hepatocytes were plated and as described in Chapter 2.2.2.2 and Chapter 2.2.2.3. After the second collagen layer polymerised, *in vitro* steatosis was induced as outlined in Chapter 2.2.8. After 72 h, hepatocytes were treated with 1 ml of 3.16 mM, 10 mM and 31.6 mM hydroxyproline and glycolate and with 1 ml of 0.316 mM, 1 mM and 3.16 mM glyoxylate for 48 h at 37°C and 5% CO_2. All concentrations of all substances were dissolved in all three media variants: FM, 0.1667 mM BSA and 1 mM OA/0.1667 mM BSA. 48, supernatants and protein extracts were collected.

2.2.11 Glucagon treatment of *ob/+* and *ob/ob* mice *in vivo* and *in vitro*

2.2.11.1 Injection of glucagon into *ob/+* and *ob/ob* mice

Nine mice were put into single cages overnight prior to the treatment with full access to food and water. On the next day, three mice of each genotype were intraperitoneally injected with 3 µg/g body weight glucagon or PBS, which served as a vehicle control. After the injections, the mice were put back into their single cages and had again access to food. After 3 h the mice were sacrificed, and liver tissue was collected for qRT-PCR and immunoblot analyses.

2.2.11.2 Treatment of primary hepatocytes from *ob/+* and *ob/ob* mice with glucagon

Primary hepatocytes were isolated from *ob/+* and *ob/ob* mice and cultivated in a collagen sandwich on top system as described in Chapter 2.2.2.2. After 24 h of cultivation, the primary hepatocytes were washed two times with William's E medium without additives and treated with 10 nM and 100 nM glucagon for 15 min, 30 min, 45 min, 1 h, 3 h, 6 h and 24 h. RNA and protein extracts were collected for each time point for qRT-PCR and immunoblot analyses.

2.2.12 Glucagon treatment of 6 weeks western diet mice *in vivo* and *in vitro*

2.2.12.1 Glucagon injection in 6 weeks WD-fed and NCD-fed mice

Prior to the treatment, six mice of 6 weeks WD-fed, and six mice of 6 weeks NCD-fed mice were starved overnight with access to water. Thereafter, three mice of each group were injected intraperitoneally with either 3 µg/g body weight glucagon or PBS, which served as a vehicle control. The mice were put back into their cages and had no access to food. After 3 h the mice were sacrificed, and liver tissue was collected for qRT-PCR and immunoblot analyses.

2.2.12.2 Glucagon exposure of primary hepatocytes from 6 weeks WD-fed and NCD-fed mice

Primary hepatocytes were isolated from 6 weeks WD-fed and NCD-fed mice and cultivated in a collagen sandwich on top system as described in Chapter 2.2.2.2. The glucagon treatment and collection time points were identical with the experiment in primary hepatocytes from

ob/+ and *ob/ob* mice (Chapter 2.2.11.2). After each time point, RNA and protein extracts were collected.

2.2.13 Glucagon treatment of primary mouse hepatocytes with *in vitro* steatosis

Primary mouse hepatocytes were isolated from wild type mice and cultivated in a collagen sandwich on top system as described in Chapter 2.2.2.2. After the second collagen layer polymerised, *in vitro* steatosis was induced as outlined in Chapter 2.2.8. After 72 h, all hepatocytes were treated with 10 nM glucagon, which was dissolved in all of three media variants (FM, 0.1667 mM BSA and 1 mM OA/0.1667 mM BSA). After 30 min, 1 h, 3 h, 6 h and 24 h of exposure, protein and RNA extracts were collected for each time point for immunoblotting and qRT-PCR analysis.

2.2.14 Treatment of primary human hepatocytes with glucagon

Primary human hepatocytes from Lonza™ were cultivated in a collagen sandwich on top system as described in Chapter 2.2.2.3. After 24 h, the hepatocytes were treated with 10 nM glucagon for 30 min, 1 h, 3 h, 6 h and 24 h. extracts for RNA and protein isolation were collected after each time point and analysed via qRT-PCR and immunoblots, respectively.

2.2.15 Transduction of primary *ob/+* and *ob/ob* hepatocytes with adeno-associated viral particles

Adeno-associated vector particles were generated by VectorBuilder. The particles contained either a pAAV-CMV-EGFP or a pAAV-CMV-mitochondrial Agxt vector. The human cytomegalovirus (CMV) promoter has been shown to be active in a wide range of cell types and is the most commonly used promoter in mammalian expression plasmids (Xia et al. 2006). Isolated primary hepatocytes of *ob/+* and *ob/ob* mice were cultivated in a collagen sandwich on top system (Chapter 2.2.2.2) for 24 h at 37°C and 5% CO_2. Subsequently, 0.85 x 10^5 cells were incubated with 10^5 and 5 x 10^5 genome copies (GC)/cell of viral particles with the pAAV-CMV-EGFT and pAAV-CMV-mAgxt constructs dissolved in full medium for 24 h at 37°C and 5% CO_2 for the first experiment. All further experiments were conducted with and 5 x 10^5 genome copies (GC)/cell of viral particles (n=5). On the next day, the cells were rinsed with William's E medium without additives and treated with 10 mM and 31.6 mM hydroxyproline in full medium for 72 h at 37°C and 5% CO_2. Thereafter, supernatants, protein and RNA extracts were collected in order to measure the hydroxyproline induced oxalate excretion, and the protein and mRNA expression of Agxt, respectively.

2.2.16 Quantification of oxalate and glycolate by Liquid Chromatography Tandem Mass Spectrometry

Oxalate and/or glycolate concentrations in urine samples (acidified), in plasma or cell supernatants (in serum-free medium) was quantified by LC-MS/MS as described before (Schriewer et al. 2017) with modifications. During this thesis, a LC-MS/MS system consisting of a QTrap5500 mass spectrometer coupled to a Shimadzu Prominence LC20 XR system was

used. Urine samples were diluted accordingly, while cell culture supernatants and plasma samples remained and were first subjected to precipitation to remove proteins. Oxalate and glycolate were quantified by using ^{13}C-labelled internal standards (Cambridge Isotope Laboratories, Inc.). The mobile phase consisted of 0.1% formic acid in water (v/v) and acetonitrile post column. The flow rate was set to 0.2ml/min and the injection volume was 30 µL. For ionisation, electrospray ionisation in negative mode was used. Analytes were fragmented by a collision gas and its product ions were analysed. Measurements and quantifications were carried out by the IfADo core unit of Analytical Chemistry (Dr. Jörg Reinders).

2.2.17 Colorimetric quantification of creatinine in urine

Creatinine is a product of muscle metabolism and excreted by the kidneys (Skorecki et al. 2015). The excreted creatinine amount is often used as a benchmark for the concentration of urine. In this thesis, the urinary creatinine concentration was used to normalise the excreted oxalate amount since the daily excreted urine volumes differed. Urinary creatinine was determined *via* the Jaffé reaction (Jaffe 1886). Creatinine reacts with picric acid under alkaline conditions and forms an orange complex with a maximum absorbance at 492 nm. Urine samples were diluted accordingly in distilled water and mixed with basic picric acid solution. Murine urine was diluted 1:20 with ultrapure water in a 1.5 ml tube, mixed and centrifuged at 6000xg for 5 minutes to remove potential fine particles. The supernatants were transferred to new tubes. Creatinine standards were prepared in water at a concentration range from 0 mg/ml to 70 mg/ml. 50 µL of each standard and sample were pipetted to a well of a transparent 96 microtiter plate with flat bottom. Moreover, 50 µL of two control urines (1:50 diluted) with different creatinine concentrations were used as a quality control. 10 ml of 0.25 M NaOH-solution were mixed with 4.365 mM picric acid. 200 µL of this alkaline picric acid solution were added to each well and incubated in the dark for 45 min. Next, the absorbance at 492 nm was measured in a microplate reader (Tecan Infinite 200PRO plate reader) and a calibration curve was used for quantification.

2.2.18 Histologic staining of paraffin embedded tissue

2.2.18.1 Fixation and paraffin embedding of tissue

After the collection in histological cassettes, liver and kidney tissues were fixed in 4% PFA at 4 °C for two days. The cassettes were shortly rinsed with sterile 1xPBS and then incubated in 1xPBS at 4 °C for two additional days ahead of the embedding of the tissue in paraffin. Tissue infiltration with paraffin was carried out with the STP120 processor (Thermo Fisher Scientific). During the process the tissues were first dehydrated with an ethanol gradient, incubated in xylene and finally infiltrated with paraffin. Detailed procedure information is listed in the Table 2.21.

Table 2-21: Programme for paraffin infiltration of tissue

Step	Solution	Time [min]

1	70% Ethanol	30
2	70% Ethanol	60
3	90% Ethanol	30
4	90% Ethanol	30
5	99% Ethanol	30
6	99% Ethanol	35
7	99% Ethanol	60
8	Xylol	30
9	Xylol	35
10	Xylol	60
11	Paraffin Histowax	80
12	Paraffin Histowax	105

Thereafter, the tissues were embedded in paraffin with the Microm HM450 automated embedding device. 4 µm-thick formalin-fixed paraffin-embedded liver and kidney tissue sections were used for tissue staining and immunohistochemistry. Sections were obtained with a feather blade type N35HR in a HM 450 Sliding Microtome (Thermo Fisher Scientific). The tissue sections were mounted on glass slides during a 20 min incubation at 60 °C. Before usage, the tissue slides were stored at 4 °C.

2.2.18.2 Haematoxylin and eosin staining

Tissue sections were deparaffinised in Roti®-Histol four times for 10 min before being rehydrated through a decreasing ethanol gradient (5 min in 100%, 95%, 90%, and 70% each) to ultrapure water. Next, the slides were incubated in freshly filtered haematoxylin for 5 min. The tissue was blued under running tap water for 10 min. Hereafter, the sections were stained with freshly filtered 1 % Eosin Y for 3 min, then shortly rinsed in ultrapure water and dehydrated through an increasing ethanol gradient (70%, 90%, 95%, 2x100%, 5 s each), ending in Roti®-Histol. Last, the tissue was mounted on a glass slide with Entellan®. The optical microscope Olympus BX41 was used for imaging.

2.2.18.3 Immunohistochemistry using Avidin-Bioting-Complex (ABC) method

Antibody based immunohistochemistry (IHC) can be used to visualise specific antigens, mainly proteins, directly on tissue. IHC was used to identify the distribution of different enzymes of the glyoxylate metabolism.

The paraffin slides were deparaffinized and rehydrated as described previously. Once fixed, proteins can be cross linked to formaldehyde leading to a weak or negative signal. In order to unmask the proteins, the sections were heated up in citrate buffer (10 mM, pH=6.0) for two times à seven minutes. After the slides cooled down, they were washed in 1xPBS two times for 5 min each. Endogenous peroxidase and background signals were blocked by treatment with 3% H_2O_2 in 1xPBS. The slides were washed thrice with 1xPBS for 5 min each and subsequently blocked with 3% BSA/3% Tween80 in 1xPBS in a humidified chamber for 60 min at room temperature. Next, the specific antibody was diluted in 0.3% BSA/3% Tween80 in 1xPBS appropriately (see Table 2.22) and the tissue samples were incubated over night at 4 °C in a

humidified chamber. On the next day, the tissue sections were washed three times à 5 min in 1xPBS to completely remove the primary antibody. The secondary antibody against rabbit was mixed with blocking reagent, both from the ABC kit, in 2 ml 1xPBS and added onto the slides for 30 min at room temperature. Then, the samples were washed again three times à 5 min in 1xPBS. Avidin (reagent A) and biotinylated horseradish peroxidase (reagent B) were mixed with 2 ml 1xPBS and incubated onto the samples for 30 min at room temperature. Again, the slides were washed three times à 5 min in 1xPBS. Five drops of 3, 3'-diaminobenzidine (DAB) were mixed with two drops H_2O_2 and two drops of buffer solution in 5 ml water; this solution was added onto the slides for 2 – 10 min until the development of a brown colour. Next, the samples were washed for 5 min under running tap water before they were stained with haematoxylin for 2 min. The haematoxylin solution was removed, and the slides were washed in running tap water for 10 min. The samples were dehydrated by an increasing ethanol gradient (70%, 90%, 95%, 2x100%, 5 s each), followed by Roti®-Histol before mounted with Entellan®. For imaging, the optical microscope (Olympus BX41) was used.

Table 2-22: Dilutions of primary antibodies used for IHC

Antibody	Host	Dilution
anti Agxt	Rabbit	1:1000

2.2.19 Methylation analysis of Agxt promoter

The methylation analysis of the *Agxt* promoter was performed by Dr. Nina Gasparoni of the genetic/epigenetic research group of Prof. Jörn Walter at Saarland University.

2.2.19.1 Sample preparation

Five million isolated primary mouse hepatocytes were transferred to a reaction tube and centrifuged for 1 min at 4 °C and 400xg. The supernatant was discarded, and the cell pellet was carefully washed with 1xPBS. The samples were centrifuged again at the same conditions and the supernatants were again discarded while the cell pellet was snap frozen in liquid nitrogen. The cells were stored at -80 °C prior to transporting them on dry ice to the Saarland University.

2.2.19.2 Targeted deep sequencing

In order to validate DMRs targeted deep sequencing was performed. Therefore, genomic DNA was treated with bisulphite using the EZ-DNA Methylation Gold kit (Zymo Research). The bisulphite treated DNA was amplified *via* PCRs with specific forward and reverse primers. Amplicons were generated by using fusion primers which contained a 3' sequence-specific part and a universal 5'-part with the nucleotide sequences for Illumina sequencing. The sequences of the specific Agxt fusion primers and conditions are listed below (Table 2.23). Next, the PCR products were separated on a 1.2% agarose gel and purified with Ampure XP beads (Beckman Coulter) by following the manufacturer's protocol. In the next step, the purified products were measured with the Qubit Fluorometer (Qubit HS-Kit, Thermo Fisher Scientific) and diluted to 4 nM. NGS tags were completed by a second PCR and a final clean-

up step. Afterwards, the samples were diluted to 10 nM, pooled and sequenced on an Illumina MiSeq (Illumina v3 chemistry, 2 × 300 bp paired end). Next, the raw data was extracted and pre-processed. Data analysis was performed with BiQHT and in-house R scripts of the research group at Saarland University (Lutsik et al. 2011). The number of cytosine and thymine at CpG positions were quantified, showing methylated and unmethylated cytosines in the *Agxt* promoter, respectively. Hereby, the methylation status of the *Agxt* promoter could be determined.

Table 2-23: Primer sequences used to. F: Forward primer, R: Reverse primer, Temp.: Annealing temperature, X: sample-specific barcode sequences.

DMR	Target region	Primer sequence (5' – 3')	Temp. (°C)
Agxt (1)	mm10: chr1: 93134656 - 93135047	F: GTGTAATGTGTTTTGGTGAAATTTATTTT R: ACTTCTTCAAAAATCAAAAAACAAATACC	54
Agxt (2)	mm10: chr1: 93135215 - 93135618	F: TTGATAATAAAAGGGTTGGAGAAATAGG R: ACTTCTTCAAAAATCAAAAAACAAATACC	58
Universal primer tags (fusion primer)		F: TCTTTCCCTACACGACGCTCTTCCGATCT R: GTGACTGGAGTTCAGACGTGTGCTCTTCCGATCT	
2nd PCR primers		F: CAAGCAGAAGACGGCATACGAGATXXXXXXGTGAC TGGAGTTCAGACGTGTGCTCTTCCGATCT R: AATGATACGGCGACCACCGAGATCTACACXXXXXXT CTTTCCCTACACGACGCTCTTCCGATC	

2.2.20 Paediatric NAFLD cohort

A collection of liver biopsies with biopsy-proven NAFLD and corresponding 24 h urine samples from overweight and obese children and adolescents (aged 10-17 years) was available from the Charité in Berlin (Hudert et al. 2019). The liver biopsies were evaluated and scored by pathologists by using the histological scoring system for non-alcoholic fatty liver disease (NAFLD) by the NASH clinical Research Network (NASH CRN). The scoring of steatosis, lobular inflammation and hepatocellular ballooning was included in this method. In order to obtain

the NAFLD activity score (NAS), the scores from the different features were aggregated. Acidified 24 h urine samples were collected from 31 patients, whereas one sample was excluded due to under-collection. For analysis, age-related reference for non-pathophysiological urinary excretion as well as body surface area (BSA) information were considered (normal value of oxalate excretion in 24-hour urine sample: <0.50 mmol/1.73m2/day for all ages; normal values of oxalate/creatinine molar ratio: <70-82 mmol/mol for 5-14 years and <40 mmol/mol for >16 years) (Hoppe 2012). The BSA was calculated as BSA = SQR [Bw (kg) x Ht (cm)/3600].

2.2.21 Statistics

All experiments were performed with three or more biological replicates if stated differently. In order to determine significant differences between groups an unpaired t test, two sided was used. P values of <0.05 were considered statistically significant. All data are shown as mean ± standard deviation (SD), except for plasma/urine where data are shown as mean ± standard error of the mean (SEM). The calculations were performed using GraphPad PRISM 7.

3 Results

In a previous study, the downregulation of AGXT in steatosis has been validated in primary human hepatocytes, in the liver and hepatocytes of *ob/ob* mice, in the liver of a western diet mouse model, as well as in *in vitro* steatosis of primary mouse hepatocytes and Huh7 cells (Chapter 1.81.; Gianmoena 2017). In order to obtain a better overview of the steatosis associated alterations within the glyoxylate metabolism, further enzymes of the metabolism were analysed. The peroxisomal enzyme Hao1 was shown to be downregulated on mRNA level in the liver of *ob/ob* mice. Since Hao1 catalyses the oxidation of glycolate to glyoxylate, this suggests a lower ability of *ob/ob* mice to generate peroxisomal glyoxylate (Gianmoena 2017). Moreover, in steatotic human hepatocytes the mRNA expression of *GRHPR*, which converts glyoxylate to glycolate within the mitochondria and in the cytosol, was significantly reduced compared to non-steatotic hepatocytes. The detoxification in steatotic human hepatocytes seemed to be impaired in the peroxisomes and additionally in the mitochondria. The consequences of these alterations remained unclear (Gianmoena 2017). Furthermore, DNA methylation analysis revealed a hypermethylation of the *AGXT* promoter in isolated hepatocytes of *ob/ob* mice, as well as in steatotic human hepatocytes. This was validated by amplicon sequencing with specific primers for the *Agxt* promoter. Since promoter hypermethylation is associated to a decreased gene expression, this illustrated a possible explanation for the downregulation of *AGXT* in steatotic conditions (Gianmoena 2017).

3.1 *Ldha* mRNA expression is elevated in *ob/ob* mice

In recent studies, *Ldha* has been reported as a possible target for reducing hepatic oxalate production and preventing calcium oxalate crystal depositions in mouse models of primary hyperoxaluria (Lai et al. 2018; Wood et al. 2019). Therefore, the expression of *Ldha* was analysed in *ob/ob* mice in order to explore whether *Ldha* might contribute to the steatosis associated increased hepatic oxalate production in these mice. Quantitative real-time PCR (qRT-PCR) revealed an upregulation of the *Ldha* mRNA expression by a fold change of 1.56 ± 0.17 in the livers of *ob/ob* mice compared to *ob/+* mice (n=5; Fig. 3.1 A). However, this could not be confirmed on protein level (Figure 3.1 B). Since the elevated *Ldha* mRNA expression is not reflected on protein level, the role of Ldha in steatosis associated hepatic oxalate production might be not relevant in *ob/ob* mice.

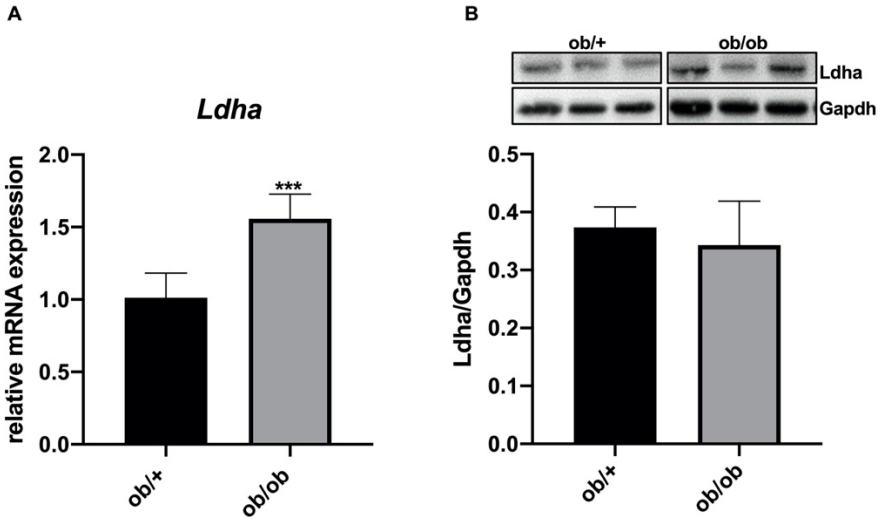

Figure 3.1: Upregulation of *Ldha* mRNA expression in *ob/ob* mouse liver. QRT-PCR showed elevated *Ldha* mRNA expression in the liver of *ob/ob* mice compared to *ob/+* (n=5). Eif2a was used as endogenous control (A). This could not be confirmed on protein level *via* immunoblotting. The means ± SD are shown. *** p < 0.001. Student's t test, unpaired, two sided.

3.2 Increased oxalate excretion due to hydroxyproline treatment in hepatocytes of *ob/ob* mice can be attributed to *Agxt* downregulation

In a previous work (Gianmoena 2017), primary hepatocytes from *ob/ob* and *ob/+* mice were treated with the oxalate precursors glycolate, hydroxyproline and glyoxylate in order to analyse the influence of the gene expression changes observed in *ob/ob* mice (including the downregulation of *Agxt*) on their capacity to metabolise oxalate precursors and to detoxify glyoxylate. Primary *ob/ob* hepatocytes excreted increased amounts of oxalate when treated with hydroxyproline compared to *ob/+* hepatocytes (Gianmoena 2017).

3.2.1 Primary *ob/ob* hepatocytes from male and female mice excrete more oxalate upon hydroxyproline treatment

The oxalate precursor challenges were repeated during this thesis in order to confirm the observed increased susceptibility of *ob/ob* hepatocytes towards hydroxyproline. Furthermore, it was investigated whether female *ob/ob* hepatocytes display the same results or react in a very different way. The precursor treatments were conducted as described in Chapter 2.2.10.2. Oxalate and glycolate levels in the supernatants were measured with LC/MS-MS.

Primary *ob/ob* hepatocytes from male mice excreted more oxalate than *ob/+* hepatocytes upon treatment with 31.6 mM hydroxyproline (*ob/ob* with 31.6 mM: 17.30 ± 5.11 nmol/mg protein; *ob/+* with 31.6 mM: 7.93 ± 1.80 nmol/mg protein) while the other precursors increased the oxalate excretion in both *ob/+* and *ob/ob* hepatocytes to the same extent (Fig. 3.2 A). This confirmed the results from the previous study (Gianmoena 2017). Additionally, the hepatocytes from male *ob/ob* mice produced more glycolate when treated with 10 mM (2.39 ± 1.55-fold change) and 31.6 mM hydroxyproline (2.73 ± 0.99-fold change) compared to *ob/+*

hepatocytes whereas glyoxylate exposure increased the glycolate excretion to the same extent in both genotypes (Fig. 3.2 B).

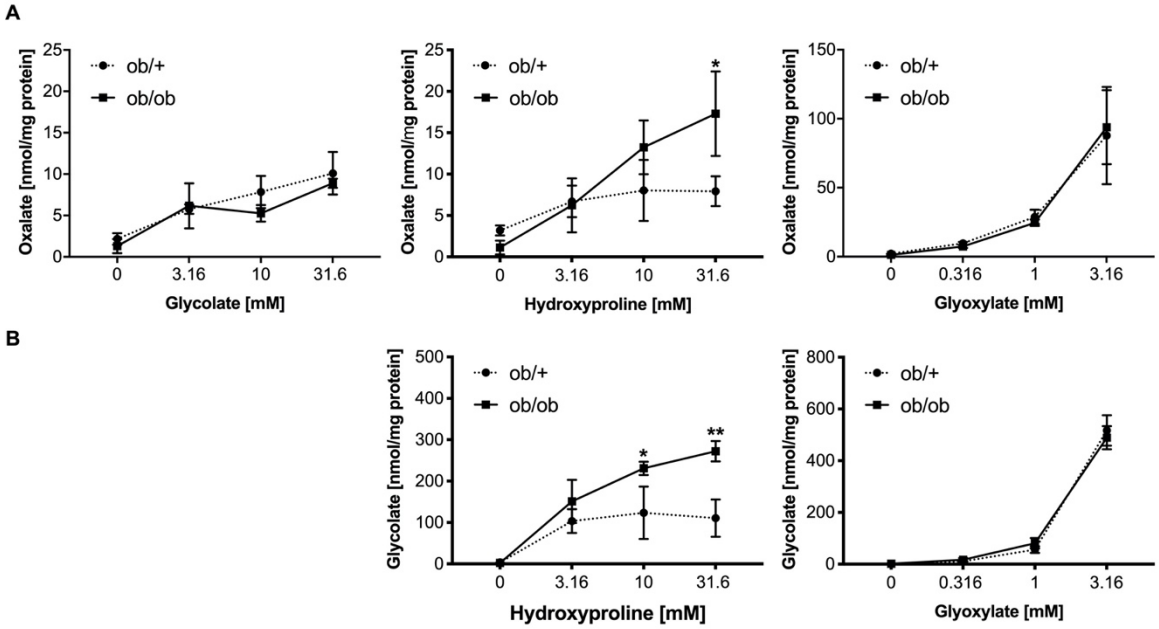

Figure 3.2: Oxalate precursor challenge of primary hepatocytes from male *ob/+* and *ob/ob* mice. Primary hepatocytes of male *ob/ob* mice excreted higher amounts of oxalate when treated with 31.6 mM hydroxyproline compared to *ob/+* hepatocytes. Glycolate and glyoxylate exposure enhanced the oxalate excretion in both genotypes to the same extent (A). Hydroxyproline treatment resulted in elevated glycolate excretion from *ob/ob* hepatocytes compared to *ob/+* while glyoxylate increased the glycolate release in ob/+ and ob/ob hepatocytes without any differences between the two groups (B). The means ± SD are shown. * p < 0.05, ** p < 0.01. Student's t test, unpaired, two sided.

In female mice, treatment with 10 mM (11.77 ± 2.15 nmol/mg protein) and 31.6 mM hydroxyproline (13.93 ± 1.40 nmol/mg protein) resulted in an increase oxalate excretion of *ob/ob* hepatocytes compared to wildtype (wt) control hepatocytes (10 mM hydroxyproline: 7.70 ± 0.78 nmol/mg protein; 31.6 mM hydroxyproline: 7.33 ± 1.20 nmol/mg protein; Fig. 3.3 A). Glyoxylate and glycolate treatment elevated the oxalate excretion in both wt and *ob/ob* female hepatocytes without any differences between the genotypes (Fig. 3.3 A). Further, exposure to 31.6 mM hydroxyproline led to higher glycolate excretion from female *ob/ob* hepatocytes compared to wt controls. Glyoxylate challenge gradually increased the glycolate excretion to the same extent in both genotypes (Fig. 3.3 B). These results mirrored the ones obtained from male *ob/ob* and *ob/+* hepatocytes. Moreover, there were no pronounced differences in oxalate and glycolate excretion due to the treatments of the different precursors when comparing male to female control hepatocytes, except for a slightly higher generation of oxalate from glycolate in males. This may be explained by a previously reported male-predominant expression of Hao1 (Breljak et al. 2015).

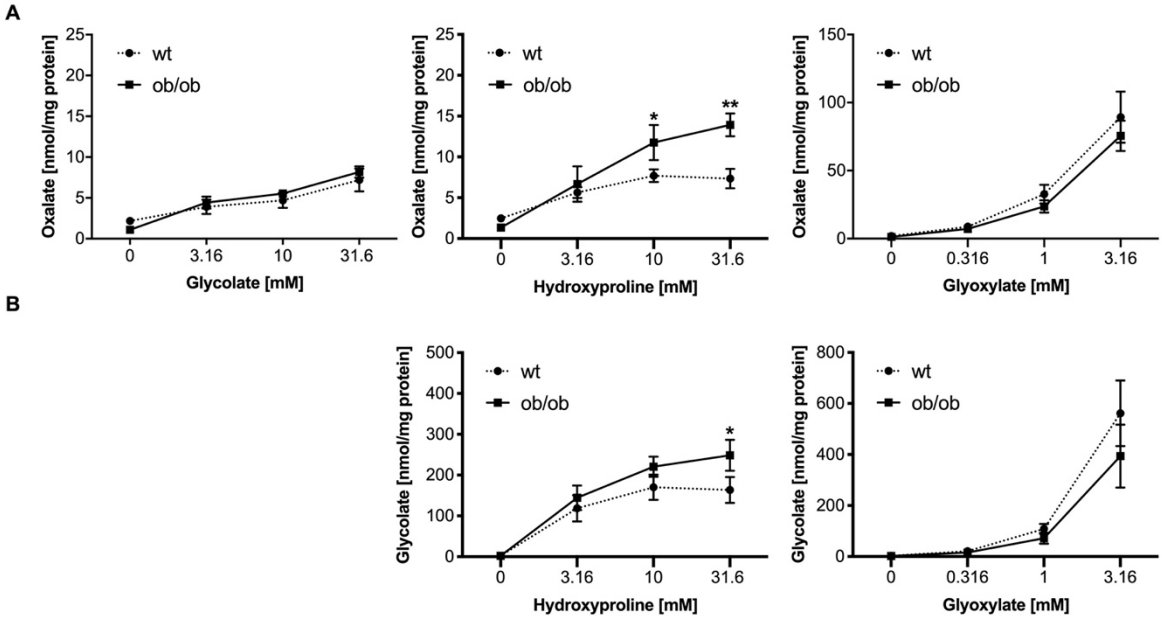

Figure 3.3: Treatment of primary hepatocytes from female wt and *ob/ob* mice with oxalate precursors. Exposure to glyoxylate and glycolate increased the oxalate excretion in *ob/+* and *ob/ob* mice to the same extent whereas hydroxyproline treatment led to higher oxalate excretion from *ob/ob* hepatocytes compared to *ob/+* (A). Glycolate excretion was higher in *ob/ob* hepatocytes when treated with 31.6 mM hydroxyproline compared to *ob/+* hepatocytes. Glyoxylate treatment increased glycolate excretion to the same extent in both genotypes (B). * p < 0.05, ** p < 0.01. Student's t test, unpaired, two sided.

These results confirmed the increased susceptibility of *ob/ob* male hepatocytes towards hydroxyproline regarding oxalate and glycolate excretion which was further verified in female *ob/ob* hepatocytes. Since the expression of enzymes catabolising hydroxyproline to glyoxylate was not altered, the elevation in oxalate production of *ob/ob* hepatocytes due to hydroxyproline treatment can be interpreted as the consequence of the *Agxt* downregulation. Altogether, the hydroxyproline catabolism seems to be the critical pathway leading to enhanced oxalate and glycolate generation in the hepatocytes of male and female *ob/ob* mice.

3.2.2 Treatment of primary *ob/+* and *ob/ob* hepatocytes with hydroxyproline influences protein expression of Agxt and Hao1

Whether the treatment of primary hepatocytes with oxalate precursors influences the expression of Agxt and Hao1 on protein level was investigated *via* immunoblotting. In control ob/+ hepatocytes, protein levels of Agxt were increased by the treatment with 31.6 mM hydroxyproline (0.91 ± 0.05 Agxt/β-actin-ratio) compared to the non-treated control cells (0.69 ± 0.09 Agxt/β-actin-ratio). However, Agxt expression in *ob/ob* hepatocytes was not altered by hydroxyproline (Fig. 3.4 B). The treatment with glycolate and glyoxylate did not influence Agxt protein expression neither in *ob/+* nor in *ob/ob* hepatocytes (Fig. 3.4 A, C). On the other hand, the Hao1 protein expression in *ob/+* cells was elevated by all hydroxyproline concentrations. However, exposure of *ob/ob* hepatocytes to hydroxyproline did not lead to an increase of Hao1 protein expression (Fig. 3.4 E). The glyoxylate and glycolate challenges increased the density of the Hao1 protein band on the immunoblots but densitometrical analysis revealed no statistical significance due to high standard deviations for both genotypes (Fig. 3.4 D, F). Furthermore, the downregulation of Agxt and Hao1 in *ob/ob* hepatocytes can

be seen (Fig. 3.4 B, C, and E). The combination of the lower Agxt protein levels and the missing increase upon hydroxyproline treatment in *ob/ob* hepatocytes might further contribute to the higher susceptibility of *ob/ob* hepatocytes towards hydroxyproline.

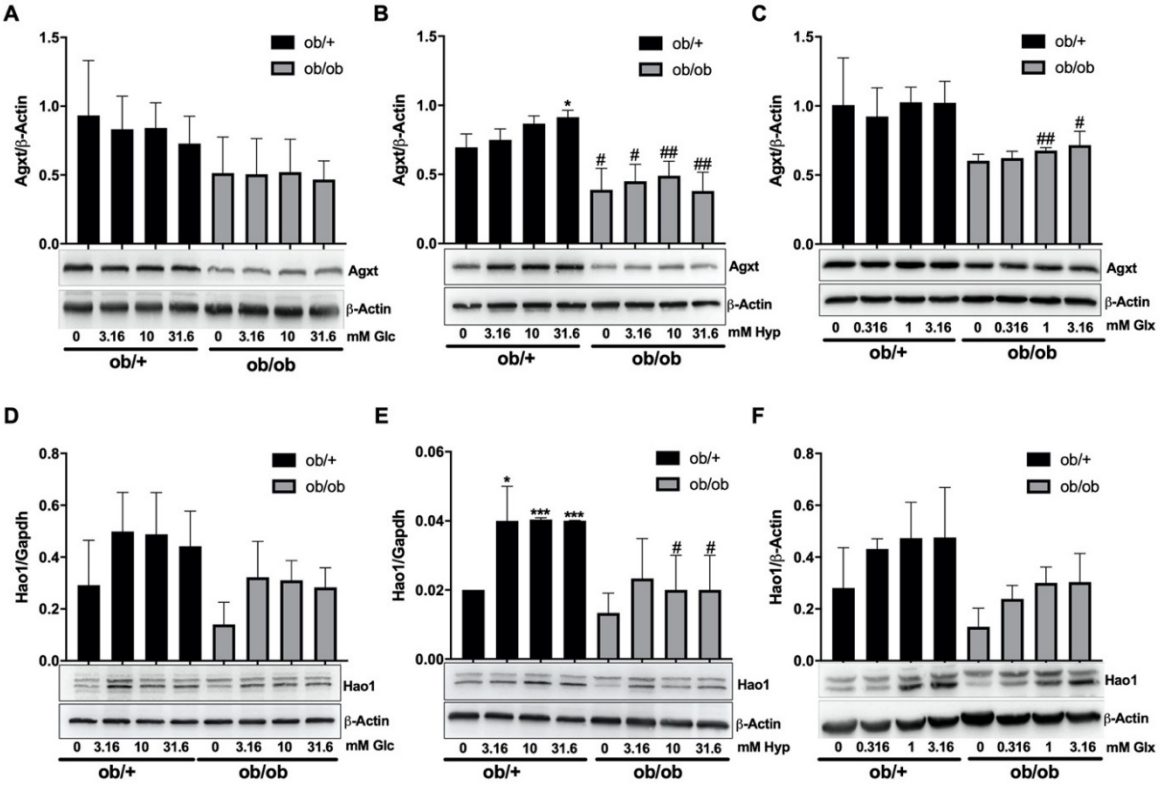

Figure 3.4: Influence of oxalate precursor exposure on Agxt and Hao1 protein expression in primary *ob/+* and *ob/ob* hepatocytes. Glycolate challenge (A) and glyoxylate treatment (C) did not influence Agxt protein expression while the highest hydroxyproline concentration slightly elevated Agxt protein levels in *ob/+* hepatocytes (B). Hao1 protein expression was not significantly influenced by glycolate and glyoxylate treatment (D + F) but hydroxyproline increased Hao1 protein levels in ob/+ and ob/ob hepatocytes (E). The bar graphs above each immunoblot represents the densitometric quantification of the corresponding blot below. Glc = glycolate; Hyp = hydroxyproline; Glx = glyoxylate. The means ± SD of three independent experiments are shown. * p < 0.05, ** p < 0.01, *** p < 0.001 for comparison between treated and non-treated (FM) cells. # p < 0.05, ## p < 0.01 for comparing *ob/ob* and *ob/+*. Student's t test, unpaired, two sided.

3.2.3 Inhibition of Prodh2 in hydroxyproline challenged primary hepatocytes leads to reduced oxalate production

The importance of the hydroxyproline pathway in the glyoxylate metabolism in primary *ob/+* and *ob/ob* mice was analysed further. Therefore, the proline dehydrogenase 2 (Prodh2), which catalyses the first step in hydroxyproline catabolism (Adams and Frank 1980), was inhibited in primary *ob/+* and *ob/ob* by using tetrahydrofuroic acid (THFA), a known Prodh2 inhibitor (Zhang et al. 2004). THFA replaces the nitrogen atom in proline and hence prevents opening of the ring during the enzymatic reaction. The experiment was conducted as described in Chapter 2.2.10.3. Oxalate levels in the supernatants were measured by LC/MS-MS and adjusted by protein content of the same sample (Fig. 3.5).

The treatment with hydroxyproline increased the oxalate excretion in *ob/+* and *ob/ob* hepatocytes as reported before (Fig. 3.5, (Gianmoena 2017). The oxalate production of *ob/ob* (22.57 ± 2.33 nmol oxalate/mg protein) hepatocytes was significantly higher compared to *ob/+* (14.96 ± 1.96 nmol oxalate/mg protein) when treated with 31.6 mM hydroxyproline, showing the already mentioned higher susceptibility of *ob/ob* hepatocytes towards hydroxyproline (Gianmoena 2017). Furthermore, the treatment with 10 mM THFA led to a significantly decreased oxalate excretion for all hydroxyproline concentrations in *ob/+* hepatocytes compared to the corresponding samples without THFA (black bar, Fig. 3.5). This effect of THFA could be observed in *ob/ob* hepatocytes treated with 31.6 mM hydroxyproline (without THFA: 22.57 ± 2.33 nmol oxalate/mg protein; with 10 mM THFA: 16.6 ± 2.87; nmol oxalate/mg protein; Fig. 3.5). Remarkably, the THFA treatment lowered the oxalate excretion to the level of *ob/+* hepatocytes. These results underpin the crucial role of the hydroxyproline catabolism in *ob/ob* hepatocytes. The inhibition of hydroxyproline breakdown leads to a decreased production of mitochondrial glyoxylate which is detoxified by mitochondrial Agxt or Grhpr (Wu et al. 2011; Fargue et al. 2018). Without THFA treatment, the *ob/ob* hepatocytes were not able to detoxify glyoxylate efficiently due to the Agxt downregulation, and therefore produced more oxalate than *ob/+* hepatocytes. Due to the THFA-mediated inhibition of mitochondrial glyoxylate production, *ob/ob* hepatocytes decreased their oxalate production to the same extent as *ob/+* hepatocytes. Therefore, this result supports the hypothesis that the insufficient mitochondrial Agxt might be the reason for the increased oxalate production of *ob/ob* hepatocytes upon hydroxyproline exposure.

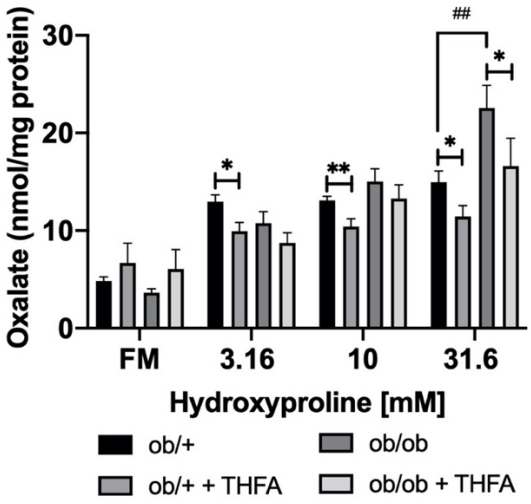

Figure 3.5: THFA treatment lowers oxalate production from hydroxyproline catabolism in primary *ob/+* and *ob/ob* hepatocytes. Hydroxyproline led to elevated oxalate excretion in *ob/+* and *ob/ob* hepatocytes, while the oxalate production of *ob/ob* hepatocytes was higher compared to *ob/+* when treated with 31.6 mM hydroxyproline. Oxalate excretion was decreased upon treatment with 10 mM THFA for all used hydroxyproline concentrations in *ob/+* hepatocytes. This effect could also be observed for *ob/ob* hepatocytes upon treatment with the highest hydroxyproline concentration. THFA = tetrahydrofuroic acid. The means ± SD are shown. * p < 0.05, ** p < 0.01 for comparison of with and without THFA treatment. ## p < 0.01 for comparison between *ob/+* and *ob/ob*. Student's t test, unpaired, two sided.

3.2.4 Rescuing *Agxt* expression in *ob/ob* hepatocytes reduced hydroxyproline-derived oxalate excretion

To further investigate the contribution of the *Agxt* downregulation to the increased hydroxyproline-derived oxalate excretion from *ob/ob* hepatocytes, primary hepatocytes from *ob/+* and *ob/ob* mice were transduced with adeno-associated viral particles containing either a pAAV-CMV-EGFP control vector or a pAAV-CMV-mAgxt vector (n=5) which enables expression of mitochondrial Agxt. The transduction was performed as described in Chapter 2.2.15. The Agxt expression was verified with qRT-PCR and immunoblotting.

Agxt mRNA levels showed a trend to increase upon pAAV-CMV-mAgxt transduction in both *ob/+* and *ob/ob* hepatocytes (Fig. 3.6 A). Immunoblots revealed an upregulation of Agxt protein expression in *ob/ob* but surprisingly not in *ob/+* hepatocytes (Fig. 3.6 B). This was confirmed in immunoblots from all five independent experiments (data not shown). Hence, it seems like *ob/+* hepatocytes may translate the *Agxt* mRNA less efficiently. This data does not differentiate whether this is a general or Agxt specific problem.

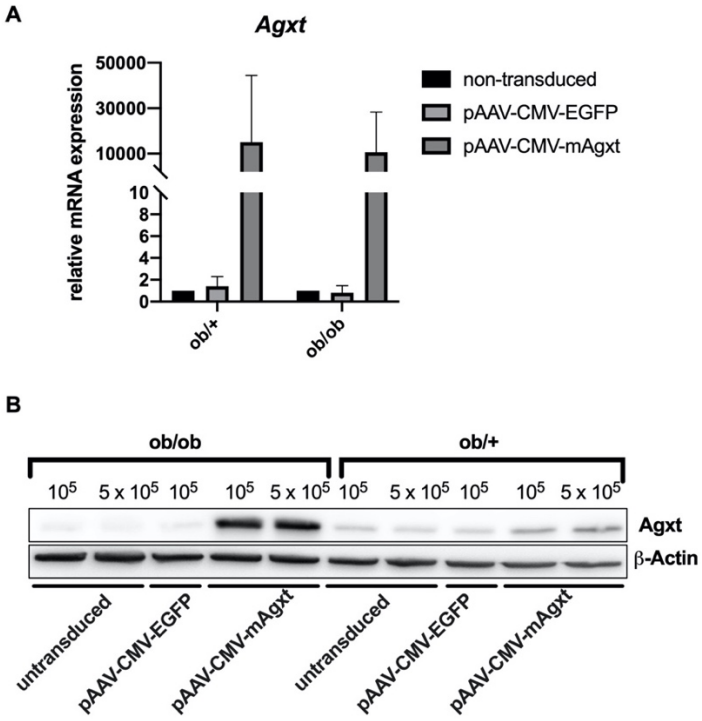

Figure 3.6: Agxt expression in pAAV-CMV-mAgxt transduced primary hepatocytes from *ob/+* and *ob/ob* mice. *Agxt* mRNA expression was elevated upon transduction with pAAV-CMV-Agxt in *ob/+* and *ob/ob* hepatocytes (n=5; A). Representative immunoblot from the first experiment showing the upregulation of Agxt protein expression in *ob/ob* hepatocytes which were transduced with pAAV-CMV-mAgxt. Protein expression of Agxt was not altered by pAAV-CMV-mAgxt transduction in *ob/+* hepatocytes. Transductions were carried out with 10^5 and 5 x 10^5 genome copies (GC)/cell of viral particles (B).

Oxalate measurements in the supernatants showed that *ob/ob* hepatocytes, which were transduced with the pAAV-CMV-mAgxt containing viral particles, displayed a significantly reduced oxalate excretion when exposed to 31.6 mM hydroxyproline compared to pAAV-CMV-EGFP transduced hepatocytes (Fig. 3.7). Thus, overexpressing Agxt in *ob/ob* hepatocytes reduced the production of oxalate after hydroxyproline catabolism. This effect was not

observed in *ob/+* hepatocytes (Fig. 3.7). This suggests, that the mitochondrial Agxt expression is pivotal for preventing hydroxyproline-derived oxalate production within primary hepatocytes of *ob/ob* mice.

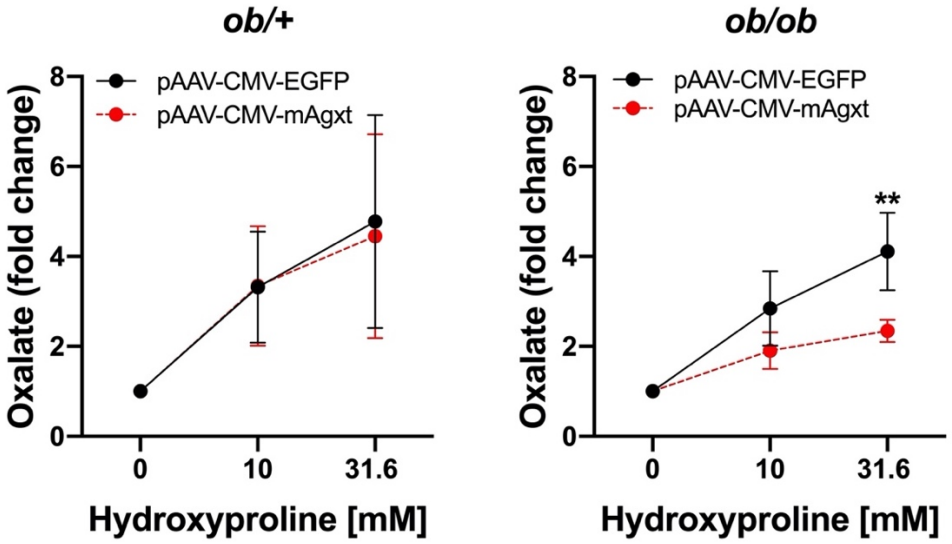

Figure 3.7: Oxalate levels in the supernatants of primary hepatocytes from *ob/+* and *ob/ob* which were transduced with pAAV-CMV-mAgxt and pAAV-CMV-EGFP after metabolising of hydroxyproline (n=5). Primary hepatocytes from *ob/ob* mice (B) exhibited a reduced oxalate excretion after 31.6 mM hydroxyproline exposure when transduced with pAAV-CMV-mAgxt compared to pAAV-CMV-EGFP. This was not observed in primary hepatocytes from *ob/+* mice. The means ± SD are shown. ** p < 0.01. Student's t test, unpaired, two sided.

3.3 Impact of dietary hydroxyproline in *ob/+* and *ob/ob* mice *in vivo*

The consequences of a deregulated glyoxylate metabolism upon hydroxyproline treatment in hepatocytes of *ob/ob* mice have been studied *in vitro*. Whether these results can be confirmed *in vivo* was studied next. Also, the question whether hydroxyproline leads to increased oxalate production by the liver and increased oxalate levels in the urine of *ob/ob* mice needed to be clarified. Finally, also a potential damage and calcium oxalate stone formation in kidney tissue was analysed as well.

For this purpose, *ob/ob* and *ob/+* mice were either fed a normal chow diet (NCD) or a hydroxyproline enriched diet (1% Hyp) for 10 days (n=5). Parameters like water intake, food intake and body weight were recorded daily. After seven days, 24 h urine sample were collected as outlined in Chapter 2.2.4 for three consecutive days. Again, food and water intake, as well as the urine volume were recorded daily. Afterwards, the mice were put back into normal cages and were sacrifice the next day. Tissue from the liver and kidney was collected for histological staining, mRNA and protein expression analyses, as well as triglyceride content measurements. Plasma was collected from the portal vein, hepatic vein and the right heart chamber for oxalate measurements in order to understand the hepatic inflow and outflow of oxalate as well as the systemic plasma oxalate concentration (Fig. 3.8). Urinary and plasma oxalate levels were analysed by LC/MS-MS.

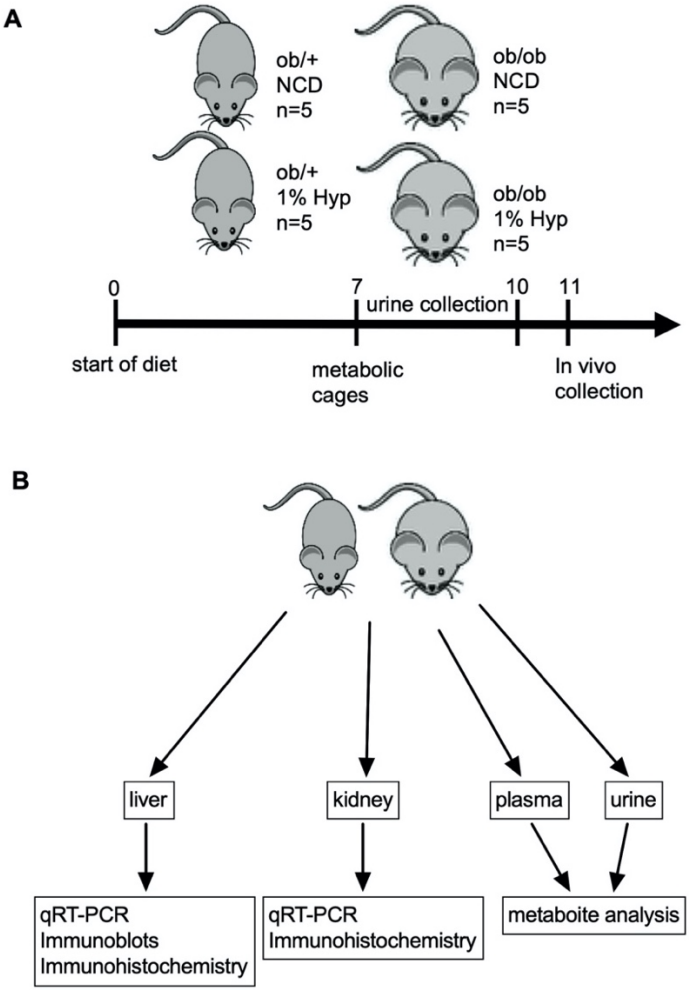

Figure 3.8: Schematic illustration of experimental design for hydroxyproline enriched diet in *ob/+* and *ob/ob* mice. Experimental design and time course for hydroxyproline challenge *in vivo* in *ob/+* and *ob/ob* mice (n=5; A). Scheme showing different approaches for analysing possible consequences of hydroxyproline enriched diet (B).

3.3.1 Basic parameters of NCD-fed and 1%Hyp-fed *ob/ob* and *ob/+* mice

All *ob/ob* mice displayed elevated body weight, liver weight and an increased liver to body weight ratio compared to their lean counterparts (Fig. 3.9 A). The hepatic triglyceride levels were significantly elevated in the *ob/ob* mice compared to *ob/+* (Fig. 3.9 B). None of these parameters were influenced by the 1% Hyp diet neither in *ob/+* nor in the *ob/ob* mice. The *ob/ob* mice showed an elevated food consumption (6.07 ± 1.55 g/day for *ob/ob* NCD) compared to *ob/+* mice (4.38 ± 0.49 g/day for *ob/+* NCD), in agreement with their reporter hyperphagia (Mayer et al. 1953; Garthwaite et al. 1980). The amount of consumed food was not influenced by the 1% Hyp diet, neither in *ob/+* (4.07 ± 0.52 g/day) nor in *ob/ob* mice (5.79 ± 1.05 g/day; Fig. 3.9 C). The water intake did not differ between the genotypes. In the case of *ob/ob* mice the 1% Hyp diet (5.17 ± 0.8 mL/day) led to a decreased water consumption compared to *ob/ob* on NCD (6.12 ± 0.6 mL/day; Fig. 3.9 C). Further, the urine volume of *ob/ob* mice were increased by 3- (*ob/ob* NCD vs. ob/+ NCD) and 2- fold (*ob/ob* 1% Hyp vs. *ob/+* 1% Hyp) compared to their lead counterparts on the same diet. The higher urine volume in the *ob/ob* mouse groups was reflected by the decreased urinary creatinine concentration

Creatinine contents in *ob/+* and *ob/ob* were not impacted by dietary hydroxyproline (Fig. 3.9 C). Since the amount of creatinine excretion per day (mg/24 h) was not different between the groups (data not shown), the elevated urine volume and decreased creatinine concentrations in *ob/ob* mice suggest an increased water excretion.

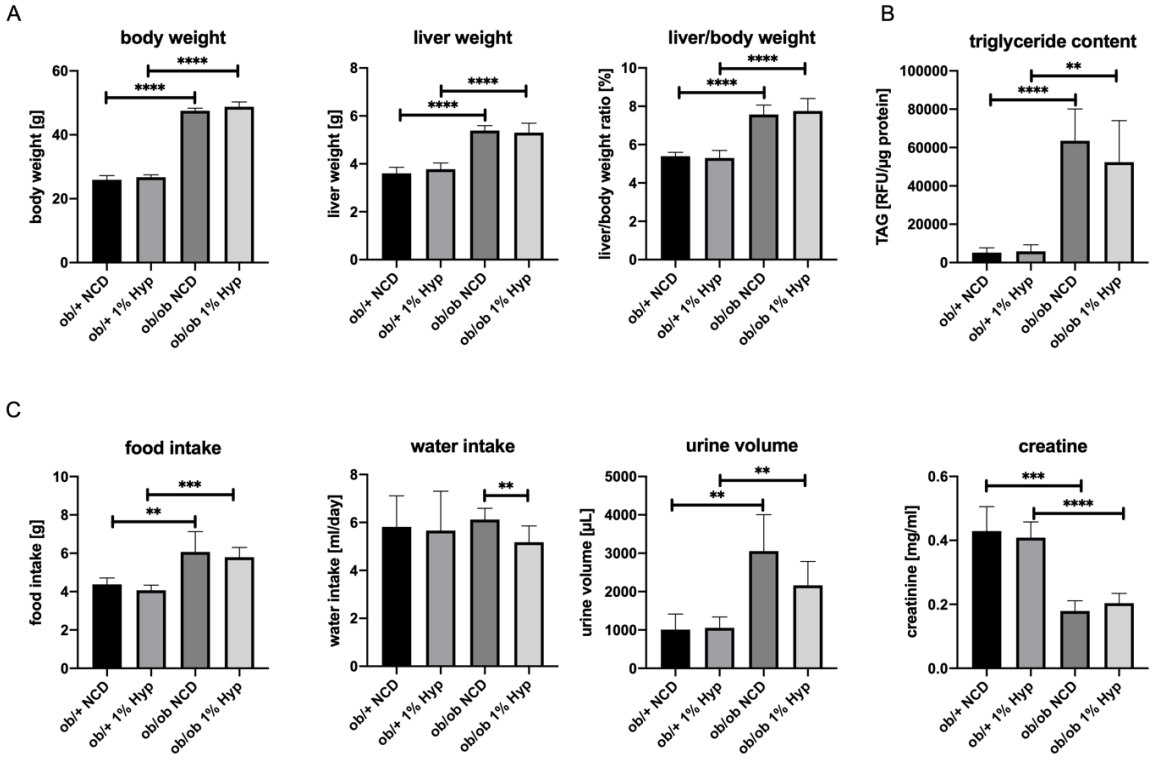

Figure 3.9: Basic parameters of *ob/+* and *ob/ob* mice fed with normal chow diet and 1% Hyp diet. Body weight, liver weight and liver to body weight ratio were increased in *ob/ob* mice fed with NCD and 1% Hyp (A). Elevated triglyceride levels in *ob/ob* livers compared to *ob/+* (B). 1% Hyp diet did not impact parameters depicted in A - C) The food intake and urine volume were higher in *ob/ob* mice independently of their diet. Creatinine concentrations were decreased in *ob/ob* mice compared to *ob/+* and not influenced by the diet in both genotypes. There was no difference in water intake when comparing *ob/ob* to *ob/+*. *Ob/ob* mice on 1% Hyp diet exhibit a lower water intake compared to NCD. The means ± SD are shown. * p < 0.05, ** p < 0.01, *** p < 0.001. Student's t test, unpaired, two sided.

3.3.2 Hydroxyproline leads to a higher urinary oxalate excretion in *ob/+* and *ob/ob* mice

The urinary oxalate excretion was analysed by LC/MS-MS measurements in 24 h-urine collected on three consecutive days from *ob/+* and *ob/ob* mice which were fed either a NCD or 1% Hyp diet (n=5; Fig. 3.10). The oxalate concentration was normalised for the daily urinary creatinine excretion or the 24 h-urine volume in order to determine the oxalate/creatinine ratio as well as the 24 h oxalate excretion, respectively. The hydroxyproline enriched diet caused increased urinary oxalate excretion in *ob/+* (542.6 ± 18.40 mg oxalate/g creatinine) and *ob/ob* mice (942.4 ± 55.64 mg oxalate/g creatinine) compared to ob/+ NCD (126.6 ± 3.99 mg oxalate/g creatinine) and ob/ob NCD (230.1 ± 10.47 mg oxalate/g creatinine). Furthermore, the *ob/ob* plus 1% Hyp group exhibited significantly elevated urinary oxalate amounts compared to 1% Hyp-fed *ob/+* mic (Fig. 3.10) even after adjustment for the higher food and hydroxyproline intake of *ob/ob* mice (data not shown). These results were also

observed when normalising the oxalate levels for the 24 h-urine volume (Fig. 3.10). Additionally, the hyperoxaluria of *ob/ob* mice which was observed in a previous study could also be confirmed for these animals (Fig. 3.10). Taken together, this data shows the ability of hydroxyproline metabolism to impact urinary oxalate excretion in both genotypes, but this effect is stronger in *ob/ob* mice due to the deregulated hepatic glyoxylate metabolism.

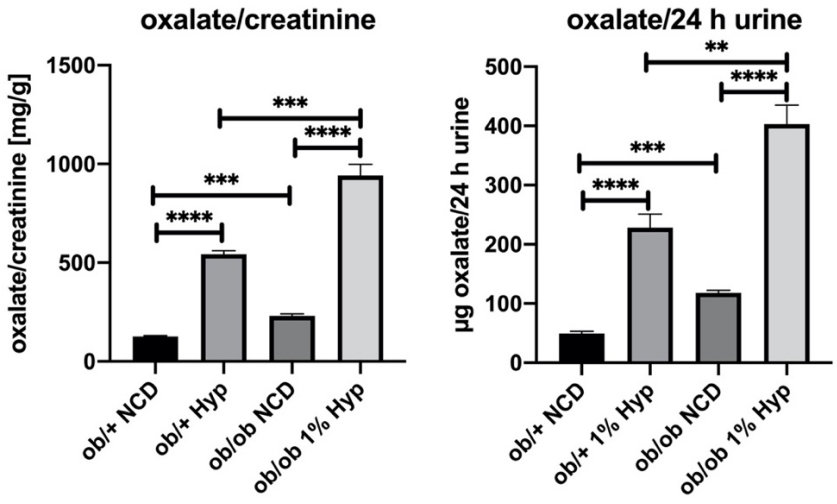

Figure 3.10: Urinary oxalate levels in the 24 h-urine of *ob/+* and *ob/ob* fed either a normal chow or 1% Hyp diet. The urinary oxalate concentrations were measured by LC/MS-MS and normalised for the daily creatinine excretion or 24 h-urine volume. For both normalisations, the 1% Hyp diet resulted in significantly elevated urinary oxalate excretion in *ob/+* and *ob/ob* mice compared to the corresponding NCD groups. Also, the *ob/ob* plus 1% Hyp group displayed higher urinary oxalate levels compared to the *ob/+* plus 1% Hyp group for both normalisations. The means ± SEM are shown. ** p < 0.01, *** p < 0.001. Student's t test, unpaired, two sided.

3.3.3 Plasma concentration of oxalate is elevated in 1%-Hyp-fed *ob/ob* mice

As already introduced, plasma from the portal vein and hepatic vein was collected from each mouse to analyse the rate of oxalate flowing into and out of the liver, respectively. Also, the oxalate concentration in the plasma obtained from the right heart chamber was collected to analyse the systemic oxalate levels in the different groups of mice. Measurements with LC/MS-MS revealed a significantly increased oxalate concentration in the plasma obtained from the hepatic vein of 1% Hyp-fed *ob/ob* mice (41.53 ± 4.04 µM) compared to the other groups (ob/+ NCD: 18.05 ± 3.82 µM; *ob/+* 1% Hyp: 18.55 ± 1.83 µM; *ob/ob* NCD: 22.53 ± 3.9 µM; Fig. 3.11). Adjustment of these values to the higher Hyp intake of *ob/ob* mice did not alter the results (data not shown). Further, the ratio of the hepatic oxalate outflow (hepatic vein) to the inflow into the liver (portal vein) was also elevated in the *ob/ob* plus 1% Hyp group (Fig. 3.11). These results suggest that, the steatotic liver of *ob/ob* mice produce more oxalate *in vivo* only when challenged with dietary hydroxyproline. This is consistent with the *in vitro* results from previous studies (Gianmoena 2017). A systemic increase of oxalate was not observed (Fig. 3.11). This might be due to a dilution of the blood from hepatic vein by venous blood from the general circulation. Additionally, the renal excretion of oxalate might also play a role.

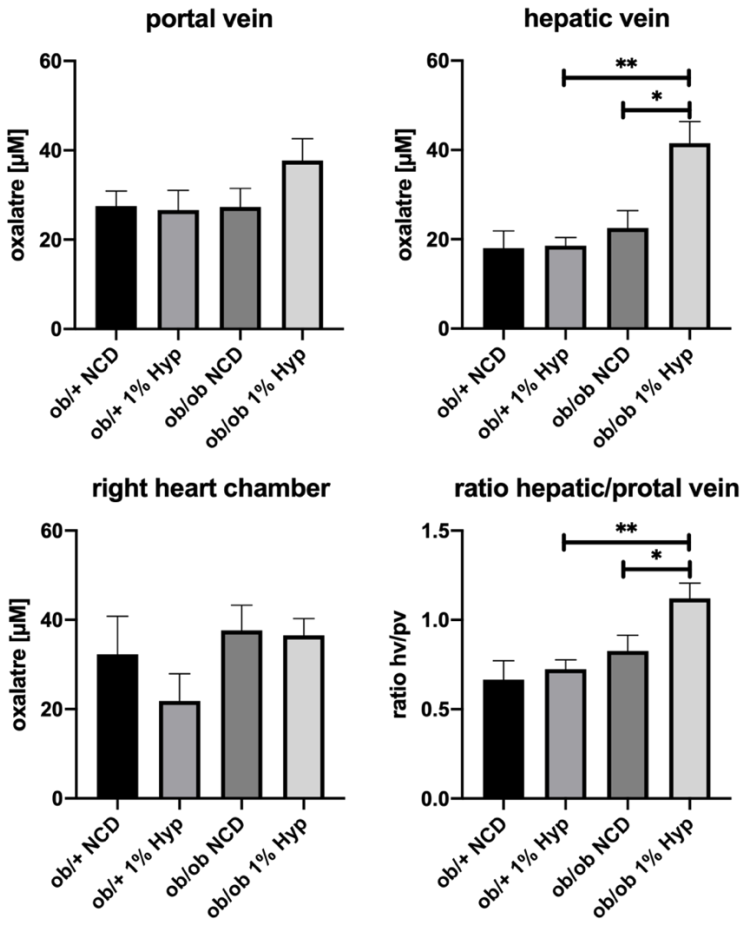

Figure 3.11: Oxalate concentrations in the plasma obtained from portal vein, hepatic vein and right heart chamber of *ob/+* and *ob/ob* mice fed with NCD or 1%Hyp. Increased oxalate concentration could be observed in the plasma from hepatic vein of *ob/ob* mice fed a 1% Hyp diet compared to the other groups. Also, the oxalate ratio of hepatic to portal vein was significantly enhanced in the same group. The means ± SEM are shown. * p < 0.05, ** p < 0.01. Student's t test, unpaired, two sided.

3.3.4 Expression of glyoxylate metabolism enzymes in 1% Hyp-fed mice

Whether the hydroxyproline enriched diet influences the hepatic and renal gene expression of glyoxylate metabolism enzymes was analysed *via* qRT-PCR and/or immunoblotting in the liver and kidney tissue of *ob/+* and *ob/ob* mice.

3.3.4.1 Expression of hepatic glyoxylate metabolism enzymes is influence by dietary hydroxyproline

The already mentioned deregulations in *Agxt*, *Hao1* and *Ldha* in the livers of *ob/ob* mice compared to *ob/+* were further confirmed in these animals (Fig. 3.12 A). There were no changes detected in the mRNA levels of *Grhpr*, *Prodh2* and *Hoga1* between the genotype (Fig. 3.12 B). Furthermore, the 1% Hyp diet did not influence the gene expression of *Hao1*, *Ldha*, *Grhpr*, *Prodh2* and *Hoga1* in both genotypes. However, the dietary Hyp slightly decreased the Agxt mRNA in the livers *ob/ob* fed 1% Hyp compared to *ob/ob* mice on NCD (fold change of -1.3 ± 0.19; Fig. 3.12 A).

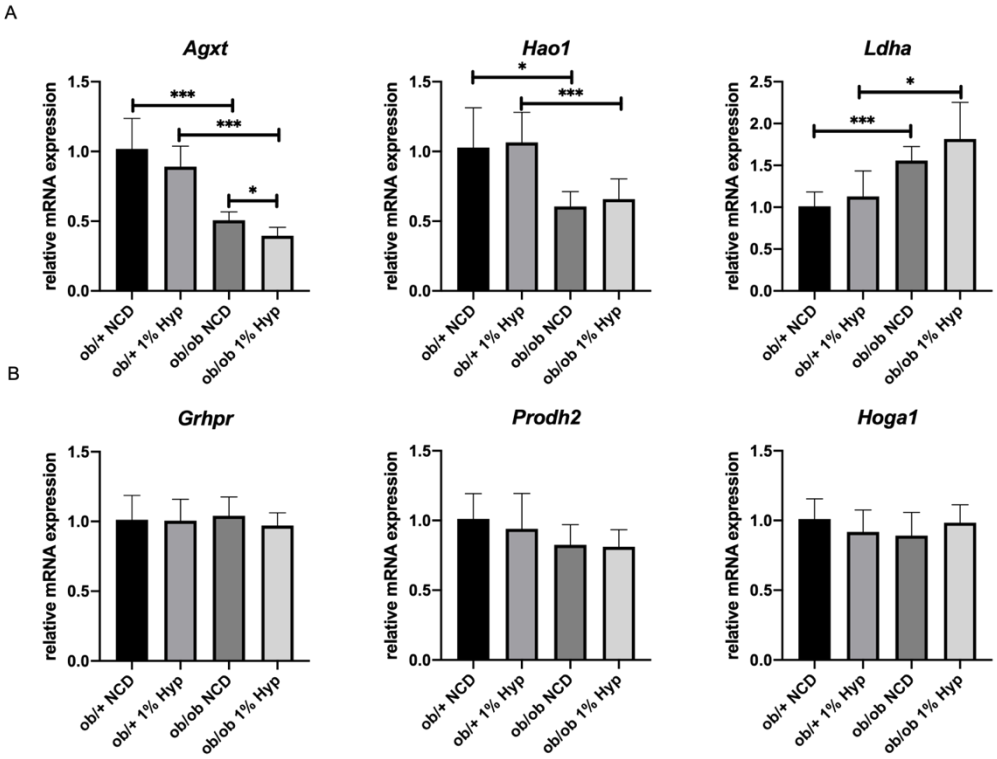

Figure 3.12: Gene expression of glyoxylate metabolism enzymes in livers of *ob/+* and *ob/ob* fed a NCD and 1% Hyp diet. The mRNA expression of *Agxt* and *Hao1* was decreased and *Ldha* mRNA levels were increased in both *ob/ob* groups. The 1% Hyp diet decreased *Agxt* mRNA levels in the livers of *ob/ob* but did not impact the expression of *Hao1* or *Ldha* (A). There were no changes detected in the mRNA levels of *Grhpr*, *Prodh2* and *Hoga1* between the genotypes and the hydroxyproline enriched diet did not influence the mRNA expression of these genes (B). Eif2a was used as endogenous control. n=5 for all groups. The means ± SD are shown. * p < 0.05, ** p < 0.01, *** p < 0.001. Student's t test, unpaired, two sided.

The protein levels of Agxt were decreased in the livers of both dietary *ob/ob* groups. The 1% Hyp diet not affect Agxt protein expression neither in *ob/+* nor in *ob/ob* mice (Fig. 3.13 A). The hepatic downregulation of Hao1 protein expression in *ob/ob* mice was also confirmed for these animals. As already seen *in vitro* in primary *ob/+* hepatocytes (Fig. 3.4), the protein levels of Hao1 increased in the livers of *ob/+* mice upon hydroxyproline (0.34 ± 0.03 Hao1/Gapdh ratio for NCD vs. 0.55 ± 0.03 Hao1/Gapdh-ratio for 1% Hyp). Additionally, dietary hydroxyproline enhanced the Hao1 protein levels also *in vivo* in the liver of *ob/ob* mice with 1% Hyp (0.49 ± 0.06 Hao1/Gapdh-ratio) compared to *ob/ob* mice on NCD (0.16 ± 0.02 Hao1/Gapdh-ratio; Fig. 3.13 B). Furthermore, densitometric analysis of Ldha protein levels revealed no differences when comparing the phenotypes but a slight downregulation by 1% Hyp diet in the livers of *ob/+* mice (0.37 ± 0.04 Ldha/Gapdh ratio for NCD vs. 0.3 ± 0.02 Ldha/Gapdh-ratio for 1% Hyp; Fig. 3.13 C).

The hydroxyproline induced upregulation of Hao1 accompanied by the missing effect on Agxt expression leads to an enhanced Hao1 to Agxt ratio in the livers of *ob/ob* fed the 1% Hyp diet. This might result in a higher glyoxylate production and a decreased detoxification, subsequently leading to elevated hepatic oxalate levels. The decreased protein expression for Ldha in *ob/+* mice plus 1% Hyp group might be due to an increased glyoxylate detoxification to glycolate *via* Grhpr in the mitochondria. The slight 1% Hyp-triggered downregulation of

Agxt mRNA in the livers of *ob/ob* mice could not be confirmed on protein levels, and hence might not be physiologically relevant.

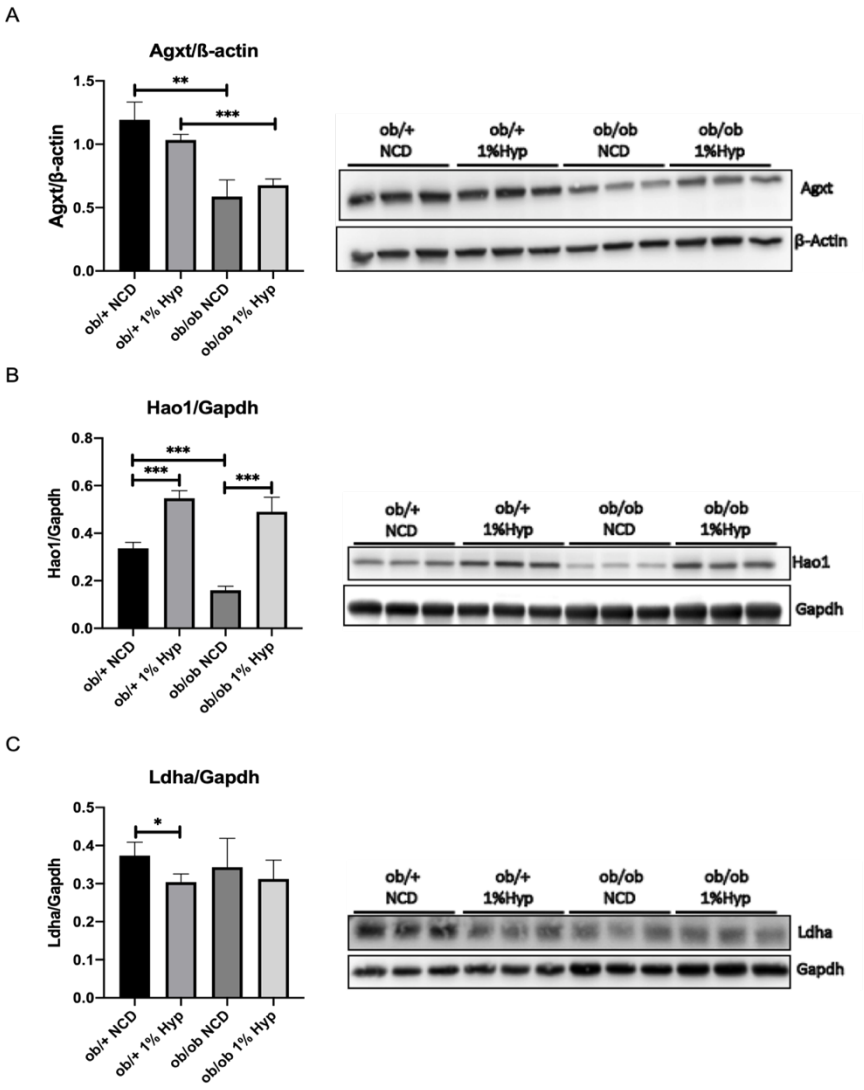

Figure 3.13: Protein expression of glyoxylate metabolism enzymes in the livers of *ob/+* and *ob/ob* mice fed either a NCD or 1% Hyp diet. The Agxt protein levels were significantly decreased in the livers of both *ob/ob* diet groups. β-Actin was used as loading control (A). Dietary hydroxyproline elevated hepatic protein levels of Hao1 in *ob/+* and *ob/ob* mice. Gapdh was used as loading control (B). Densitometric analysis showed no difference between *ob/ob* and *ob/+* in the protein expression of Ldha, a slight decrease was observed in the livers of 1% Hyp fed *ob/+* mice. Gapdh was used as loading control (C). The means ± SD are shown. * p < 0.05, ** p < 0.01, *** p < 0.001. Student's t test, unpaired, two sided.

3.3.4.2 Renal expression of hydroxyproline catabolism enzymes in *ob/ob* mice

The influence of obesity and a 1% Hyp diet on the mRNA expression of glyoxylate metabolism enzymes in the kidneys of *ob/+* and *ob/ob* mice was analysed *via* qRT-PCR. The mRNA expression of *Grhpr*, *Hao1* and *Agxt* did not differ in the kidneys of *ob/ob* mice compared to *ob/+.* Contrary, alterations in mRNA expression were detected for *Prodh2* and *Hoga1*. The expression of *Prodh2* was upregulated in the kidney tissue of *ob/ob* mice (2.01 ± 0.36-fold change) compared to ob/+, while 1% Hyp diet did not influence the *Prodh2* mRNA level neither in *ob/+* nor in *ob/ob* mice (Fig. 3.13). Hoga1 mRNA expression was not altered in the kidney of

ob/ob mice compared to *ob/+* when fed a normal diet but it was upregulated by 1% Hyp diet in *ob/ob* mice (approx. 1.3-fold) compared to *ob/ob* mice on a normal chow diet (Fig. 3.14).

Hoga1 and *Prodh2 c*atalyse the first and the last step of mitochondrial hydroxyproline breakdown, respectively (Wu et al. 2011). Hence, upregulation of *Hoga1* due to hydroxyproline ingestion in the kidneys of *ob/ob* but not *ob/+* mice suggests that the dietary hydroxyproline may not be completely catabolised in the livers of *ob/ob* mice. Furthermore, the upregulation of *Prodh2* in the kidneys *ob/ob* mice indicate an enhanced production of mitochondrial glyoxylate out of hydroxyproline catabolism in the kidneys of *ob/ob.*

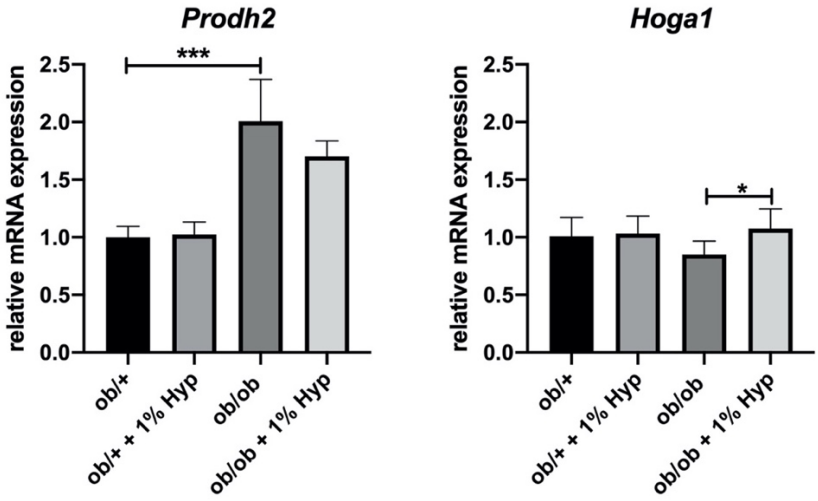

Figure 3.14: Expression *Prodh2* and *Hoga1* in the kidney of NCD-fed and 1% Hyp-fed *ob/+* and *ob/ob* mice. The mRNA expression of *Prodh2* was elevated in the kidney of *ob/ob* mice but not influenced by 1% Hyp diet in none of the genotypes. *Hoga1* mRNA expression was upregulated by 1% Hyp diet in the kidney of *ob/ob* mice but not in *ob/+* mice. The means ± SD are shown. * p < 0.05, *** p < 0.001. Student's t test, unpaired, two sided.

3.3.5 The hydroxyproline-enriched diet does not lead to histopathological alterations of the liver and kidney tissue

In order to study possible effects of dietary hydroxyproline in connection with the steatosis-related alterations of glyoxylate metabolism in the liver and kidneys of *ob/ob* mice, paraffin embedded tissue slides were stained with haematoxylin and eosin (H&E). The hydroxyproline-enriched diet did not impact the tissue structure of neither liver nor kidney (n=5; Fig. 3.15). Furthermore, cooperation partners from Munich (Prof. Hans-Joachim Anders) performed Pizzalato staining to investigate whether enhanced urinary oxalate levels after consumption of dietary hydroxyproline lead to the formation of calcium oxalate stones in the kidneys. However, no calcium oxalate deposits found in any of examined mice have been detected (data not shown).

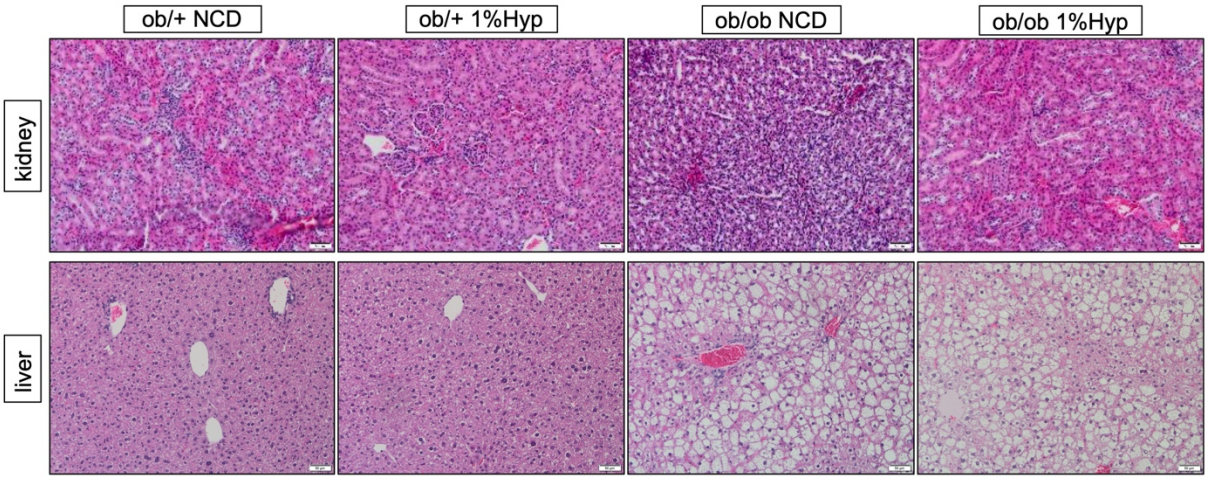

Figure 3.15: Representative images of the H&E staining of liver and kidney tissue of *ob/+* and *ob/ob* mice fed either NCD or 1% Hyp. The hydroxyproline enriched diet did not influence the structure of neither liver nor kidney tissue in *ob/+* and *ob/ob* mice. Hepatic steatosis was confirmed in both *ob/ob* dietary groups. Scale bars represent 50 µm.

3.4 Feeding a Western-type diet leads to expression and epigenetic alterations in the hepatic glyoxylate metabolism

Since the pathophysiology of NAFLD and NASH is strongly complex and comprised of a lot of different features, there are different mouse models to investigate NAFLD that recapitulate different histopathological and physiological characteristics of human NAFLD progression from steatosis to HCC (Lau et al. 2017). The *ob/ob* mouse model applied so far is a genetic model useful for studying simple steatosis but does not capture the development of NAFLD to NASH by an unhealthy lifestyle and diet (Ingalls et al. 1950; Zhang et al. 1994; Friedman et al. 1995). In order to understand whether a diet-induced steatosis also impacts the glyoxylate metabolism, the livers of mice, which were fed a western diet (WD) for 6, 12, 18, 24 and 30 weeks, were analysed in a previous study (Gianmoena 2017). It was shown that WD-induced steatosis lead to a decrease in *Agxt*, *Hao1* and *Hoga1* mRNA levels for 6-, 18- and 30-weeks Western diet while the expression of *Grhpr* was not influenced by the diet-induced steatosis (Gianmoena et al., not published). Moreover, urinary oxalate excretion was not elevated in 30 weeks WD-fed mice (Gianmoena 2017).

In this thesis, mice were fed a WD for 6 weeks and compared to aged matched controls which were fed a NCD (n=5). It could be shown that the mRNA (fold change: 1.43 ± 0.16) and protein expression of Ldha was significantly elevated in WD mice compared to NCD controls (Fig. 3.16 A, B). Further, immunoblotting confirmed a downregulation of Agxt protein expression in 6 weeks WD mice (Fig. 3.16 B). This data suggests an increased hepatic oxalate production in the livers of WD mice.

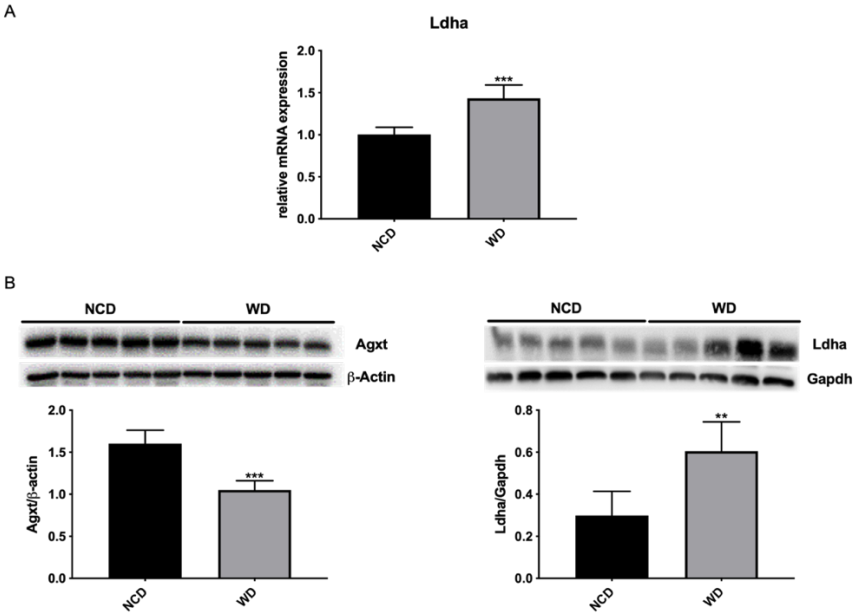

Figure 3.16: Protein and mRNA expression of Ldha and Agxt in 6 weeks WD mice. The expression of Ldha was elevated in 6 weeks WD mice on mRNA (A) and protein level (B). The downregulation of Agxt could be shown on immunoblotting for 6 weeks WD mice (B). The means ± SD are shown. ** p < 0.01, *** p < 0.001. Student's t test, unpaired, two sided.

In a former project, the IfADo participated in the German Epigenetic Programme (DEEP) in order to identify epigenetic alterations in NAFLD. DNA methylation was analysed by reduced representation bisulphite sequencing (RRBS) and revealed an *Agxt* promoter hypermethylation in the primary hepatocytes of *ob/ob* mice compared to *ob/+*. This observation was validated by targeted deep sequencing using specific primers for the *Agxt* promoter (Gianmoena et al., not published; Gianmoena 2017). For this work, isolated hepatocytes from 6 weeks WD mice and the aged matched NCD controls were analysed for DNA hypermethylation. Targeted deep sequencing showed that the promoter region Agxt(2) displayed a slightly higher methylation degree in the hepatocytes of WD mice (Fig. 3.17). Moreover, the position of one cytosine within the Agxt(2) amplicon co-localised with a half-site cAMP response element (CRE; Fig. 3.17).

All in all, these results show that the diet-induced steatosis in 6 weeks WD-fed mice leads to similar alterations in the glyoxylate metabolism as in *ob/ob* mice. Furthermore, the steatosis associated hypermethylation of the *Agxt* promoter can be observed in both mouse models.

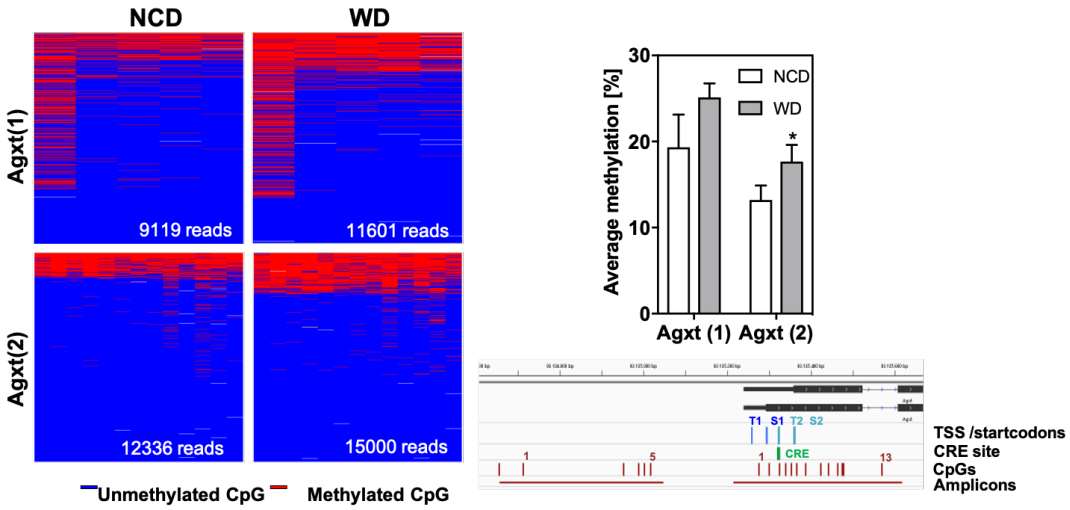

Figure 3.17: Hypermethylated *Agxt* promoter in steatotic hepatocytes of 6 weeks WD mice. Representative pattern maps of methylated CpG sites (red) in the promoter region of murine *Agxt* in hepatocytes of NCD and WD mice and the corresponding average % methylation values (n=3). Integrative Genomics Viewer showing the localisation of Agxt in the genome and the position of the two amplicons with the corresponding CpGs. A CRE sequence overlaps with the CpG at the third position in the Agxt(2) amplicon. The means ± SD are shown. * p < 0.05. Student's t test, unpaired, two sided.

3.5 Increased hepatic oxalate production results in systemic oxalaemia and not in hyperoxaluria

Since the alterations within the glyoxylate metabolism of 6 weeks WD-fed mice were similar to *ob/ob* mice and hinted towards an increased hepatic oxalate production, possible physiological consequences in 6 weeks WD-fed mice were studied in the next steps.

3.5.1 Feeding a western diet for six weeks does not lead to hyperoxaluria

In order to examine urinary oxalate excretion, 6 weeks WD-fed and NCD-fed mice (n=5) were put into metabolic cages for three consecutive days and 24 h urine was collected every morning. Body weight, food intake, water intake and urine volume were recorded. Additionally, urinary creatinine levels were quantified (Fig. 3.18). As expected, the body weight of WD-fed mice was significantly increased compared to the NCD control mice (Fig. 3.18 A). Surprisingly, there were no differences in the food intake between the groups. On the other hand, WD-fed mice displayed a decreased water consumption compared to the control group (NCD; Fig. 3.18 A). The 24 h urine volume and daily creatinine excretion were not altered in the WD-fed mice despite the reduced water intake (Fig. 3.18 B).

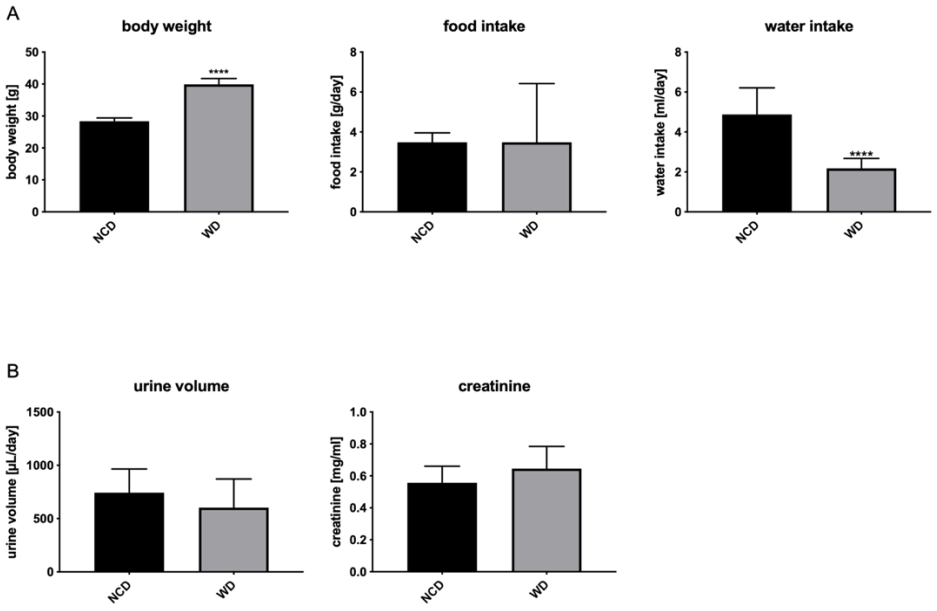

Figure 3.18: Basic parameters of 6 weeks WD-fed and NCD-fed mice during urine collection (n=5). An increased body weight of the WD-fed mice was observed while the daily food intake did not differ compared to NCD-fed control mice. Water consumption was significantly impaired in the WD group with respect to the NCD mice (A). The daily urinary volume (24 h urine) and creatinine excretion displayed no differences between the two dietary groups (B). The means ± SD are shown. *** p < 0.001. Student's t test, unpaired, two sided

The 24 h urine samples were diluted accordingly, measured by LC/MS-MS and normalised for the urinary creatinine content and for the 24 h urine volume. In both analyses, the 6 weeks WD-fed mice did not exhibit an increased urinary oxalate excretion compared to their lean counterparts (NCD; Fig. 3.19). This data show that altered glyoxylate metabolism in WD mice does not result in higher urinary oxalate excretion. This is contrary to *ob/ob* mice and not fully understood.

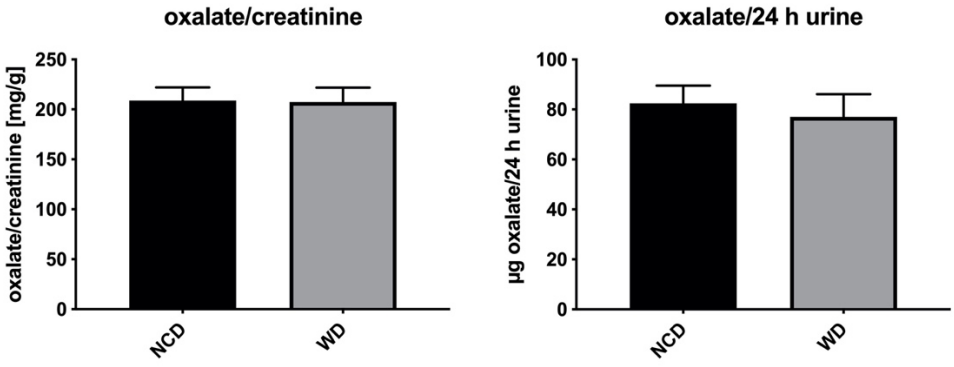

Figure 3.19: Urinary oxalate excretion in 6 weeks WD-fed and NCD-fed mice normalised for creatinine levels and 24 h urine volume (n=5). No changes were observed in the daily urinary oxalate excretion between WD-fed and NCD-fed mice. The means ± SEM are shown. Student's t test, unpaired, two sided.

3.5.2 Oxalate plasma concentration is elevated in the right heart chamber and hepatic vein of western diet mice

In the next step, it was studied whether the alterations within the glyoxylate metabolism of 6 weeks WD-fed mice result in changed hepatic oxalate excretion into the blood. Therefore, five mice on WD for 6 weeks and five aged-matched NCD controls were sacrificed and plasma samples were collected from the portal vein, hepatic vein and right heart chamber to monitor the plasma oxalate concentrations for hepatic inflow, outflow and the systemic oxalate levels, respectively.

LC/MS-MS measurements showed no difference between WD-fed and NCD-fed regarding the oxalate levels in samples collected from the portal vein (Fig. 3.20). On the contrary, the WD-fed mice displayed significantly elevated oxalate concentrations in the hepatic vein (29.74 ± 2.59 µM oxalate) and the right heart chamber (33.98 ± 4.64 µM oxalate) compared to the NCD-fed controls (hepatic vein NCD: 19.36 ± 1.01 µM oxalate; right heart chamber NCD: 23.06 ± 0.78 µM oxalate; Fig. 3.20). Additionally, the ratio of hepatic outflow to inflow of oxalate (hepatic vein/portal vein) was increased in 6 weeks WD-fed mice compared to the NCD group (Fig. 3.20). These results indicate that the altered glyoxylate metabolism in 6 weeks WD-fed mice results in an elevated hepatic oxalate production and excretion into the hepatic vein, leading to a systemic oxalaemia.

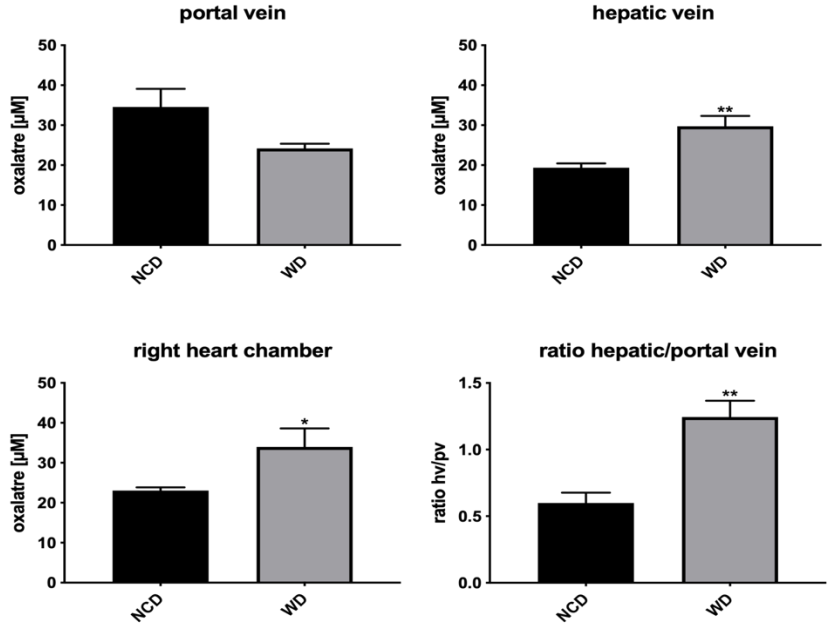

Figure 3.20: Plasma oxalate concentrations in 6 weeks WD-fed and NCD-fed mice. Oxalate levels are significantly elevated in plasma samples from the hepatic vein and right heart chamber of 6 weeks WD-fed mice. No changes were found in samples from the portal vein of the WD group compared to NCD. The ratio of the oxalate levels in the hepatic vein to those in the portal vein was significantly elevated in the WD-fed mice. Each group consisted of five mice (n=5). The means ± SEM are shown. * p < 0.05, ** p < 0.01. Student's t test, unpaired, two sided.

3.6 Primary hepatocytes from 6 weeks WD-fed mice display increased susceptibility towards hydroxyproline

The 6 weeks WD-fed mice displayed similar expression changes in the hepatic glyoxylate metabolism like *ob/ob* mice (Chapter 3.4). Whether these changes affect the hepatic glyoxylate detoxification function of WD-fed mice was investigated by treating isolated hepatocytes from 6 weeks WD-fed and NCD-fed mice with different concentrations of the oxalate precursors hydroxyproline, glycolate and glyoxylate for 48 h (Chapter 2.2.10.4). Oxalate and glycolate levels in the supernatants were measured *via* LC/MS-MS and normalised for protein content of the corresponding sample.

3.6.1 Hydroxyproline leads to increased oxalate production in primary hepatocytes from 6 weeks WD-fed mice

The treatment with glycolate and glyoxylate resulted in a concentration-dependent increase of oxalate excretion from WD and NCD hepatocytes without differences between the two groups (Fig. 3.21 A). Oxalate levels in the supernatants were also elevated upon hydroxyproline exposure in both groups whereas the WD hepatocytes produced a significantly higher amount of oxalate when treated with 10 mM hydroxyproline (NCD with 10 mM hydroxyproline: 5.14 ± 1.22 nmol/mg protein; WD with 10 mM hydroxyproline: 11.93 ± 2.37 nmol/mg protein; Fig. 3.21 A). Glycolate levels in the supernatant were also quantified. The highest glyoxylate concentration led to a strong increase of glycolate excretion of WD and NCD hepatocytes without difference between the groups (Fig. 3.21 B). On the other hand, already the lowest hydroxyproline concentration resulted in an elevated glycolate excretion in both groups while increasing hydroxyproline concentrations did not lead to further increase of glycolate. However, the hydroxyproline-derived excretion of glycolate was significantly higher in WD hepatocytes for all used hydroxyproline concentrations compared to NCD (Fig. 3.21 B). Therefore, similar to *ob/ob* hepatocytes, the WD hepatocytes are more susceptible to hydroxyproline compared to the NCD control hepatocytes. Since, the expression of enzymes which are active in the hydroxyproline catabolism are not altered in the livers of 6 weeks WD-fed mice, the enhanced oxalate and glycolate excretion from WD hepatocytes upon hydroxyproline treatment are attributed to impaired glyoxylate detoxification resulting from *Agxt* downregulation. Exogenously added glyoxylate and glycolate is probably converted by to glycolate and/or oxalate by Grhpr and Ldha already in the cytosol, which is not affected by the *Agxt* downregulation.

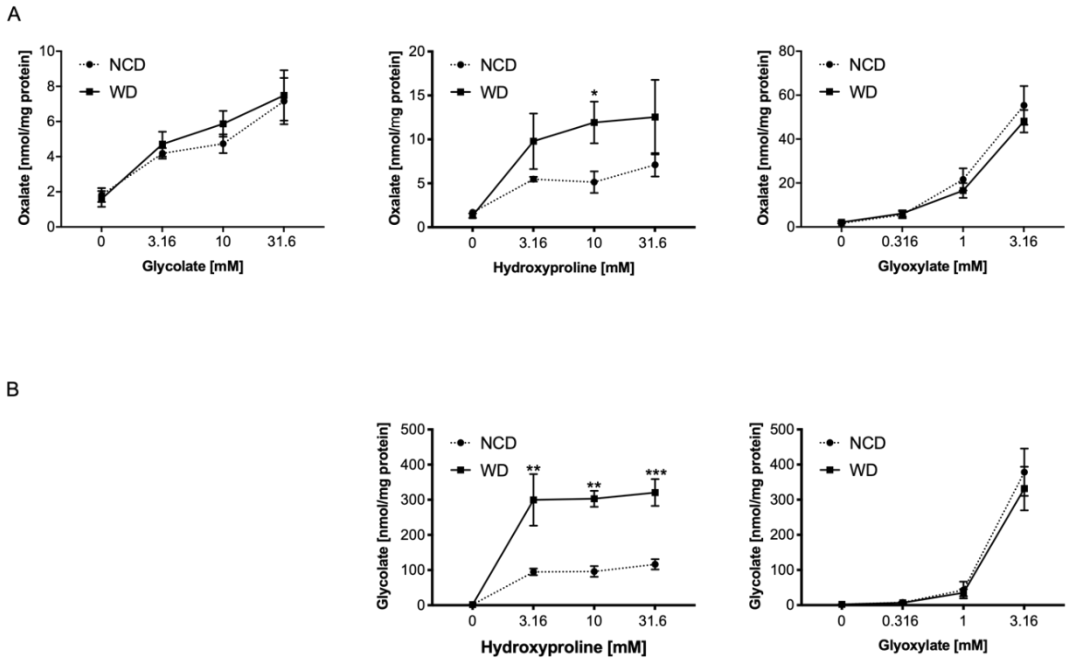

Figure 3.21: Oxalate precursor challenges on primary hepatocytes of 6 weeks WD-fed and NCD-fed mice. All three precursors resulted in an elevated oxalate excretion in both groups, while hydroxyproline led to higher oxalate excretion in WD hepatocytes compared to NCD (A). Glyoxylate treatment increased glycolate excretion in both groups. Hydroxyproline challenge enhanced the glycolate excretion of WD hepatocytes significantly stronger than in NCD hepatocytes (B). The means ± SD are shown. * p < 0.05 ** p < 0.01, *** p < 0.001 for comparison between WD and NCD. Student's t test, unpaired, two sided.

3.6.2 Influence of precursor challenges on protein expression of primary hepatocytes from WD-fed mice

The effects of oxalate precursors on the oxalate and glycolate excretion in cultivated primary hepatocytes from 6 weeks WD-fed and NCD-fed prompted the question whether the exposure to these substances might have an impact on the protein expression of Agxt and Hao1. Therefore, the protein extracts from primary hepatocytes which were exposed to oxalate precursors (Chapter 3.6.1) were analysed *via* immunoblotting. The signals were quantified by densitometrical analysis (Fig. 3.22).

The exposure to glycolate and hydroxyproline did not alter the Agxt protein expression neither in WD nor in NCD hepatocytes (Fig. 3.22 A + B). Only the highest glyoxylate concentration slightly increased the protein levels of Agxt in NCD hepatocytes compared to the untreated control (Fig. 3.22 C). Remarkably, the immunoblotting revealed a decreased Hao1 protein expression in the untreated hepatocytes of 6 weeks WD mice (0.34 ± 0.09 Hao1/β-Actin ratio) compared to the NCD controls (0.38 ± 0.02 Hao1/β-Actin ratio; Fig. 3.22 E). This was not expected, since a previous analysis had revealed no differences in Hao1 mRNA levels in the liver tissue of 6 weeks WD compared to NCD mice. This suggest that, immunoblotting with isolated hepatocytes serve more specific results regarding the expression of glyoxylate metabolism enzymes within hepatocytes since other cell types in the liver tissue might influence the protein signal. Furthermore, the treatment with all used concentrations of glycolate and hydroxyproline elevated the Hao1 protein levels in both WD and NCD

hepatocytes (Fig. 3.22 D + E). The incubation with 1 mM and 3.16 mM glyoxylate significantly increased the Hao1 protein expression in the hepatocytes of NCD mice. This effect was only significant for 1 mM glyoxylate in the case of WD hepatocytes (Fig. 3.22 F). Like in the steatotic *ob/ob* hepatocytes, the protein expression of Agxt could not be altered by hydroxyproline treatment, whereas Hao1 protein levels were significantly elevated in WD and NCD hepatocytes. This shifted Hao1 to Agxt ratio and the downregulation of Hao1 in WD hepatocytes might explain the elevated glycolate excretion in the supernatant of WD hepatocytes compared to NCD controls (Fig. 3.22 B).

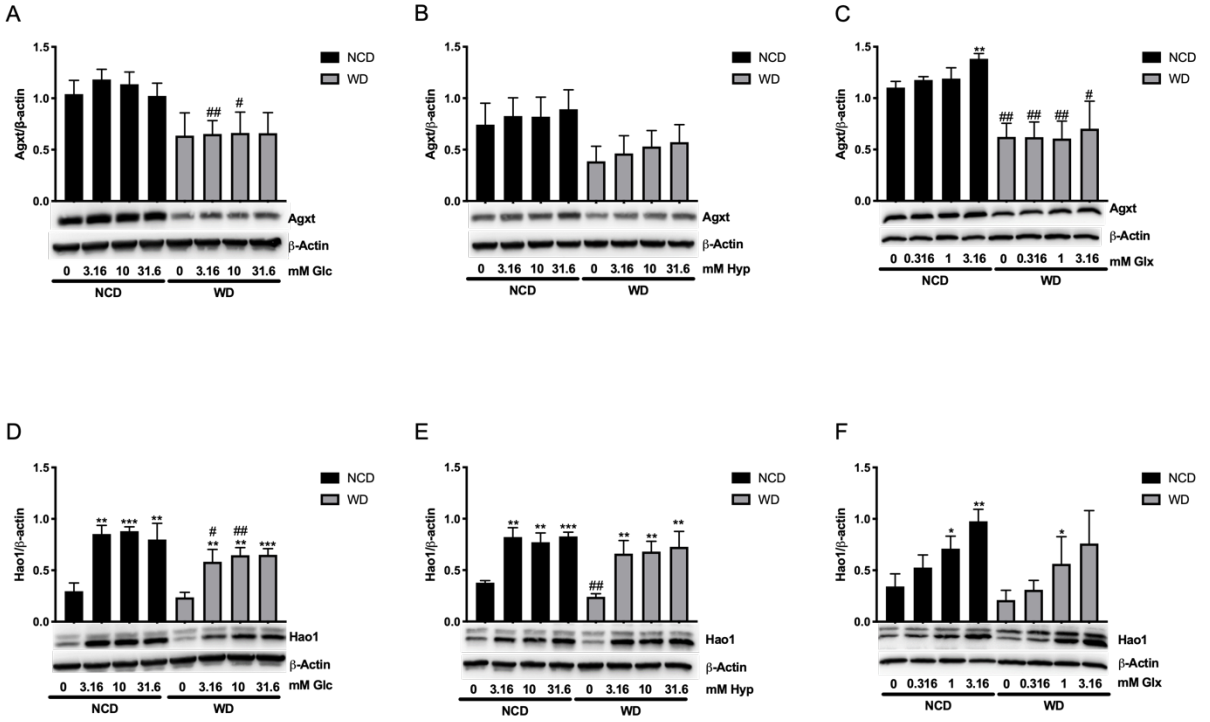

Figure 3.22: Agxt and Hao1 protein expression in primary hepatocytes of 6 weeks WD-fed and NCD-fed mice treated with oxalate precursors. The bar graphs above each western blot represents the densitometric quantification of the corresponding blot below. Agxt protein levels were elevated by 3.16 mM glyoxylate in NCD hepatocytes (C) whereas Hao1 protein expression was increased by all precursors in both WD and NCD hepatocytes (D-F). Glc = glycolate; Hyp = hydroxyproline; Glx = glyoxylate. The means ± SD are shown. * p < 0.05, ** p < 0.01, *** p < 0.001 for comparison between treated and non-treated (0 mM) cells. # p < 0.05, ## p < 0.01 for comparing WD and NCD. Student's t test, unpaired, two sided.

3.7 Agxt deficiency is sufficient for increased hepatic and urinary oxalate excretion

Whether the increased hepatic oxalate production and excretion can be attributed to the missing glyoxylate detoxification by Agxt was investigated in primary hepatocytes of Agxt knockout mice (*Agxt*$^{-/-}$). *Agxt*$^{-/-}$ mice were obtained from Prof. Dr. Eduardo Salido who kindly allowed our group to use these mice for our research purposes. Generation of the *Agxt*$^{-/-}$ mice as described in detail and already published (Salido et al. 2006a).

3.7.1 *Agxt*$^{-/-}$ hepatocytes excrete more oxalate when exposed to oxalate precursors

Primary hepatocytes were isolated from *Agxt*$^{-/-}$ mice and from aged-matched wild type (wt) controls and plated in a collagen sandwich on top system as described before (Chapter 2.2.2.2). The oxalate precursor treatments are specified in Chapter 2.2.10.5. Oxalate and glycolate levels in the supernatants were measured by LC/MS-MS and normalised for the corresponding protein content. Immunoblotting showed the Agxt deficiency on protein level (Fig. 3.23).

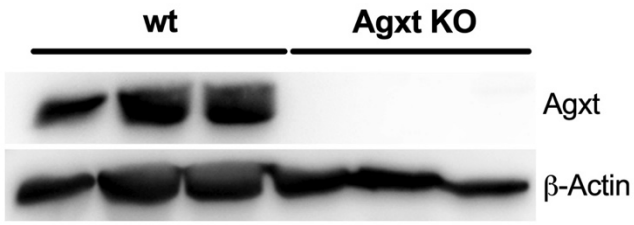

Figure 3.23: Immunoblotting of primary hepatocytes from wt and *Agxt*$^{-/-}$ mice. Agxt protein expression is not detectable via immunoblotting in primary hepatocytes from *Agxt*$^{-/-}$ mice. Agxt KO = Agxt knockout, wt = wild type

The lowest (3.16 mM) and highest (31.6 mM) concentrations of glycolate provoked a significantly higher oxalate excretion from *Agxt*$^{-/-}$ hepatocytes compared to the wt controls (Fig. 3.24 A). All hydroxyproline concentrations increased oxalate concentrations in the supernatants of *Agxt*$^{-/-}$ hepatocytes compared to wt (Fig. 3.24 A). Moreover, glyoxylate challenge elevated oxalate production in both genotypes while 0.316 nM glyoxylate resulted in a higher oxalate excretion from *Agxt*$^{-/-}$ hepatocytes compared to wt (Fig. 3.24 A). Additionally, glycolate excretion upon hydroxyproline challenge was elevated in both genotypes but significantly higher in the supernatants of *Agxt*$^{-/-}$ hepatocytes for all hydroxyproline concentrations compared to wt controls (Fig. 3.24 B). Glyoxylate treatment increased glycolate excretion to the same extent from hepatocytes of both genotypes (Fig. 3.24 B).

These results show Agxt that deficiency is responsible for the elevated oxalate and glycolate excretion in response to hydroxyproline treatment as well as for the increased oxalate excretion upon glycolate exposure. The fact that only the lowest concentration of glyoxylate resulted in a higher oxalate excretion from *Agxt*$^{-/-}$ hepatocytes and there was no difference between the genotypes in glycolate excretion when exposed to glyoxylate treatment might be due to the cytosolic glyoxylate conversion to oxalate or glycolate by Ldha and/or Grhpr, respectively. Since glyoxylate treatment elevated oxalate and glycolate excretion from hepatocytes of both genotypes to the same extent, exogenously added glyoxylate seems not to reach the peroxisomes or mitochondria where Agxt is located and is therefore not affected by the Agxt deficiency. Furthermore, these results show that a complete knockout of *Agxt* leads to an increased susceptibility towards all three oxalate precursors in contrast to an *Agxt* downregulation in *ob/ob* hepatocytes which resulted in the excretion of higher oxalate amounts only when treated with hydroxyproline.

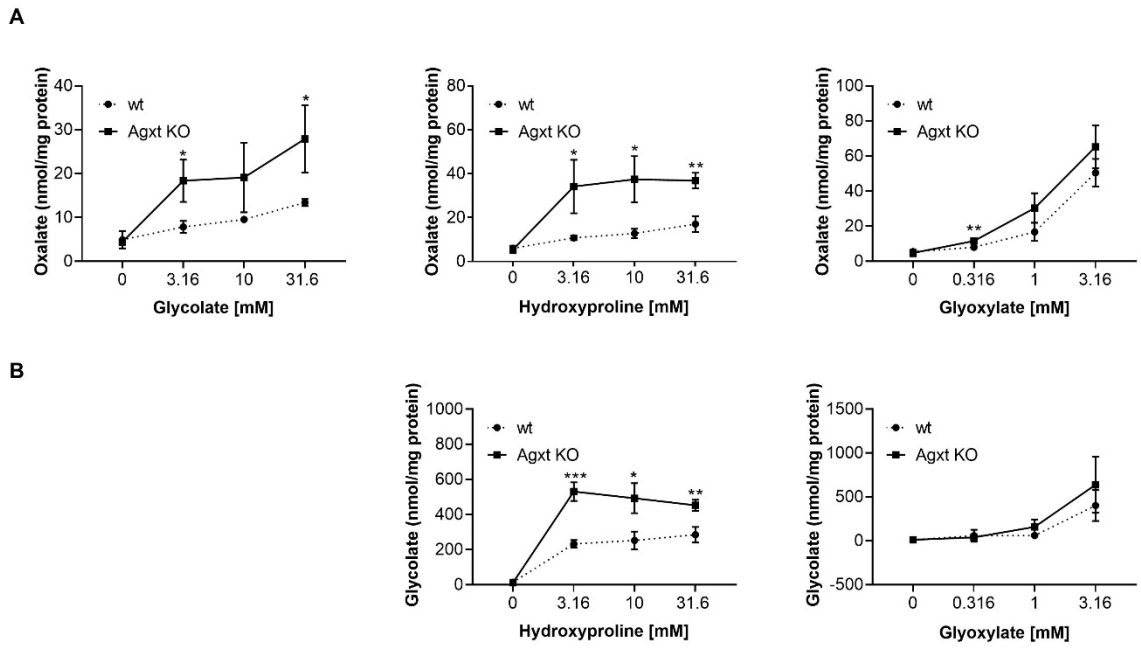

Figure 3.24: Oxalate precursor challenge in primary hepatocytes from *Agxt*$^{-/-}$ mice and wt controls. Glycolate and hydroxyproline treatment increased oxalate excretion from primary hepatocytes of *Agxt*$^{-/-}$ mice compared to wt controls (A). Oxalate excretion was increased by glyoxylate exposure in both genotypes, while 0.316 mM glyoxylate led to higher oxalate concentrations in the supernatants of *Agxt*$^{-/-}$ hepatocytes compared to the wt controls (A). Glycolate excretion upon hydroxyproline was significantly higher in *Agxt*$^{-/-}$ hepatocytes for all used hydroxyproline concentrations compared to wt controls (B). Glyoxylate treatment increased the glycolate excretion in both genotypes to the same extent (B). *Agxt* KO = Agxt knockout; wt = wild type. The means ± SD are shown. * p < 0.05, ** p < 0.01, *** p < 0.001 for comparison between wt and Agxt KO. Student's t test, unpaired, two sided.

3.7.2 Elevated plasma and urinary oxalate concentrations in *Agxt*$^{-/-}$ mice

In order to examine whether *Agxt*$^{-/-}$ mice exhibit increased hepatic and urinary oxalate excretion, plasma samples from the right heart chamber and 24 h urine samples from three consecutive days were collected and oxalate levels were measured by LC/MS-MS. *Agxt*$^{-/-}$ mice displayed increased oxalate levels in the plasma samples compared to wt mice, suggesting an increased hepatic oxalate production due to Agxt deficiency (Fig. 3.25 A). Moreover, both the concentration of oxalate in urine and the total 24-hour urinary oxalate excretion were significantly increased in *Agxt*$^{-/-}$ mice (Fig. 3.25 B), which has already been reported before (Salido et al. 2006). This suggests that hepatic Agxt deficiency is responsible for the increase hepatic and urinary oxalate excretion *in vivo,* resulting in hyperoxaluria and oxalaemia.

.

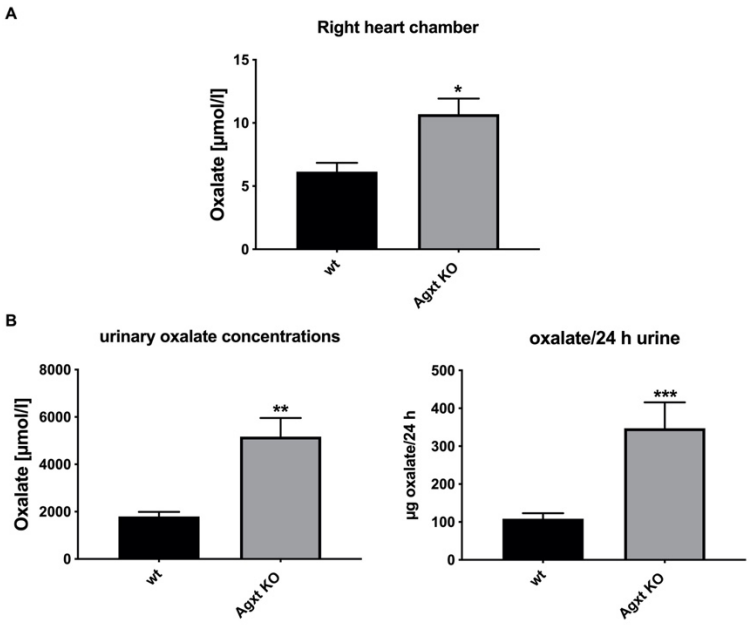

Figure 3.25: Plasma and urinary oxalate levels are elevated in *Agxt*$^{-/-}$ mice. Oxalate levels are elevated in the plasma from the right heart chamber (A) and in 24 h urine samples (B) of Agxt-/- mice compared to wt controls. The means ± SEM are shown. * p < 0.05, ** p < 0.01, *** p < 0.001. Student's t test, unpaired, two sided.

3.8 Steatosis grade correlates with urinary oxalate excretion in obese children and adolescents

In a next step the translational relevance of the findings in the NAFLD mouse models was investigated by analysing oxalate excretion in human NAFLD. In a previous study, the correlation between reduced *AGXT* expression and increased TAG content in primary human hepatocytes (PHHs) from steatotic and healthy donors was reported (Gianmoena 2017). *AGXT* mRNA expression inversely correlated with increasing TG content in PHHs and when stratified into low and high TAG content, the *AGXT* mRNA expression was significantly lower in PHHs with a high TAG content (Gianmoena 2017). In addition to *AGXT*, *GRHPR* and *HOGA1* mRNA expression also displayed an inverse correlation with the TG content in PHHs, indicating steatosis-associated alterations in the human glyoxylate metabolism involving all three primary hyperoxaluria linked genes (Gianmoena 2017).

Whether these alterations exhibit physiological consequences in human NAFLD patients was investigated in a cohort of overweight or obese children and adolescents with biopsy proven NAFLD recruited at the Charité Berlin from which corresponding 24 h urine samples were available (n=30; Chapter 2.2.20). Urinary oxalate levels were measured *via* LC/MS-MS and normalised to the urinary creatinine content and to the body surface area (BSA). The percentage steatosis positively correlated with the urinary oxalate to creatinine ratio (rho = 0.366, p = 0.047) as well as with the total amount of excreted oxalate when corrected for BSA (rho = 0.427, p = 0.019; Fig. 3.26). There was no association of the daily urinary oxalate excretion with fibrosis, inflammation, ballooning or NAFLD activity score (NAS) observed. These results suggest that also in human NAFLD the hepatic fat accumulation is the key factor leading to increased urinary oxalate excretion.

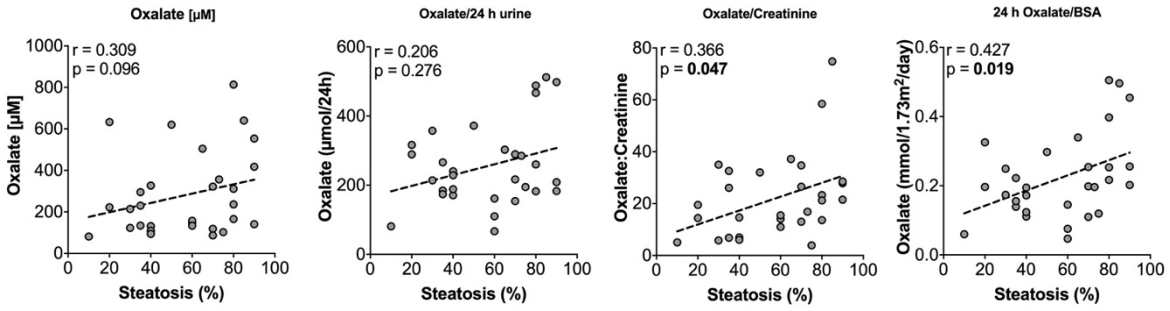

Figure 3.26: Urinary oxalate levels of overweight or obese children and adolescents with biopsy proven NAFLD. Scatter plots showed that hepatic percentage steatosis positively correlated with the oxalate to creatinine and 24 h oxalate to BSA ratio of the corresponding donors. The Spearman correlation coefficient and corresponding p-values are shown

3.9 Primary human hepatocytes excrete more oxalate from glycolate than from hydroxyproline

The results obtained in the children NAFLD cohort indicated a relationship between steatosis and oxalate excretion but due to missing information on dietary habits the source of oxalate could not be identified. Therefore, the response of primary human hepatocytes (PHHs) towards oxalate precursor treatments was analysed in the following experiment. To this aim, primary human hepatocytes purchased from Lonza, BioIVT or obtained from the University of Leipzig were treated with hydroxyproline, glycolate and glyoxylate as described in Chapter 2.2.20.6. Oxalate and glycolate levels in the supernatants were measured by LC/MS-MS and normalised for the protein content of the corresponding sample. The results obtained from female donors Hum4229, Hum 4108, Hum181761 and IPH and the male donors L1, L2 and IAN are depicted in Figure 3.27 and 3.28, respectively.

When exposed to 10 mM, 31.6 mM and 100 mM glycolate, female donors displayed a significantly elevated oxalate excretion compared to the untreated controls. The highest glycolate concentrations increased oxalate expression by an approximately 5-fold change compared to the untreated controls (Fig. 3.27 A). Interestingly, treatment with only 31.6 mM hydroxyproline slightly increased oxalate levels in the supernatants of the female hepatocytes, whereas all other hydroxyproline concentrations did have an effect. Further, all used glyoxylate concentrations significantly enhanced the oxalate excretion in from the primary hepatocytes of female donors compared to the untreated control (Fig. 3.27 A). Glycolate excretion was significantly increased by all three hydroxyproline concentrations (Fig. 3.27 B) and the treatment with 3.16 mM and 10 mM glyoxylate could markedly increase the glycolate levels in the supernatants compared to untreated hepatocytes (Fig. 3.27 B).

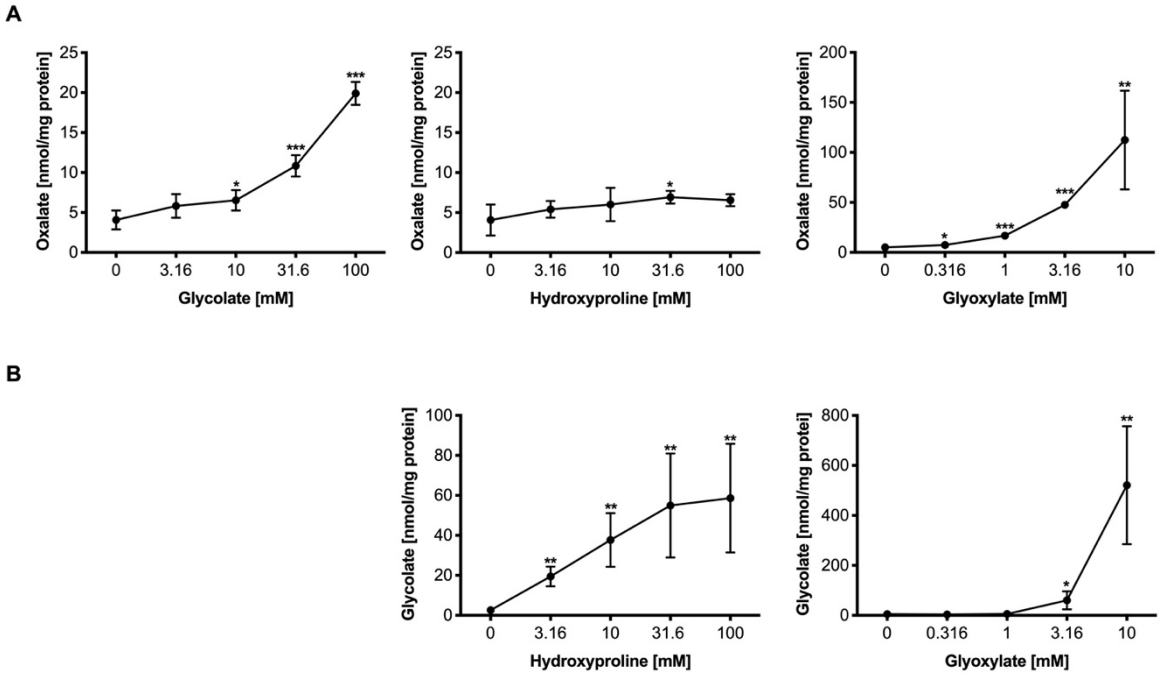

Figure 3.27: Oxalate precursor challenge in PHHs from female donors (n=4). Oxalate excretion was significantly increased by all glycolate concentrations, while hydroxyproline did not influence oxalate production in female PHHs. Glyoxylate elevated the oxalate excretion in a concentration dependent manner (A). Glycolate levels in the supernatant of female PHHs significantly increased upon hydroxyproline exposure in a concentration dependent manner. Treatment with 3.16 mM and 10 mM glyoxylate markedly elevated the glycolate levels in the supernatant of female PHHs (B). The means ± SD are shown. * p < 0.05, ** p < 0.01, *** p < 0.001. Student's t test, unpaired, two sided.

In male donors, the oxalate excretion into the supernatant were significantly elevated upon 100 mM glycolate treatment by 2.4-fold compared to the untreated controls whereas hydroxyproline challenge failed to increase the oxalate production. Further, glyoxylate exposure increased the oxalate excretion into the supernatants of male donors in a concentration dependent manner (Fig. 3.28 A). There was a trend in increasing glycolate levels upon treatment with increasing hydroxyproline concentrations. However, this was not significant. Glyoxylate treatment increased the glycolate excretion concentration dependently (Fig. 3.28 B).

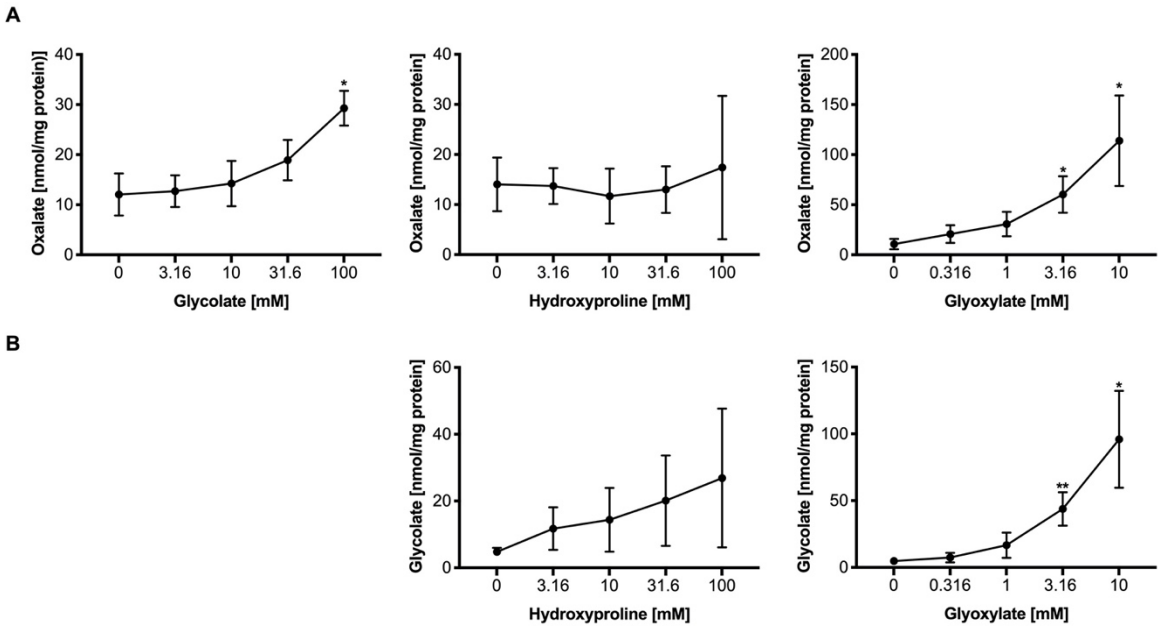

Figure 3.28: Oxalate precursor challenge in PHHs from male donors (n=3). Increased oxalate excretion was measured upon treatment with 100 mM glycolate. Hydroxyproline did not influence the oxalate production in male PHHs. Treatment with glyoxylate elevated the oxalate levels in the supernatant of male PHHs in a concentration dependent manner (A). Glycolate levels tend to gradually increase upon hydroxyproline treatment. 3.16 mM and 10 mM glyoxylate significantly enhanced the glycolate excretion in male PHHs (B). The means ± SD are shown. * p < 0.05, ** p < 0.01. Student's t test, unpaired, two sided.

These results show, that PHHs are more susceptible to glycolate towards oxalate production than to hydroxyproline like in primary mouse hepatocytes. The difference to primary mouse hepatocytes probably arises from the exclusive peroxisomal localisation of AGXT in the human liver while murine Agxt localised in the mitochondria and peroxisomes (Takada and Noguchi 1982; Birdsey et al. 2004). Furthermore, the analysed female donors seem to be more sensitive towards glycolate treatment, since they produced 5-fold more oxalate from 100 mM glycolate compared to the male donors, which displayed a fold-change of 2.4. Moreover, the female donors excrete more oxalate from glyoxylate (10 mM glyoxylate females: 22-fold; 10 mM glyoxylate males: 10.6-fold). Also, the fold-change in glycolate excretion upon hydroxyproline and glyoxylate is higher in female donors compared to male donors. Altogether, these findings suggest a gender difference in the glyoxylate metabolism in PHHs. This has to be validated with more experiments on more female and male donors.

3.10 *Agxt* transcription in response to glucagon in the livers and primary hepatocytes of *ob/+* and *ob/ob* mice

Various studies over the years have reported an upregulation of mitochondrial Agxt expression by glucagon in rats and mice as described in Chapter 1.6.1. Li and colleagues reported that the promoter sequence of the mouse Agxt gene contains a CRE sequence, which is known to respond to glucagon. Also, they showed that an intraperitoneal (IP) injection of 3 µg/g body weight of glucagon for 3 h increased the level of the mitochondrial Agxt transcript in mouse liver (Li et al. 1999). In a previous work, it was reported that the *Agxt* promoter is hypermethylated in the isolated hepatocytes of *ob/ob* mice (Gianmoena 2017). Interestingly,

the CRE sequence in the promoter sequence of mitochondrial Agxt lies within the hypermethylated region (Li et al. 1999). Whether this might influence the responsiveness of Agxt towards glucagon stimulation in *ob/ob* mice was investigated next.

3.10.1 *Agxt* mRNA expression in response to glucagon injection is impaired in the livers of *ob/ob* mice

To analyse the possible consequences of the hypermethylation at the CRE sequence on the transcriptional response of *Agxt* to glucagon, *ob/+* and *ob/ob* mice were injected intraperitoneally with 3 µg/g body weight glucagon or PBS (Chapter 2.2.11.1). After 3 h the mice were sacrificed, and liver tissue was collected for immunohistochemistry, qRT-PCR and immunoblot analyses (Fig. 3.29).

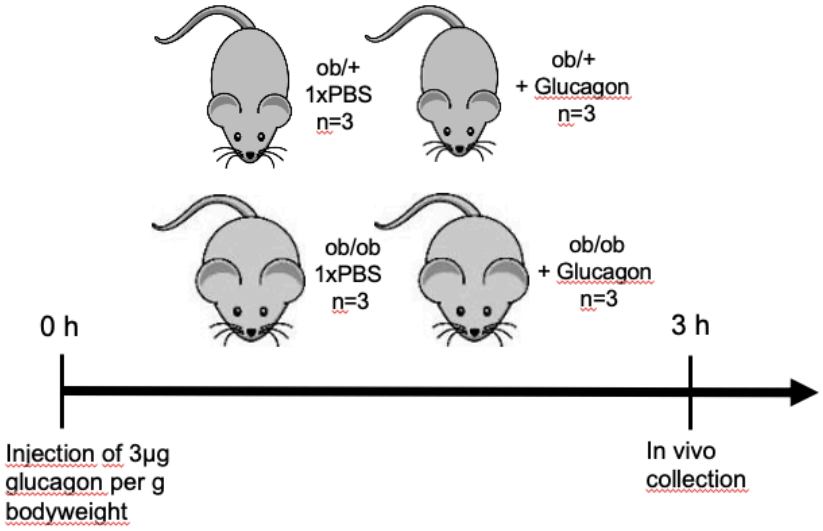

Figure 3.29: Experimental set up for glucagon treatment in *ob/+* and *ob/ob* mice. IP injection of 3 µg/g body weight glucagon or 1xPBS into *ob/+* and *ob/ob* (n=3). Mice were sacrificed after 3 h and liver tissue was collected for immunohistochemistry, qRT-PCR and immunoblotting. Mice were not starved prior or during this experiment.

Analysis of *Agxt* mRNA levels in the livers of glucagon treated *ob/+* and *ob/ob* mice revealed an 11.27 ± 3.10-fold upregulation of *Agxt* mRNA in response to glucagon in *ob/+* mice. This confirmed previous results (Li et al. 1999). On the other hand, the mRNA expression of *Agxt* was not significantly enhanced by glucagon treatment in the livers of *ob/ob* mice (2.90 ± 1.72-fold change; Fig. 3.30). The missing response of *Agxt* mRNA expression upon glucagon treatment in the livers of *ob/ob* might be due to the hypermethylated CRE sequence in the *Agxt* promoter

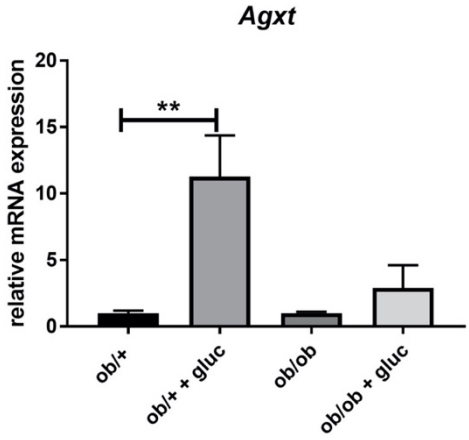

Figure 3.30: QRT-PCR analysis of *Agxt* mRNA expression in the livers of glucagon treated *ob/+* and *ob/ob* mice. *Agxt* mRNA levels were significantly upregulated in response to glucagon in the livers of *ob/+* but not of *ob/ob* mice. Eif2a was used as an endogenous control. The means ± SD are shown. ** p < 0.01. Student's t test, unpaired, two sided.

Next, the response of Agxt to glucagon in the livers of *ob/+* and *ob/ob* was analysed on protein level *via* immunoblotting and immunohistochemistry (Fig. 3.31). No elevation of Agxt protein expression could be detected neither in immunoblotting (Fig. 3.31 A) nor in the immunohistochemical staining (Fig. 3.31 B). This shows that 3h after glucagon stimulation the enhanced transcription of mitochondrial Agxt is not yet followed by enhanced translation.

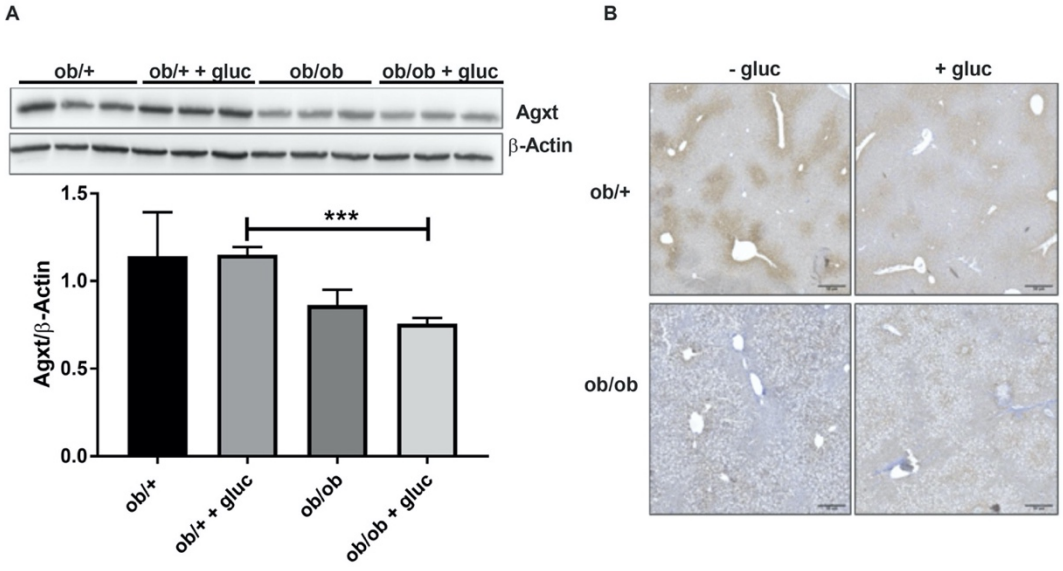

Figure 3.31: Analysis of Agxt protein expression in the livers of glucagon treated *ob/+* and *ob/ob* mice and the vehicle controls. Densitometric analysis of the immunoblot showed no increase of Agxt protein expression upon glucagon treatment (A). Representative pictures of paraffin-embedded liver slides from glucagon treated *ob/+* and *ob/ob* mice and the corresponding vehicle controls. No changes in Agxt expression could be observed (B). Scale bars represent 50 µm. The means ± SD are shown. *** p < 0.001. Student's t test, unpaired, two sided.

3.10.2 Phosphorylation of Creb does not increase upon glucagon treatment in the livers of *ob/+* and *ob/ob* mice

One possible explanation for the decreased transcriptional upregulation of Agxt in response to glucagon in *ob/ob* mice could be that the glucagon signalling pathway is compromised in these mice. A key signalling protein is Creb, which becomes phosphorylated by the PKA as part of glucagon signalling. Therefore, to investigate the glucagon pathway in in the livers of *ob/+* and *ob/ob* mice, the phosphorylation status of Creb was analysed *via* immunoblotting (Fig. 3.32). The ratio of phosphorylated Creb (pCreb) to β-Actin and total Creb (tCreb) to β-Actin was determined by densitometric analysis in order to calculate the pCreb/tCreb ratio.

Protein levels of total Creb were stable upon glucagon treatment in *ob/+* and *ob/ob* mice compared to the vehicle controls (Fig. 3.32). Surprisingly, a slight decrease in pCreb/Creb ratio was observed in the livers of glucagon treated *ob/+* mice (1.93 ± 0.04 pCreb/tCreb-ratio) with respect to the vehicle controls (3.13 ± 0.58 pCreb/tCreb-ratio; Fig. 3.32). Densitometrical analyses did not display any changes in pCreb/tCreb ratio upon glucagon treatment in the livers of *ob/ob* mice (Fig. 3.32). These data show no increase on the phosphorylation status of Creb in the liver of *ob/+* and *ob/ob* mice in response to glucagon possibly due to a small animal number and interfering signal from different cell types within the liver tissue.

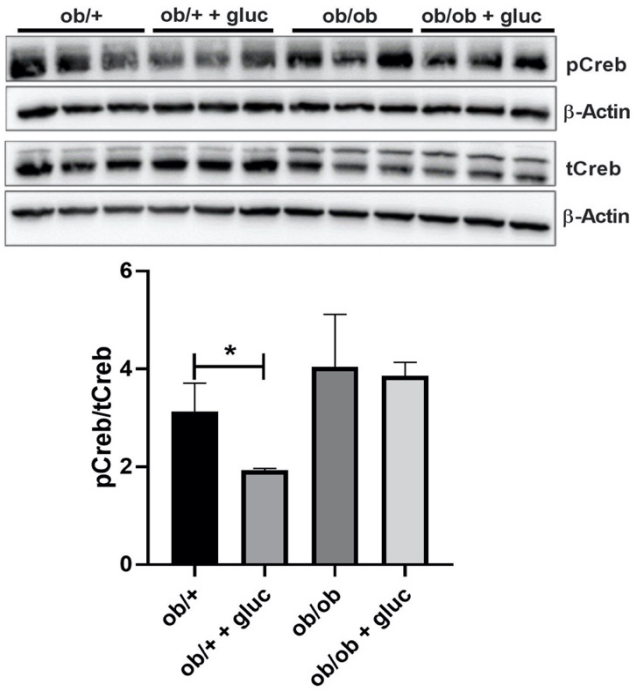

Figure 3.32: Immunoblotting and corresponding densitometrical analysis of phosphorylated and total Creb in the livers of glucagon treated *ob/+* and *ob/ob*. A slight decrease in phosphorylated Creb in the livers of glucagon treated *ob/+* mice was detected whereas no changes upon glucagon treatment were observed in *ob/ob* mice. No changes in the protein levels of total Creb were observed in both genotypes. pCreb = phosphorylated CRE binding protein; tCreb = total CRE binding protein. The mean ± SD is show. * p < 0.05. Student's t test, unpaired, two sided.

3.10.3 Time course of *Agxt* mRNA expression in glucagon treated primary hepatocytes from *ob/+* and *ob/ob* mice

Whether the missing glucagon stimulated *Agxt* mRNA expression could also be confirmed *in vitro* was addressed next. Therefore, *ob/+* and *ob/ob* hepatocytes were treated with 10 nM and 100 nM glucagon as described in Chapter 2.2.11.2. For qRT-PCR analysis the fold changes were calculated relative to the non-treated control of every collection time point.

Glucagon treatment of *ob/+* hepatocytes resulted in a significant increase of *Agxt* mRNA levels after 3 h for 100 nM (2.18 ± 0.67 fold change), after 6 h for both 10 nM (3.31 ± 0.54 fold change) and 100 nM glucagon (3.25 ± 0.55 fold change) and after 24 h for 10 nM glucagon (3.96 ± 0.78 fold change) compared to the untreated control of each time point, respectively (Fig. 3.33 A). The higher glucagon concentration (100 nM) did not lead to a further increase on the mRNA levels of *Agxt* in the hepatocytes of *ob/+* mice (Fig. 3.33 A). However, expression of *Agxt* upon glucagon treatment was not significantly elevated in the hepatocytes of *ob/ob* mice at any analysed time point (Fig. 3.33 A). Furthermore, after 6 h of glucagon exposure *ob/+* hepatocytes exhibited significantly higher *Agxt* mRNA levels than *ob/ob* hepatocytes for 10 nM and 100 nM glucagon and after 24 h for 10 nM glucagon (Fig. 3.33 A). Since 100 nM glucagon did not show a stronger effect on the *Agxt* mRNA expression, only the impact of 10 nM glucagon on the Agxt protein expression was analysed *via* immunoblotting (Fig. 3.33 B). Densitometrical analysis revealed no impact of glucagon on the protein expression of Agxt neither in *ob/+* nor in *ob/ob* hepatocytes (Fig. 3.33 B). This data confirms the results observed *in vivo* (Chapter 3.10.1) and shows a time course of the effect of glucagon on the induction of *Agxt* mRNA expression in control hepatocytes *in vitro,* that is not shared by hepatocytes from steatotic mice.

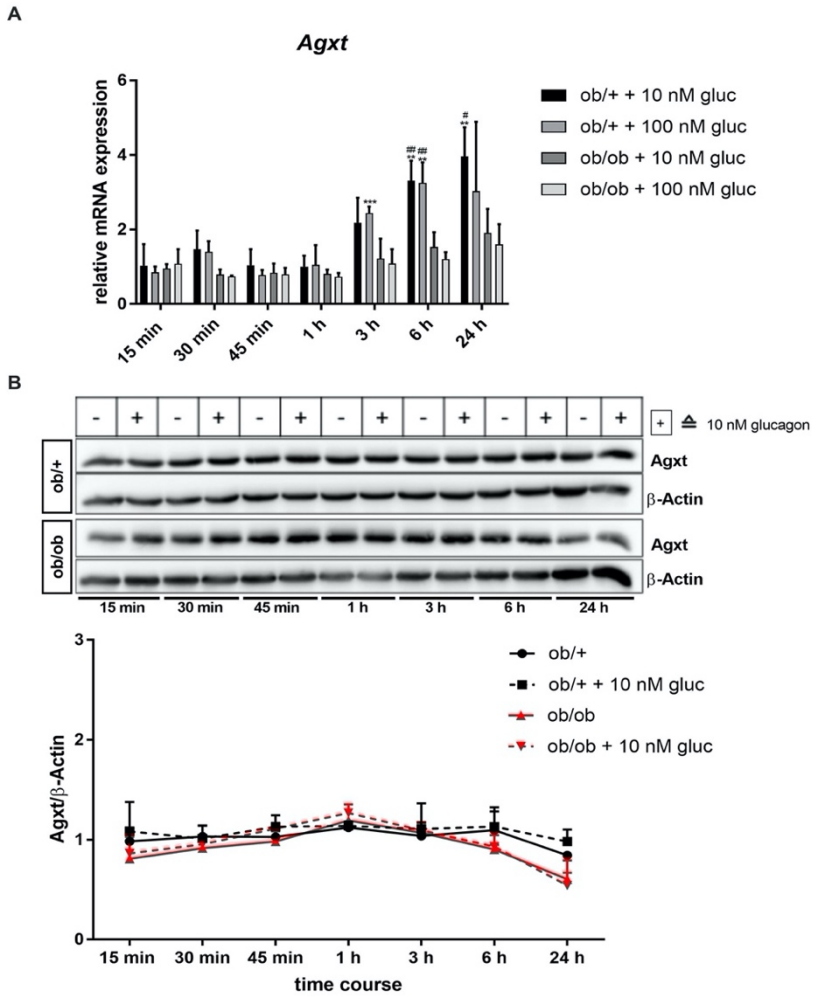

Figure 3.33: Agxt mRNA and protein expression in glucagon treated *ob/+* and *ob/ob* mice in a time course. QRT-PCR analysis revealed an upregulation of *Agxt* mRNA after 3 h for 10 nM, after 6 h for 10 nM and 100 nM glucagon and after 24 h for 10 nM glucagon in *ob/+* hepatocytes compared to *Agxt* mRNA levels of untreated hepatocytes at the corresponding time points. No increase of *Agxt* mRNA expression was observed in *ob/ob* hepatocytes, whereas the *Agxt* mRNA levels in *ob/+* hepatocytes were significantly higher after 6 h for both glucagon concentrations and after 24 h for 10 nM compared to the corresponding *ob/ob* hepatocytes (A). No changes in Agxt protein levels in response to glucagon were observed neither in *ob/+* nor in *ob/ob* hepatocytes for any time point (B). The means ± SD are shown. ** $p < 0.01$ for comparison to untreated hepatocytes at the corresponding time points. # $p < 0.05$, ## $p < 0.01$ for comparing *ob/ob* and *ob/+*. Student's t test, unpaired, two sided.

3.10.4 Phosphorylation of Creb in response to glucagon decreases earlier in *ob/ob* hepatocytes

In order to understand the differential upregulation of the Agxt transcript in response to glucagon in the cultivated hepatocytes of *ob/+* and *ob/ob* mice, the glucagon signalling pathway was investigated. For this purpose, the phosphorylation of Creb in response to glucagon treatment of primary *ob/+* and *ob/ob* hepatocytes was analysed *via* immunoblotting and subsequent densitometrical analysis.

Glucagon treatment (10 nM) was able to elevate the phosphorylation of Creb in both *ob/+* and *ob/ob* hepatocytes already after 15 min of exposure (Fig. 3.34). The phosphorylation of Creb

could be observed until 3 h of treatment in both phenotypes, whereas after 6 h the Creb phosphorylation is only detectable in *ob/+* hepatocytes and not in *ob/ob* hepatocytes. Densitometrical analysis from three independent experiments revealed the pCreb/tCreb ratio of *ob/ob* hepatocytes after 6 h of glucagon treatment to be significantly lower compared to *ob/+* hepatocytes. After 24 h, the Creb phosphorylation was not observable in both genotypes (Fig. 3.34). No changes were observed in the protein expression of total Creb in both genotypes in response to glucagon treatment or due to time effects (Fig. 3.34). This suggests that the activation of the glucagon signalling pathway leads to Creb phosphorylation in both *ob/+* and *ob/ob* hepatocytes to a similar extent until 3 h after stimulation but the phosphorylation declines faster in steatotic *ob/ob* hepatocytes. Although the underlying mechanism for this observation remain unclear, this may be related to the reduced transcriptional upregulation of Agxt after stimulation with glucagon.

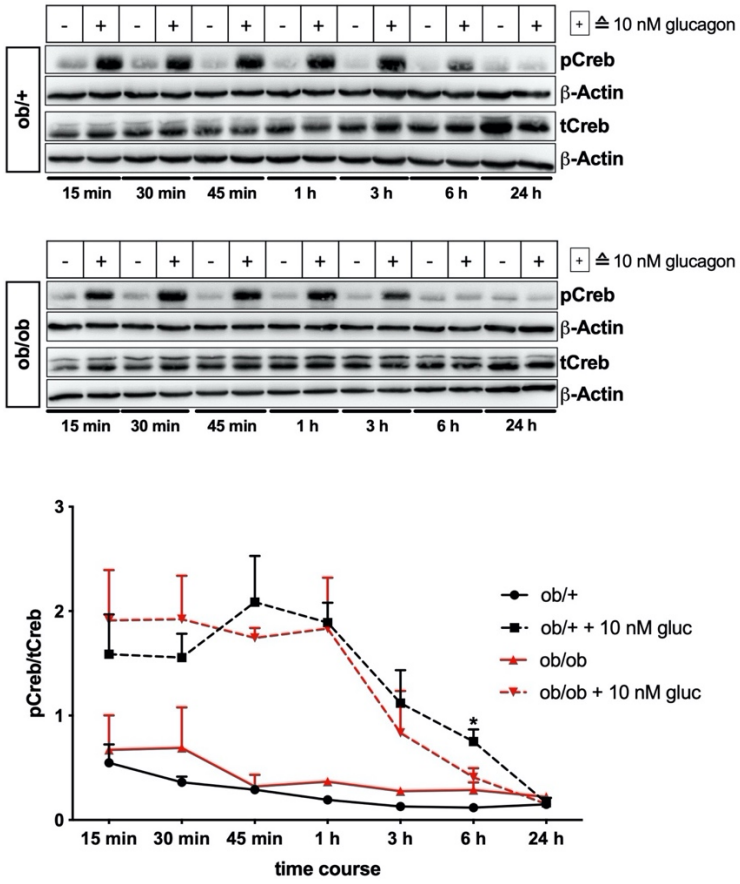

Figure 3.34: Representative immunoblots and corresponding densitometrical analysis of pCreb and tCreb in glucagon treated *ob/+* and *ob/ob* hepatocytes. Creb phosphorylation is induced by glucagon treatment in both genotypes until 3 h of exposure. After 6 h, the phosphorylation of Creb is only detectable in *ob/+* and not in *ob/ob* hepatocytes. Glucagon exposure for 24 h did not lead to a Creb phosphorylation in both genotypes. Gluc = glucagon; pCreb = phosphorylated Creb; tCreb = total Creb. The means ± SD are shown. * $p < 0.05$. Student's t test, unpaired, two sided.

3.10.5 Glucagon treatment in primary *ob/+* and *ob/ob* hepatocytes does not reduce hydroxyproline induced oxalate production

Takayama and colleagues reported that urinary oxalate excretion in rats, which was elevated by an injection of hydroxyproline, was significantly decreased by glucagon stimulated activity of mitochondrial Agxt (Takayama et al. 2003; Ichiyama 2011). Whether the simultaneous treatment of *ob/+* and *ob/ob* hepatocytes with hydroxyproline and glucagon reduces the oxalate excretion was investigated in the next step. Therefore, primary hepatocytes from *ob/+* and *ob/ob* mice were exposed to either different concentrations of hydroxyproline or to a combination of the different hydroxyproline concentrations together with 10 nM glucagon for 48 h (Chapter 2.2.10.2 and 2.2.11.2). Oxalate levels were measured by LC/MS-MS and normalised for the protein content of the corresponding sample (Fig. 3.35).

Both concentrations of hydroxyproline increased the oxalate excretion into the supernatant of *ob/+* and *ob/ob* hepatocytes (Fig. 3.35 A + B). Treatment with glucagon did not influence the hydroxyproline induced oxalate excretion neither in *ob/+* nor *ob/ob* hepatocytes (Fig. 3.35 A + B). It was expected that the glucagon-induced elevation of mitochondrial *Agxt* mRNA levels lead to an increased detoxification of mitochondrial glyoxylate, and hence result in a reduced oxalate excretion. Since glucagon is very unstable, the *in vitro* system might not be the right choice for this experiment. Altogether, these results could not confirm data obtained from literature (Takayama et al. 2003; Ichiyama 2011).

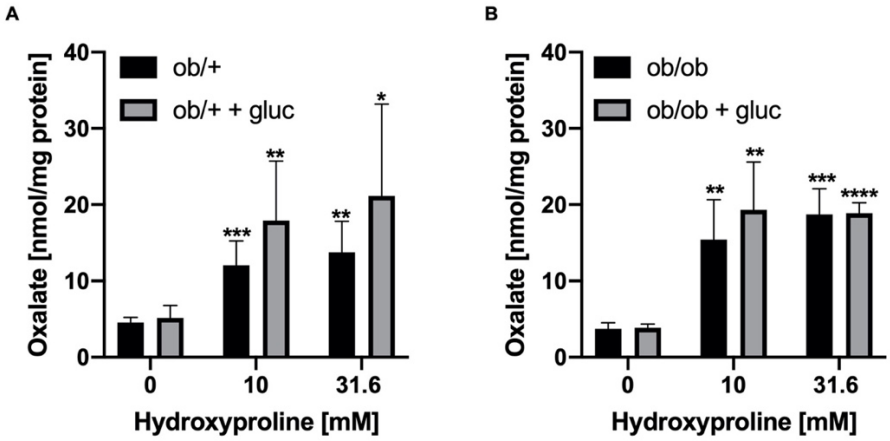

Figure 3.35: Hydroxyproline and glucagon challenge in primary hepatocytes of *ob/+* and *ob/ob* mice. 10 mM and 31.6 mM hydroxyproline increased the oxalate excretion of *ob/+* (A) and *ob/ob* hepatocytes (B). The treatment with 10 nM glucagon did not impact hydroxyproline stimulated oxalate production in neither *ob/+* nor *ob/ob* hepatocytes. The means ± SD are shown. * p < 0.05, ** p < 0.01, *** p < 0.01 for comparison of hydroxyproline treated to untreated. Student's t test, unpaired, two sided.

3.11 Response of Agxt to glucagon in the livers and primary mouse hepatocytes from WD-fed mice

Next, it was investigated whether the weakened response of *Agxt* mRNA expression to glucagon and earlier loss of Creb phosphorylation observed in steatotic ob/ob hepatocytes could be confirmed in a WD- induced NAFLD. The Agxt promoter hypermethylation observed in hepatocytes of 6 weeks WD-fed mice suggested that the transcription of *Agxt* in response

to glucagon might also be impaired in this model. Therefore, the treatment with glucagon in 6 weeks WD-fed and NCD-fed mice was conducted as described in Chapter 2.2.12.1 (Fig. 3.36).

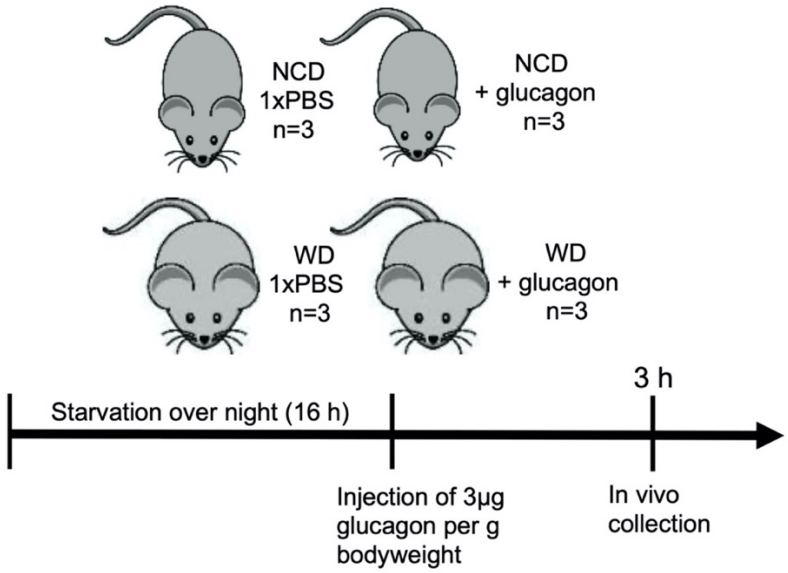

Figure 3.36: Scheme of experimental setup of glucagon treatment in 6 weeks WD-fed and NCD-fed mice. The mice were put into single cages and starved overnight. Next, 3µg/g body weight glucagon or 1 x PBS (vehicle) were injected intraperitoneally into three mice of each group (n=3). The mice were put back into their single cages without access to food. After 3 h the mice were scarified, and liver tissue was collected for qRT-PCR and immunoblotting.

3.11.1 Transcriptional response *of Agxt* mRNA expression towards glucagon in the livers of 6 weeks WD-fed mice

The Agxt expression in response to glucagon was analysed via qRT-PCR and immunoblot on mRNA and protein level, respectively.

Glucagon treatment elevated *Agxt* mRNA levels in the NCD + glucagon (gluc) group by 6.5-fold compared and in the WD + gluc by 7-fold compared to the corresponding control groups (Fig. 3.37 A). Despite the elevated *Agxt* mRNA, the Agxt protein expression was not influenced by glucagon treatment neither in NCD-fed nor in WD-fed mice at this time point (Fig. 3.37 B). In contrast to the situation in *ob/ob* mice, the Agxt mRNA expression in response to glucagon is not attenuated in the hepatic steatosis of 6 weeks WD-fed mice. These results suggest, that the *Agxt* promoter hypermethylation in 6 weeks WD-fed mice does not impact the *Agxt* mRNA expression responsiveness towards glucagon treatment.

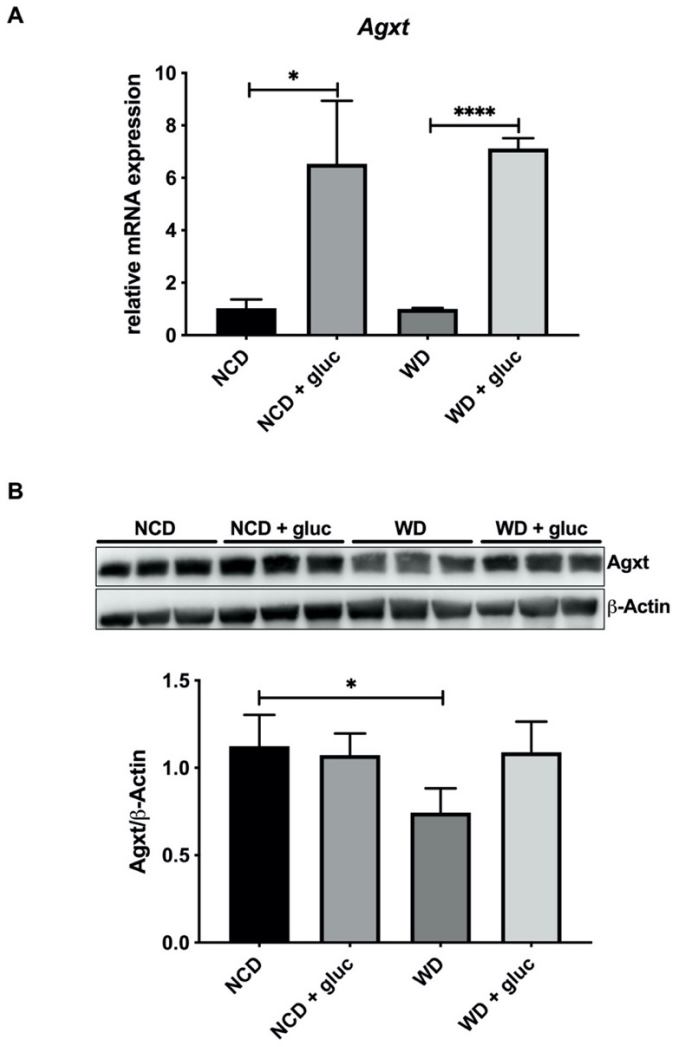

Figure 3.37: *Agxt* mRNA and protein expression in 6 weeks WD-fed and NCD-fed mice after glucagon treatment. Agxt mRNA levels are increased by glucagon treatment by 6.5-fold in 6 weeks NCD-fed and by 7-fold in 6 weeks WD-fed mice compared to the corresponding vehicle control groups (A). Densitometric analysis of Agxt immunoblot revealed that glucagon treatment did not influence Agxt protein expression in the livers of neither 6 weeks WD-fed nor NCD-fed mice. Gluc = glucagon. The means ± SD are shown. * $p < 0.05$, *** $p < 0.01$. Student's t test, unpaired, two sided.

3.11.2 Phosphorylation of Creb in the livers of WD-fed mice

Next, the phosphorylation of Creb in response to glucagon treatment in 6 weeks WD-fed and NCD-fed mice was analysed *via* immunoblotting of liver tissue extracts to better understand the contribution of the glucagon signalling pathway in the upregulation of *Agxt*. At the experimental time point analysed (3h after glucagon), the pCreb/tCreb ratio was not significantly altered in WD-fed mice compared to NCD-fed mice. Moreover, glucagon treatment did not influence the pCreb/tCreb ratio neither in NCD-fed nor in WD-fed mice (Fig. 3.38).

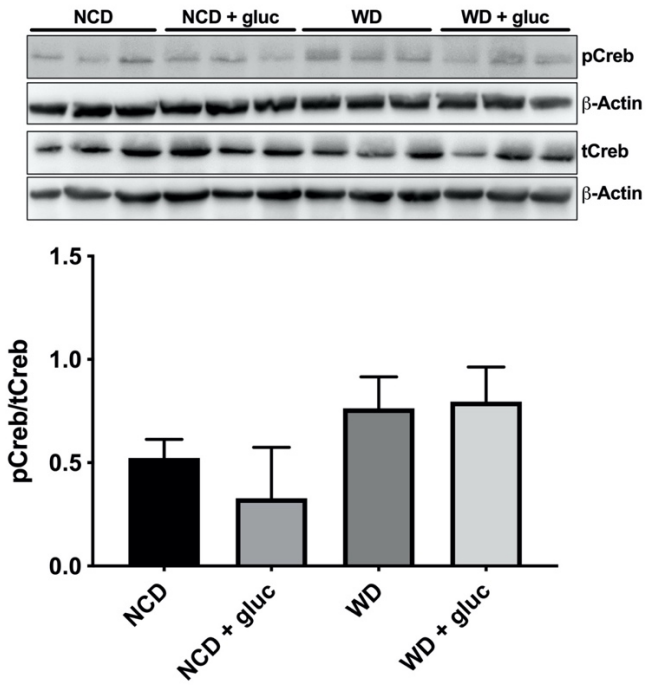

Figure 3.38: Immunoblot and densitometric analysis of pCreb/tCreb ratio in the livers of glucagon treated 6 weeks WD-fed and NCD-fed mice. The pCreb/tCreb ratio was not altered in WD-fed mice compared to NCD-fed controls. Furthermore, glucagon treatment did not impact the pCreb/tCreb ratio in the livers of neither NCD-fed nor WD-fed mice.

3.11.3 Time course of *Agxt* mRNA expression in glucagon-treated primary hepatocytes from WD-fed mice

Next, the Agxt expression in response to glucagon was investigated in a time dependent manner *in vitro* in primary mouse hepatocytes from 6 weeks WD-fed and NCD-fed mice. Glucagon treatment was performed like in the description of Chapter 2.2.12.2. For qRT-PCR analysis, all mRNA levels are calculated with respect to the untreated full media controls of each time point.

In primary hepatocytes from 6 weeks NCD-fed mice, the *Agxt* mRNA expression was increased upon treatment with 10 nM glucagon after 24 h (3.88 $\pm$ 0.85-fold change) and upon 100 nM glucagon after 6 h (1.90 $\pm$ 0.49-fold change) and 24 h (4.56 $\pm$ 1.20-fold change) of exposure compared to the untreated controls of the corresponding time points (Fig. 3.39 A). Glucagon treatment significantly elevated the *Agxt* mRNA levels in primary hepatocytes of WD-fed mice after 3 h (1.87 $\pm$ 0.08-fold change) and 6 h (2.15 $\pm$ 0.25-fold change) for 10 nM glucagon and after 6 h (2.29 $\pm$ 0.01-fold change) and 24 h (2.83 $\pm$ 1.03-fold change) for 100 nM glucagon compared to the full media controls of the corresponding time points (Fig. 3.39 A). There was no difference in glucagon stimulated *Agxt* mRNA expression between the hepatocytes of NCD-fed and WD-fed mice (Fig. 3.39 A). Protein expression of Agxt was not altered by 10 nM glucagon treatment neither in the hepatocytes of NCD-fed nor WD-fed mice (Fig. 3.39 B). This data confirms the results obtained *in vivo*, where glucagon treatment elevated *Agxt* mRNA

expression in NCD-fed and WD-fed mice to the same extent and had no influence on the Agxt protein expression (Chapter 3.11.1).

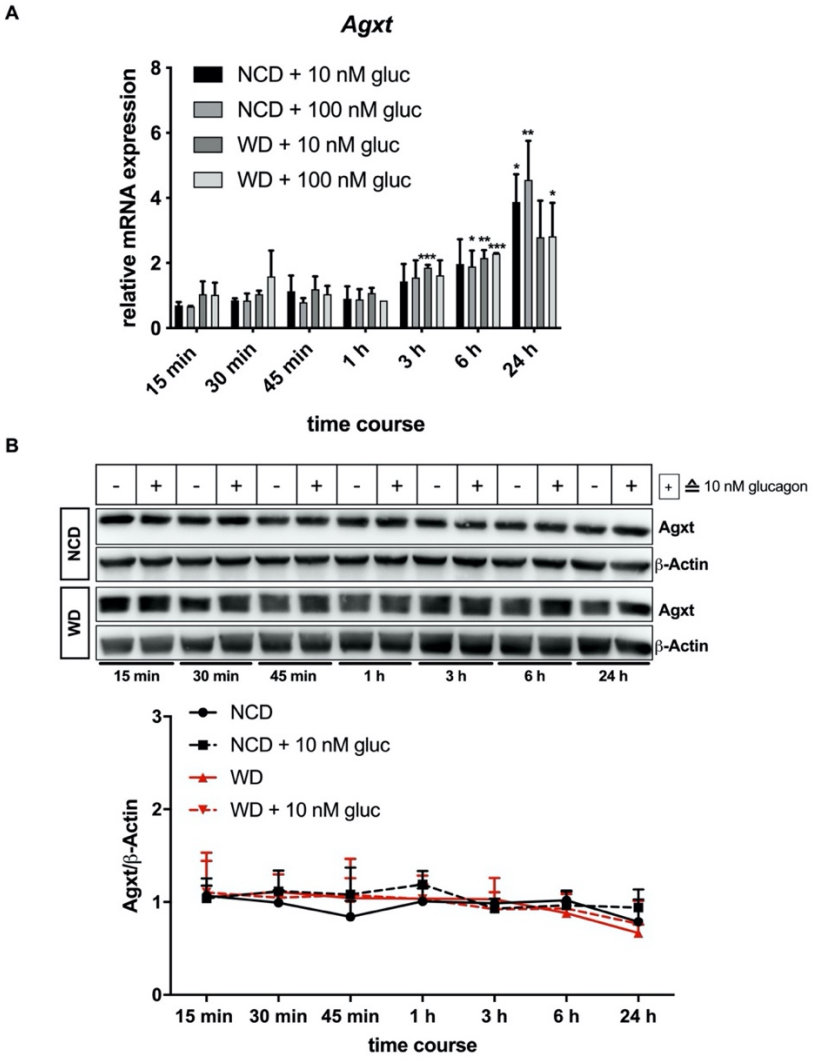

Figure 3.39: *Agxt* mRNA and protein expression in response to glucagon in primary hepatocytes of 6 weeks NCD-fed and WD-fed mice. Glucagon treatment increased *Agxt* mRNA expression in NCD hepatocytes after 24 h of exposure for 10 nM and after 6 h and 24 h for 100 nM glucagon. *Agxt* mRNA levels were elevated upon glucagon exposure after 3 h and 6 h for 10 nM and after 6 h and 24 h of exposure for 100 nM glucagon in WD hepatocytes. There was no difference in glucagon induced *Agxt* mRNA expression between NCD and WD hepatocytes (A). Agxt protein expression was not altered by glucagon treatment neither in NCD nor in WD hepatocytes (B). Gluc = glucagon. The means ± SD are shown. * $p < 0.05$, *** $p < 0.01$ for comparison of glucagon treated to untreated hepatocytes at the corresponding time points. Student's t test, unpaired, two sided.

3.11.4 Phosphorylation of Creb decreases earlier in WD hepatocytes in response to glucagon

The glucagon induced phosphorylation of Creb was investigated in 6 weeks WD-fed mice *via* immunoblotting in order to study possible influences of the Western diet on the glucagon pathway. Representative immunoblots of pCreb and tCreb in 6 weeks NCD-fed and WD-fed mice and densitometrically determined pCreb/tCreb ratios out of four independent experiments are depicted in Figure 3.40 (n=4).

Exposure to glucagon resulted in an increased Creb phosphorylation in both groups. However, the pCreb/tCreb ratio was significantly lower in WD hepatocytes (0.38 ± 0.12 pCreb/tCreb ratio) compared to NCD hepatocytes (1.03 ± 0.43 pCreb/tCreb ratio) after 6 h of glucagon treatment (Fig. 3.40). This confirms the observation made in *ob/ob* hepatocytes in a further NAFLD mouse model, and hence the independency of the earlier loss of pCreb phosphorylation to the genetic *ob/ob* model. Hence, this effect seems to be associated with hepatic steatosis, but the underlying molecular process remains unclear. Moreover, there seems be no connection between the earlier loss in Creb phosphorylation to the glucagon stimulated transcriptional response of *Agxt* in 6 weeks WD-fed mice.

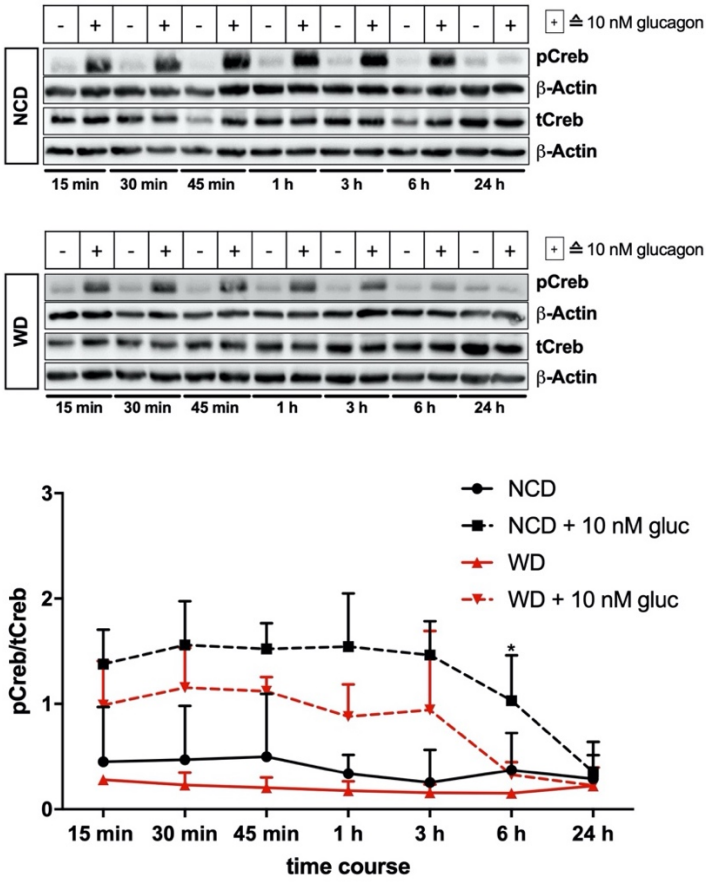

Figure 3.40: Representative immunoblots showing pCreb/tCreb ration in glucagon treated primary hepatocytes from 6 weeks WD-fed and NCD-fed mice. The pCreb/tCreb ratio was significantly decreased in WD hepatocytes compared to NCD hepatocytes after 6 h of glucagon treatment. Gluc = glucagon. The means ± SD are shown. * $p < 0.05$. Student's t test, unpaired, two sided.

3.12 Treatment of primary mouse hepatocytes with oleic acid and glucagon

Next, it was investigated whether the impaired response of *Agxt* mRNA expression towards glucagon and the earlier dephosphorylation of Creb in steatotic primary mouse hepatocytes is caused by the accumulation of lipids itself. For this purpose, *in vitro* steatosis was induced successfully induced in primary mouse hepatocytes which were subsequently treated with glucagon (Chapter 2.2.13) The experimental setup is depicted in Figure 3.41.

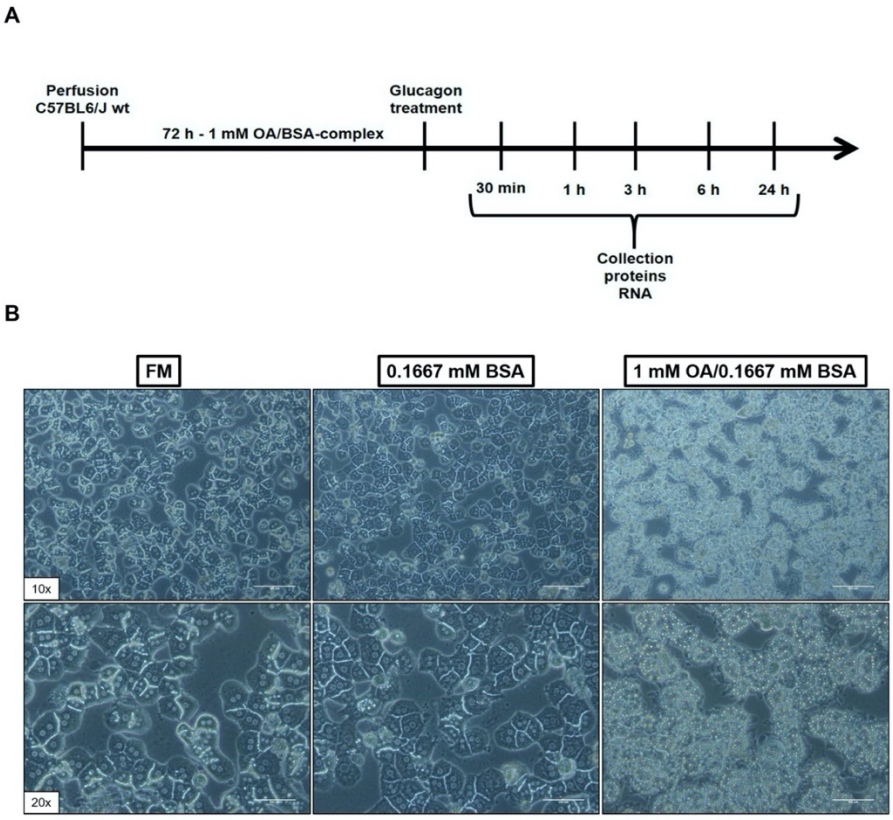

Figure 3.41: Experimental setup for establishing *in vitro* steatosis in primary mouse hepatocytes combined with a subsequent glucagon treatment. The isolated hepatocytes were incubated with control medium (FM), 0.1667 mM BSA-medium and 1 mM OA-medium for 72 h. Subsequently, the cells were treated with 10 nM glucagon for 30 min, 1 h, 3 h, 6 h and 24. Protein and RNA extracts were collected after each time point (A). Pictures showing the *in vitro* steatosis in the primary mouse hepatocytes after 72 h (B). Scale bars represents 200 µm.

3.12.1 *Agxt* mRNA expression response to glucagon is impaired by oleic acid treatment

The response of *Agxt* mRNA expression towards glucagon treatment in primary mouse hepatocytes cultivated in FM-medium (FM + 10 nM gluc), BSA-medium (BSA + 10 nM gluc) and OA-medium (OA + 10 nM gluc) was analysed *via* qRT-PCR. The values are calculated with respect to the FM untreated control group for each time point. The mRNA levels of the treated groups were compared with the levels of the groups cultivated in the same medium but not exposed to glucagon, e.g. OA + 10 nM gluc was compared with the OA group (*). Furthermore, in order to evaluate whether the lipid accumulation impacted the responsiveness of *Agxt* mRNA levels to glucagon, the OA + 10 nM group was compared to the FM + 10 nM gluc (#) and BSA + 10 nM gluc group (§; Fig. 3.42).

Glucagon treatment led to a significant elevation of *Agxt* mRNA levels in the FM + 10 nM gluc compared to FM control after 3 h (6.27 $\pm$ 1.23-fold change), 6 h (9.49 $\pm$ 5.01-fold change) and 24 h (5.64 $\pm$ 0.24-fold change) of glucagon challenge (*). An increase of *Agxt* mRNA expression could also be detected in the BSA + 10 nM gluc group compared to the BSA group after 3 h (5.90 $\pm$ 2.49-fold change) and 6 h (9.04 $\pm$ 2.73-fold change) of glucagon treatment (*), whereas *Agxt* mRNA levels did not response to glucagon in the OA + 10 nM gluc group compared to the OA group (Fig. 3.42). Furthermore, BSA itself influenced the *Agxt* mRNA expression after 24 h,

since Agxt mRNA levels increased approximately by 1.8-fold in the BSA + 10 nM gluc group compared to the FM + 10 nM gluc group after 24 h of treatment. Importantly, OA treatment resulted in a decreased *Agxt* mRNA expression when treated with glucagon compared to BSA + 10 nM gluc after 30 min, 1 h, 3 h and 6 h of glucagon exposure (§, Fig. 3.44). This effect was also observable when comparing OA + 10 nM gluc group to FM + 10 nM gluc after 1 h, 3 h and 24 h of incubation with glucagon (#; Fig. 3.42). These results suggest, that the accumulation of lipids itself, induced by OA/BSA treatment, impairs the responsiveness of *Agxt* mRNA expression towards glucagon.

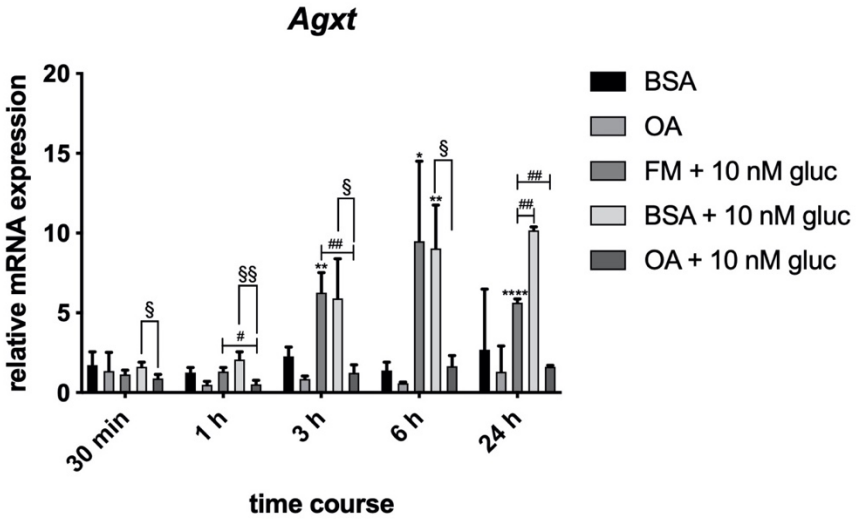

Figure 3.42: *Agxt* mRNA expression in response to glucagon in primary mouse hepatocytes with *in vitro* steatosis. Glucagon treatment increased *Agxt* mRNA levels in the FM + 10 nM gluc group after 3 h, 6 h and 24 h (*) of exposure compared to FM control and in the BSA + 10 nM gluc group for the 3 h and 6 h (*) time points compared to the BSA control group. *Agxt* mRNA expression was not elevated by glucagon in the OA + 10 nM gluc group with respect to the OA group. When compared to FM + 10 nM gluc and BSA + 10 nM gluc, the *Agxt* mRNA expression was decreased in the OA + 10 nM group after 1 h, 3 h, 24 h (#) and 30 min, 1h, 3 h, 6 h (§) of glucagon treatment, respectively. Gluc = glucagon. The means ± SD are shown. * p < 0.05, ** p < 0.01, *** p < 0.001 for comparisons between glucagon treated and untreated groups. # p < 0.05, ## p < 0.01 for comparison of FM + 10 nM gluc to BSA + 10 nM gluc and OA + 10 nM gluc. § p < 0.05, §§ p < 0.01 for comparison of BSA + 10 nM gluc to OA + 10 nM gluc. Student's t test, unpaired, two sided.

3.12.2 Treatment with oleic acid leads to earlier loss of Creb phosphorylation in response to glucagon

The phosphorylation of Creb upon glucagon treatment was analysed *via* immunoblotting to investigate whether the OA/BSA-induced steatosis influenced the glucagon signalling pathway.

The pCreb/tCreb ratio was decreased in the OA + 10 nM gluc group compared to FM + 10 nM gluc after 1 h and 3 h of glucagon treatment. Interestingly, BSA influenced the Creb phosphorylation, since the pCreb/tCreb ratio in the BSA + 10 nM gluc group was elevated only after 1 h of glucagon exposure compared to OA + 10 nM gluc, and hence displayed different effects than the FM + 10 nM gluc group (Fig. 3.43). This could be due the additional proteins added to the cells *via* BSA. The additional amino acids in combination with glucagon are able

to prolong gluconeogenesis, and hence the Creb phosphorylation (Aikawa et al. 1972). Taken together these result show that the accumulation of lipids in an *in vitro* steatosis model leads to an earlier loss of Creb phosphorylation compared to the FM and BSA control groups in primary mouse hepatocytes.

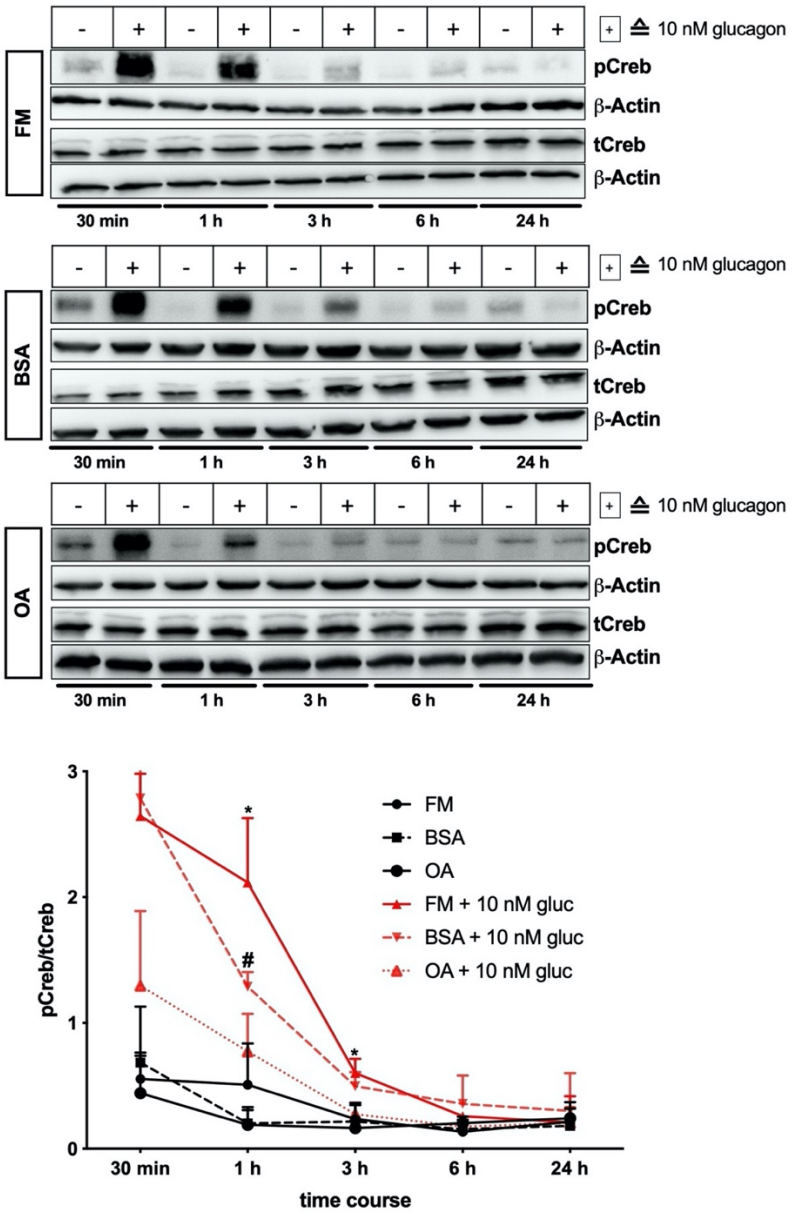

Figure 3.43: Representative immunoblots of pCreb and tCreb in OA-treated primary mouse hepatocytes upon glucagon exposure. The accumulation of lipids due to OA/BSA complex treatment leads to an earlier loss of Creb phosphorylation compared FM + 10 nM gluc and BSA + 10 nM gluc after 1 h and 3 h and after 1 h of glucagon treatment, respectively. Gluc = glucagon; pCreb – phosphorylate Creb; tCreb = total Creb. The means ± SD are shown. * $p < 0.05$ for comparing FM + 10 nM gluc to OA + 10 nM gluc. # $p < 0.05$ for comparing BSA + 10 nM gluc to OA + 10 nM gluc. Student's t test, unpaired, two sided.

3.13 Effects of glucagon treatment on primary human hepatocytes

In the next step it was studied whether the *Agxt* mRNA expression and Creb phosphorylation in response to glucagon exposure is altered in steatotic PHHs. Therefore, the PHHs from the

female donors Hum4229 and Hum4108 were chosen in order to simulate non-steatotic and steatotic conditions, since Hum4108 exhibited a 5-fold higher TAG compared to Hum4229 (Fig. 3.44 A). Glucagon treatment was performed as described in Chapter 2.2.14.

Glucagon treatment did not influence the *AGXT* mRNA expression in Hum4108 hepatocytes while in Hum4229 the *AGXT* mRNA levels increased after 24 h of glucagon exposure (Fig. 3.44 B). This suggests, that the steatotic donor Hum4108 displays an impaired *AGXT* mRNA expression upon glucagon treatment compared to the lean donor Hum4229, which supports the results seen in primary mouse hepatocytes. The response of human *AGXT* expression towards glucagon was surprising since the human *AGXT* gene does not display an CRE sequence (Purdue et al. 1991b). The glucagon induced gluconeogenesis might exhibit in indirect effect on the expression of *AGXT*. Whether the difference in *AGXT* mRNA expression responsiveness towards glucagon between the donors is due to the different TAG content remains unanswered. Therefore, this experiment has to be repeated with further non-steatotic and steatotic donor pairs in order to verify this hypothesis.

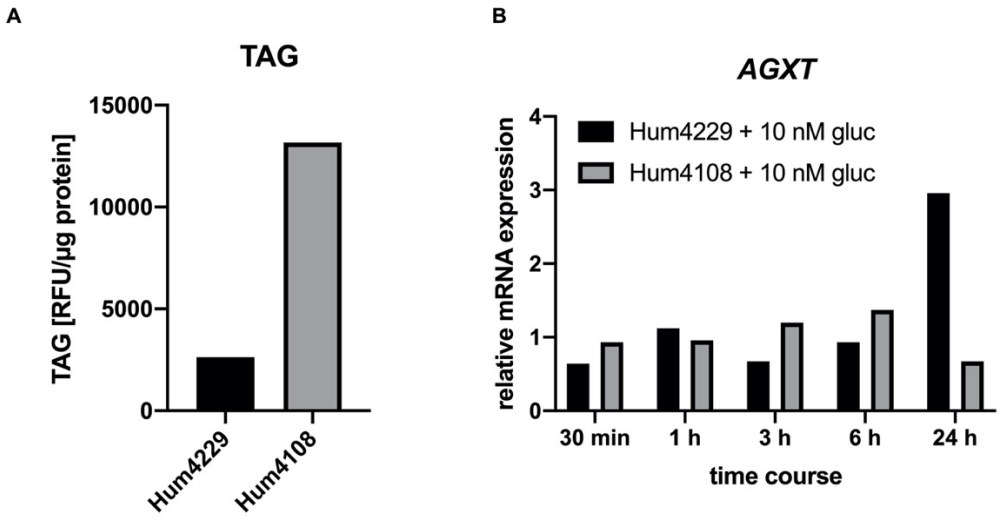

Figure 3.44: *AGXT* mRNA expression upon glucagon treatment in PHHs from Hum4229 and Hum4108. Glucagon treatment resulted in an elevation of *AGXT* mRNA levels in Hum4229 after 24 h but did not influence *AGXT* mRNA expression in Hum4108. Gluc = glucagon.

Whether the phosphorylation of Creb upon glucagon treatment differed between the non-steatotic Hum4229 and steatotic Hum4108 donor was investigated *via* immunoblotting (Fig.3.45). The pCreb signal in Hum4108 hepatocytes appeared to be weaker after 3 h and 6 h of glucagon treatment compared to Hum4229 (Fig. 3.45 A). For a better comparison the untreated and treated samples from the time points of 1 h, 3 h and 6 h of both donors were analysed on the same membrane (Fig. 3.45 B). The immunoblot showed an impaired pCreb signal in Hum4108 hepatocytes after 3 h and 6 h of glucagon treatment and confirmed the previously mentioned observation from Fig. 3.45 A. The effect of an earlier loss of Creb phosphorylation under steatotic condition seems also to be true for this pair of PHHs. For further validation, more experiments with non-steatotic and steatotic pairs of primary human hepatocytes have to be done.

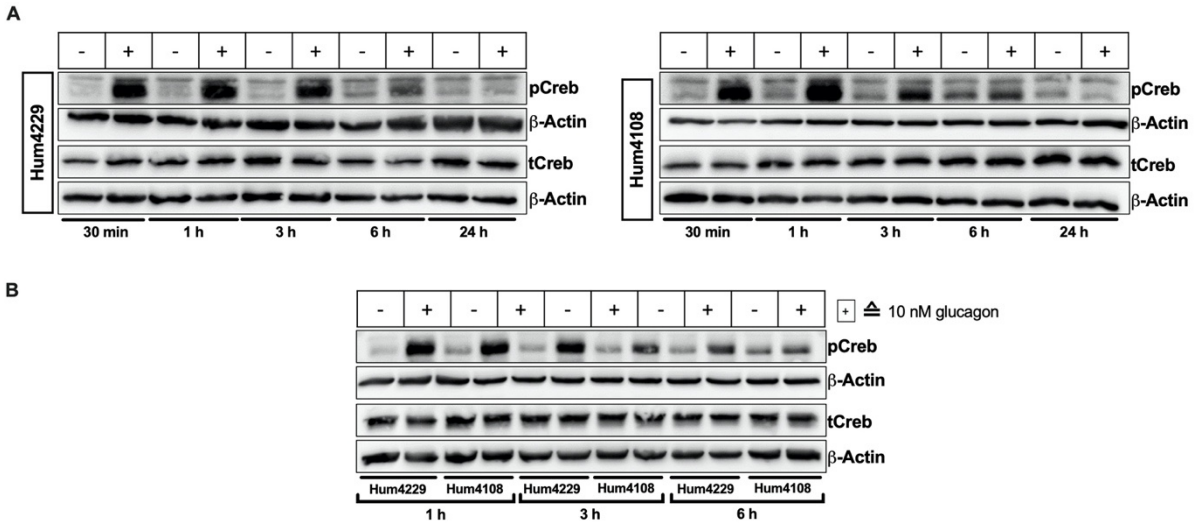

Figure 3.45: Creb phosphorylation upon glucagon treatment in PHHs from Hum4229 and Hum4108. The signal of pCreb appeared to be weaker in Hum4108 after 3 h and 6 h of glucagon treatment compared to Hum4229 (A). Protein extracts from both donors for the time points 1 h, 3 h and 6 h were analysed on the same immunoblot. Again, the pCreb signal in Hum4108 hepatocytes after 3 h and 6 h of glucagon exposure appeared to be weaker compared to the corresponding samples of Hum4229. Gluc = glucagon.

4 Discussion

NAFLD is the most common cause of liver disease worldwide and highly relevant due to its potential to progress to severe liver diseases such as cirrhosis or hepatocellular cancer (HCC). Furthermore, the metabolic syndrome, an increased risk of cardiovascular diseases (Misra et al. 2009) and renal diseases, like CKD (Musso et al. 2014b) and urolithiasis (Nam et al. 2016), are also strongly associated with NAFLD. The underlying molecular mechanism explaining the connection of NAFLD to urolithiasis remained unknown.

In a previous study, the downregulation of the glyoxylate detoxifying enzyme alanine-glyoxylate aminotransferase (AGXT) was found to be associated with lipid accumulation in NAFLD mouse models, in an *in vitro* steatosis model as well as in steatotic primary human hepatocytes (PHHs). AGXT is essential for preventing excessive formation of oxalate from glyoxylate. Patients with primary hyperoxaluria type 1 (PH1) carry mutations in the *AGXT* gene which lead to an insufficient or missing AGXT enzyme activity, and subsequently to an accumulation of oxalate within the kidneys which results in the recurrent formation of calcium oxalate deposits and severe kidney damage. The downregulation of *Agxt* in steatotic conditions was proposed as one possible mechanism linking NAFLD and the formation of calcium oxalate kidney stones. Besides its downregulation, the *AGXT* promoter was found to be hypermethylated upon steatosis in the hepatocytes of *ob/ob* mice and in steatotic primary human hepatocytes (PHHs). Therefore, it was proposed, that the *AGXT* downregulation in steatosis might be caused by the hypermethylation of its promotor (Gianmoena 2017). In addition to its role in glyoxylate detoxification, Agxt is reported to play a role in gluconeogenesis due to its ability of catalysing the conversion of serine and pyruvate to hydroxypyruvate and alanine (Remesy et al. 1983). In line with a role in gluconeogenesis, it was shown, that the rodent *Agxt* gene sequence contains a CRE sequence (Oda et al. 1993; Li et al. 1999a), which is bound by the transcription factor Creb in response to glucagon. In several studies, glucagon was shown to enhance *Agxt* mRNA and protein expression as well as the Agxt activity in mice and rat (Tsubaki and Hiraiwa 1971b; Fukushima et al. 1978b; Biochem 1989). Interestingly, the CRE sequence in the *Agxt* promotor is located within the steatosis-associated hypermethylated region. Therefore, a working hypothesis was that hypermethylation of CRE sequence may prevent transcriptional upregulation of *Agxt* in response to glucagon.

In the course of this PhD thesis, consequences of the steatosis-associated deregulation of the hepatic glyoxylate metabolism were examined *in vivo* in two different NAFLD mouse models, as well as *in vitro* in cultivated primary mouse hepatocytes isolated from these mouse models. These experiments revealed an increased production of oxalate in steatotic hepatocytes after catabolism of hydroxyproline. Evidence for a causal role of the *Agxt* downregulation on increased oxalate generation was achieved by rescuing Agxt levels in steatotic hepatocytes *via* adeno-associated virus (AAV)-mediated gene transfer. Analysis of *Agxt* knockout ($Agxt^{-/-}$) mice confirmed the pivotal role of Agxt deficiency. Moreover, in order to understand potential

consequences of the steatosis dependent hypermethylation in the *Agxt* promoter, the responsiveness of the Agxt expression towards glucagon in steatosis was investigated. In addition to the *Agxt* promoter hypermethylation, a steatosis-associated earlier loss of Creb phosphorylation upon glucagon treatment was detected in primary mouse hepatocytes from both NAFLD mouse models and in an *in vitro* steatosis model. This indicated that not only the methylation status of the *Agxt* promoter but also the intensity and duration of the signal transduction pathway might play an important role. Finally, the translational relevance of the findings in NAFLD mice was studied in a children cohort of NAFLD and in cultivated human hepatocytes. The most important findings are discussed below in detail.

4.1 Alterations in the expression of glyoxylate metabolism enzymes predispose to elevated oxalate generation from hydroxyproline catabolism

In order to understand the steatosis-dependent deregulations within the glyoxylate metabolism, the expression of glyoxylate metabolism enzymes was analysed on mRNA and protein level in *ob/ob* and 6 weeks WD-fed mice. In addition to the downregulation of *Agxt*, the focus was on upstream enzymes that lead to glyoxylate production both in the peroxisome (Hao1) and in the mitochondria (e.g. Prodh2), but also on the *Ldha* isoform of the lactate dehydrogenase, which converts glyoxylate to oxalate.

A downregulation of *Hao1* mRNA and protein levels in *ob/ob* mice indicated an impaired peroxisomal glyoxylate formation. In the mitochondria however, the pathway of hydroxyproline catabolism, which leads to the formation of mitochondrial glyoxylate, was not downregulated. In combination with a downregulation of *Agxt*, this subsequently leads to an overall increased hepatic oxalate production in the liver of *ob/ob* mice. The glyoxylate metabolism in 6 weeks Western diet-fed (WD-fed) mice displayed slightly different alterations. While the downregulation of *Agxt* on mRNA and protein level in the livers of 6 weeks WD-fed mice was similar to *ob/ob* mice, the upregulation of *Ldha* mRNA and protein expression was not observed in the *ob/ob* mouse model. Also, the downregulation of Hao1 protein expression could only be detected in primary hepatocytes of 6 weeks WD mice, similar to primary hepatocytes from *ob/ob* mice. However, in summary, the steatosis induced alterations of the glyoxylate metabolism in the livers of 6 weeks WD-fed mice predispose for an elevated hepatic oxalate production. Furthermore, these results obtained in *ob/ob* and WD-fed mice indicate that changes in glyoxylate metabolism are independent of the NAFLD mouse model and can be attributed to the condition of hepatic steatosis. This is supported by data from a previous study which showed a downregulation of *Agxt*, *Hao1* and *Grhpr* upon an induction of *in vitro* steatosis in primary mouse hepatocytes (Gianmoena 2017). These findings suggest that triglyceride accumulation within hepatocytes may have a causal role in the gene expression changes observed in the glyoxylate metabolism pathway.

The steatosis-associated altered expression of the glyoxylate metabolism enzymes predisposed towards increased hepatic oxalate generation in both NAFLD mouse models.

Whether these alterations lead to higher oxalate excretion from steatotic hepatocytes was investigated by analysing the oxalate formation from different oxalate precursors. Furthermore, it was a major aim of this work to understand possible extrahepatic pathophysiological effects of an increased steatosis-associated hepatic oxalate generation *in vivo*.

A previous study already showed a higher oxalate formation from hydroxyproline catabolism in primary *ob/ob* hepatocytes compared to *ob/+* hepatocytes, demonstrating an increased susceptibility of *ob/ob* hepatocytes towards oxalate production from hydroxyproline (Gianmoena 2017). This was attributed to the insufficient detoxification of mitochondrial glyoxylate due to the steatosis-induced downregulation of Agxt (Gianmoena 2017). By these means, the hydroxyproline metabolism was identified as a crucial pathway leading to elevated oxalate production in conditions of steatosis (Gianmoena 2017). In the present study, the steatosis-associated increased susceptibility towards hydroxyproline was confirmed in another NAFLD mouse model, since primary hepatocytes from 6 weeks WD-fed mice also excreted significantly increased amounts of oxalate and glycolate upon hydroxyproline treatment compared to their lean counterparts.

Consistent with the *in vitro* results, plasma oxalate concentrations in the hepatic vein of *ob/ob* mice, showing the oxalate excretion out of the liver, were elevated upon hydroxyproline enriched (1% Hyp) diet. Daily urinary oxalate excretion was elevated by 1% Hyp diet in both genotypes whereas 1% Hyp fed *ob/ob* mice displayed the highest urinary oxalate concentrations. Hence, the livers of *ob/ob* mice are not able to sufficiently detoxify the glyoxylate generated from dietary hydroxyproline. This is likely the consequence of the steatosis-induced alterations in glyoxylate metabolism leading to an enhanced hepatic oxalate excretion into the plasma and consequently elevated urinary oxalate amounts. This approach is of human relevance since dietary meat contains between 0.3 and 0.7 % hydroxyproline and gelatine exhibits 9-15 % of hydroxyproline (Miyada and Tappel 1956; Knight et al. 2006).

It is important to note that the hyperoxaluria observed after consumption of hydroxyproline enriched diet did not lead to the development of calcium oxalate deposits within the kidneys of *ob/ob* mice. Hyperoxaluria is expected to have pathophysiological consequences, since excess oxalate can accumulate within the kidneys and subsequently might lead to the formation of calcium oxalate deposits and ultimately to severe kidney damage (Romero et al. 2010a). Furthermore, oxalate represents a risk factor for CKD progression (Waikar et al. 2019). It has been reported that kidneys of *ob/ob* mice exhibit an increased susceptibility towards glyoxylate-induced crystal formation (Fujii et al. 2013). The lack of urolithiasis in our study may be due to the observed increased urine volume of *ob/ob* mice, which probably results from increased glucose levels in the plasma and kidney tubules. This leads to osmotic diuresis (Lindström 2007, 2010), which is a reported factor for the prevention of calcium oxalate supersaturation (Mulay and Anders 2017). The formation of kidney stones is a highly complex process with multiple steps which are affected by multiple aspects beside the oxalate concentration (Basavaraj et al. 2007). This is supported by a study from Salido and colleagues,

where despite a complete *Agxt* deficiency and a much stronger hyperoxaluria than in *ob/ob* mice, only half of the analysed *Agxt*$^{-/-}$ mice developed calcium oxalate urinary stones and just a few exhibited calcium oxalate deposits in the kidneys under normal conditions. Severe kidney stone disease could only be seen after enhancement of oxalate production by 0.7% ethylene glycol administration (Salido et al. 2006a). Agxt is downregulated in hepatic steatosis of *ob/ob* mice, but not completely absent. This might explain the missing calcium oxalate kidney stones in *ob/ob* mice despite the increased hepatic oxalate production and hyperoxaluria.

Increased hepatic oxalate production in 6 weeks WD-fed mice, caused by glyoxylate metabolism changes, was reflected in higher plasma oxalate levels in the hepatic vein and right heart chamber. In contrast to *ob/ob* mice, 6 weeks WD-fed mice were not hyperoxaluric. The reason for this discrepancy is not fully understood, but hyperoxaluria may perhaps only develop when challenged with a dietary precursor. Although no 1% Hyp-enriched diet was given to these mice *in vivo*, the results obtained in cultivated primary hepatocytes isolated from 6 weeks WD-fed mice suggest that they may also excrete more oxalate when fed with hydroxyproline. Another reason for the lack of hyperoxaluria in this mouse model could be changes in endogenous collagen turnover. It has been reported, that not only dietary but also tissue collagen turnover-derived hydroxyproline contributes to the daily urinary oxalate excretion (Knight et al. 2006b; Li et al. 2016; Fargue et al. 2018). Furthermore, NAFLD is known to affect collagen-rich tissues, such as bone and muscle tissue, in human and mice (Lindström 2007; Abrigo et al. 2016; Poggiogalle et al. 2017). Therefore, NAFLD-induced reduction of lean body mass might influence the endogenous hydroxyproline concentrations, and hence lead to reduced oxalate excretion. Additionally, a decreased collagen turnover from endogenous tissue in PH1 patients has been reported, indicating a complex negative feedback mechanism/organ crosstalk which remains not fully understood (Fargue et al. 2018).

All in all, this work provides evidence for an increased formation of the kidney stone-promoting factor oxalate in hepatic steatosis. Although, as mentioned before, the formation of kidney stones is a highly complex mechanism which consists of multiple steps and is influenced by several factors (Basavaraj et al. 2007; Romero et al. 2010b), the increased hepatic oxalate production by the steatotic liver may be a key initial event leading to a cascade that might result in the formation of kidney stones or worsen a pre-existing kidney disease (Einollahi et al. 2013; Musso et al. 2014b; Nam et al. 2016; Mantovani et al. 2018; Qin et al. 2018; Waikar et al. 2019).

4.2 Downregulation of Agxt is a key factor for increasing hydroxyproline-derived oxalate production in hepatic steatosis

An important goal of this work was to investigate whether the steatosis-induced downregulation of *Agxt* is sufficient to result in an increased oxalate generation from the hydroxyproline catabolism. This hypothesis was supported by the fact that the inhibition of Prodh2, which catalyses the first and rate-limiting step of hydroxyproline catabolism, reduced

the oxalate excretion from primary *ob/ob* hepatocytes upon hydroxyproline exposure to the level of *ob/+* control hepatocytes. This emphasises the importance of the hydroxyproline pathway as a source of increased oxalate production in *ob/ob* hepatocytes. In addition, the fact that rescuing the Agxt expression in *ob/ob* hepatocytes also reduced the hydroxyproline-derived oxalate excretion provided evidence for the causal role of *Agxt* downregulation in the oxalate overproduction of *ob/ob* hepatocytes. Finally, the phenotype caused by *Agxt* downregulation in steatotic hepatocytes could be compared to that of *Agxt*$^{-/-}$ mice. A complete deficiency of *Agxt* leads to excessive oxalate production from glycolate and hydroxyproline, which are converted to glyoxylate in the peroxisomes and in the mitochondria respectively. This is in contrast to a milder phenotype in steatotic hepatocytes, where *Agxt* downregulation only affects detoxification of hydroxyproline-derived glyoxylate. These results provided evidence that either only mitochondrial Agxt is downregulated in hepatic steatosis or that mitochondrial glyoxylate detoxification is particularly affected by the downregulation of Agxt.

4.3 Steatosis grade correlates with increased urinary oxalate excretion in human NAFLD

In a previous work, the *AGXT* hypermethylation and downregulation were shown to correlate with the TAG content of PHHs isolated from control and steatotic donors (Gianmoena 2017), demonstrating an important similarity between human and mouse NAFLD. In this work, the significant correlation observed between the daily urinary oxalate and the steatosis percentage in a paediatric cohort of biopsy proven NAFLD indicated that also the human steatotic liver produces more oxalate. Weaknesses of this study are on the one hand the small sample size, and on the other hand the lack of information regarding dietary oxalate precursors.

In order to gain information about the metabolization of glyoxylate precursors by human hepatocytes in vitro experiments similar to those with primary mouse hepatocytes were performed. Treating PHHs with oxalate precursors showed an increased oxalate production from glycolate but not from hydroxyproline. This was in contrast to primary mouse hepatocytes, which released oxalate formed from the hydroxyproline catabolism. The observed effect results most probably due to high expression of *GRHPR* in human mitochondria, which reduces glyoxylate to glycolate (Salido et al. 2012). In agreement, glycolate excretion was increased in human hepatocytes exposed to hydroxyproline. AGXT is exclusively localised in peroxisomes in the human liver (Danpure 2006b). Therefore, it is possible that reduced expression of *AGXT* in human steatotic hepatocytes would only affect glyoxylate generation in this organelle. So far, the only reaction known to generate glyoxylate in the peroxisome is the oxidation of glycolate to glyoxylate by HAO1 (Salido et al. 2012). Therefore, to examine the consequences of steatosis in the human hepatocytes, experiments with steatotic and non-steatotic donors exposed to glycolate have to be done in the future.

4.4 The altered transcriptional response of *Agxt* to glucagon in steatosis – possible mechanisms

Many studies have shown that the *Agxt* expression is elevated upon glucagon treatment due to the CRE sequence in the *Agxt* promoter (Rowsell et al. 1969; Tsubaki and Hiraiwa 1971a; Fukushima et al. 1978a; Miyajima et al. 1989; Oda et al. 1993; Uchida et al. 1994; Li et al. 1999a).

Understanding whether hypermethylation of the *Agxt* promoter in conditions of hepatic steatosis has a causal contribution in the downregulation of *Agxt* and/or its response to glucagon was one focus of this thesis. One hypothesis was that the steatosis-associated *Agxt* hypermethylation of the Cre sequence in the *Agxt* promoter observed in steatotic hepatocytes may repress the binding of the transcription factor Creb, which is activated by the glucagon receptor-cyclic adenosine monophosphate-protein kinase A (GCGR-cAMP-PKA) pathway, leading to a missing or reduced upregulation of *Agxt* mRNA expression in response to glucagon. To investigate this hypothesis, the transcriptional upregulation of Agxt after treatment with glucagon was investigated in both the *ob/ob* and WD-induced NAFLD mouse models both in vivo and in vitro.

In *ob/ob* mice, the injection of glucagon did not lead to an increased *Agxt* mRNA expression in contrast to *ob/+* control mice, which was confirmed in *in vitro* experiments in primary hepatocytes from *ob/+* and *ob/ob* mice. This indicated a compromised transcriptional upregulation of *Agxt* in *ob/ob* mice. In contrast, glucagon injection in WD-fed mice resulted in an increased *Agxt* mRNA expression that was comparable to that of NCD-fed mice, and similar results were obtained in *in vitro* experiments. When relating this behaviour to the degree of methylation in the *Agxt* promoter, the average hypermethylation in the analysed promoter region was increased by approximately 2.5-fold in *ob/ob* hepatocytes and 1.5-fold in WD hepatocytes compared to their lean counterparts. Hence, the higher methylation in the *Agxt* promoter of *ob/ob* mice was in agreement with the loss of responsiveness to glucagon, while in 6 weeks WD-fed mice the weaker methylation was in line with the successful glucagon-induced upregulation. This supports the role of the promoter hypermethylation regarding the suppression of *Agxt* mRNA expression in response to glucagon, since the promoter hypermethylation may repress the binding of pCreb to the CRE sequence within the *Agxt* promoter and hence impair the *Agxt* expression.

Interestingly, in an *in vitro* steatosis model of oleic acid (OA) -induced lipid accumulation in primary mouse hepatocytes, a strongly attenuated transcriptional response of *Agxt* mRNA to glucagon was also observed. While this confirms that the accumulation of lipids in hepatic steatosis impairs the *Agxt* mRNA expression in response to glucagon, the involved mechanism in this case may not be a steatosis-associated hypermethylation of the *Agxt* promoter, since *de novo* DNA methylation could not be induced in primary hepatocytes cultivated *in vitro* (Gianmoena 2017).

Considering that the impaired glucagon-induced transcriptional upregulation of *Agxt* observed in steatosis could also arise from a dysfunctional glucagon signalling pathway, the phosphorylation of Creb was analysed as a representative for pathway activation. An earlier loss of Creb phosphorylation in response to glucagon was observed in the hepatocytes from *ob/ob* and 6 weeks WD-fed mice as well as in the *in vitro* steatosis model. This attenuated glucagon signalling may contribute to the impaired transcriptional upregulation of *Agxt* in *ob/ob* hepatocytes and in the OA-induced steatosis *in vitro*. However, in 6 weeks WD-fed mice *Agxt* becomes successfully upregulated by glucagon despite a faster dephosphorylation of Creb. This is not yet understood. The molecular mechanism leading to the earlier loss of Creb phosphorylation also remains unclear. In literature, GCGR desensitisation and internalisation have been extensively discussed as a possible mechanisms driving steatosis associated attenuation of the glucagon signalling pathway (Authier et al. 1992; Charbonneau et al. 2005a, 2007; Krilov et al. 2008, 2011). However, our data suggest that the observed effects arise from steatosis-associated alterations downstream of the GCGR. An upregulation of phosphatases which dephosphorylate Creb faster in steatotic conditions, a feedback mechanism leading to a faster termination of signalling, an inhibition of the adenylate cyclase, an increased degradation of cAMP or the suppression of PKA could all be potential underlying mechanism explaining the acquired results.

In control PHHs, the upregulation of *AGXT* mRNA levels due to glucagon treatment was surprising since the human *AGXT* promoter does not contain a CRE sequence (Purdue et al. 1991b). Hence, the mechanism of glucagon-induced *AGXT* upregulation may not be conserved between both species. It might result from branches of the glucagon signalling pathway that do not involve CREB phosphorylation as well as from increased substrate availability (Jahoor et al. 1990; Goldstein and Hager 2018). Interestingly, human hepatocytes with a higher TAG content failed to upregulate *AGXT* in response to glucagon, which was paralleled by an earlier lost in CREB phosphorylation. Thus, lipid accumulation affects AGXT in human and mice in a similar way. However, additional experiments are needed in order to validate the obtained results.

4.5 Steatosis-associated impaired transcriptional response of Agxt towards glucagon might reduce hyperglycaemia

A further aim of this thesis was to understand the potential physiological consequences and benefits resulting from an impaired transcriptional response of Agxt towards glucagon in hepatic steatosis.

Assuming that Agxt plays a role in gluconeogenesis by providing gluconeogenic substrates, it can be speculated that the steatosis-induced attenuation of the hepatic glucagon signalling meant to upregulate Agxt might be a negative feedback mechanism in order to prevent further increase of hepatic glucose production in NAFLD, which is strongly associated with hyperglycaemia, insulin resistance, and T2D (Marchesini et al. 1999; Hatziagelaki et al. 2012; Williams et al. 2013). Furthermore, the upregulation of *Agxt* by glucagon in rats has been

shown to reduce hydroxyproline-derived urinary oxalate excretion due to the increased glyoxylate detoxification (Takayama et al. 2003). All in all, downregulating *Agxt* may help prevent excessive hyperglycaemia but may result in hyperoxaluria.

Surprisingly, a reduced oxalate production due to the glucagon-induced increase of *Agxt* mRNA expression could not be observed in our *in vitro* experiments, in which primary hepatocytes from *ob/+* and *ob/ob* mice were treated with glucagon and hydroxyproline simultaneously. This is most likely due to lack of translation of Agxt protein in response to glucagon treatment, since no increase in Agxt protein levels could be detected in cultivated hepatocytes in response to glucagon despite higher Agxt mRNA levels. *In vitro* conditions might not be suitable for this experiment due to expressional alterations happening in cultivated primary mouse hepatocytes (Godoy et al. 2016). This cultivation-dependent loss of hepatic gene expression may be responsible for the less efficient translation of Agxt. Importantly, also, after transduction of the viral Agxt construct, *ob/+* hepatocytes did not display a significant higher Agxt protein expression even though mRNA levels were elevated already 24 h after transduction. In conclusion, cultivated primary mouse hepatocytes seem to have protein translation difficulties regarding Agxt, which might explain why glucagon treatment did not reduce oxalate excretion in hydroxyproline treated primary hepatocytes. Furthermore, it might also be possible that the subcellular distribution of the Agxt enzymes changes in response to glucagon instead of an overall increase of Agxt protein expression. However, the exact underlying molecular reason remains unclear. To circumvent these difficulties, experiments in mice should be performed.

4.6 Future perspectives

This study has demonstrated that the *Agxt* downregulation is a key event leading to steatosis-associated increased hepatic oxalate production from hydroxyproline catabolism, as observed in primary hepatocytes from both *ob/ob* mice (Gianmoena 2017) and Western-diet (WD)-fed mice.

Increased hepatic oxalate production and mild hyperoxaluria have been shown to be pathophysiological consequences of the steatosis-linked *Agxt* downregulation in *ob/ob* mice, which were both further increased by dietary hydroxyproline. Since, rescuing *Agxt* expression in cultivated *ob/ob* hepatocytes *in vitro* reduced the oxalate production upon hydroxyproline treatment, future *in vivo* experiments will be necessary to clarify whether the rescue of the *Agxt* expression reverses the hyperoxaluria in *ob/ob* mice. In addition, rescue experiments by adeno-associated virus-(AAV) mediated delivery of *Agxt* should be conducted in WD-fed mice, where the influence of dietary hydroxyproline on the hepatic and urinary oxalate excretion still remains to be investigated. This will strengthen the connection between hepatic steatosis and increased hepatic oxalated production followed by an elevated urinary oxalate excretion *via Agxt* in the two different NAFLD mouse models.

One question that was not addressed within this thesis is whether the downregulation of *Agxt* in mouse NAFLD affects both subcellular pools of Agxt, the mitochondrial and the peroxisomal.

While the results obtained provide strong evidence for a reduced mitochondrial pool it cannot be excluded that also the peroxisomal Agxt is reduced, and hence plays a role in the observed pathology. For this purpose, peroxisomal and mitochondrial targeting Agxt constructs will be delivered by AAV transduction and the effects regarding the increased hepatic oxalate excretion and hyperoxaluria will be studied. Furthermore, this should be combined with a hydroxyproline- or a glycolate-enriched diet in order to understand the roles of peroxisomal and mitochondrial Agxt towards exogenously added oxalate precursors *in* vivo in the context of NAFLD.

Although the downregulation of *Agxt* has been shown in both mouse models of NAFLD studied, they differed in the transcriptional response of *Agxt* to glucagon. Because, in contrast to *ob/ob* mice, an impaired responsiveness of *Agxt* mRNA expression towards glucagon was not observed in 6 weeks WD-fed mice. This was most probably due to the less distinct promoter hypermethylation in WD-fed mice compared to *ob/ob* mice. Therefore, studying both *Agxt* promoter methylation and the *Agxt* response towards glucagon in mice that were fed with a WD for longer periods of time would be important in order to understand whether the hypermethylation of *Agxt* increases by prolonged diet-induced steatosis and whether this is connected to loss of transcriptional regulation by glucagon. Furthermore, the influence of NAFLD progression on the transcriptional response of *Agxt* to glucagon should be investigated, since cirrhosis is reported to be associated with impaired glucagon signalling (Keller et al. 1982).

Furthermore, it is still unclear by which molecular mechanism the accumulation of lipids leads to the downregulation of *Agxt* in hepatic steatosis. The oversupply of lipids has been reported to result in an accumulation of lipotoxic intermediates, which in turn drive the development of insulin resistance (Erion and Shulman 2010; Yazıcı and Sezer 2017). It could be possible, that lipotoxicity and insulin resistance might lead to the downregulation of *Agxt*, since in addition to glucagon, also insulin is reported to regulate *Agxt* expression (Miyajima et al. 1989). However, this has to be extensively analysed in future experiments, e.g. in our *in vitro* steatosis model. Moreover, the mechanism leading to the steatosis-associated hypermethylation in the *Agxt* promoter still needs to be clarified. DNA methyltransferase 1 (DNMT1) has been reported to be increased in obesity (Kim et al. 2015). Therefore, analysing DNMT1 and other DNMTs might be a starting point for the purpose of elucidating the key mechanism leading to *Agxt* promoter hypermethylation in hepatic steatosis. Additionally, a transfection assay with a CpG free luciferase reporter vector (Klug and Rehli 2006) could be used to analyse whether the hypermethylation of the Agxt promoter results in silencing or repression of the Agxt gene expression.

One finding of this study, the altered glucagon signalling pathway, deserves future research since it may have important implications in the regulation of hepatic gluconeogenesis and thus hyperglycaemia. The underlying mechanism leading to the earlier dephosphorylation of Creb in all steatotic conditions studied - in primary hepatocytes from *ob/ob* and WD-fed mice, in an *in vitro* steatosis model as well as in primary human hepatocytes (PHHs) with an increased

triglyceride content - has to be clarified in further experiments by manipulating and monitoring different components of the glucagon signal transduction pathway. Finally, the physiological consequence for glucose production and the translational relevance of the observed attenuated glucagon signalling in hepatic steatosis has to be investigated in human NAFLD patients.

Moreover, PHHs from female donors exhibited a higher susceptibility towards the oxalate precursors glycolate and glyoxylate compared to male PHHs. Since, male individuals are more likely to develop NAFLD and kidney stone disease (Liang et al. 2014; Ballestri et al. 2017), our observations are contrary to the literature. Therefore, the obtained results should be confirmed with further PHH donors. Also, it is important to analyse the underlying molecular mechanisms leading to the observed gender difference by studying a possible gender-predominant expression of the different glyoxylate metabolism enzymes. Interventions such as inhibition and/or overexpression analyses of e.g. HAO1 and LDHA might help to understand the gender difference in the glyoxylate metabolism on a molecular level. Furthermore, investigating the influence of sexual hormones like estradiol or testosterone on the expression of glyoxylate metabolism enzymes, might also help to elucidate the molecular mechanisms underlying the gender differences. Moreover, the impact of lipid accumulation on the oxalate production from different oxalate precursors should be investigated in steatotic PHHs or in an *in vitro* steatosis model in future. This should help to identify the glyoxylate precursors that sensitize to overproduction of oxalate in human NAFLD. Both male and female hepatocytes from NAFLD patients should be studied as well, in order to investigate whether the lipid accumulation alters gender differences that are observed in the healthy state. Understanding the gender differences in the glyoxylate metabolism in combination with NAFLD is important, since female and male individuals with and without NAFLD might need specialised treatments against kidney stone disease.

The analysis in the cohort of overweight and obese children and adolescents showed a positive correlation between the steatosis percentage and increased urinary oxalate excretion, supporting the connection of human NAFLD to an increased risk of kidney stone formation. In order to strengthen this hypothesis, the sample size has to be increased and information regarding dietary oxalate precursors have to be collected. Finally, follow-up studies with the same participants over the next years would be interesting in order to track the progression of NAFLD, and whether this increases the urinary oxalate excretion and the development of calcium oxalate deposits.

5 Bibliography

Abe Y, Shodai T, Muto T, et al (2000) Structural basis of presequence recognition by the mitochondrial protein import receptor Tom20. Cell 100:551–560. https://doi.org/10.1016/s0092-8674(00)80691-1

Abrigo J, Rivera JC, Aravena J, et al (2016) High Fat Diet-Induced Skeletal Muscle Wasting Is Decreased by Mesenchymal Stem Cells Administration: Implications on Oxidative Stress, Ubiquitin Proteasome Pathway Activation, and Myonuclear Apoptosis. Oxid Med Cell Longev 2016:1–13. https://doi.org/10.1155/2016/9047821

Adachi M, Brenner DA (2008) High molecular weight adiponectin inhibits proliferation of hepatic stellate cells via activation of adenosine monophosphate-activated protein kinase. Hepatology 47:677–685. https://doi.org/10.1002/hep.21991

Adams E, Frank L (1980) Metabolism of Proline and the Hydroxyprolines. Annu Rev Biochem 49:1005–1061. https://doi.org/10.1146/annurev.bi.49.070180.005041

Adams LA, Lymp JF, St Sauver J, et al (2005) The natural history of nonalcoholic fatty liver disease: a population-based cohort study. Gastroenterology 129:113–121. https://doi.org/10.1053/j.gastro.2005.04.014

Ahrens M, Ammerpohl O, von Schönfels W, et al (2013) DNA Methylation Analysis in Nonalcoholic Fatty Liver Disease Suggests Distinct Disease-Specific and Remodeling Signatures after Bariatric Surgery. Cell Metab 18:296–302. https://doi.org/10.1016/j.cmet.2013.07.004

Aikawa T, Matsutaka H, Takezawa K, Ishikawa E (1972) Gluconeogenesis and amino acid metabolism I. Comparison of various precursors for hepatic gluconeogenesis in vivo. Biochim Biophys Acta BBA - Gen Subj 279:234–244. https://doi.org/10.1016/0304-4165(72)90139-0

Akarken I, Zorlu F (2015) original Visceral obesity : A new risk factor for stone disease. 9:

Alberti KGMM, Christensen NJ, Iversen J, Ørskov H (1975) ROLE OF GLUCAGON AND OTHER HORMONES IN DEVELOPMENT OF DIABETIC KETOACIDOSIS. The Lancet 305:1307–1311. https://doi.org/10.1016/S0140-6736(75)92315-6

Anstee Q, Daly A, Day C (2011) Genetics of Alcoholic and Nonalcoholic Fatty Liver Disease. Semin Liver Dis 31:128–146. https://doi.org/10.1055/s-0031-1276643

Anstee QM, Goldin RD (2006) Mouse models in non-alcoholic fatty liver disease and steatohepatitis research. Int J Exp Pathol 87:1–16. https://doi.org/10.1111/j.0959-9673.2006.00465.x

Anstee QM, Reeves HL, Kotsiliti E, et al (2019a) From NASH to HCC: current concepts and future challenges. Nat Rev Gastroenterol Hepatol 16:411–428. https://doi.org/10.1038/s41575-019-0145-7

Anstee QM, Reeves HL, Kotsiliti E, et al (2019b) From NASH to HCC: current concepts and future challenges. Nat Rev Gastroenterol Hepatol 16:411–428. https://doi.org/10.1038/s41575-019-0145-7

Arita Y, Kihara S, Ouchi N, et al (1999) Paradoxical decrease of an adipose-specific protein,

adiponectin, in obesity. Biochem Biophys Res Commun 257:79–83. https://doi.org/10.1006/bbrc.1999.0255

Arslan U, Türkoğlu S, Balcioğlu S, et al (2007) Association between nonalcoholic fatty liver disease and coronary artery disease. Coron Artery Dis 18:433–436. https://doi.org/10.1097/MCA.0b013e3282583c0d

Authier F, Desbuquois B, De Galle B (1992) Ligand-mediated internalization of glucagon receptors in intact rat liver. Endocrinology 131:447–457. https://doi.org/10.1210/endo.131.1.1319325

Axelsen L, Keung W, Pedersen H, et al (2012) Glucagon and a glucagon-GLP-1 dual-agonist increases cardiac performance with different metabolic effects in insulin-resistant hearts: Glucagon and GLP-1 in insulin-resistant hearts. Br J Pharmacol 165:2736–2748. https://doi.org/10.1111/j.1476-5381.2011.01714.x

Baffy G, Brunt EM, Caldwell SH (2012) Hepatocellular carcinoma in non-alcoholic fatty liver disease: An emerging menace. J Hepatol 56:1384–1391. https://doi.org/10.1016/j.jhep.2011.10.027

Baker PRS, Cramer SD, Kennedy M, et al (2004) Glycolate and glyoxylate metabolism in HepG2 cells. Am J Physiol Cell Physiol 287:C1359–C1365. https://doi.org/10.1152/ajpcell.00238.2004

Ballestri S, Nascimbeni F, Baldelli E, et al (2017) NAFLD as a Sexual Dimorphic Disease: Role of Gender and Reproductive Status in the Development and Progression of Nonalcoholic Fatty Liver Disease and Inherent Cardiovascular Risk. Adv Ther 34:1291–1326. https://doi.org/10.1007/s12325-017-0556-1

Basavaraj DR, Biyani CS, Browning AJ, Cartledge JJ (2007) The Role of Urinary Kidney Stone Inhibitors and Promoters in the Pathogenesis of Calcium Containing Renal Stones. EAU-EBU Update Ser 5:126–136. https://doi.org/10.1016/j.eeus.2007.03.002

Behnam JT, Williams EL, Brink S, et al (2006) Reconstruction of human hepatocyte glyoxylate metabolic pathways in stably transformed Chinese-hamster ovary cells. Biochem J 394:409–416. https://doi.org/10.1042/BJ20051397

Belostotsky R, Seboun E, Idelson GH, et al (2010) Mutations in DHDPSL are responsible for primary hyperoxaluria type III. Am J Hum Genet 87:392–399. https://doi.org/10.1016/j.ajhg.2010.07.023

Benedict M, Zhang X (2017) Non-alcoholic fatty liver disease: An expanded review. World J Hepatol 9:715–732. https://doi.org/10.4254/wjh.v9.i16.715

Bergman A, Tan B, Somayaji VR, et al (2017) A 4-week study assessing the pharmacokinetics, pharmacodynamics, safety, and tolerability of the glucagon receptor antagonist PF-06291874 administered as monotherapy in subjects with type 2 diabetes mellitus. Diabetes Res Clin Pract 126:95–104. https://doi.org/10.1016/j.diabres.2017.01.019

Biochem J (1989) Induction of Mitochondrial Serine : Pyruvate Aminotransferase Liver by Glucagon and Insulin through Different Mechanisms of Rat Hiroaki Miyajima ,*,** Toshiaki Oda ,* and Arata Ichiyama * of Biochemistry and -D epartment of Medicine , Hamamatsu of Medicin. 504:500–504

Birdsey GM, Lewin J, Cunningham AA, et al (2004) Differential Enzyme Targeting As an Evolutionary Adaptation to Herbivory in Carnivora. Mol Biol Evol 21:632–646. https://doi.org/10.1093/molbev/msh054

Boden G, Chen X, Mozzoli M, Ryan I (1996) Effect of fasting on serum leptin in normal human subjects. J Clin Endocrinol Metab 81:3419–3423. https://doi.org/10.1210/jcem.81.9.8784108

Bonventre JV, Yang L, Bonventre JV, Yang L (2011) Cellular pathophysiology of ischemic acute kidney injury Find the latest version : Science in medicine Cellular pathophysiology of ischemic acute kidney injury. Sci Med 121:4210–4221. https://doi.org/10.1172/JCI45161.4210

Breljak D, Brzica H, Vrhovac I, et al (2015) In female rats, ethylene glycol treatment elevates protein expression of hepatic and renal oxalate transporter sat-1 (Slc26a1) without inducing hyperoxaluria. Croat Med J 56:447–459. https://doi.org/10.3325/cmj.2015.56.447

Browning JD, Szczepaniak LS, Dobbins R, et al (2004) Prevalence of hepatic steatosis in an urban population in the United States: Impact of ethnicity. Hepatology 40:1387–1395. https://doi.org/10.1002/hep.20466

Brunt EM, Kleiner DE, Wilson LA, et al (2011) Nonalcoholic fatty liver disease (NAFLD) activity score and the histopathologic diagnosis in NAFLD: Distinct clinicopathologic meanings. Hepatology 53:810–820. https://doi.org/10.1002/hep.24127

Brushia R J (1999) Phosphorylase kinase: the complexity of its regulation is reflected in the complexity of its structure. Front Biosci 4:d618. https://doi.org/10.2741/Brushia

Bruun JM, Lihn AS, Verdich C, et al (2003) Regulation of adiponectin by adipose tissue-derived cytokines: in vivo and in vitro investigations in humans. Am J Physiol-Endocrinol Metab 285:E527–E533. https://doi.org/10.1152/ajpendo.00110.2003

Buchanan KD, Mccarroll AM (1972) ABNORMALITIES OF GLUCAGON METABOLISM IN UNTREATED DIABETES MELLITUS. The Lancet 300:1394–1395. https://doi.org/10.1016/S0140-6736(72)92964-9

Burgess SC, He T, Yan Z, et al (2007) Cytosolic Phosphoenolpyruvate Carboxykinase Does Not Solely Control the Rate of Hepatic Gluconeogenesis in the Intact Mouse Liver. Cell Metab 5:313–320. https://doi.org/10.1016/j.cmet.2007.03.004

Buzzetti E, Pinzani M, Tsochatzis EA (2016) The multiple-hit pathogenesis of non-alcoholic fatty liver disease (NAFLD). Metabolism 65:1038–1048. https://doi.org/10.1016/j.metabol.2015.12.012

Cedar H (1988) DNA methylation and gene activity. Cell 53:3–4. https://doi.org/10.1016/0092-8674(88)90479-5

Cegla J, Troke RC, Jones B, et al (2014) Coinfusion of Low-Dose GLP-1 and Glucagon in Man Results in a Reduction in Food Intake. Diabetes 63:3711–3720. https://doi.org/10.2337/db14-0242

Cejvan K, Coy DH, Efendic S (2003) Intra-Islet Somatostatin Regulates Glucagon Release via Type 2 Somatostatin Receptors in Rats. Diabetes 52:1176–1181. https://doi.org/10.2337/diabetes.52.5.1176

Cellini B, Bertoldi M, Montioli R, et al (2007) Human wild-type alanine:glyoxylate aminotransferase and its naturally occurring G82E variant: functional properties and physiological implications. Biochem J 408:39–50. https://doi.org/10.1042/BJ20070637

Chai W, Liebman M, Kynast-Gales S, Massey L (2004) Oxalate absorption and endogenous oxalate synthesis from ascorbate in calcium oxalate stone formers and non-stone formers. Am J Kidney Dis 44:1060–1069. https://doi.org/10.1053/j.ajkd.2004.08.028

Chalasani N, Younossi Z, Lavine JE, et al (2012) The diagnosis and management of non-alcoholic fatty liver disease: Practice Guideline by the American Association for the Study of Liver Diseases, American College of Gastroenterology, and the American Gastroenterological Association. Hepatology. https://doi.org/10.1002/hep.25762

Charbonneau A, Couturier K, Gauthier MS, Lavoie JM (2005a) Evidence of hepatic glucagon resistance associated with hepatic steatosis: Reversal effect of training. Int J Sports Med 26:432–441. https://doi.org/10.1055/s-2004-821225

Charbonneau A, Melancon A, Lavoie C, Lavoie J-M (2005b) Alterations in hepatic glucagon receptor density and in $G_s\alpha$ and $G_i\alpha_2$ protein content with diet-induced hepatic steatosis: effects of acute exercise. Am J Physiol-Endocrinol Metab 289:E8–E14. https://doi.org/10.1152/ajpendo.00570.2004

Charbonneau A, Unson CG, Lavoie JM (2007) High-fat diet-induced hepatic steatosis reduces glucagon receptor content in rat hepatocytes: Potential interaction with acute exercise. J Physiol 579:255–267. https://doi.org/10.1113/jphysiol.2006.121954

Chen Z, Prosperi M, Bird VY (2019) Prevalence of kidney stones in the USA: The National Health and Nutrition Evaluation Survey. J Clin Urol 12:296–302. https://doi.org/10.1177/2051415818813820

Cheung O, Puri P, Eicken C, et al (2008) Nonalcoholic steatohepatitis is associated with altered hepatic MicroRNA expression. Hepatology 48:1810–1820. https://doi.org/10.1002/hep.22569

Chomzynski P (1987) Single-Step Method of RNA Isolation by Acid Guanidinium Thiocyanate–Phenol–Chloroform Extraction. Anal Biochem 162:156–159. https://doi.org/10.1006/abio.1987.9999

Clemmensen C, Chabenne J, Finan B, et al (2014) GLP-1/glucagon coagonism restores leptin responsiveness in obese mice chronically maintained on an obesogenic diet. Diabetes 63:1422–1427. https://doi.org/10.2337/db13-1609

Cochat P, Deloraine A, Rotily M, et al (1995) Epidemiology of primary hyperoxaluria type 1. Nephrol Dial Transplant 10:3–7. https://doi.org/10.1093/ndt/10.supp8.3

Coe FL (2005) Kidney stone disease. J Clin Invest 115:2598–2608. https://doi.org/10.1172/JCI26662

Conarello SL, Jiang G, Mu J, et al (2006) Glucagon receptor knockout mice are resistant to diet-induced obesity and streptozotocin-mediated beta cell loss and hyperglycaemia. Diabetologia 50:142–150. https://doi.org/10.1007/s00125-006-0481-3

Cousin SP, Hügl SR, Wrede CE, et al (2001) Free Fatty Acid-Induced Inhibition of Glucose and Insulin-Like Growth Factor I-Induced Deoxyribonucleic Acid Synthesis in the Pancreatic β-Cell Line INS-1 [1]. Endocrinology 142:229–240. https://doi.org/10.1210/endo.142.1.7863

Cramer SD, Ferree PM, Lin K, et al (1999) The gene encoding hydroxypyruvate reductase (GRHPR) is mutated in patients with primary hyperoxaluria type II. Hum Mol Genet 8:2063–2069. https://doi.org/10.1093/hmg/8.11.2063

Crespo J (2001) Gene expression of tumor necrosis factor [alpha] and TNF-receptors, p55 and p75, in nonalcoholic steatohepatitis patients. Hepatology 34:1158–1163. https://doi.org/10.1053/jhep.2001.29628

Curhan GC, Willett WC, Speizer FE, Stampfer MJ (2001) Twenty-four–hour urine chemistries and the risk of kidney stones among women and men. Kidney Int 59:2290–2298. https://doi.org/10.1046/j.1523-1755.2001.00746.x

Cusi K (2009) Nonalcoholic fatty liver disease in type 2 diabetes mellitus: Curr Opin Endocrinol Diabetes Obes 16:141–149. https://doi.org/10.1097/MED.0b013e3283293015

Czaja MJ (2010) JNK regulation of hepatic manifestations of the metabolic syndrome. Trends Endocrinol Metab 21:707–713. https://doi.org/10.1016/j.tem.2010.08.010

Danpure CJ (1997) Variable peroxisomal and mitochondrial targeting of alanine: Glyoxylate aminotransferase in mammalian evolution and disease. BioEssays 19:317–326. https://doi.org/10.1002/bies.950190409

Danpure CJ (2006a) Primary hyperoxaluria type 1: AGT mistargeting highlights the fundamental differences between the peroxisomal and mitochondrial protein import pathways. Biochim Biophys Acta BBA - Mol Cell Res 1763:1776–1784. https://doi.org/10.1016/j.bbamcr.2006.08.021

Danpure CJ (2006b) Primary hyperoxaluria type 1: AGT mistargeting highlights the fundamental differences between the peroxisomal and mitochondrial protein import pathways. Biochim Biophys Acta - Mol Cell Res 1763:1776–1784. https://doi.org/10.1016/j.bbamcr.2006.08.021

Danpure CJ, Cooper PJ, Wise PJ, Jennings PR (1989) An enzyme trafficking defect in two patients with primary hyperoxaluria type 1: peroxisomal alanine/glyoxylate aminotransferase rerouted to mitochondria. J Cell Biol 108:1345–1352. https://doi.org/10.1083/jcb.108.4.1345

Day CP (2002) Pathogenesis of steatohepatitis. Best Pract Res Clin Gastroenterol 16:663–678. https://doi.org/10.1053/bega.2002.0333

Day CP, James OFW (1998) Steatohepatitis: A tale of two “hits”? Gastroenterology 114:842–845. https://doi.org/10.1016/S0016-5085(98)70599-2

Day JW, Ottaway N, Patterson JT, et al (2009) A new glucagon and GLP-1 co-agonist eliminates obesity in rodents. Nat Chem Biol 5:749–757. https://doi.org/10.1038/nchembio.209

de Mello VD, Matte A, Perfilyev A, et al (2017) Human liver epigenetic alterations in non-alcoholic steatohepatitis are related to insulin action. Epigenetics 12:287–295. https://doi.org/10.1080/15592294.2017.1294305

Dicker A, Zhao J, Cannon B, Nedergaard J (1998) Apparent thermogenic effect of injected glucagon is not due to a direct effect on brown fat cells. Am J Physiol-Regul Integr Comp Physiol 275:R1674–R1682. https://doi.org/10.1152/ajpregu.1998.275.5.R1674

Dongiovanni P, Valenti L, Rametta R, et al (2010) Genetic variants regulating insulin receptor signalling are associated with the severity of liver damage in patients with non-alcoholic fatty liver disease. Gut 59:267–273. https://doi.org/10.1136/gut.2009.190801

Donini S, Ferrari M, Fedeli C, et al (2009) Recombinant production of eight human cytosolic aminotransferases and assessment of their potential involvement in glyoxylate metabolism. Biochem J 422:265–272. https://doi.org/10.1042/BJ20090748

Donnelly KL, Smith CI, Schwarzenberg SJ, et al (2005) Sources of fatty acids stored in liver and secreted via lipoproteins in patients with nonalcoholic fatty liver disease. J Clin Invest 115:1343–1351. https://doi.org/10.1172/JCI23621

Duncan SH, Richardson AJ, Kaul P, et al (2002) Oxalobacter formigenes and Its Potential Role in Human Health. Appl Environ Microbiol 68:3841–3847. https://doi.org/10.1128/AEM.68.8.3841-3847.2002

Eccleston HB, Andringa KK, Betancourt AM, et al (2011) Chronic exposure to a high-fat diet induces hepatic steatosis, impairs nitric oxide bioavailability, and modifies the mitochondrial proteome in mice. Antioxid Redox Signal 15:447–459. https://doi.org/10.1089/ars.2010.3395

Einollahi B, Naghii MR, Sepandi M (2013) Association of nonalcoholic fatty liver disease (NAFLD) with urolithiasis. Endocr Regul 47:27–32. https://doi.org/10.4149/endo_2013_01_27

Eissing L, Scherer T, Tödter K, et al (2013) De novo lipogenesis in human fat and liver is linked to ChREBP-β and metabolic health. Nat Commun 4:1528. https://doi.org/10.1038/ncomms2537

Ekstedt M, Franzén LE, Mathiesen UL, et al (2006) Long-term follow-up of patients with NAFLD and elevated liver enzymes. Hepatol Baltim Md 44:865–873. https://doi.org/10.1002/hep.21327

Erion DM, Shulman GI (2010) Diacylglycerol-mediated insulin resistance. Nat Med 16:400–402. https://doi.org/10.1038/nm0410-400

European Association for the Study of the Liver (EASL) (2016) EASL–EASD–EASO Clinical Practice Guidelines for the management of non-alcoholic fatty liver disease. Diabetologia. https://doi.org/10.1007/s00125-016-3902-y

Evan AP (2010) Physiopathology and etiology of stone formation in the kidney and the urinary tract. Pediatr Nephrol 25:831–841. https://doi.org/10.1007/s00467-009-1116-y

Faggioni R, Fantuzzi G, Gabay C, et al (1999) Leptin deficiency enhances sensitivity to endotoxin-induced lethality. Am J Physiol-Regul Integr Comp Physiol 276:R136–R142. https://doi.org/10.1152/ajpregu.1999.276.1.R136

Fang YL, Chen H, Wang CL, Liang L (2018) Pathogenesis of non-alcoholic fatty liver disease in children and adolescence: From “two hit theory” to “multiple hit model.” World J Gastroenterol 24:2974–2983. https://doi.org/10.3748/wjg.v24.i27.2974

Fargue S, Knight J, Holmes RP, et al (2016) Effects of alanine:glyoxylate aminotransferase variants and pyridoxine sensitivity on oxalate metabolism in a cell-based cytotoxicity assay. Biochim Biophys Acta BBA - Mol Basis Dis 1862:1055–1062. https://doi.org/10.1016/j.bbadis.2016.02.004

Fargue S, Lewin J, Rumsby G, Danpure CJ (2013) Four of the most common mutations in primary hyperoxaluria type 1 unmask the cryptic mitochondrial targeting sequence of alanine:glyoxylate aminotransferase encoded by the polymorphic minor allele. J Biol Chem 288:2475–2484. https://doi.org/10.1074/jbc.M112.432617

Fargue S, Milliner DS, Knight J, et al (2018) Hydroxyproline Metabolism and Oxalate Synthesis in Primary Hyperoxaluria. J Am Soc Nephrol 29:1615–1623. https://doi.org/10.1681/ASN.2017040390

Fehlmann M, LeCam A, Freychet P (1979) Insulin and glucagon stimulation of amino acid transport in isolated rat hepatocytes. JBiolChem 254:10431–10437

Ferrara CT, Wang P, Neto EC, et al (2008) Genetic networks of liver metabolism revealed by integration of metabolic and transcriptional profiling. PLoS Genet 4:. https://doi.org/10.1371/journal.pgen.1000034

Fitzpatrick GF, Meguid MM, Gitlitz PH, Brennan MF (1977) Glucagon infusion in normal man: Effects on 3-mthylhistidine excretion and plasma amino acids. Metabolism 26:477–485. https://doi.org/10.1016/0026-0495(77)90091-9

Franklin ZJ, O'Harte FPM, Irwin N (2014) Effects of short-term chemical ablation of glucagon signalling by peptide-based glucagon receptor antagonists on insulin secretion and glucose homeostasis in mice. Biol Chem 395:433–442. https://doi.org/10.1515/hsz-2013-0224

Friedman JM, Halaas JL, Gajiwala KS, et al (1995) Weight-reducing effects of the plasma protein encoded by the obese gene. Science 269:543–546. https://doi.org/10.1126/science.7624777

Fujii Y, Okada A, Yasui T, et al (2013) Effect of Adiponectin on Kidney Crystal Formation in Metabolic Syndrome Model Mice via Inhibition of Inflammation and Apoptosis. PLoS ONE 8:. https://doi.org/10.1371/journal.pone.0061343

Fukunishi S, Sujishi T, Takeshita A, et al (2014) Lipopolysaccharides accelerate hepatic steatosis in the development of nonalcoholic fatty liver disease in Zucker rats. J Clin Biochem Nutr 54:39–44. https://doi.org/10.3164/jcbn.13-49

Fukushima M, Aihara Y, Ichiyama A (1978a) Immunochemical studies on induction of rat liver mitochondrial serine:pyruvate aminotransferase by glucagon. J Biol Chem 253:1187–1194

Fukushima M, Aihara Y, Ichiyama A (1978b) Immunochemical studies on induction of rat liver mitochondrial serine:pyruvate aminotransferase by glucagon. J Biol Chem 253:1187–1194

Gambardella R (1977) The pathways of oxalate formation from phenylalanine, tyrosine, tryptophan and ascorbic acid in the rat. Biochim Biophys Acta BBA - Gen Subj 499:156–168. https://doi.org/10.1016/0304-4165(77)90238-0

Garthwaite TL, Martinson DR, Tseng LF, et al (1980) A Longitudinal Hormonal Profile of the

Genetically Obese Mouse*. Endocrinology 107:671–676. https://doi.org/10.1210/endo-107-3-671

Gastaldelli A (2010) Fatty liver disease: the hepatic manifestation of metabolic syndrome. Hypertens Res 33:546–547. https://doi.org/10.1038/hr.2010.60

Gastaldelli A, Baldi S, Pettiti M, et al (2000) Influence of obesity and type 2 diabetes on gluconeogenesis and glucose output in humans: a quantitative study. Diabetes 49:1367–1373. https://doi.org/10.2337/diabetes.49.8.1367

Geary N (2013) Glucagon. In: Handbook of Biologically Active Peptides. Elsevier, pp 1118–1122

Gelling RW, Du XQ, Dichmann DS, et al (2003) Lower blood glucose, hyperglucagonemia, and pancreatic cell hyperplasia in glucagon receptor knockout mice. Proc Natl Acad Sci 100:1438–1443. https://doi.org/10.1073/pnas.0237106100

Gianmoena K (2017) Metabolic alterations in non-alcoholic fatty liver disease (NAFLD): consequences of AGXT downregulation on glyoxylate detoxification. https://doi.org/10.17877/DE290R-18100

Gianmoena K, Gasparoni N, Jashari A, et al Epigenetic and transcriptional profiling identifies impaired glyoxylate detoxification in NAFLD as a risk factor for hyperoxaluria. 84

Gluvic Z, Zaric B, Resanovic I, et al (2016) Link between Metabolic Syndrome and Insulin Resistance. Curr Vasc Pharmacol 15:30–39. https://doi.org/10.2174/1570161114666161007164510

Godoy P, Widera A, Schmidt-Heck W, et al (2016) Gene network activity in cultivated primary hepatocytes is highly similar to diseased mammalian liver tissue. Arch Toxicol 90:2513–2529. https://doi.org/10.1007/s00204-016-1761-4

Goldstein I, Hager GL (2018) The Three Ds of Transcription Activation by Glucagon: Direct, Delayed, and Dynamic. Endocrinology 159:206–216. https://doi.org/10.1210/en.2017-00521

Gordon RS, Cherkes A (1956) UNESTERIFIED FATTY ACID IN HUMAN BLOOD PLASMA 1. J Clin Invest 35:206–212. https://doi.org/10.1172/JCI103265

Grander C, Grabherr F, Moschen AR, Tilg H (2016) Non-Alcoholic Fatty Liver Disease: Cause or Effect of Metabolic Syndrome. Visc Med 32:329–334. https://doi.org/10.1159/000448940

Gu W, Yan H, Winters KA, et al (2009) Long-Term Inhibition of the Glucagon Receptor with a Monoclonal Antibody in Mice Causes Sustained Improvement in Glycemic Control, with Reversible α-Cell Hyperplasia and Hyperglucagonemia. J Pharmacol Exp Ther 331:871–881. https://doi.org/10.1124/jpet.109.157685

Guan H-P, Yang X, Lu K, et al (2015) Glucagon receptor antagonism induces increased cholesterol absorption. J Lipid Res 56:2183–2195. https://doi.org/10.1194/jlr.M060897

Hædersdal S, Lund A, Knop FK, Vilsbøll T (2018) The Role of Glucagon in the Pathophysiology and Treatment of Type 2 Diabetes. Mayo Clin Proc 93:217–239. https://doi.org/10.1016/j.mayocp.2017.12.003

Halaas J, Gajiwala K, Maffei M, et al (1995) Weight-reducing effects of the plasma protein

encoded by the obese gene. Science 269:543–546. https://doi.org/10.1126/science.7624777

Harris KS, Richardson KE (1980) Glycolate in the diet and its conversion to urinary oxalate in the rat. Invest Urol 18:106–109

Harte AL, da Silva NF, Creely SJ, et al (2010) Elevated endotoxin levels in non-alcoholic fatty liver disease. J Inflamm 7:15. https://doi.org/10.1186/1476-9255-7-15

Hatziagelaki E, Karageorgopoulos DE, Chounta A, et al (2012) Predictors of Impaired Glucose Regulation in Patients with Non-Alcoholic Fatty Liver Disease. Exp Diabetes Res 2012:1–7. https://doi.org/10.1155/2012/351974

Higuchi R, Fockler C, Dollinger G, Watson R (1993) Kinetic PCR Analysis: Real-time Monitoring of DNA Amplification Reactions. Nat Biotechnol 11:1026–1030. https://doi.org/10.1038/nbt0993-1026

Holland PM, Abramson RD, Watson R, Gelfand DH (1991) Detection of specific polymerase chain reaction product by utilizing the 5'----3' exonuclease activity of Thermus aquaticus DNA polymerase. Proc Natl Acad Sci 88:7276–7280. https://doi.org/10.1073/pnas.88.16.7276

Holmes RP, Assimos DG (1998) Glyoxylate synthesis, and its modulation and influence on oxalate synthesis. J Urol 160:1617–1624. https://doi.org/10.1016/S0022-5347(01)62363-2

Holmes RP, Goodman HO, Assimos DG (2001) Contribution of dietary oxalate to urinary oxalate excretion. Kidney Int 59:270–276. https://doi.org/10.1046/j.1523-1755.2001.00488.x

Holmes RP, Knight J, Assimos DG (2016) Lowering urinary oxalate excretion to decrease calcium oxalate stone disease. Urolithiasis 44:27–32. https://doi.org/10.1007/s00240-015-0839-4

Hoppe B (2003) Diagnostic and therapeutic approaches in patients with secondary hyperoxaluria. Front Biosci 8:e437-443. https://doi.org/10.2741/1135

Hoppe B (2012) An update on primary hyperoxaluria. Nat Rev Nephrol 8:467–475. https://doi.org/10.1038/nrneph.2012.113

Hoppe B, Beck BB, Milliner DS (2009) The primary hyperoxalurias. Kidney Int 75:1264–1271. https://doi.org/10.1038/ki.2009.32

Hotamisligil GS (2006) Inflammation and metabolic disorders. Nature 444:860–867. https://doi.org/10.1038/nature05485

Huang PL (2009) A comprehensive definition for metabolic syndrome. Dis Model Mech 2:231–237. https://doi.org/10.1242/dmm.001180

Hudert CA, Selinski S, Rudolph B, et al (2019) Genetic determinants of steatosis and fibrosis progression in paediatric non-alcoholic fatty liver disease. Liver Int 39:540–556. https://doi.org/10.1111/liv.14006

Ichiyama A (2011) Studies on a unique organelle localization of a liver enzyme, serine:pyruvate (or alanine:glyoxylate) aminotransferase. Proc Jpn Acad Ser B Phys Biol Sci 87:274–286. https://doi.org/10.2183/pjab.87.274

Ikejima K (2001) Leptin augments inflammatory and profibrogenic responses in the murine liver induced by hepatotoxic chemicals. Hepatology 34:288–297. https://doi.org/10.1053/jhep.2001.26518

Ingalls AM, Dickie MM, Snell GD (1950) OBESE, A NEW MUTATION IN THE HOUSE MOUSE*. J Hered 41:317–318. https://doi.org/10.1093/oxfordjournals.jhered.a106073

Ito M, Suzuki J, Tsujioka S, et al (2007) Longitudinal analysis of murine steatohepatitis model induced by chronic exposure to high-fat diet: Longitudinal analysis of diet-induced NASH model. Hepatol Res 37:50–57. https://doi.org/10.1111/j.1872-034X.2007.00008.x

Jaenisch R, Bird A (2003) Epigenetic regulation of gene expression: how the genome integrates intrinsic and environmental signals. Nat Genet 33:245–254. https://doi.org/10.1038/ng1089

Jaffe M (1886) Ueber den Niederschlag, welchen Pikrinsäure in normalem harn erzeugt und über eine neue Reaction des Kreatinins. Z Für Physiol Chem 391

Jahoor F, Peters EJ, Wolfe RR (1990) The relationship between gluconeogenic substrate supply and glucose production in humans. Am J Physiol-Endocrinol Metab 258:E288–E296. https://doi.org/10.1152/ajpendo.1990.258.2.E288

Jiang G, Zhang BB (2003) Glucagon and regulation of glucose metabolism. Am J Physiol-Endocrinol Metab 284:E671–E678. https://doi.org/10.1152/ajpendo.00492.2002

Jin T, Weng J (2016) Hepatic functions of GLP-1 and its based drugs: current disputes and perspectives. Am J Physiol - Endocrinol Metab 311:E620–E627. https://doi.org/10.1152/ajpendo.00069.2016

Junker AE, Gluud LL, van Hall G, et al (2016) Effects of glucagon-like peptide-1 on glucagon secretion in patients with non-alcoholic fatty liver disease. J Hepatol 64:908–915. https://doi.org/10.1016/j.jhep.2015.11.014

Kadlec AO, Greco K, Fridirici ZC, et al (2012) Metabolic syndrome and urinary stone composition: What factors matter most? Urology 80:805–810. https://doi.org/10.1016/j.urology.2012.05.011

Kakuma T, Lee Y, Higa M, et al (2000) Leptin, troglitazone, and the expression of sterol regulatory element binding proteins in liver and pancreatic islets. Proc Natl Acad Sci 97:8536–8541. https://doi.org/10.1073/pnas.97.15.8536

Kamada Y, Tamura S, Kiso S, et al (2003) Enhanced carbon tetrachloride-induced liver fibrosis in mice lacking adiponectin. Gastroenterology 125:1796–1807. https://doi.org/10.1053/j.gastro.2003.08.029

Kapoor A, Sanyal AJ (2009) Endoplasmic Reticulum Stress and the Unfolded Protein Response. Clin Liver Dis 13:581–590. https://doi.org/10.1016/j.cld.2009.07.004

Kawamori D, Kurpad AJ, Hu J, et al (2009) Insulin Signaling in α Cells Modulates Glucagon Secretion In Vivo. Cell Metab 9:350–361. https://doi.org/10.1016/j.cmet.2009.02.007

Kazda CM, Ding Y, Kelly RP, et al (2016) Evaluation of efficacy and safety of the glucagon receptor antagonist LY2409021 in patients with type 2 diabetes: 12-and 24-week phase 2 studies. Diabetes Care 39:1241–1249. https://doi.org/10.2337/dc15-1643

Keller U, Sonnenberg E, Burckhardt D, Perruchoud A (1982) Evidence for an Augmented Glucagon Dependence of Hepatic Glucose Production in Cirrhosis of the Liver*. J Clin Endocrinol Metab 54:961–968. https://doi.org/10.1210/jcem-54-5-961

Kelly RP, Garhyan P, Raddad E, et al (2015) Short-term administration of the glucagon receptor antagonist LY2409021 lowers blood glucose in healthy people and in those with type 2 diabetes. Diabetes Obes Metab 17:414–422. https://doi.org/10.1111/dom.12446

Khan RS, Bril F, Cusi K, Newsome PN (2019) Modulation of Insulin Resistance in Nonalcoholic Fatty Liver Disease. Hepatology 70:711–724. https://doi.org/10.1002/hep.30429

Kim AY, Park YJ, Pan X, et al (2015) Obesity-induced DNA hypermethylation of the adiponectin gene mediates insulin resistance. Nat Commun 6:7585. https://doi.org/10.1038/ncomms8585

Kim CH, Younossi ZM (2008) Nonalcoholic fatty liver disease: A manifestation of the metabolic syndrome. Cleve Clin J Med 75:721–728. https://doi.org/10.3949/ccjm.75.10.721

Kim K-A, Gu W, Lee I-A, et al (2012a) High fat diet-induced gut microbiota exacerbates inflammation and obesity in mice via the TLR4 signaling pathway. PloS One 7:e47713. https://doi.org/10.1371/journal.pone.0047713

Kim W-D, Lee Y, Kim M-H, et al (2012b) Human Monoclonal Antibodies against Glucagon Receptor Improve Glucose Homeostasis by Suppression of Hepatic Glucose Output in Diet-Induced Obese Mice. PLoS ONE 7:e50954. https://doi.org/10.1371/journal.pone.0050954

Klug M, Rehli M (2006) Functional Analysis of Promoter CPG-Methylation using a CpG-Free Luciferase Reporter Vector. Epigenetics 1:127–130. https://doi.org/10.4161/epi.1.3.3327

Knight J, Jiang J, Assimos DG, Holmes RP (2006) Hydroxyproline ingestion and urinary oxalate and glycolate excretion. Kidney Int 70:1929–1934. https://doi.org/10.1038/sj.ki.5001906

Kopp N, Leumann E (1995) Changing pattern of primary hyperoxaluria in Switzerland. Nephrol Dial Transplant 10:2224–2227. https://doi.org/10.1093/ndt/10.12.2224

Kostic A, King TA, Yang F, et al (2018) A first-in-human pharmacodynamic and pharmacokinetic study of a fully human anti-glucagon receptor monoclonal antibody in normal healthy volunteers. Diabetes Obes Metab 20:283–291. https://doi.org/10.1111/dom.13075

Krilov L, Nguyen A, Miyazaki T, et al (2011) Dual Mode of glucagon receptor internalization: Role of PKCα, GRKs and β-arrestins. Exp Cell Res 317:2981–2994. https://doi.org/10.1016/j.yexcr.2011.10.001

Krilov L, Nguyen A, Miyazaki T, et al (2008) Glucagon receptor recycling: role of carboxyl terminus, beta-arrestins, and cytoskeleton. Am J Physiol Cell Physiol 295:C1230-7. https://doi.org/10.1152/ajpcell.00240.2008

Kurland IJ, Pilkis SJ (1995) Covalent control of 6-phosphofructo-2-kinase/fructose-2,6-bisphosphatase: Insights into autoregulation of a bifunctional enzyme: Covalent control of 6PF-2-K/Fru-2,6-P $_2$ ase. Protein Sci 4:1023–1037. https://doi.org/10.1002/pro.5560040601

Lai C, Pursell N, Gierut J, et al (2018) Specific Inhibition of Hepatic Lactate Dehydrogenase Reduces Oxalate Production in Mouse Models of Primary Hyperoxaluria. Mol Ther 26:1983–1995. https://doi.org/10.1016/j.ymthe.2018.05.016

Lambert JE, Ramos–Roman MA, Browning JD, Parks EJ (2014) Increased De Novo Lipogenesis Is a Distinct Characteristic of Individuals With Nonalcoholic Fatty Liver Disease. Gastroenterology 146:726–735. https://doi.org/10.1053/j.gastro.2013.11.049

Larcher F, Del Rio M, Serrano F, et al (2001) A cutaneous gene therapy approach to human leptin deficiencies: correction of the murine *ob/ob* phenotype using leptin-targeted keratinocyte grafts. FASEB J 15:1529–1538. https://doi.org/10.1096/fj.01-0082com

Lau J, Behrens C, Sidelmann UG, et al (2007) New β-Alanine Derivatives Are Orally Available Glucagon Receptor Antagonists. J Med Chem 50:113–128. https://doi.org/10.1021/jm058026u

Lau JKC, Zhang X, Yu J (2017) Animal models of non-alcoholic fatty liver disease: current perspectives and recent advances. J Pathol 241:36–44. https://doi.org/10.1002/path.4829

Leclercq IA, Farrell GC, Schriemer R, Robertson GR (2002) Leptin is essential for the hepatic fibrogenic response to chronic liver injury. J Hepatol 37:206–213. https://doi.org/10.1016/S0168-8278(02)00102-2

Lee J, Friso S, Choi S-W (2014) Epigenetic Mechanisms Underlying the Link between Non-Alcoholic Fatty Liver Diseases and Nutrition. Nutrients 6:3303–3325. https://doi.org/10.3390/nu6083303

Lee J, Kim Y, Friso S, Choi S-W (2017) Epigenetics in non-alcoholic fatty liver disease. Mol Aspects Med 54:78–88. https://doi.org/10.1016/j.mam.2016.11.008

Lee SML, Schelcher C, Demmel M, et al (2013) Isolation of human hepatocytes by a two-step collagenase perfusion procedure. J Vis Exp JoVE. https://doi.org/10.3791/50615

Lee Y, Berglund ED, Wang M -y., et al (2012) Metabolic manifestations of insulin deficiency do not occur without glucagon action. Proc Natl Acad Sci 109:14972–14976. https://doi.org/10.1073/pnas.1205983109

Lee Y, Wang M-Y, Du XQ, et al (2011) Glucagon Receptor Knockout Prevents Insulin-Deficient Type 1 Diabetes in Mice. Diabetes 60:391–397. https://doi.org/10.2337/db10-0426

Lefkowitz RJ (1998) G Protein-coupled Receptors: III. NEW ROLES FOR RECEPTOR KINASES AND β-ARRESTINS IN RECEPTOR SIGNALING AND DESENSITIZATION. J Biol Chem 273:18677–18680. https://doi.org/10.1074/jbc.273.30.18677

Lefkowitz RJ, Pitcher J, Krueger K, Daaka Y (1997) Mechanisms of β-Adrenergic Receptor Desensitization and Resensitization. In: Advances in Pharmacology. Elsevier, pp 416–420

Leiper JM, Oatey PB, Danpure CJ (1996) Inhibition of alanine:glyoxylate aminotransferase 1 dimerization is a prerequisite for its peroxisome-to-mitochondrion mistargeting in primary hyperoxaluria type 1. J Cell Biol 135:939–951. https://doi.org/10.1083/jcb.135.4.939

Li X, Knight J, Fargue S, et al (2016) Metabolism of13C5-hydroxyproline in mouse models of Primary Hyperoxaluria and its inhibition by RNAi therapeutics targeting liver glycolate oxidase and hydroxyproline dehydrogenase. Biochim Biophys Acta - Mol Basis Dis 1862:233–239. https://doi.org/10.1016/j.bbadis.2015.12.001

Li XM, Salido EC, Shapiro LJ (1999a) The mouse alanine:glyoxylate aminotransferase gene

(Agxt1): Cloning, expression, and mapping to chromosome 1. Somat Cell Mol Genet 25:67–77. https://doi.org/10.1023/B:SCAM.0000007142.36524.58

Li XM, Salido EC, Shapiro LJ (1999b) The mouse alanine:glyoxylate aminotransferase gene (Agxt1): Cloning, expression, and mapping to chromosome 1. Somat Cell Mol Genet 25:67–77. https://doi.org/10.1023/B:SCAM.0000007142.36524.58

Li Y-Y (2012) Genetic and epigenetic variants influencing the development of nonalcoholic fatty liver disease. World J Gastroenterol 18:6546. https://doi.org/10.3748/wjg.v18.i45.6546

Liang L, Li L, Tian J, et al (2014) Androgen Receptor Enhances Kidney Stone-CaOx Crystal Formation via Modulation of Oxalate Biosynthesis & Oxidative Stress. Mol Endocrinol 28:1291–1303. https://doi.org/10.1210/me.2014-1047

Liang Y, Osborne MC, Monia BP, et al (2004) Reduction in Glucagon Receptor Expression by an Antisense Oligonucleotide Ameliorates Diabetic Syndrome in db/db Mice. Diabetes 53:410–417. https://doi.org/10.2337/diabetes.53.2.410

Lin HV, Accili D (2011) Hormonal Regulation of Hepatic Glucose Production in Health and Disease. Cell Metab 14:9–19. https://doi.org/10.1016/j.cmet.2011.06.003

Lindström P (2007) The Physiology of Obese-Hyperglycemic Mice [*ob/ob* Mice]. Sci World J 7:666–685. https://doi.org/10.1100/tsw.2007.117

Lindström P (2010) β-Cell Function in Obese-Hyperglycemic Mice [ob/ob Mice]. In: Islam MdS (ed) The Islets of Langerhans. Springer Netherlands, Dordrecht, pp 463–477

Livak KJ, Schmittgen TD (2001) Analysis of Relative Gene Expression Data Using Real-Time Quantitative PCR and the 2−ΔΔCT Method. Methods 25:402–408. https://doi.org/10.1006/meth.2001.1262

Lonardo A, Ballestri S, Marchesini G, et al (2015) Nonalcoholic fatty liver disease: A precursor of the metabolic syndrome. Dig Liver Dis 47:181–190. https://doi.org/10.1016/j.dld.2014.09.020

Longuet C, Robledo AM, Dean ED, et al (2013) Liver-Specific Disruption of the Murine Glucagon Receptor Produces -Cell Hyperplasia: Evidence for a Circulating -Cell Growth Factor. Diabetes 62:1196–1205. https://doi.org/10.2337/db11-1605

Loomba R, Sanyal AJ (2013) The global NAFLD epidemic. Nat Rev Gastroenterol Hepatol 10:686–690. https://doi.org/10.1038/nrgastro.2013.171

Lorenzo V, Torres A, Salido E (2014) Hiperoxaluria primaria. Nefrologia 34:398–412. https://doi.org/10.3265/Nefrologia.pre2014.Jan.12335

Lutsik P, Feuerbach L, Arand J, et al (2011) BiQ Analyzer HT: locus-specific analysis of DNA methylation by high-throughput bisulfite sequencing. Nucleic Acids Res 39:W551–W556. https://doi.org/10.1093/nar/gkr312

Mantovani A, Zaza G, Byrne CD, et al (2018) Nonalcoholic fatty liver disease increases risk of incident chronic kidney disease: A systematic review and meta-analysis. Metabolism 79:64–76. https://doi.org/10.1016/j.metabol.2017.11.003

Marchesini G, Brizi M, Morselli-Labate AM, et al (1999) Association of nonalcoholic fatty liver disease with insulin resistance. Am J Med 107:450–455. https://doi.org/10.1016/S0002-9343(99)00271-5

Marí M, Caballero F, Colell A, et al (2006) Mitochondrial free cholesterol loading sensitizes to TNF- and Fas-mediated steatohepatitis. Cell Metab 4:185–198. https://doi.org/10.1016/j.cmet.2006.07.006

Mashiter K, Harding PE, Chou M, et al (1975) Persistent Pancreatic Glucagon but not Insulin Response to Arginine in Pancreatectomized Dogs. Endocrinology 96:678–693. https://doi.org/10.1210/endo-96-3-678

Massey LK, Liebman M, Kynast-Gales SA (2005) Ascorbate Increases Human Oxaluria and Kidney Stone Risk. J Nutr 135:1673–1677. https://doi.org/10.1093/jn/135.7.1673

Matteoni CA, Younossi ZM, Gramlich T, et al (1999) Nonalcoholic fatty liver disease: a spectrum of clinical and pathological severity. Gastroenterology 116:1413–1419. https://doi.org/10.1016/s0016-5085(99)70506-8

Mayer J, Russell RE, Bates MW, Dickie MM (1953) Metabolic, nutritional and endocrine studies of the hereditary obesity-diabetes syndrome of mice and mechanism of its development. Metabolism 2:9–21

Medina-Santillán R, López-Velázquez JA, Chávez-Tapia N, et al (2013) Hepatic manifestations of metabolic syndrome: Liver and Metabolic Syndrome. Diabetes Metab Res Rev n/a-n/a. https://doi.org/10.1002/dmrr.2410

Miller RA, Birnbaum MJ (2016) Glucagon: acute actions on hepatic metabolism. Diabetologia 59:1376–1381. https://doi.org/10.1007/s00125-016-3955-y

Milliner DS, Wilson DM, Smith LH (2001) Phenotypic expression of primary hyperoxaluria: Comparative features of types I and II. Kidney Int 59:31–36. https://doi.org/10.1046/j.1523-1755.2001.00462.x

Misra VL, Khashab M, Chalasani N (2009) Nonalcoholic fatty liver disease and cardiovascular risk. Curr Gastroenterol Rep 11:50–55. https://doi.org/10.1007/s11894-009-0008-4

Miyada DS, Tappel AL (1956) Colorimetric Determination of Hydroxyproline. Anal Chem 28:909–910. https://doi.org/10.1021/ac60113a039

Miyajima H, Oda T, Ichiyama A (1989) Induction of Mitochondrial Serine: Pyruvate Aminotransferase of Rat Liver by Glucagon and Insulin through Different Mechanisms. J Biochem (Tokyo) 105:500–504. https://doi.org/10.1093/oxfordjournals.jbchem.a122695

Monico CG, Rossetti S, Belostotsky R, et al (2011) Primary hyperoxaluria type III gene HOGA1 (Formerly DHDPSL) as a possible risk factor for idiopathic calcium oxalate urolithiasis. Clin J Am Soc Nephrol 6:2289–2295. https://doi.org/10.2215/CJN.02760311

Motley A, Lumb MJ, Oatey PB, et al (1995a) Mammalian alanine/glyoxylate aminotransferase 1 is imported into peroxisomes via the PTS1 translocation pathway. Increased degeneracy and context specificity of the mammalian PTS1 motif and implications for the peroxisome-to-mitochondrion mistargeting of AGT in primary hyperoxaluria type 1. J Cell Biol 131:95–109.

https://doi.org/10.1083/jcb.131.1.95

Motley A, Lumb MJ, Oatey PB, et al (1995b) Ronald J. A. W.anders, ~ Henk F. Tabak,* and Christopher J. Danpure*. 95–109

Moylan CA, Pang H, Dellinger A, et al (2014) Hepatic gene expression profiles differentiate presymptomatic patients with mild versus severe nonalcoholic fatty liver disease: Hepatology. Hepatology 59:471–482. https://doi.org/10.1002/hep.26661

Mu J, Qureshi SA, Brady EJ, et al (2012) Anti-Diabetic Efficacy and Impact on Amino Acid Metabolism of GRA1, a Novel Small-Molecule Glucagon Receptor Antagonist. PLoS ONE 7:e49572. https://doi.org/10.1371/journal.pone.0049572

Mulay SR, Anders H-J (2017) Crystal nephropathies: mechanisms of crystal-induced kidney injury. Nat Rev Nephrol 13:226–240. https://doi.org/10.1038/nrneph.2017.10

Müller TD, Finan B, Clemmensen C, et al (2017) The new biology and pharmacology of glucagon

Müller WA, Faloona GR, Unger RH (1971) The effect of experimental insulin deficiency on glucagon secretion. J Clin Invest 50:1992–1999. https://doi.org/10.1172/JCI106691

Musso G, Gambino R, Tabibian JH, et al (2014a) Association of Non-alcoholic Fatty Liver Disease with Chronic Kidney Disease: A Systematic Review and Meta-analysis. PLoS Med 11:e1001680. https://doi.org/10.1371/journal.pmed.1001680

Musso G, Gambino R, Tabibian JH, et al (2014b) Association of Non-alcoholic Fatty Liver Disease with Chronic Kidney Disease: A Systematic Review and Meta-analysis. PLoS Med 11:. https://doi.org/10.1371/journal.pmed.1001680

Nam IC, Yoon JH, Park SH, et al (2016) Association of non-alcoholic fatty liver disease with renal stone disease detected on computed tomography. Eur J Radiol Open 3:195–199. https://doi.org/10.1016/j.ejro.2016.07.004

Negri AL, Spivacow FR, Del Valle EE, et al (2008) Role of overweight and obesity on the urinary excretion of promoters and inhibitors of stone formation in stone formers. Urol Res 36:303–307. https://doi.org/10.1007/s00240-008-0161-5

Noguchi T, Minatogawa Y, Takada Y, et al (1978) Subcellular distribution of pyruvate (glyoxylate) aminotransferases in rat liver. Biochem J 170:173–175. https://doi.org/10.1042/bj1700173

Noguchi T, Takada Y (1978) Peroxisomal localization of serine:pyruvate aminotransferase in human liver. J Biol Chem 253:7598–7600

Nonaka K, Toyoshima H, Yoshida T, et al (1977) The Nature of Hyperglucagonemia in Diabetes Mellitus. In: Foà PP, Bajaj JS, Foà NL (eds) GLUCAGON: Its Role in Physiology and Clinical Medicine. Springer New York, New York, NY, pp 663–677

Nyati KK, Masuda K, Zaman MM-U, et al (2017) TLR4-induced NF-κB and MAPK signaling regulate the IL-6 mRNA stabilizing protein Arid5a. Nucleic Acids Res 45:2687–2703. https://doi.org/10.1093/nar/gkx064

Obita T, Muto T, Endo T, Kohda D (2003) Peptide Library Approach with a Disulfide Tether to Refine the Tom20 Recognition Motif in Mitochondrial Presequences. J Mol Biol 328:495–504. https://doi.org/10.1016/S0022-2836(03)00288-2

Oda T, Funai T, Ichiyama A (1990) Generation from a single gene of two mRNAs that encode the mitochondrial and peroxisomal serine:pyruvate aminotransferase of rat liver. J Biol Chem 265:7513–7519

Oda T, Nishiyama K, Ichiyama A (1993) Characterization and Sequence Analysis of Rat Serine:Pyruvate/Alanine:Glyoxylate Aminotransferase Gene. Genomics 17:59–65. https://doi.org/10.1006/geno.1993.1283

Okamoto H, Kim J, Aglione J, et al (2015) Glucagon Receptor Blockade With a Human Antibody Normalizes Blood Glucose in Diabetic Mice and Monkeys. Endocrinology 156:2781–2794. https://doi.org/10.1210/en.2015-1011

Ota T, Takamura T, Kurita S, et al (2007) Insulin Resistance Accelerates a Dietary Rat Model of Nonalcoholic Steatohepatitis. Gastroenterology 132:282–293. https://doi.org/10.1053/j.gastro.2006.10.014

Pacifico L, Cantisani V, Ricci P, et al (2008) Nonalcoholic fatty liver disease and carotid atherosclerosis in children. Pediatr Res 63:423–427. https://doi.org/10.1203/PDR.0b013e318165b8e7

Palmer JP, Werner PL, Benson JW, Ensinck JW (1976) Immunoreactive glucagon responses to arginine in three pancreatectomized humans. Metabolism 25:1483–1485. https://doi.org/10.1016/S0026-0495(76)80173-4

Panera N (2014) MicroRNAs as controlled systems and controllers in non-alcoholic fatty liver disease. World J Gastroenterol 20:15079. https://doi.org/10.3748/wjg.v20.i41.15079

Paradies G (2014) Oxidative stress, cardiolipin and mitochondrial dysfunction in nonalcoholic fatty liver disease. World J Gastroenterol 20:14205. https://doi.org/10.3748/wjg.v20.i39.14205

Park SW, Zhou Y, Lee J, et al (2010) The regulatory subunits of PI3K, p85α and p85β, interact with XBP-1 and increase its nuclear translocation. Nat Med 16:429–437. https://doi.org/10.1038/nm.2099

Pearson MJ, Unger RH, Holland WL (2016) Clinical Trials, Triumphs, and Tribulations of Glucagon Receptor Antagonists. Diabetes Care 39:1075–1077. https://doi.org/10.2337/dci15-0033

Pelleymounter M, Cullen M, Baker M, et al (1995) Effects of the obese gene product on body weight regulation in ob/ob mice. Science 269:540–543. https://doi.org/10.1126/science.7624776

Pessayre D, Fromenty B (2005) NASH: a mitochondrial disease. J Hepatol 42:928–940. https://doi.org/10.1016/j.jhep.2005.03.004

Petersen MC, Shulman GI (2018) Mechanisms of Insulin Action and Insulin Resistance. Physiol Rev 98:2133–2223. https://doi.org/10.1152/physrev.00063.2017

Phang J, Hu C-AA, Valle D (2001) Disorders of proline and hydroxyproline metabolism. Metab Mol Bases Inherit Dis 1821–1838

Pierantonelli I, Svegliati-Baroni G (2019) Nonalcoholic Fatty Liver Disease: Basic Pathogenetic Mechanisms in the Progression From NAFLD to NASH. Transplantation 103:e1–e13. https://doi.org/10.1097/TP.0000000000002480

Pikarsky E, Porat RM, Stein I, et al (2004) NF-κB functions as a tumour promoter in inflammation-associated cancer. Nature 431:461–466. https://doi.org/10.1038/nature02924

Pilkis SJ, El-Maghrabi MR, McGrane M, et al (1982) Regulation by glucagon of hepatic pyruvate kinase, 6-phosphofructo 1-kinase, and fructose-1,6-bisphosphatase. Fed Proc 41:2623–2628

Podrini C, Borghesan M, Greco A, et al (2013) Redox Homeostasis and Epigenetics in Non-alcoholic Fatty Liver Disease (NAFLD). Curr Pharm Des 19:2737–2746. https://doi.org/10.2174/1381612811319150009

Poggiogalle E, Donini LM, Lenzi A, et al (2017) Non-alcoholic fatty liver disease connections with fat-free tissues: A focus on bone and skeletal muscle. World J Gastroenterol 23:1747. https://doi.org/10.3748/wjg.v23.i10.1747

Pogribny IP, Tryndyak VP, Bagnyukova TV, et al (2009) Hepatic epigenetic phenotype predetermines individual susceptibility to hepatic steatosis in mice fed a lipogenic methyl-deficient diet. J Hepatol 51:176–186. https://doi.org/10.1016/j.jhep.2009.03.021

Polat EC, Ozcan L, Cakir SS, et al (2015) Relationship between calcium stone disease and metabolic syndrome. Urol J 12:2391–2395

Postic C, Girard J (2008) Contribution of de novo fatty acid synthesis to hepatic steatosis and insulin resistance: lessons from genetically engineered mice. J Clin Invest 118:829–838. https://doi.org/10.1172/JCI34275

Purdue PE, Allsop J, Isaya G, et al (1991a) Mistargeting of peroxisomal L-alanine:glyoxylate aminotransferase to mitochondria in primary hyperoxaluria patients depends upon activation of a cryptic mitochondrial targeting sequence by a point mutation. Proc Natl Acad Sci U S A 88:10900–10904. https://doi.org/10.1073/pnas.88.23.10900

Purdue PE, Lumb MJ, Fox M, et al (1991b) Characterization and chromosomal mapping of a genomic clone encoding human alanine:Glyoxylate aminotransferase. Genomics 10:34–42. https://doi.org/10.1016/0888-7543(91)90481-S

Purdue PE, Takada Y, Danpure CJ (1990) Identification of mutations associated with peroxisome-to-mitochondrion mistargeting of alanine/glyoxylate aminotransferase in primary hyperoxaluria type 1. J Cell Biol 111:2341–2351. https://doi.org/10.1083/jcb.111.6.2341

Qin S, Wang S, Wang X, Wang J (2018) Non-alcoholic fatty liver disease and the risk of urolithiasis: A systematic review and meta-analysis. Medicine (Baltimore) 97:e12092. https://doi.org/10.1097/MD.0000000000012092

Ramaswamy K, Shah O (2014) Metabolic syndrome and nephrolithiasis. Transl Androl Urol 3:285–295. https://doi.org/10.3978/j.issn.2223-4683.2014.06.03

Ratziu V, Bellentani S, Cortez-Pinto H, et al (2010) A position statement on NAFLD/NASH based on the EASL 2009 special conference. In: Journal of Hepatology

Remesy C, Fafournoux P, Demigne C (1983) Control of hepatic utilization of serine, glycine and threonine in fed and starved rats. J Nutr 113:28–39. https://doi.org/10.1093/jn/113.1.28

Rinella ME, Sanyal AJ (2016) Management of NAFLD: A stage-based approach. Nat Rev Gastroenterol Hepatol 13:196–205. https://doi.org/10.1038/nrgastro.2016.3

Robertson WG (2004) Kidney Models of Calcium Oxalate Stone Formation. Nephron Physiol 98:p21–p30. https://doi.org/10.1159/000080260

Rokka A, Antonenkov VD, Soininen R, et al (2009) Pxmp2 is a channel-forming protein in mammalian peroxisomal membrane. PLoS ONE 4:. https://doi.org/10.1371/journal.pone.0005090

Romeo S, Kozlitina J, Xing C, et al (2008) Genetic variation in PNPLA3 confers susceptibility to nonalcoholic fatty liver disease. Nat Genet 40:1461–1465. https://doi.org/10.1038/ng.257

Romero V, Akpinar H, Assimos DG (2010a) Kidney Stones: A Global Picture of Prevalence, Incidence, and Associated Risk Factors Kidney Stones: A Global Perspective. Rev Urol Rev Urol 1212:86–96. https://doi.org/10.3909/riu0459

Romero V, Akpinar H, Assimos DG (2010b) Kidney stones: a global picture of prevalence, incidence, and associated risk factors. Rev Urol 12:e86-96. https://doi.org/10.3909/riu0459

Rowsell EV, Snell K, Carnie JA, Al-Tai AH (1969) Liver-L-alanine-glyoxylate and L-serine-pyruvate aminotransferase activities: an apparent association with gluconeogenesis. Biochem J 115:1071–1073. https://doi.org/10.1042/bj1151071

Salem V, Izzi-Engbeaya C, Coello C, et al (2016) Glucagon increases energy expenditure independently of brown adipose tissue activation in humans. Diabetes Obes Metab 18:72–81. https://doi.org/10.1111/dom.12585

Salido E, Pey AL, Rodriguez R, Lorenzo V (2012) Primary hyperoxalurias: Disorders of glyoxylate detoxification. Biochim Biophys Acta - Mol Basis Dis 1822:1453–1464. https://doi.org/10.1016/j.bbadis.2012.03.004

Salido EC, Li XM, Lu Y, et al (2006a) Alanine-glyoxylate aminotransferase-deficient mice, a model for primary hyperoxaluria that responds to adenoviral gene transfer. Proc Natl Acad Sci 103:18249–18254. https://doi.org/10.1073/pnas.0607218103

Salido EC, Li XM, Lu Y, et al (2006b) Alanine-glyoxylate aminotransferase-deficient mice, a model for primary hyperoxaluria that responds to adenoviral gene transfer. Proc Natl Acad Sci U S A 103:18249–18254. https://doi.org/10.1073/pnas.0607218103

Samuel VT, Shulman GI (2016) The pathogenesis of insulin resistance: integrating signaling pathways and substrate flux. J Clin Invest 126:12–22. https://doi.org/10.1172/JCI77812

Sanyal A, Poklepovic A, Moyneur E, Barghout V (2010) Population-based risk factors and resource utilization for HCC: US perspective. Curr Med Res Opin 26:2183–2191. https://doi.org/10.1185/03007995.2010.506375

Sato M (2002) Functional analysis of the 5 P - £ anking region of the human alanine : glyoxylate aminotransferase gene AGXT. 1574:205–209

Savage A, Zeng L, Houslay MD (1995) A role for protein kinase C-mediated phosphorylation in eliciting glucagon desensitization in rat hepatocytes. Biochem J 307:281–285. https://doi.org/10.1042/bj3070281

Schattenberg JM, Galle PR (2010) Animal Models of Non-Alcoholic Steatohepatitis: Of Mice and Man. Dig Dis 28:247–254. https://doi.org/10.1159/000282097

Schattenberg JM, Singh R, Wang Y, et al (2006) Jnk1 but not jnk2 promotes the development of steatohepatitis in mice. Hepatology 43:163–172. https://doi.org/10.1002/hep.20999

Schriewer A, Brink M, Gianmoena K, et al (2017) Oxalic acid quantification in mouse urine and primary mouse hepatocyte cell culture samples by ion exclusion chromatography–mass spectrometry. J Chromatogr B 1068–1069:239–244. https://doi.org/10.1016/j.jchromb.2017.10.032

Schulman JL, Carleton JL, Whitney G, Whitehorn JC (1957) *Effect of Glucagon on Food Intake and Body Weight in Man*. J Appl Physiol 11:419–421. https://doi.org/10.1152/jappl.1957.11.3.419

Schultz JR (2000) Role of LXRs in control of lipogenesis. Genes Dev 14:2831–2838. https://doi.org/10.1101/gad.850400

Schulze MB (2019) Metabolic health in normal-weight and obese individuals. Diabetologia 62:558–566. https://doi.org/10.1007/s00125-018-4787-8

Scott RV, Bloom SR (2018) Problem or solution: The strange story of glucagon. Peptides 100:36–41. https://doi.org/10.1016/j.peptides.2017.11.013

Seghieri M, Christensen AS, Andersen A, et al (2018) Future Perspectives on GLP-1 Receptor Agonists and GLP-1/glucagon Receptor Co-agonists in the Treatment of NAFLD. Front Endocrinol 9:649. https://doi.org/10.3389/fendo.2018.00649

Seglen PO (1976) Chapter 4 Preparation of Isolated Rat Liver Cells. In: Methods in Cell Biology. Elsevier, pp 29–83

Seki S, Kitada T, Sakaguchi H (2005) Clinicopathological significance of oxidative cellular damage in non-alcoholic fatty liver diseases. Hepatol Res 33:132–134. https://doi.org/10.1016/j.hepres.2005.09.020

Seo YY, Cho YK, Bae J-C, et al (2013) Tumor Necrosis Factor-α as a Predictor for the Development of Nonalcoholic Fatty Liver Disease: A 4-Year Follow-Up Study. Endocrinol Metab Seoul Korea 28:41–45. https://doi.org/10.3803/EnM.2013.28.1.41

Shapiro AL, Viñuela E, V. Maizel J (1967) Molecular weight estimation of polypeptide chains by electrophoresis in SDS-polyacrylamide gels. Biochem Biophys Res Commun 28:815–820. https://doi.org/10.1016/0006-291X(67)90391-9

Shavit L, Ferraro PM, Johri N, et al (2015) Effect of being overweight on urinary metabolic risk factors for kidney stone formation. Nephrol Dial Transplant 30:607–613. https://doi.org/10.1093/ndt/gfu350

Shen H, Lipka S, Kumar A, Mustacchia P (2014) Association between nonalcoholic fatty liver disease and colorectal adenoma: a systemic review and meta-analysis. J Gastrointest Oncol 5:440–446. https://doi.org/10.3978/j.issn.2078-6891.2014.061

Shin J-A, Lee J-H, Lim S-Y, et al (2013) Metabolic syndrome as a predictor of type 2 diabetes, and its clinical interpretations and usefulness. J Diabetes Investig 4:334–343. https://doi.org/10.1111/jdi.12075

Siener R, Glatz S, Nicolay C, Hesse A (2004) The Role of Overweight and Obesity in Calcium Oxalate Stone Formation. Obes Res 12:106–113. https://doi.org/10.1038/oby.2004.14

Siener R, Hönow R, Voss S, et al (2006) Oxalate Content of Cereals and Cereal Products. J Agric Food Chem 54:3008–3011. https://doi.org/10.1021/jf052776v

Singh S, Allen AM, Wang Z, et al (2015) Fibrosis Progression in Nonalcoholic Fatty Liver vs Nonalcoholic Steatohepatitis: A Systematic Review and Meta-analysis of Paired-Biopsy Studies. Clin Gastroenterol Hepatol 13:643-654.e9. https://doi.org/10.1016/j.cgh.2014.04.014

Skorecki K, Chertow GM, Marsden PA, et al (2015) Brenner and Rector's The Kidney. Elsevier Health Sciences

Smith PK, Krohn RI, Hermanson GT, et al (1985) Measurement of protein using bicinchoninic acid. Anal Biochem 150:76–85. https://doi.org/10.1016/0003-2697(85)90442-7

Smits MM, Ioannou GN, Boyko EJ, Utzschneider KM (2013) Non-alcoholic fatty liver disease as an independent manifestation of the metabolic syndrome: Results of a US national survey in three ethnic groups: Fatty liver and the metabolic syndrome. J Gastroenterol Hepatol 28:664–670. https://doi.org/10.1111/jgh.12106

Stern JH, Smith GI, Chen S, et al (2019) Obesity dysregulates fasting-induced changes in glucagon secretion. J Endocrinol 243:149–160. https://doi.org/10.1530/JOE-19-0201

Stojsavljević S, Gomerčić Palčić M, Virović Jukić L, et al (2014) Adipokines and proinflammatory cytokines, the key mediators in the pathogenesis of nonalcoholic fatty liver disease. World J Gastroenterol 20:18070–18091. https://doi.org/10.3748/wjg.v20.i48.18070

Suppli MP, Bagger JI, Lund A, et al (2020) Glucagon Resistance at the Level of Amino Acid Turnover in Obese Subjects with Hepatic Steatosis. Diabetes db190715–db190715. https://doi.org/10.2337/db19-0715

Suppli MP, Lund A, Bagger JI, et al (2016) Involvement of steatosis-induced glucagon resistance in hyperglucagonaemia. Med Hypotheses 86:100–103. https://doi.org/10.1016/j.mehy.2015.10.029

Takada Y, Noguchi T (1982) Subcellular distribution, and physical and immunological properties of hepathic alanine: Glyoxylate aminotransferase isoenzymes in different mammalian species. Comp Biochem Physiol Part B Comp Biochem 72:597–604. https://doi.org/10.1016/0305-0491(82)90512-0

Takayama T, Fujita K, Suzuki K, et al (2003) Control of oxalate formation from L-hydroxyproline in liver mitochondria. J Am Soc Nephrol 14:939–946.

https://doi.org/10.1097/01.ASN.0000059310.67812.4F

Tan TM, Field BCT, McCullough KA, et al (2013) Coadministration of Glucagon-Like Peptide-1 During Glucagon Infusion in Humans Results in Increased Energy Expenditure and Amelioration of Hyperglycemia. Diabetes 62:1131–1138. https://doi.org/10.2337/db12-0797

Targher G, Bertolini L, Padovani R, et al (2007) Prevalence of nonalcoholic fatty liver disease and its association with cardiovascular disease among type 2 diabetic patients. Diabetes Care 30:1212–1218. https://doi.org/10.2337/dc06-2247

Targher G, Day CP, Bonora E (2010) Risk of Cardiovascular Disease in Patients with Nonalcoholic Fatty Liver Disease. N Engl J Med 363:1341–1350. https://doi.org/10.1056/NEJMra0912063

Taylor EN (2005) Obesity, Weight Gain, and the Risk of Kidney Stones. JAMA 293:455. https://doi.org/10.1001/jama.293.4.455

Tian Y, Wong VW-S, Chan HL-Y, Cheng AS-L (2013) Epigenetic regulation of hepatocellular carcinoma in non-alcoholic fatty liver disease. Semin Cancer Biol 23:471–482. https://doi.org/10.1016/j.semcancer.2013.08.010

Tilg H, Hotamisligil GS (2006) Nonalcoholic Fatty Liver Disease: Cytokine-Adipokine Interplay and Regulation of Insulin Resistance. Gastroenterology 131:934–945. https://doi.org/10.1053/j.gastro.2006.05.054

Tilg H, Moschen AR (2010) Evolution of inflammation in nonalcoholic fatty liver disease: The multiple parallel hits hypothesis. Hepatology 52:1836–1846. https://doi.org/10.1002/hep.24001

Tilg H, Moschen AR (2006) Adipocytokines: mediators linking adipose tissue, inflammation and immunity. Nat Rev Immunol 6:772–783. https://doi.org/10.1038/nri1937

Tollefsbol TO (2011) Epigenetics. In: Handbook of Epigenetics. Elsevier, pp 1–6

Tomita K (2006) Tumour necrosis factor signalling through activation of Kupffer cells plays an essential role in liver fibrosis of non-alcoholic steatohepatitis in mice. Gut 55:415–424. https://doi.org/10.1136/gut.2005.071118

Torricelli FCM, De SK, Gebreselassie S, et al (2014) Dyslipidemia and Kidney Stone Risk. J Urol 191:667–672. https://doi.org/10.1016/j.juro.2013.09.022

Tsochatzis E, Papatheodoridis GV, Archimandritis AJ (2006) The Evolving Role of Leptin and Adiponectin in Chronic Liver Diseases. Am J Gastroenterol 101:2629–2640. https://doi.org/10.1111/j.1572-0241.2006.00848.x

Tsochatzis E, Papatheodoridis GV, Hadziyannis E, et al (2008) Serum adipokine levels in chronic liver diseases: Association of resistin levels with fibrosis severity. Scand J Gastroenterol 43:1128–1136. https://doi.org/10.1080/00365520802085387

Tsubaki M, Hiraiwa H (1971a) Short Communications. Chem Eng 35:376-380,a1. https://doi.org/10.1252/kakoronbunshu1953.35.376

Tsubaki M, Hiraiwa H (1971b) Short Communications. Chem Eng 35:376-380,a1.

https://doi.org/10.1252/kakoronbunshu1953.35.376

Uchida C, Funai T, Oda T, et al (1994) Regulation of glucagon of serine:pyruvate/alanine:glyoxylate aminotransferase gene expression in cultured rat hepatocytes. J Biol Chem 269:8849–8856

Unger R, Orci L (1975) THE ESSENTIAL ROLE OF GLUCAGON IN THE PATHOGENESIS OF DIABETES MELLITUS. The Lancet 305:14–16. https://doi.org/10.1016/S0140-6736(75)92375-2

Unger RH, Madison LL, Muller WA (1972) Abnormal Alpha Cell Function in Diabetics Response to Insulin. Diabetes 21:301–307. https://doi.org/10.2337/diab.21.5.301

Vajda EG, Logan D, Lasseter K, et al (2017) Pharmacokinetics and pharmacodynamics of single and multiple doses of the glucagon receptor antagonist LGD-6972 in healthy subjects and subjects with type 2 diabetes mellitus. Diabetes Obes Metab 19:24–32. https://doi.org/10.1111/dom.12752

van Dongen MGJ, Geerts BF, Morgan ES, et al (2015) First proof of pharmacology in humans of a novel glucagon receptor antisense drug. J Clin Pharmacol 55:298–306. https://doi.org/10.1002/jcph.396

van Woerden CS (2003) Primary hyperoxaluria type 1 in The Netherlands: prevalence and outcome. Nephrol Dial Transplant 18:273–279. https://doi.org/10.1093/ndt/18.2.273

Vatner DF, Majumdar SK, Kumashiro N, et al (2015) Insulin-independent regulation of hepatic triglyceride synthesis by fatty acids. Proc Natl Acad Sci 112:1143–1148. https://doi.org/10.1073/pnas.1423952112

Vernon G, Baranova A, Younossi ZM (2011) Systematic review: the epidemiology and natural history of non-alcoholic fatty liver disease and non-alcoholic steatohepatitis in adults: Systematic review: epidemiology of NAFLD and NASH. Aliment Pharmacol Ther 34:274–285. https://doi.org/10.1111/j.1365-2036.2011.04724.x

Volzke H, Robinson D-M, Kleine V, et al (2005) Hepatic steatosis is associated with an increased risk of carotid atherosclerosis. World J Gastroenterol 11:1848–1853. https://doi.org/10.3748/wjg.v11.i12.1848

Waikar SS, Srivastava A, Palsson R, et al (2019) Association of Urinary Oxalate Excretion With the Risk of Chronic Kidney Disease Progression. JAMA Intern Med 179:542. https://doi.org/10.1001/jamainternmed.2018.7980

Wainwright P, Byrne C (2016) Bidirectional Relationships and Disconnects between NAFLD and Features of the Metabolic Syndrome. Int J Mol Sci 17:367. https://doi.org/10.3390/ijms17030367

Wang H, Zhao M, Sud N, et al (2016) Glucagon regulates hepatic lipid metabolism via cAMP and Insig-2 signaling: Implication for the pathogenesis of hypertriglyceridemia and hepatic steatosis. Sci Rep 6:1–11. https://doi.org/10.1038/srep32246

Wang M, Kaufman RJ (2014) The impact of the endoplasmic reticulum protein-folding environment on cancer development. Nat Rev Cancer 14:581–597. https://doi.org/10.1038/nrc3800

Wildman RP (2008) The Obese Without Cardiometabolic Risk Factor Clustering and the Normal Weight With Cardiometabolic Risk Factor Clustering: Prevalence and Correlates of 2 Phenotypes Among the US Population (NHANES 1999-2004). Arch Intern Med 168:1617. https://doi.org/10.1001/archinte.168.15.1617

Williams KH, Shackel NA, Gorrell MD, et al (2013) Diabetes and Nonalcoholic Fatty Liver Disease: A Pathogenic Duo. Endocr Rev 34:84–129. https://doi.org/10.1210/er.2012-1009

Williams T (2015) Metabolic Syndrome: Nonalcoholic Fatty Liver Disease. FP Essent 435:24–29

Winnay JN, Boucher J, Mori MA, et al (2010) A regulatory subunit of phosphoinositide 3-kinase increases the nuclear accumulation of X-box–binding protein-1 to modulate the unfolded protein response. Nat Med 16:438–445. https://doi.org/10.1038/nm.2121

Wong RJ, Cheung R, Ahmed A (2014) Nonalcoholic steatohepatitis is the most rapidly growing indication for liver transplantation in patients with hepatocellular carcinoma in the U.S. Hepatology 59:2188–2195. https://doi.org/10.1002/hep.26986

Wong VWS, Wong GLH, Choi PCL, et al (2010) Disease progression of non-alcoholic fatty liver disease: A prospective study with paired liver biopsies at 3 years. Gut 59:969–974. https://doi.org/10.1136/gut.2009.205088

Wood KD, Holmes RP, Erbe D, et al (2019) Reduction in urinary oxalate excretion in mouse models of Primary Hyperoxaluria by RNA interference inhibition of liver lactate dehydrogenase activity. Biochim Biophys Acta BBA - Mol Basis Dis 1865:2203–2209. https://doi.org/10.1016/j.bbadis.2019.04.017

Wu G, Bazer FW, Burghardt RC, et al (2011) Proline and hydroxyproline metabolism: implications for animal and human nutrition. Amino Acids 40:1053–1063. https://doi.org/10.1007/s00726-010-0715-z

Wullaert A, van Loo G, Heyninck K, Beyaert R (2007) Hepatic Tumor Necrosis Factor Signaling and Nuclear Factor-κB: Effects on Liver Homeostasis and Beyond. Endocr Rev 28:365–386. https://doi.org/10.1210/er.2006-0031

Xia W, Bringmann P, McClary J, et al (2006) High levels of protein expression using different mammalian CMV promoters in several cell lines. Protein Expr Purif 45:115–124. https://doi.org/10.1016/j.pep.2005.07.008

Xu A, Wang Y, Keshaw H, et al (2003) The fat-derived hormone adiponectin alleviates alcoholic and nonalcoholic fatty liver diseases in mice. J Clin Invest 112:91–100. https://doi.org/10.1172/JCI200317797

Xue HH, Fujie M, Sakaguchi T, et al (1999) Flux of the L-serine metabolism in rat liver: The predominant contribution of serine dehydratase. J Biol Chem 274:16020–16027. https://doi.org/10.1074/jbc.274.23.16020

Yamato E, Noma Y, Tahara Y, et al (1990) Suppression of synthesis and release of glucagon by glucagon-like peptide-1 (7–36 amide) without affect on mRNA level in isolated rat islets. Biochem Biophys Res Commun 167:431–437. https://doi.org/10.1016/0006-291X(90)92041-W

Yan H, Gu W, Yang J, et al (2009) Fully Human Monoclonal Antibodies Antagonizing the Glucagon Receptor Improve Glucose Homeostasis in Mice and Monkeys. J Pharmacol Exp Ther 329:102–111. https://doi.org/10.1124/jpet.108.147009

Yang K, Zhang XJ, Cao LJ, et al (2014) Toll-Like Receptor 4 Mediates Inflammatory Cytokine Secretion in Smooth Muscle Cells Induced by Oxidized Low-Density Lipoprotein. PLoS ONE 9:e95935. https://doi.org/10.1371/journal.pone.0095935

Yang SQ, Lin HZ, Lane MD, et al (1997) Obesity increases sensitivity to endotoxin liver injury: Implications for the pathogenesis of steatohepatitis. Proc Natl Acad Sci 94:2557–2562. https://doi.org/10.1073/pnas.94.6.2557

Yang Z, Sugawara M, Ponath PD, et al (1990) Interferon gamma response region in the promoter of the human DPA gene. Proc Natl Acad Sci 87:9226–9230. https://doi.org/10.1073/pnas.87.23.9226

Yazıcı D, Sezer H (2017) Insulin Resistance, Obesity and Lipotoxicity. In: Engin AB, Engin A (eds) Obesity and Lipotoxicity. Springer International Publishing, Cham, pp 277–304

Yki-Järvinen H (2014a) Non-alcoholic fatty liver disease as a cause and a consequence of metabolic syndrome. Lancet Diabetes Endocrinol 2:901–910. https://doi.org/10.1016/S2213-8587(14)70032-4

Yki-Järvinen H (2014b) Non-alcoholic fatty liver disease as a cause and a consequence of metabolic syndrome. Lancet Diabetes Endocrinol 2:901–910. https://doi.org/10.1016/S2213-8587(14)70032-4

Younossi Z, Anstee QM, Marietti M, et al (2018) Global burden of NAFLD and NASH: Trends, predictions, risk factors and prevention. Nat Rev Gastroenterol Hepatol 15:11–20. https://doi.org/10.1038/nrgastro.2017.109

Younossi ZM, Marchesini G, Pinto-Cortez H, Petta S (2019) Epidemiology of Nonalcoholic Fatty Liver Disease and Nonalcoholic Steatohepatitis: Implications for Liver Transplantation. Transplantation 103:22–27. https://doi.org/10.1097/TP.0000000000002484

Zeybel M, Mann DA, Mann J (2013) Epigenetic modifications as new targets for liver disease therapies. J Hepatol 59:1349–1353. https://doi.org/10.1016/j.jhep.2013.05.039

Zhang M, White TA, Schuermann JP, et al (2004) Structures of the *Escherichia coli* PutA Proline Dehydrogenase Domain in Complex with Competitive Inhibitors †, ‡. Biochemistry 43:12539–12548. https://doi.org/10.1021/bi048737e

Zhang X, Roe SM, Hou Y, et al (2003) Crystal structure of alanine:glyoxylate aminotransferase and the relationship between genotype and enzymatic phenotype in primary hyperoxaluria type 1. J Mol Biol 331:643–652. https://doi.org/10.1016/S0022-2836(03)00791-5

Zhang Y, Proenca R, Maffei M, et al (1994) Positional cloning of the mouse obese gene and its human homologue. Nature 372:425–432. https://doi.org/10.1038/372425a0

6 Appendix

6.1 List of figures

6.2 List of tables

6.3 Publications

6.3.1 Articles

Hurst, J.; Kuehn, S.; **Jashari, A**.; Tsai, T.; Bartz-Schmidt, K. U.; Schnichels, S.; Joachim, S. C**. A Novel Porcine *Ex Vivo* Retina Culture Model for Oxidative Stress Induced by H_2O_2.** *Altern. Lab. Anim.* **2017**, *45* (1), 11–25. https://doi.org/10.1177/026119291704500105.

Kuehn, S.; Hurst, J.; **Jashari, A**.; Ahrens, K.; Tsai, T.; Wunderlich, I. M.; Dick, H. B.; Joachim, S. C.; Schnichels, S. **The Novel Induction of Retinal Ganglion Cell Apoptosis in Porcine Organ Culture by NMDA** — An Opportunity for the Replacement of Animals in Experiments. *Altern. Lab. Anim.* **2016**, *44* (6), 557–568. https://doi.org/10.1177/026119291604400608.

6.3.2 Contribution on congresses

Talk: **Downregulation of AGXT in NAFLD - a molecular link to kidney injury.** Cadenas C, **Jashari A**, Hengstler JG. 2nd European Fatty Liver Conference (EFLC 2018), Maastrich NL

Poster: **Epigenetic and transcriptional profiling identifies impaired glyoxylate detoxification in NAFLD as a risk factor for hyperoxaluria. Jashari A,** Gianmoena K, Cadenas C, Hengstler JG. EMBO/EMBL Symposium: Metabolism meets Epigenetics, November 2019 in Heidelberg, Germany.

6.4 Eidesstattliche Versicherung (Affidavit)

Name, Vorname
(Surname, first name)

Matrikel-Nr.
(Enrolment number)

Belehrung:

Wer vorsätzlich gegen eine die Täuschung über Prüfungsleistungen betreffende Regelung einer Hochschulprüfungsordnung verstößt, handelt ordnungswidrig. Die Ordnungswidrigkeit kann mit einer Geldbuße von bis zu 50.000,00 € geahndet werden. Zuständige Verwaltungsbehörde für die Verfolgung und Ahndung von Ordnungswidrigkeiten ist der Kanzler/die Kanzlerin der Technischen Universität Dortmund. Im Falle eines mehrfachen oder sonstigen schwerwiegenden Täuschungsversuches kann der Prüfling zudem exmatrikuliert werden, § 63 Abs. 5 Hochschulgesetz NRW.

Die Abgabe einer falschen Versicherung an Eides statt ist strafbar.

Wer vorsätzlich eine falsche Versicherung an Eides statt abgibt, kann mit einer Freiheitsstrafe bis zu drei Jahren oder mit Geldstrafe bestraft werden, § 156 StGB. Die fahrlässige Abgabe einer falschen Versicherung an Eides statt kann mit einer Freiheitsstrafe bis zu einem Jahr oder Geldstrafe bestraft werden, § 161 StGB.

Die oben stehende Belehrung habe ich zur Kenntnis genommen:

Official notification:

Any person who intentionally breaches any regulation of university examination regulations relating to deception in examination performance is acting improperly. This offence can be punished with a fine of up to EUR 50,000.00. The competent administrative authority for the pursuit and prosecution of offences of this type is the chancellor of the TU Dortmund University. In the case of multiple or other serious attempts at deception, the candidate can also be unenrolled, Section 63, paragraph 5 of the Universities Act of North Rhine-Westphalia.

The submission of a false affidavit is punishable.

Any person who intentionally submits a false affidavit can be punished with a prison sentence of up to three years or a fine, Section 156 of the Criminal Code. The negligent submission of a false affidavit can be punished with a prison sentence of up to one year or a fine, Section 161 of the Criminal Code.

I have taken note of the above official notification.

Ort, Datum
(Place, date)

Unterschrift
(Signature)

Titel der Dissertation:
(Title of the thesis):

Ich versichere hiermit an Eides statt, dass ich die vorliegende Dissertation mit dem Titel selbstständig und ohne unzulässige fremde Hilfe angefertigt habe. Ich habe keine anderen als die angegebenen Quellen und Hilfsmittel benutzt sowie wörtliche und sinngemäße Zitate kenntlich gemacht.
Die Arbeit hat in gegenwärtiger oder in einer anderen Fassung weder der TU Dortmund noch einer anderen Hochschule im Zusammenhang mit einer staatlichen oder akademischen Prüfung vorgelegen.

I hereby swear that I have completed the present dissertation independently and without inadmissible external support. I have not used any sources or tools other than those indicated and have identified literal and analogous quotations.

The thesis in its current version or another version has not been presented to the TU Dortmund University or another university in connection with a state or academic examination.*

*Please be aware that solely the German version of the affidavit ("Eidesstattliche Versicherung") for the PhD thesis is the official and legally binding version.

Ort, Datum
(Place, date)

Unterschrift
(Signature)

6.5 Acknowledgement

Completing my PhD thesis was challenging, and I could not have done it on my own without the guidance and support of numerous people who encouraged me to keep going and helped me in various ways.

First, I would like to thank **Prof. Hengstler** for giving me the opportunity to work in his laboratory and for his continuous support and guidance during the last years. He was always accessible for questions and discussions. Without his ideas, I would have been stuck many times.

My deepest gratitude goes to **Dr. Cristina Cadenas** for her outstanding guidance and for always being there as a supervisor as well as a human being. You were always positive and full of joy which helped me to stay on track and never give up. Honestly, you are the best supervisor someone could wish for.

I also want to thank the team from the Analytical Chemistry Unit at IfADo, in particular Dr. Jörg Reinders, Michael Porta and Beate Aust, for analysing hundreds of samples for us. Moreover, thank you to all our cooperation partners, who contributed to this thesis, especially Dr. Nina Gasparoni from the Epigenetic Unit (University of Saarland) and Dr. Christian Hudert (Charité Berlin).

I am truly grateful for my colleagues who made the everyday lab life more fun and exciting. Thank you, **Philipp Gabrys** and **Katharina Grgas** for always making me laugh, and helping and supporting me so much in the lab, especially during my pregnancy. Without you, this thesis would have not been possible. Thank you, **Katharina Belgasmi** for the “thousands of thounsands” of perfusions. Thank you, **Annika Glotzbach, Daniela Gonzales, Maiju Myllus and Wiebke Albrecht** for not only being my colleagues but becoming my friends.

Mein Dank geht auch an meine liebsten Freunde **Pina Eichert** und **Sugina Thavalingam** fürs Immerdasein, Bestärken und Unterstützen seit nun fast 10 Jahren. Danke auch an meine Familie für alles was sie für mich getan haben.

Mein größter Dank geht an meinen besten Freund und Ehemann **Miro Kerckhoff** für seine unermüdliche Unterstützung und vielen Aufmunterungen, die ich nach langen Tagen gebraucht habe. Danke, dass du mir gezeigt hast, dass es Wichtigeres gibt als Agxt und mich in Allem was ich tue immer bestärkst. Ohne dich wäre ich heute nicht der Mensch, der ich bin. Ich freue mich auf unsere gemeine Zukunft und die Ankunft unseres Babys.